

# The Importance of Magnitude Spectra in the Discrimination of Visual and Tactile Textures

By

**Mohammad Faizun**

Submitted in accordance with the requirements for the degree of  
Doctor of Philosophy

The University of Leeds  
School of Mechanical Engineering

August 2020

# Acknowledgements

Undertaking this PhD programme has been a truly life-changing experience for me and it would not have been possible to complete it without the support and guidance that I received from many people.

I would like to express my deepest appreciation all those who have helped me to complete this thesis.

A special gratitude I give to my supervisors Dr Brian Henson, Dr Donna Lloyd, and Dr Jongrae Kim who gave me the chance to pursue the research and provided me with patient guidance, encouragement, and helpful discussions along the research and the thesis writing process. I have been extremely lucky to have supervisors who cared so much about my work, and who responded to my questions, queries, and problems so promptly.

I would like to thank the LPDP (Indonesia Endowment Fund for Education), not only for providing the funding which allowed me to pursue this PhD programme, but also for giving me the opportunity to attend conferences and meet so many interesting people. Thanks are also due to my supervisor Dr Brian Henson for providing partial financial support.

I thank to all my colleagues in The Institute of Design, Robotics and Optimisation for the support they provided. Special thank to Aws Ali who have been my best friend since the beginning of my PhD programme.

And finally, I would also like to say a heartfelt thank you to my wife Yolanda and family who have been by my side in all circumstances, giving me support and love to always encourage me to follow my dreams.

## Declaration of Originality

I thereby declare that this thesis has not been and will not be submitted in whole or in part to another university for the award of any other degree.

Mohammad Faizun

---

(Signature)

# Abstract

Surface texture is one of the key parameters in the affective design of products. It can give tactile sensations which influence customers' appreciation and preference to the product. Among other tactile sensations, perceptual roughness is the most important. However, designing a surface texture which satisfies the aimed tactile-sensation is still challenging. To characterize roughness perception, roughness parameters have been used and they were found to not reflect the perceived roughness.

In this research, instead of using roughness parameters, the surface contours were represented by using image textures. This method was motivated by two evidences; first, there is a strong indication that visual and tactile perception is related in some degree; second, the researches in image recognition are more mature and the knowledge in that field can be useful to model the tactile perception.

There are at least four types of image features; statistical, structural, model-based methods, and spectral-based features. In this study, the FT spectra-based features were selected because they are more related to the frequency of textures. Furthermore, as there are two parts of FT spectra, this research was aimed to determine the importance of the magnitude and phase spectra of images in the discrimination of visual and tactile textures.

In order to do so, some sets of tactile stimuli were designed by transforming pixels' value of image into the height of stimuli's asperities. The designs which are in 3D CAD files were then printed using a 3D printer. Four set of experiments were made; the first set was to investigate the similarity between visual and tactile perception in discriminating irregular textures; the second set was to investigate the influence of magnitude and phase spectra on the hybrid image appearance; the third set was to measure the magnitude dominance of images using power-spectra based features; the fourth set was to investigate the presence of natural textures which are magnitude dominant.

The results show that the magnitudes are more important than the phases and the magnitude-based features can be used to measure the magnitude and phase dominance of textures. Beside that, the results also show that both visual and tactile perception have a similar pattern which indicates that it is possible to model the tactile perception using image textures.



## Abbreviations

<i>1D</i>	One-Dimensional
<i>2D</i>	Two-Dimensional
<i>3D</i>	Three-Dimensional
ACF	auto-correlation function
<i>ASCII</i>	American Standard Code for Information Interchange
CAD	Computer Aided Design
FFT	Fast Fourier Transform
FO	First-Order
IFFT	Inverse Fast Fourier Transform
MDS	Multidimensional Scaling
SO	Second-Order
TO	Third-Order

# Contents

<b>1</b>	<b>Introduction</b>	<b>1</b>
1.1	Overview . . . . .	1
1.1.1	Tactual perception dimension . . . . .	2
1.1.2	Roughness texture of surface . . . . .	2
1.1.3	Image textures used to represent roughness . . . . .	3
1.2	Problem Statement . . . . .	5
1.3	Aim of Research . . . . .	6
1.4	Original Contributions . . . . .	6
1.5	Outline of the thesis . . . . .	7
<b>2</b>	<b>Literature Review</b>	<b>10</b>
2.1	Physical Roughness . . . . .	10
2.1.1	2D roughness parameters . . . . .	13
2.1.2	3D roughness parameters . . . . .	16
2.2	Roughness Perception . . . . .	16
2.2.1	Mechanoreceptive afferents in glabrous skin . . . . .	17
2.2.2	Un-myelinated mechanoreceptive afferents . . . . .	22
2.2.3	Tactile spatial acuity . . . . .	23
2.2.4	Perception of roughness magnitude . . . . .	25
2.2.5	Tactual perceptual field . . . . .	28
2.2.6	Human perception on tactual patterns . . . . .	29
2.2.7	Cross-modal interactions between visual perception and touch perception . . . . .	31
2.3	Relationship between Physical Roughness and Perceived Roughness	32
2.3.1	Vibratory cues approach . . . . .	32
2.3.2	Physical properties approach . . . . .	34
2.4	Image Textures . . . . .	35
2.4.1	Extraction methods of image features . . . . .	36
2.5	The Importance of Magnitude and Phase in Signal . . . . .	37

---

2.5.1	Justifications of the argument that phase is more important than magnitude . . . . .	38
2.5.2	Magnitude can be more important than phase . . . . .	41
2.5.3	Quantitative measurements on phase dominance . . . . .	43
2.5.4	Fourier transform-based features . . . . .	45
2.6	Summary . . . . .	47
<b>3</b>	<b>Magnitude Estimation of Roughness</b>	<b>48</b>
3.1	Experiment Rationale . . . . .	48
3.2	Method . . . . .	50
3.2.1	Participants . . . . .	50
3.2.2	Stimuli . . . . .	51
3.2.3	The computer codes for creating textures . . . . .	53
3.2.4	Procedure . . . . .	56
3.2.5	Analysis . . . . .	58
3.3	Result and Discussion . . . . .	59
3.3.1	Visual experiment . . . . .	59
3.3.2	Tactile experiment . . . . .	75
3.3.3	Comparison between the roughness scales of the visual and the tactile textures . . . . .	91
3.4	Conclusion . . . . .	96
<b>4</b>	<b>The Influence of Magnitude and Phase Spectra in the Discrimination of Images</b>	<b>98</b>
4.1	Experiment Rationale . . . . .	98
4.2	Method . . . . .	100
4.2.1	Stimuli . . . . .	100
4.2.2	Participants . . . . .	102
4.2.3	Procedure . . . . .	103
4.2.4	Analysis . . . . .	104
4.3	Result and Discussion . . . . .	107
4.3.1	The effect of the type of the signals to the magnitude's dominance . . . . .	109
4.3.2	The effect of the frequency of MP to the magnitude's dominance . . . . .	112
4.3.3	The effect of the rotation angle of MPs to the magnitude dominance . . . . .	116

---

4.3.4	The effect of the combination between the type and the frequency of MPs to the magnitude's dominance . . . . .	119
4.3.5	Power spectra-based features to measure the magnitude's dominance . . . . .	121
4.4	Conclusion . . . . .	128
<b>5</b>	<b>The Influence of Scaling Transformation to the Magnitude Dominance of Images</b>	<b>130</b>
5.1	Experiment Rationale . . . . .	130
5.2	Method . . . . .	132
5.2.1	Stimuli . . . . .	132
5.2.2	Participants . . . . .	133
5.2.3	Procedure . . . . .	134
5.2.4	Analysis . . . . .	136
5.3	Result and Discussion . . . . .	137
5.3.1	The appearance and disappearance of PPs in the hybrid image . . . . .	137
5.3.2	The ratio of the resized MPs . . . . .	139
5.3.3	A Logistic regression to model the relationship between a set of power spectra-based features and the visual responses	141
5.4	Conclusion . . . . .	147
<b>6</b>	<b>Magnitude Dominance of Natural Textures in the Visual and Tactile Perception</b>	<b>149</b>
6.1	Experiment Rationale . . . . .	149
6.2	Method . . . . .	150
6.2.1	Stimuli . . . . .	150
6.2.2	Participants . . . . .	157
6.2.3	Procedure . . . . .	157
6.2.4	Analysis . . . . .	158
6.3	Result and Discussion . . . . .	161
6.4	Conclusion . . . . .	166
<b>7</b>	<b>General Discussion and Conclusion</b>	<b>167</b>
7.1	Overview . . . . .	167
7.2	General Discussion . . . . .	169
7.3	Conclusions and Recommendations . . . . .	172
7.3.1	Conclusions . . . . .	172

---

7.3.2	Recommendations for future work . . . . .	173
<b>A</b>	<b>Computer Codes to Create Image Textures and CAD Models</b>	<b>175</b>
A.1	Java™ code to create the first-, second-, and third-order patterns .	175
A.2	Java™ codes to convert a 2D array into an image and an <i>.stl</i> file of boxels . . . . .	177
A.3	Python™ code to convert and save a 2D array into an <i>.stl</i> file . .	181
<b>B</b>	<b>Parent Images with Standard Signals</b>	<b>184</b>
<b>C</b>	<b>Power Spectra-Based Features</b>	<b>187</b>
C.1	Features Derived by Liu and Jernigan . . . . .	187
C.2	Proposed Features . . . . .	188
C.2.1	Maximum value-based threshold of features . . . . .	188
C.2.2	Circular boundary-based threshold of features . . . . .	190
C.2.3	Quadrant area-based features . . . . .	191
C.2.4	Wedge area-based features . . . . .	192
C.2.5	Standardized spectrum-based features . . . . .	193
<b>D</b>	<b>Results of Post-hoc Pairwise Comparisons Tests</b>	<b>194</b>
D.1	Post-hoc pairwise comparisons of Chi-squared test . . . . .	199
	<b>References</b>	<b>230</b>

# List of Figures

1.1	Homogeneous particles with unfamiliar texture . . . . .	3
2.1	Example of machined surface topography. Length of the axis is 750 $\mu m$ . . . . .	11
2.2	Example of the result of stylus-based measurement . . . . .	12
2.3	Filtered profile: primary (top), waviness (middle) and roughness (bottom) profiles . . . . .	12
2.4	Mechanoreceptors in glabrous skin . . . . .	18
2.5	For a variety of factors, the elliptical shape (b) is perceived as round hoop . . . . .	29
3.1	First-order textures with transition probabilities from 10% to 50% in the upper row, and 60% to 90% in the lower row. . . . .	51
3.2	Second-order textures with transition probabilities from 10% to 50% in the upper row, and 60% to 90% in the lower row. . . . .	52
3.3	Third-order textures with transition probabilities from 10% to 50% in the upper row, and 60% to 90% in the lower row. . . . .	53
3.4	Image (a) to roughness pattern (b) transformation . . . . .	54
3.5	A sample of CAD model of the tactile stimulus. . . . .	55
3.6	Image textures in the visual experiment. The subjects were asked to assign a roughness value for the test stimulus by referring to the reference images. . . . .	57
3.7	Percent of Markov Order vs Actual Roughness. . . . .	58
3.8	Scales of the perceived roughness of the visual textures with first- , second-, and third-order statistics. The horizontal axis is the category of textures with each point indicates the percentage of the transient probabilities of the corresponding texture. The vertical axis is the scales of the perceived magnitude of the textures. . . . .	59

- 
- 3.9 Multiple comparisons of the scales' means of the perceived roughness between all pairs of the first-order visual textures. The blue error bars indicate that the difference of scales' means for the corresponding pair is not statistically significant ( $p\text{-Tukey} \geq .05$ ). If the error bar is red, the scales' means for the corresponding pairs is statistically significant ( $p\text{-Tukey} \leq .05$ ). . . . . 61
- 3.10 Boxplot of subjective scale for each of first-order visual texture. The horizontal axis is the category of textures with each point indicating the percentage of the transient probabilities of the corresponding texture. The vertical axis is the scales of the perceived roughness of the textures. . . . . 62
- 3.11 Subjects' roughness sensation on the visual textures with first-order statistics. The horizontal axis is the category of textures with each point indicates the percentage of the transient probabilities of the corresponding texture. The vertical axis is the scales of the perceived roughness of the textures. . . . . 63
- 3.12 The correlation between transition probabilities of the first-order visual textures and the scales of perceived roughness for each subject. The subject with positive correlation means that he/she perceived the scale of roughness to increase as the transition probability increases. Zero correlation indicates the roughness perception is either constant, concave or convex. Negative correlation indicates that the scales of perceived roughness decreases. . . . . 64
- 3.13 Polynomial regressions of the perceived roughness of the visual textures with first-order statistics. The red scattered-dots are the mean of the scales of perceived roughness of each texture. There are four polynomial functions with different degrees to fit. . . . . 66
- 3.14 Multiple comparisons of the scales' means of the perceived roughness between all pairs of the second-order visual textures. The blue error bars indicate that the difference of scales' means for the corresponding pair is not statistically significant ( $p\text{-Tukey} \geq .05$ ). If the error bar is red, the scales' means for the corresponding pairs is statistically significant ( $p\text{-Tukey} \leq .05$ ). . . . . 67

- 
- 3.15 The boxplot of subjective scale for each of second-order visual texture. The horizontal axis is the category of textures with each point indicates the percentage of the transient probabilities of the corresponding texture. The vertical axis is the scale of the perceived roughness of the textures. . . . . 67
- 3.16 Subjects' roughness sensation on the visual textures with second-order statistics. The horizontal axis is the category of textures with each point indicates the percentage of the transient probabilities of the corresponding texture. The vertical axis is the scales of the perceived roughness of the textures. . . . . 68
- 3.17 The correlation between transition probabilities of the second-order visual textures and the perceived scales of their roughness for each subject. The subject with positive correlation means he/she perceived the the roughness scale to increase as the transition probability increases. Zero correlation indicates the roughness perception is either constant, concave or convex. Negative correlations indicate that the scales of perceived roughness decreases . . . . . 69
- 3.18 Polynomial regressions of the perceived roughness of the visual textures with second-order statistics. The red scattered dots are the scales' mean of the perceived roughness of each texture. There are four polynomial functions with different degrees to fit. . . . . 70
- 3.19 Multiple comparisons of the scales' means of the perceived roughness between all pairs of the third-order visual textures. The blue error bars indicate that the difference of scales' means for the corresponding pair is not statistically significant ( $p\text{-Tukey} \geq .05$ ). If the error bar is red, the scales' means for the corresponding pairs is statistically significant ( $p\text{-Tukey} \leq .05$ ). . . . . 71
- 3.20 The boxplot of subjective scale for each of third-order visual texture. The horizontal axis is the category of textures with each point indicates the percentage of the transient probabilities of the corresponding texture. The vertical axis is the scales of the perceived roughness of the textures. . . . . 72
- 3.21 Subjects' roughness sensation on the visual textures with third-order statistics. The horizontal axis is the category of textures with each point indicates the percentage of the transient probabilities of the corresponding texture. The vertical axis is the scales of the perceived roughness of the textures. . . . . 73



- 
- 3.22 The correlation between transition probabilities of the third-order visual textures and the perceived scales of their roughness for each subject. The subject with positive correlation means he/she perceived the the roughness scale to increase as the transition probability increases. Zero correlation indicates the roughness perception is either constant, concave or convex. Negative correlation indicates that the scales of perceived roughness decreases. . . . . 73
- 3.23 Polynomial regressions of the perceived roughness of the visual textures with third-order statistics. The red scattered dots are the mean of the roughness of each texture. There are four polynomial functions with different degrees to fit. . . . . 75
- 3.24 Perceived magnitude-scales of the roughness of the tactile textures with first-, second-, and third-order statistics. The horizontal axis is the category of textures with each point indicates the percentage of the transient probabilities of the corresponding texture. The vertical axis is the scales of the perceived magnitude of the textures. 76
- 3.25 Multiple comparisons of the scales' means of the perceived roughness between all pairs of the first-order tactile textures. The blue error bars indicate that the difference of scales' means for the corresponding pair is not statistically significant ( $p\text{-Tukey} \geq .05$ ). If the error bar is red, the scales' means for the corresponding pairs is statistically significant ( $p\text{-Tukey} \leq .05$ ). . . . . 77
- 3.26 The boxplot of subjective scale for each of first-order tactile texture. The horizontal axis is the category of textures with each point indicates the percentage of the transient probabilities of the corresponding texture. The vertical axis is the scales of the perceived magnitude of the textures. . . . . 78
- 3.27 Subjects' roughness sensation on the tactile textures with first-order statistics. The horizontal axis is the category of textures with each point indicates the percentage of the transient probabilities of the corresponding texture. The vertical axis is the scales of the perceived magnitude of the textures. . . . . 79

- 
- 3.28 The correlation between transition probabilities of the first-order tactile textures and the perceived scales of their roughness for each subject. The subject with positive correlation means he/she perceived the the roughness scale to increase as the transition probability increases. Zero correlation indicates the roughness perception is either constant, concave or convex. Negative correlation indicate the roughness perception decreases . . . . . 80
- 3.29 Polynomial regressions of the perceived roughness of the tactile textures with first-order statistics. The red scattered dots are the mean of the roughness of each texture. There are four polynomial functions with different degrees to fit. . . . . 81
- 3.30 Multiple comparisons of the scales' means of the perceived roughness between all pairs of the second-order tactile textures. The blue error bars indicate that the difference of scales' means for the corresponding pair is not statistically significant ( $p\text{-Tukey} \geq .05$ ). If the error bar is red, the scales' means for the corresponding pairs is statistically significant ( $p\text{-Tukey} \leq .05$ ). . . . . 83
- 3.31 The boxplot of subjective scale for each of second-order tactile texture. The horizontal axis is the category of textures with each point indicates the percentage of the transient probabilities of the corresponding texture. The vertical axis is the scales of the perceived magnitude of the textures. . . . . 83
- 3.32 Subjects' roughness sensation on the tactile textures with second-order statistics. The horizontal axis is the category of textures with each point indicates the percentage of the transient probabilities of the corresponding texture. The vertical axis is the scales of the perceived magnitude of the textures. . . . . 84
- 3.33 The correlation between transition probabilities of the second-order tactile textures and the perceived scales of their roughness for each subject. The subject with positive correlation means he/she perceived the the roughness scale to increase as the transition probability increases. Zero correlation indicates the roughness perception is either constant, concave or convex. Negative correlation indicate the roughness perception decreases . . . . . 85

- 
- 3.34 Polynomial regressions of the perceived roughness of the tactile textures with second-order statistics. The red scattered dots are the mean of the roughness of each texture. There are four polynomial functions with different degrees to fit. . . . . 86
- 3.35 Multiple comparisons of the scales' means of the perceived roughness between all pairs of the third-order tactile textures. The blue error bars indicate that the difference of scales' means for the corresponding pair is not statistically significant ( $p\text{-Tukey} \geq .05$ ). If the error bar is red, the scales' means for the corresponding pairs is statistically significant ( $p\text{-Tukey} \leq .05$ ). . . . . 87
- 3.36 The boxplot of subjective scale for each of third-order tactile texture. The horizontal axis is the category of textures with each point indicates the percentage of the transient probabilities of the corresponding texture. The vertical axis is the scales of the perceived magnitude of the textures. . . . . 88
- 3.37 Subjects' roughness sensation on the tactile textures with third-order statistics. The horizontal axis is the category of textures with each point indicates the percentage of the transient probabilities of the corresponding texture. The vertical axis is the scales of the perceived magnitude of the textures. . . . . 89
- 3.38 The correlation between transition probabilities of the third-order tactile textures and the perceived scales of their roughness for each subject. The subject with positive correlation means he/she perceived the the roughness scale to increase as the transition probability increases. Zero correlation indicates the roughness perception is either constant, concave or convex. Negative correlation indicate the roughness perception decreases . . . . . 90
- 3.39 Polynomial regressions of the perceived roughness of the tactile textures with third-order statistics. The red scattered dots are the mean of the roughness of each texture. There are four polynomial functions with different degrees to fit. . . . . 91
- 3.40 Polynomial regressions of the perceived roughness of the first-order statistical visual and tactile textures. The red scattered dots are the mean of the roughness of the visual textures and the blue scattered dots are the mean of the roughness of the tactile textures. 93

---

3.41	Polynomial regressions of the perceived roughness of the second-order statistical visual and tactile textures. The red scattered dots are the mean of the roughness of the visual textures and the blue scattered dots are the mean of the roughness of the tactile textures.	94
3.42	Polynomial regressions of the perceived roughness of the third-order statistical visual and tactile textures. The red scattered dots are the mean of the roughness of the visual textures and the blue scattered dots are the mean of the roughness of the tactile textures.	95
4.1	Phase components have more influence to image recognition (Zisserman, 2014).	100
4.2	Magnitude component seems to have more influence to image recognition.	101
4.3	A sample of twelve images selected from thirty six parent images that were used as stimuli in this experiment. The complete set of the parent images can be found in Appendix (B). Here, their sizes are adjusted for sake of clarity. Their actual size is $420 \times 420$ . Images in row A have sawtooth type of signal with their frequency from left is 1, 3, and 9 respectively. In row B, the signal type is sinusoidal, in row C is square, and in row D is triangle and their frequencies follow the pattern of row A.	102
4.4	The scheme of a pair of images displayed on computer screen. Here, the sizes of the image stimuli are reduced for sake of clarity. The actual size of each image is $420 \times 420$ .	103
4.5	Four periodic signals which were used to generate the parent images and their power spectra. The left side plots are the periodic signals. From the top to the bottom is: sinusoidal, triangle, square, and sawtooth signal. The right side plots are the power spectra of each corresponding signal at the left side.	105
4.6	The power spectra of each periodic signals in three different frequencies. From the top to the bottom is the spectrum of the: sinusoidal, triangle, square, and sawtooth signal.	106

- 
- 4.7 Frequency distribution of the responses for each the type of MP. Each x-axis label indicates the type, the frequency, and the rotation angle of the signal. The signal's types are coded as Saw, Sin, Squ, and Too which stands for Sawtooth, Sinusoidal, Square, and Square-wave respectively. Each type of MP were paired with 980 of PP. Therefore, this number also indicates the total number of responses for each type of the stimuli. The error bar represents the corresponding standard deviation value. . . . . 108
- 4.8 Frequency distribution of the responses filtered by the type of MP (left) and filtered by the type of PP (right). Each of the x-axis label stands for Sinusoidal (Sin), Triangle (Tri), Square-wave (Squ), and Sawtooth (Saw). They indicate the signal's type. Every type of MP (PP) were paired with 8820 of PP (MP) of all types. Therefore, this number also indicates the total number of responses for each type of the stimuli. . . . . 109
- 4.9 The percentage of the number of the response 0 and the response 1 for each type of MP when they are paired with each type of PP. The total responses for each pair is 2268 if the signal type is different and 2016 for the pair with the same type of signal. The upper lines are the plot of the percentage of 1s, and the bottom ones are the plot of the percentage of 0s. . . . . 112
- 4.10 Frequency distribution of the responses filtered by the signal's frequency of MP (left) and by the signal's frequency of PP (right). Each MP (PP) with a particular signal's frequency were paired with 11760 of PP (MP) of all types. . . . . 113
- 4.11 The number of 0s and 1s for each type of signal in every frequency of MP (left), and in every frequency of PP (right). Each type of MP is paired with the same type of PP. Therefore, the effect of pairing of different signals can be suppressed. The total number of response for each frequency is 672 responses. . . . . 115
- 4.12 The percentage of the number of the response 0 and the response 1 for each type of MP when they are paired with each frequency of PP. The total number of responses for each frequency of MP at each frequency of PP is 1008 responses for the pair with different frequencies, and is 924 responses for the pair with the same frequency. 116

---

4.13	Frequency distribution of the responses filtered by the rotation angle of MP (left) and the rotation angle of PP (right). The total number of responses is 1760 for each rotation angle. . . . .	117
4.14	The percentage of the number of the response 0 and the response 1 for each type of MP when they are paired with each angle of PP. The total number of responses is 1008 when the rotation angles of MP and PP are different, and it is 924 when the rotation angles are the same. . . . .	119
4.15	The percentage of response 1s and the response 0s for each type of MP when they are paired with PP which has the same rotation angle. . . . .	120
4.16	A set of power spectra-based features that are most correlated with the type of signal . . . . .	123
4.17	A set of power spectra-based features that are most correlated with the frequency of signal. . . . .	124
4.18	A set of power spectra-based features that are most correlated to the combination of the type and the frequencies of signal of MP .	125
4.19	The error function used to estimate the relationship between the magnitude's dominance and the phase's dominance. The sum of their values at any point along the feature axis is always 1.0. For example, a value of the feature which corresponds to an image with 80% magnitude's dominance will imply that the phase's dominance of that image can also be known directly from that value which, therefore is 20%. It is assumed that as the value of the feature increases, the magnitude's dominance also increases. . . . .	126
4.20	Constant C is the inverse of $\lambda$ (the penalty term's constant). The larger the C value, the logistic regression becomes more similar to the ordinary logistic regression. The coefficients become large. To shrink the coefficient, the C value must be adjusted to the smaller level. The closer the value of C to the zero, the bigger the penalty applied to the loss-function which eventually makes the logistic regression's coefficients shrink. . . . .	127
4.21	The coefficients of each feature ( $\beta$ ) of the logistic regression which is supposed to give the best performance (See Equation 4.9). . . .	128

- 
- 5.1 The error function can be used to estimate the magnitude dominance of an image based on its features. An image cannot be both magnitude dominant and phase dominant at the same time. However, by changing the frequency of its texture, the magnitude dominance of an image can be modified. Increasing the frequency will improve the magnitude dominance of the image and therefore, a phase dominant image can become magnitude dominant. Reducing the frequency will result the contrary effect. . . . . 131
- 5.2 The set of parent images which were used as the source of the power spectra (MP). From the top left to the bottom right, the patterns are labelled as MP-1 to MP-5 respectively. Here, the sizes of the image stimuli are reduced for sake of clarity. The actual size of each image is  $256 \times 256$ . . . . . 133
- 5.3 The set of parent images which were used as the source of the phase spectra (PP). From the top left to the bottom right, the image are labelled as PP-1 to PP-9 respectively. These images were displayed along with the hybrid image and their texture was not modified. Thus, their phase spectra did not change. Here, the sizes of the image stimuli are reduced for sake of clarity. The actual size of each image is  $256 \times 256$ . . . . . 134
- 5.4 The scheme of a pair of images displayed on computer screen for the left-setup experiment. The left image is PP which contribute phase spectrum and was not transformed. The right image is the hybrid image which is changing if the slider is moved due to its power spectrum changing too. If the slider is move to the right, the texture of the left image (PP) will probably and slowly appear in the hybrid image. Here, the sizes of the image stimuli are reduced for sake of clarity. The actual size of each image is  $420 \times 420$  pixels. 135
- 5.5 The scheme of a pair of images displayed on computer screen for the right-setup experiment. The slider was initially set the right side which indicates that the scaling ratio of MP is 1.0. At this condition, the texture of PP will probably appear in the hybrid image (right side). If the slider is moved to the left side, the texture will slowly disappear. Here, the sizes of the image stimuli are reduced for sake of clarity. The actual size of each image is  $420 \times 420$ . . . . . 136

- 
- 5.6 The histogram of the gathered scaling ratios of transformed MPs for the left-setup and the right-setup experiments. The frequency of scaling ratios is not normally distributed for both experiments. 140
- 5.7 The optimal C value is shown by the vertical red dashed-line. The ordinate value of crossing points between this line and the feature paths become the coefficient value of each corresponding feature in the logistic regression model which can give the best prediction. 142
- 5.8 Features that are correlated each other above the threshold and would be excluded from the regression model. . . . . 143
- 5.9 Using either training or validation data, the accuracy of the binary logistic regression model is seen to not improve for the C ( $1/\lambda$ ) value larger than 10. A GridSearch-CV method gave C equals to 28 to obtain the best accuracy. . . . . 144
- 5.10 The coefficients of each feature ( $\beta_j$ ) of the logistic regression which is estimated to give the best performance. . . . . 145
- 5.11 Scatter plots of 3240 responses. An MDS method was used to transform the dataset from one hundred and seven into two dimensions so that they can be visualized using scatter plots. The blue points indicates that the scaled images is magnitude dominant and the red ones for phase dominant images. Upper left is the plot of subjects' responses; upper right is the plot of clustered responses using K-means clustering method; bottom left is the plot of the clustered response from the binary logistic regression model using transformed-features (Equation 4.8); bottom right is the plot using the same binary logistic regression model but the features were from the MPs only. . . . . 147
- 6.1 One hundred and thirteen labels of images are arranged based on their relative closeness. Image 112 has sinusoidal texture and here, it is the most magnitude dominant. Image 113 is a Chinese letter and it is most likely to have the most phase dominant. . . . . 151
- 6.2 The blue curve shows the total sum of squared distance between two data points ( $J$ ) within each cluster for every  $k$  number of clusters in range of  $[1, 16]$ . The lower value of  $J$  the better. The red line indicates the average width of the silhouettes ( $\tilde{s}(i)$ ) at each  $k$  number of cluster. The higher value of  $\tilde{s}(i)$  indicates the better degree of cluster separation. . . . . 152



- 
- 6.3 Three clusters were then generated using K-means clustering method. Each cluster is surrounded by line segments and their member of images have the same colour. All points in black colour are the centre of gravity of the corresponding cluster. The black numbers were the image chosen as the stimuli. . . . . 154
- 6.4 In the top row from left to right are M1, M2, M3, and D1. In the middle row from left to right are P1, P2, and P3. The actual size of each image is  $256 \times 256$  pixels. Here, their size is reduced for sake of the space. . . . . 155
- 6.5 The hybrid images in the first row from left to right was created using the combination of the phase spectrum of D1 and the power spectra of M1, M2, and M3 respectively. In the second row from left to right, the hybrid images were created using the power spectrum of D1 and the phase spectra of P1, P2, and P3 respectively. Their actual size is  $256 \times 256$  pixels. Here, its size is reduced for sake of the space. . . . . 156
- 6.6 A sample of CAD model of the tactile stimulus with texture of D1. All CAD models of the stimuli were created using a computer code written in Python™ programming language (Appendix A.3). . . . 157
- 6.7 The presentation of a pair of visual stimuli. The upper image is the "sample" stimulus and two lower images are the "match" stimuli. The actual size of each stimulus is  $256 \times 256$  pixels. Here, their size is reduced for sake of clarity. . . . . 158
- 6.8 The relative distance between texture of the stimuli. Textures with labels M are magnitude dominant and the ones with labels P are phase dominant. D1 is the intermediate texture. . . . . 163

# List of Tables

2.1	Arithmetic and Statistical Roughness Parameters . . . . .	14
2.2	Motif Parameters . . . . .	15
2.3	Tactual Afferent System and Their Properties . . . . .	19
3.1	Shepherd's Pi Correlation between the Visual Texture Types . . . .	60
3.2	ANOVA Test for First-Order Visual Textures: Between Textures .	61
3.3	The Criteria of Eta Squared . . . . .	61
3.4	ANOVA Test for First-Order Visual Textures: Between Subjects .	65
3.5	ANOVA Test for Second-Order Visual Textures: Between Textures	66
3.6	ANOVA Test for Second-Order Visual Textures: Between Subjects	69
3.7	ANOVA Test for Third-Order Visual Textures: Between Textures	71
3.8	ANOVA Test for Third-Order Visual Textures: Between Subjects	74
3.9	Sepherd's Pi Correlation between the Types of Tactile Textures .	75
3.10	ANOVA Test for First-Order Tactile Textures: Between Textures	77
3.11	ANOVA Test for First-Order Tactile Textures: Between Subjects .	80
3.12	ANOVA Test for Second-Order Tactile Textures: Between Textures	82
3.13	ANOVA Test for Second-Order Tactile Textures: Between Subjects	85
3.14	ANOVA Test for Third-Order Tactile Textures: Between Textures	87
3.15	ANOVA Test for Third-Order Tactile Textures: Between Subjects	89
3.16	Correlation between Roughness and Textures of the Visual and Tactile First-Order Textures . . . . .	92
3.17	Sepherd's Pi Correlation between Visual and Tactile Textures with First-Order Textures . . . . .	93
3.18	Correlation between Roughness and Textures of the Visual and Tactile Second-Order Textures . . . . .	93
3.19	Sepherd's Pi Correlation between Visual and Tactile Textures with Second-Order Textures . . . . .	94
3.20	Correlation between Roughness and Textures of the Visual and Tactile Third-Order Textures . . . . .	95

---

3.21	Sepherd's Pi Correlation between Visual and Tactile Textures with Third-Order Textures . . . . .	96
4.1	Two-Dimensional Functions of each Type of the Image Stimuli . . . . .	101
4.2	Response Summary . . . . .	107
4.3	Chi-square Analysis of Magnitude's Dominance of the MP . . . . .	108
4.4	Chi-square Test on the Prevalence of Different Magnitude's Dominance among the Types of MP . . . . .	110
4.5	Post-hoc Pairwise Comparison of Chi-squared Test between the Types of MP . . . . .	110
4.6	Chi-square Test on the Prevalence of Different Magnitude's Dominance among MPs at Different Frequencies . . . . .	113
4.7	Post-hoc Pairwise Comparison of Chi-squared Test between the Frequencies of MP . . . . .	114
4.8	Post-hoc Pairwise Comparison of Chi-squared Test between the Frequencies of PP . . . . .	114
4.9	Chi-square Test on the Prevalence of Different Magnitude's Dominance among MPs with Different Rotation Angle . . . . .	117
4.10	Post-hoc Pairwise Comparison of Chi-squared Test between the Rotation Angles of MP . . . . .	118
4.11	Post-hoc Pairwise Comparison of Chi-squared Test between the Rotation Angles of PP . . . . .	118
4.12	The Chi-square Test on the Prevalence of Magnitude's Difference within the Combination of the Types and the Frequency of the MP's Signals . . . . .	120
4.13	The Structure of the Variables and Their Data Types . . . . .	121
4.14	The Classification Report of the Logistic Regression . . . . .	128
5.1	The Summary of Responses on Appearance and Disappearance of PPs . . . . .	138
5.2	The Summary of Responses on Appearance and Disappearance of PPs for Each PP in Both Experiment Setups . . . . .	138
5.3	The Cross Tabulation of the Predicted and the Observed Responses	139
5.4	Chi-Square Test of Independence of Responses . . . . .	139
5.5	Paired T-tests on the Prevalence of Different Means of Scaling Ratio between Setups and between Rounds . . . . .	141
5.6	ANOVA tests on the Prevalence of Different Means of Scaling Ratio within MPs and PPs . . . . .	141

---

5.7	The Classification Report of the Binary Logistic Regression Model	145
6.1	Response Summary . . . . .	162
6.2	Chi-square Analyses of Responses' Difference within Round and Mode for P1, P2, and P3 . . . . .	162
6.3	T-test on the Prevalence of Different Means of Distance between the Similar and Dissimilar Stimuli . . . . .	164
6.4	T-test on the Prevalence of Different Means of Roughness between the Similar and Dissimilar Tactile Stimuli . . . . .	165
6.5	T-test on the Prevalence of Different Means of Roughness between the Similar and Dissimilar Tactile Stimuli . . . . .	165
D.1	Post-hoc pairwise comparisons of chi-squared test between FO visual textures . . . . .	194
D.2	Post-hoc pairwise comparisons of chi-squared test between SO visual textures . . . . .	195
D.3	Post-hoc pairwise comparisons of chi-squared test between TO visual textures . . . . .	196
D.4	Post-hoc pairwise comparisons of chi-squared test between FO tactile textures . . . . .	197
D.5	Post-hoc pairwise comparisons of chi-squared test between SO tactile textures . . . . .	197
D.6	Post-hoc pairwise comparisons of chi-squared test between TO tactile textures . . . . .	198
D.7	Post-hoc pairwise comparisons of chi-squared test between MPs . . . . .	199
D.8	The Value of Roughness parameters of the Six Tactile Stimuli . . . . .	202

# Chapter 1

## Introduction

This chapter first briefly introduces some basic and necessary knowledges associated with tactile sensations. After that, the background, aims and objectives, and the methodologies of this project are elaborated. A summary of this chapter will be given at the end section.

### 1.1 Overview

Functionality is a must feature of products to be considered. However, to win the market competition, a designer must go beyond functional features because customers tend to buy products based on their emotional feelings rather than logical or rational thinking [1, 2]. Consumer are more likely to buy an attractive product, even it is more expensive [3].

Nowadays, the emotional aspects of products have been put in the design process. The emotional design is commonly termed as *hedonomic/affective* design to mean a design which generates pleasurable human-product interaction [1]. Barnes and Lillford [4] defined affective design as a systematic way to analyse the relationship between user responses and the physical parameters of the candidate designs. To get the affective responses the designer prepares some alternative physical features of a product and provide related adjectives. Users are asked to make judgements and assign ratings of some adjectives subjectively for each variation of physical parameters. The best physical criteria of the product is the highest total ratings gathered.

Most studies of affective design deal with shape [4–6], colour [7, 8], and material of products [9, 10]. The surface texture, which was ignored as a parameter of product quality for many years, attributes apparent sensation and preference on the product [11–13]. For example, two products with the similar material, shape,

and colour but different tactile texture will be valued differently as seen in the effect of uses of different lacquer on the plastic product. The tactile texture is a physical property which is perceived by touching or sliding the fingerpad over the material surface. Touch tells additional information about the product that can not be provided by visual observation [14]. Therefore, this tactile texture also has an important role in object recognition and identification [15, 16].

### 1.1.1 Tactual perception dimension

Touching and sliding the fingerpad over an object's surface will create tactile sensations such as softness, warmth, roughness and slipperiness [17]. These sensations are used to determine the characteristics of the corresponding object. The number and the type of sensations will likely to vary among different people and or objects. It is believed that the number of tactile sensations is limited [18], and can be categorized into two to five orthogonal and major groups or dimensions [19]. The categorization of those dimensions were based on the multidimensional scaling methods [18, 20–22]. By investigating previous related studies, Okamoto et al. [19] argued that there are at least three fundamental dimensions of tactile sensations which always appear: fine roughness (smooth-rough), hardness (soft-hard), and warmness (cold-warm). Furthermore, they proposed to add two more dimensions: friction (dry-moist, slippery-sticky) and macro roughness (relief-uneven).

All the dimensions, except warmth sensation, are related in some degree to the vibration generated on the skin at the interface between fingerpad and the object's surface during touching or sliding [23]. They are mediated by mechanoreceptive afferents which are embedded beneath the glabrous (non-hairy) skin such as skin of the fingerpad. Those afferents will only work in the presence of the static and or dynamic deformation of the fingerpad. Therefore, the roughness dimension is the most important among the other ones [24].

### 1.1.2 Roughness texture of surface

Researchers in psychophysics field have been investigating the relationship between the human tactile feel and surface roughness parameters that evoke it. There are three main objectives of the studies: to determine the basic understanding about spatial acuity of the touching skin [25, 26], roles of the mechanoreceptive afferents in perceiving roughness [27–31], and the relationship between the particle size and the perceived roughness [24, 32, 33]. To achieve those objectives,

most of the studies were using stimuli with relatively anisotropic textures with homogeneous particles such as sandpapers [30, 33, 34], dots embossed on paper and plastic surfaces [35–38], and metal gratings [38–41].

Few researches studied the roughness perception by using stimuli with non-homogeneous texture. Eck et al. [42] used the homogeneous particles which are arranged in unfamiliar pattern (see Figure 1.1) and they reported that the roughness magnitude perception is related to average inter-dot spacing by bi-exponential function. In the haptic mode, the value of perceived roughness is increasing as the inter-dot spacing moves from  $1.5\text{mm}$  to  $3.5\text{mm}$  and the perceived roughness is decreasing when the inter-dot spacing is getting larger than  $3.5\text{mm}$ . The pattern of this result is relatively similar with previous experiments which were using stimuli with regular spacing [35, 36]. They did not make any comparison of perceived roughness between regular and non-regular arrangement of surface textures for each respective inter-dot spacing.

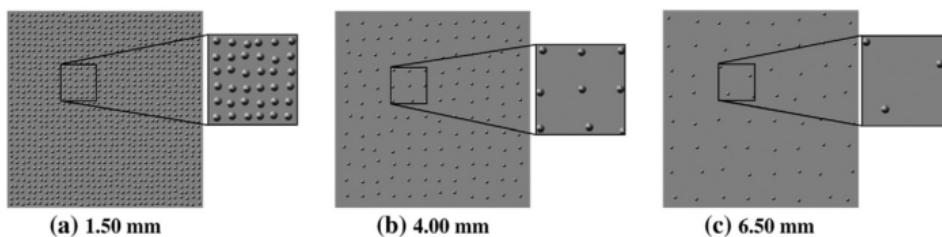


Figure 1.1: Homogeneous particles with unfamiliar texture [42].

### 1.1.3 Image textures used to represent roughness

Some researches used grayscale images as the pattern of their tactile stimuli. Each pixel's value in the image represent the elevation of the local contour of the stimuli's surface. By using this method an image texture can be transformed into a roughness texture. Culbert and Stellwagen [43] are among the first researchers to used image textures to study the tactile perception. They used forty images recommended by cartographers to create tactual patterns using a special embossage technique. Elkharraz et al. [44] designed a set of forty eight stimuli by transforming image pixels into boxels for each stimulus. They 3D printed those stimuli and then asked subjects to touch and to assign of a value of the affective response for each stimulus. Tymms et al. [45] used forty six different image textures as the surfaces' stimuli which consist of synthesized textures and natural

ones to investigate the relationship between surface roughness and the perceived roughness.

By using images as the blueprint of surfaces' stimuli, image features can be used to model the surface's topography instead of using conventional roughness parameters. There are various approaches and methods for extracting features from the image textures either directly from the spatial or from the spatial-frequency domain [46]. Bharati et al. [47] and Alaei et al. [48] proposed four categories of methods: (1) statistical methods, (2) structural methods, (3) model-based methods, and (4) transform-based methods.

*Statistical* techniques are primarily based on grayscale histograms to describe texture of patch area in images. Haralick [49] mentioned eight approaches within this statistical methods: autocorrelation function, optical transforms, digital transforms, textural edgeness, structural elements, spatial gray tone cooccurrence probabilities, gray tone run length, and autoregressive models. The first three approaches are related with spatial frequency. Fine textures are rich in high spatial frequencies while coarse textures are rich in low frequencies.

*Structural-based* techniques describe texture as the composition and orientation of texton (texture element) such as regularly spaced dots or parallel lines [49]. Three commonly used methods within this categories are auto-correlation function (ACF), edge detection, and morphological operation [48]. These methods are rarely used since they can only describe very regular textures [47]. Furthermore, finding a description and representation of primitives is difficult [50].

*Model-based* techniques generate an empirical or approximation of each pixel in the image based on a weighted average of pixel values in its neighbourhood [48]. Examples of the model-based methods are auto-regressive model, Markov random fields, and fractal models [47]. These methods have computational complexity, miss orientation selectivity, and are not suitable for describing local structures of images [48].

*Transform-based* techniques convert the image into new forms using the spatial frequency through some function transformation methods such as FFT and wavelet transform [47]. These techniques are usually called spectral-based methods. They are used to measure the overall frequency of the textures [51].

Among the above categories, only the statistical-based methods have been used in early investigation to find their correlation with affective touch responses. This method is sensitive to noise and not many of those textures are correlated to affective touch responses. Elkharraz et al. [44] investigated the correlation between 196 statistical types of image features with not only roughness but also



other tactual sensations which consist of 20 adjectives in total. They reported that among those features, there were only four that are strongly correlated with the affective responses [52, page 1]. Tymms et al. [45] used three image features suggested by Elkharraz et al. [44] to model the roughness perception. The results show that all of them have a correlation less than 0.5 with the perceptual roughness.

Compared to the statistical features, transform-based features are less sensitive to noise. This type of features are also more related to frequency or spacing of the roughness particles than the statistical types which make them more promising to model the tactile touch perception. However, so far there is not any research that use transform-based features to model the touch affective perception.

Among the transform-based methods, Fourier transform is the best method to describe the information of overall frequency of an image [53]. Therefore, in this study, the Fourier transform-based features were selected to investigate the roughness perception. As a Fourier transform has two spectra (the magnitude and phase spectrum), the textural features can be extracted from both of them. However, as there are different suggestions about which one of them is more important, investigating this problem becomes useful so that the features can be extracted from the most reliable spectrum.

The novelty of this study is to investigate the features of Fourier spectra which influence the phase and magnitude dominance of textures, to build a measure to determine these dominances, and to evaluate the built measure in visual and tactile perception.

## 1.2 Problem Statement

Physical roughness parameters have been reported to be insufficient to model the roughness perception. Some researchers made attempts to use images as the blueprints of the tactile stimuli so that instead of using roughness parameters they can use image features to model the roughness perception. Among several types of features, only the statistical-based features have been explored. It has been reported that only few of them were correlated with roughness sensation. The Fourier transform-based features which are related with frequency and, therefore, are most likely correlated with roughness have not been explored.

As there are two spectra of Fourier transform, the features can be extracted from both of them. However, not all of these spectra are useful to characterize the textures which can make a large number of extracted features might have no

correlation with the roughness. In this sense, it would be beneficial to have a method to determine the importance of each spectrum and to obtain a number of features from the most important features which correlate with roughness perception.

### 1.3 Aim of Research

This research aims to determine the phase and magnitude dominance of visual and tactile textures. To achieve this aim, the corresponding objectives are formulated:

- (a) To identify the similarity of the visual and tactile perception in perceiving irregular patterns so that representing surface roughness using image features becomes relevant.
- (b) To determine the importance of magnitudes and phases using image textures with standard signals and to extract parameters and features from the most important spectrum of image textures with standard signals.
- (c) To measure the phase and magnitude dominance of image textures using the extracted features.
- (d) To identify the similarity of the visual and tactile perception in perceiving natural textures which are either magnitude or phase dominant.

### 1.4 Original Contributions

The contributions of this study as listed here are presented against each of the research objectives.

1. This study shows that both visual and tactile perception have similar pattern in perceiving irregular textures with first-, second-, and third-order transition probabilities. The visual and tactile stimuli with coarse grain and wide distance of arrangement were perceived to be rougher.
2. By using thirty six image textures with standard signals, it is shown that the magnitude spectrum is more important than the phase spectrum. The phase and magnitude dominance of images having those types of texture is influenced by the number and arrangement's distance of the non-zero frequency components of the magnitude spectrum. One hundred features

were extracted from the power spectra of the image stimuli to characterize the magnitude dominance of the image stimuli.

3. This study provide a model to measure the influence of the value of power spectra-based features to the magnitude dominance of an using an error function. The output of the model is the influence's level which range from 0 to 1.0. A logistic regression model was developed to measure the magnitude and phase dominance of an image relative to its pair. By using the influence's level of power spectra-based features as the inputs of the developed model, the relative magnitude and phase dominance of an image can be determined with accuracy more than 85%.
4. Several evidences were obtained from this study that the power-spectra based features were useful to cluster images with natural texture into two groups of magnitude and phase dominant textures. The magnitude and phase dominance of each texture was tested in the visual and tactile experiment and the subjects' responses show that the magnitude and phase dominance of all textures was in accordance with their corresponding group. In other words, the textures in the magnitude dominant group were perceived visually and tactually as magnitude dominant too and it was so for all textures in the phase dominant group. In general, both visual and tactile perception have a similar pattern in perceiving textures. However, as pixels in images are not identical with asperities in surfaces, in some cases the same texture can be perceived differently by the visual and tactile perception.

## 1.5 Outline of the thesis

*Chapter 2* reviews surface roughness, tactile perception, comparisons between visual and tactile perception, and the image features extraction. Several methods and parameters to characterize the topography of surfaces were surveyed and discussed here. The basic concept of roughness perception including the related neural system was described. Some aspects of visual perception such as perceptual field and cross-modal interaction between visual and tactile perception were surveyed and analysed. Then, the existing implementations of image textures to represent surfaces' topography were discussed. Finally, a number of types of image features were surveyed and analysed.

*Chapter 3* compares the patterns of visual and tactile perception in perceiving irregular textures by examining Julesz's conjecture. The results of visual and tactile experiment in which subjects were perceiving and comparing the roughness of twenty seven of image and surface textures with first-, second-, and third-order transition probability were analysed and discussed.

*Chapter 4* investigates the importance of the phase and magnitude spectra of images which have textures with standard-signal. Some evidences obtained from the visual experiment which support that magnitudes are more important than phases were presented and discussed. A number of parameters and features of the power spectra of the image stimuli which influence the magnitude and phase dominance of the image stimuli were explored and analysed. A logistic regression model to measure the magnitude dominance using power spectra-based features was developed and its performance was analysed and discussed.

*Chapter 5* investigates the effect of scaling transformation on the magnitude dominance of images. This chapters was intended to examine the findings in Chapter 4 which show that the frequency of image's texture influence its magnitude dominance. A scaling transformation method used to modify the frequency of texture was described here. Finally, the results of visual experiment using the transformed images were analysed and discussed.

*Chapter 6* investigates the usefulness of the power spectra-based features to cluster images with natural textures. This chapter also describes an MDS method which was applied to the values of features prior the clustering process to reduce the dimension of the features and to determine the "relative distance" between images. The results of both visual and tactile experiments to evaluate the clustered images were analysed and discussed here.

*Chapter 7* presents an overview and general discussion which stitch all experimental chapters to provide a single story about this research. A summary is given of the conclusions of this study. Finally, several recommendations were made for future work.

*Appendix A* presents the computer codes for creating the image and stimuli textures used in the experiment reported in Chapter 3 and 6. The codes were put in three sections. First section is Java™ codes to create the stimuli with the first-, second-, and third-order transition probability. Second section also is Java™

codes to write an array into an image or *.stl* file. The third section is Python™ used in Chapter 6 to convert images into *.stl* files.

*Appendix B* shows the image stimuli having textures of standard signals used in the experiment reported in Chapter 4.

*Appendix C* present the lists of power spectra-based features used in this study. There are two sections; first section is the list of features developed by Liu and Jernigan [54]. Second section consists of five subsections. First subsection lists and describes the features which were calculated from the power spectrum with the threshold based on its maximum value. Second subsection lists and describes the features which were calculated from the power spectrum within circular boundaries. Third subsection lists and describes the features which were calculated from the power spectrum within the first and second quadrant. Fourth subsection lists and describes the features which were calculated from the power spectrum within the wedges. Fifth subsection lists two features which were calculated from the standardized power spectrum.

*Appendix D* presents seven tables related to the results of the experiment reported in Chapter 3 and one table related to Chapter 6.

# Chapter 2

## Literature Review

This chapter will discuss about physical roughness, perceived roughness, and current reports about the relationship between the touch perception and the visual one. Physical roughness refers to the asperities of a surface while perceived roughness or simply roughness refers to the roughness sensation that is perceived by human when touching a surface. The physical roughness will be elaborated to show how its parameters were established. The psychophysical and neurophysiological studies will be selected and discussed to get an overview how human perceives the surface roughness and the image texture. Some current theories of how physical roughness parameters correlate with perceived roughness will be reviewed to get more precise understanding about roughness perception.

### 2.1 Physical Roughness

The characterization and description of surface topography which is interchangeably referred as surface texture is useful and important in many applications. Due to the dynamic machining process, the real profile will likely deviate geometrically from the nominal surface, i.e. is the ideal workpiece surface as prescribed in the drawing. Petropoulos et al. [55] classified geometric deviations into two categories:

1. Macrogeometric errors
2. Microgeometric deviations

The form errors such as roundness, flatness, and straightness; and waviness fall within the first type of deviation. The second type of deviations corresponds to the micro-size irregularities which is called surface roughness or simply as

roughness (see Figure 2.1). The term roughness has the opposite meaning to the word smoothness. Surface roughness, commonly shortened as roughness, depicts the level of contour deviations in the normal direction from its mean level.

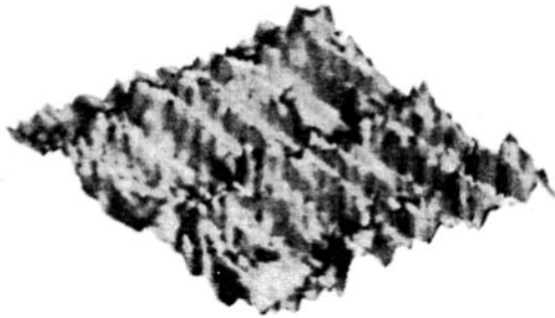


Figure 2.1: Example of mached surface topography. Length of the axis is  $750 \mu m$  [56].

Surface roughness is one of the key parameters in modelling the wear characteristics of a bearing, studying the lubrication effects, analysing bonding properties of joints, predicting the thermal and electrical conductivity of joint interfaces in electronics and computer hardware, managing the coating process, and manufacturing optical components [57]. In most applications such as wear, friction control, lubrication, and electrical and thermal conductivity the presence of roughness is not wanted or to be minimized. In machining processes, roughness cannot be avoided and it is considered as surface flaw. Some surface finishing processes such as grinding and polishing are needed to minimize the roughness within certain tolerance to meet the required specification.

However, in some applications the presence of roughness is needed. Structured roughness is important to make a stronger bonding and or a good sealing between two contact joints [58, 59]. In the area of product design, certain condition of surface roughness on the packages contributes playful perception which is important to attract consumers [60]. In this case, a textured roughness pattern can be carved across the outer surface of the product to evoke positive affective feel. An engineered roughness pattern is engraved on a surfaces to provide certain function such as giving an optimal coefficient of friction [61].

Early methods to characterize roughness were using stylus-based profilometer techniques [62]. The stylus is moved over the surface throughout several sampling trace lines to measure the altitude ( $z$ ) of different points of the surface along that line ( $x$ ). The vertical micro-movement of the stylus tip is amplified and then recorded [63]. The results are two-dimensional (2D) visual displays of the cross

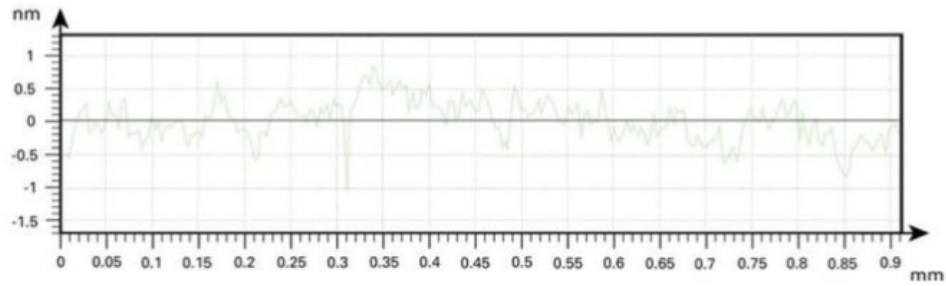


Figure 2.2: Example of the result of stylus-based measurement [64].

sectional profile ( $z(x)$ ) of the surfaces which depicts its asperity (Figure 2.2). The surface texture profile that is obtained from direct measurement is called total profile. This profile likely contains noise and imperfections such as the presence of wavelengths that are shorter than radius of the stylus tip. Filtering processes are needed to remove a range of irrelevant waves in the total profile by rejecting waves with certain lengths. At least there are three different filtering processes of a total profile [65]. The first filtering process applies a band-pass filter to remove the waves that have shorter wavelength than the diameter of the stylus tip and to suppress the long-wave components (profile geometry). The result is called a primary profile that is a superposition of roughness profile and waviness profile (Figure 2.3). The second filtering process applies a low-pass filter to obtain the waviness profile within the primary profile. Waviness profile is used to analyse macrogeometric deviations of the surface. The third filtering process uses a high-pass filter to select the roughness profile from the primary profile.

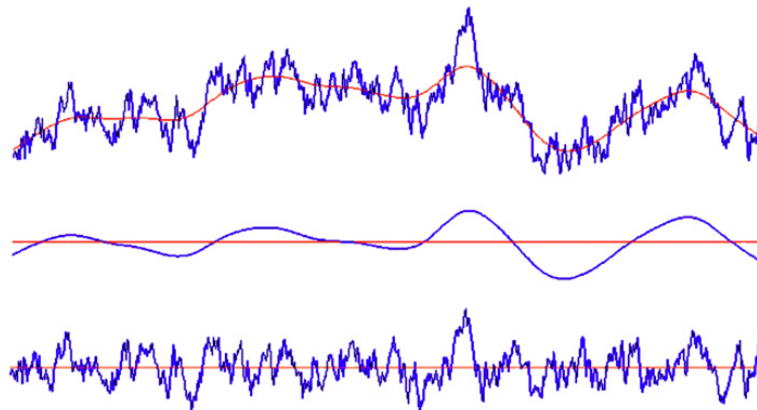


Figure 2.3: Filtered profile: primary (top), waviness (middle) and roughness (bottom) profiles [65].



### 2.1.1 2D roughness parameters

The two-dimensional (2D) roughness profile is obtained by measuring five sampling lines across the surface with the maximum spacing between two sampling lines is 20% of the tip radius [65]. The direction of the trace lines must be chosen appropriately to ensure the roughness profile is typical of the surface under inspection. For example, in the presence of lay, the trace lines must be perpendicular to the lay. The length of the sampling lines depends on the purpose of the profile characterization. ISO 4288-1998 provides the guideline for selecting the sampling length [66].

The 2D roughness profile is quantified and standardized using the two dimensional (2D) roughness parameters. These parameters are formulated based on four methods of calculations: arithmetic, statistical, morphology and fractal geometry calculations [55]. Arithmetic methods calculate the roughness parameters based on peak-to-valley height or amplitude of the profile, amplitudes distribution and spacing of the profile. The statistical methods have more complicated calculation than arithmetic method because it needs the altitude values ( $z(x)$ ) of the roughness profile instead of peaks and valleys information. This method could be applied after digital processing became available [67]. The roughness parameters in ISO 4287 are calculated based on arithmetic and statistical methods [68]. Gadelmawla et al. [69] categorised and listed arithmetic and statistical roughness parameters into three groups: amplitude parameters, spacing parameters, and hybrid parameters (Table 2.1). Each parameter is formulated based on single line profile (See [69] for the complete description). Amplitude parameters reckon the height ( $z$ ) values of the roughness profile without take into account their spread over the surface. The values of these roughness parameters will not change if, for example, the roughness profile stretches or shrinkages in longitudinal direction. Spacing parameters count features of the roughness profile along its longitudinal direction without taking into account the  $z$  values of the roughness profile. Hybrid parameters reckon the  $z$  values and their distribution along the roughness profile.

Table 2.1: Arithmetic and Statistical Roughness Parameters [After [69]]

No	Parameters Type		
	Amplitude	Spacing	Hybrid
1	Arithmetic average roughness ( $R_a$ )	High spot count ( $HSC$ )	Profile slope at mean line ( $\gamma$ )
2	Root mean square roughness ( $R_q$ )	Peak count ( $P_c$ )	Mean slope of the profile ( $\Delta_a$ )
3	Ten-point height ( $R_z$ )	Mean spacing of adjacent local peaks ( $S$ )	RMS slope of the profile ( $\Delta_q$ )
4	Maximum height of peaks ( $R_p$ )	Mean spacing at mean line ( $S_m$ )	Average wavelength ( $\lambda_a$ )
5	Maximum depth of valleys ( $R_v$ )	Number of intersections of the profiles at mean line ( $n(0)$ )	RMS wavelength ( $\lambda_q$ )
6	Mean height of peaks ( $R_p m$ )	Number of peaks in the profile ( $m$ )	Relative length of the profile ( $l_o$ )
7	Mean depth of valleys ( $R_v m$ )	Number of inflection points ( $g$ )	Bearing area length ( $t_p$ ) and bearing area curve ( $BAC$ )
8	Maximum height of the profiles ( $R_t$ ) or ( $R_{max}$ )	Mean radius of asperities ( $r_p$ )	Stepness factor of the profile ( $S_f$ )
9	Maximum peak to valley height ( $R_{ti}$ )		Waviness factor of the profile ( $W_f$ )
10	Mean of maximum peak to valley height ( $R_{tm}$ )		Roughness height uniformity ( $H_u$ )
11	Largest peak to valley height ( $R_y$ )		Roughness height skewness ( $H_s$ )
12	Third point height ( $R_{3y}$ )		Roughness pitch uniformity ( $P_u$ )
13	Mean of third point height ( $R_{3z}$ )		Roughness pitch skewness ( $P_s$ )
14	Profile solidity factor ( $k$ )		
15	Skewness ( $R_{sk}$ )		
16	Kurtosis ( $R_{ku}$ )		
17	Amplitude density function ( $ADF$ )		
18	Auto correlation function ( $ACF$ )		
19	Correlation length ( $\beta$ )		
20	Power spectral density ( $PSD$ )		

Morphological methods calculate the roughness parameters based on the primary profile instead of the roughness profile. It means that this method can separate the waviness profile without filtering process. By adopting this method ISO 12085-1997 introduced motif parameters and provided the definition of a motif as a portion of the primary profile between the highest points of two local peaks which are not necessarily adjacent [70]. There are seven motif parameters, three of which are roughness motifs and the rest are waviness motifs (See Table 2.2). Motif parameters can be calculated using a procedures as shown in ISO 12085 or an algorithm proposed by Lou et al. [71].

Table 2.2: Motif Parameters

No		Roughness motifs	Waviness motifs
1	Mean spacing	$AR$	$AW$
2	Mean Depth	$R$	$W$
3	Maximum depth	$Rx$	$Wx$
4	Total depth		$Wte$

When the resolution measurement is becoming higher, the roughness profile of a surface will be more detail because the smaller asperities will be detected. Therefore, the roughness profile obtained from the higher resolution stylus is not simply the magnification of the roughness profile from the lower resolution stylus although both seem to be similar. This property is called self-affine. The Weierstrass-Mandelbrot (W-M) fractal function can be used to represent the roughness profile which is self-affine in nature. The W-M fractal function can be characterized using two parameters, the fractal dimension ( $D$ ) and the topothesy ( $\Lambda$ ). These parameters represent intrinsic properties of the profile regardless of the stylus resolution used.  $D$  depicts the "complexity" of the profile structure while  $\Lambda$  represents the horizontal separation of profile heights corresponding to an average slop of one radian [55, 67].  $D$  and  $\Lambda$  are related to profile power spectra as shown by Thomas et al. [72]. Some discrete calculation methods for both parameters can be seen in [73].

Selecting the appropriate 2D roughness parameters is important because not all of the those parameters are useful. Most of them do not have functional significance in the application. Using a higher class of roughness which exceeds the necessary level is not advantageous [55, Page 4]. Some parameters are redundant because they are correlated with each other. The confusion of selecting the proper parameters is called parameter rash which may generate expensive cost [74]. The least significant parameter should be removed to eliminate unwanted cost. For

example, instead of including the arithmetic average height ( $R_a$ ) in an analysis it is preferably to use the root mean square roughness ( $R_q$ ) because  $R_a$  and  $R_q$  are correlated. However,  $R_a$  is less sensitive to asperity fluctuation than  $R_q$ . Therefore, a roughness parameter to be useful should represent the surface topography effectively, have statistical form, and provide function and is not correlated with another parameter [75].

### 2.1.2 3D roughness parameters

The 2D roughness profile provides only limited information on the characteristics of the surface topography. A finite number of 2D roughness parameters cannot fully describe real surface geometry [62, 69]. Furthermore, most of these parameters are not effective for representing the surface characteristics especially for the surface with anisotropic roughness [76]. In an anisotropic surface, different scanning directions will produce significantly different data for each parameter. Moreover, 2D parameters provide only little information about functional behaviour of surfaces because most of the surface function is manifest in 3-dimensions (3D) [63]. This becomes one of the reasons for developing three-dimensional (3D) surface topography [62].

The 3D roughness represents the calculation of an area of the surface instead of a single line [69]. Many 3D measurement methods have been proposed and developed [77–81] to record the surface asperities in  $z(x, y)$ . This 3D roughness profile is quantified in the 3D roughness parameters. The initial numerical parameters were developed in 1990s and are called *Birmingham 14* parameters. These parameters are categorised into four groups, they are: amplitude parameters, spacing parameters, hybrid parameters and other parameters. Most of them were derived from 2D characterization methods. New 3D roughness parameter set is intended to characterise geometrical properties in two different aspects of surfaces, namely field and feature characteristics. The details of field parameters formulations can be seen in [82]. The description of the feature parameters can be seen in [83].

## 2.2 Roughness Perception

In the previous sections the term roughness refers to physical roughness that has been defined as the degree of deviations of a surface asperities from the nominal surface. When the fingerpad slides on a surface, its asperities will generate uneven

pressure distribution and vibrations on the skin. The mechanoreceptor afferents within the skin transmit the pressure signals and vibrations signals to the brain by which then we feel the roughness sensation.

In contrast to the physical roughness which can be quantified using many parameters, the psychophysical roughness is unidimensional that means it only has magnitude comparison. In some degree the physical roughness parameters can be used to predict the magnitude of the perceived roughness. However, psychophysical roughness is not the projection of the surface topography which is being touched [84] and the exact physical roughness parameters which determine roughness perception have remained elusive [35].

Many studies in roughness perception have been conducted to understand how human perceives the surface roughness. There are two main approaches to characterize the relationship between properties of roughness stimuli and the corresponding roughness sensation, they are psychophysical and neurophysiological approaches. Psychophysical studies were intended to find the characteristic function which relates the stimuli quantity and its sensation; for example, the study to find the relationship between particle size of sandpapers and the subjective magnitude of the roughness perceived [33]. The neurophysiological studies were used to investigate what neural codes are responsible in perceiving the roughness. Most of the roughness perception studies were conducted in psychophysical mode or combination of both psychophysical and neurophysiological modes in which the objectives are mostly to determine the basic understanding about the roles of the mechanoreceptive afferents in perceiving roughness, spatial acuity of the glabrous and non-glabrous skin, and the relationship between the physical and the perceived roughness.

### **2.2.1 Mechanoreceptive afferents in glabrous skin**

Exploring the roughness of a surface will utilize mechanoreceptors which are embedded in the skin and the mechanoreceptors that are embedded in the muscles, tendons, and joints [85]. These mechanoreceptors are responsible in sensing the presence and the characteristics of the object being touched. Without these receptors in the finger's skin human will experience numbness on their finger. The finger will not be able to touch a surface firmly and to feel the texture of the surface. Finally, the hand cannot hold an object firmly.

There are four mechanoreceptors in the glabrous skin. They are Merkel disc, Meissner, Pacinian, and Ruffini corpuscles (see Figure 2.4). Those receptors are

the endings of four classes of afferent fibers, namely Slowly Adapting type 1 (SA1), Slowly Adapting type 2 (SA2), Rapid Adapting (RA) and Pacinian (PC) afferents [86]. The Merkel cells are the ending of the Slowly Adapting type 1 or SA1 afferents. SA2 afferents are believed to end in Ruffini complexes. RA afferents end in Meissner corpuscles. PC afferents end in Pacinian corpuscles. A summary of their properties can be found in Table 2.3.

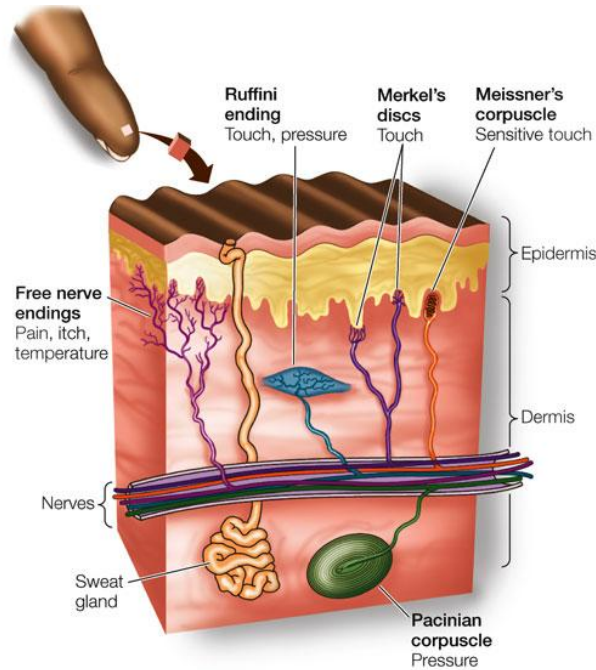


Figure 2.4: Mechanoreceptors in glabrous skin [87].

(a) SA1 Afferents

Merkel cells which are the receptors of SA1 type can be found at the bottom of epidermal ridges (Figure 2.4). This condition makes the SA1 afferent is sensitive to the stretch but not to the pressure intensity. This is the reason why SA1 system is responsible for detecting form and perceiving texture. The innervation density of the Merkel cells in the fingerpad's skin is around  $100/cm^2$  which enables the finger detect two asperities separated by  $0.5\text{ mm}$ . The edges, points, corners, curvature, groves, and ridges are detected by SA1 afferents Johnson [88].

SA1 afferents are continuously sending pulses under indentation to keep feel the contour of the surface being touched. The frequency of the pulse is approximately proportional to the indentation amplitude and it will increase

Table 2.3: Tactual Afferent System and Their Properties (After Johnson [88])

	Small receptor field		Large receptor field	
	Merkell	Meissner	Pacinian	Ruffini
Location	Tip of epidermal sweat ridges	Dermal papillae (close to skin surface)	Dermis and deeper tissue	Dermis
Axon diameter	7-11 $\mu m$	6-12 $\mu m$	6-12 $\mu m$	6-12 $\mu m$
Conduction velocity	40-65 m/s	35-70 m/s	35-70 m/s	35-70 m/s
Sensory function	Form and texture perception	Motion detection; grip control	Perception of distant events through transmitted vibrations, tool use	Tangential force; hand shape; motion direction
Effective stimuli	Edges, points, corners, curvatures	Skin motion	Vibration	Skin stretch
receptive field area	9 $mm^2$	22 $mm^2$	Entire finger or hand	60 $mm^2$
Innervation density (finger pad)	100/ $cm^2$	150/ $cm^2$	20/ $cm^2$	10/ $cm^2$
Spatial acuity	0.5 mm	3 mm	10+ mm	7+ mm
Response to sustained indentation	Sustained(SA1)	None (RA)	None(RA)	Sustained(SA2)
Frequency range	0-100 Hz	1-300 Hz	5-1000 Hz	0-? Hz
Peak sensitivity	5 Hz	50 Hz	200 Hz	0.5 Hz
Threshold for rapid indentation or vibration:				
Best	8 $\mu m$	2 $\mu m$	0.01 $\mu m$	40 $\mu m$
Mean	30 $\mu m$	6 $\mu m$	0.08 $\mu m$	300 $\mu m$

significantly when the finger is moving horizontally [28]. According to Connor et al. [35] the SAI system is a major spatial system primarily responsible for tactual *form* and roughness perception when the fingers are touching the surface directly. The SA1 spatial variation and roughness perception are highly correlated [89].

(b) SA2 Afferents

The Ruffini corpuscles are the receptors of the SA2 afferents spread within the dermis layer of the skin. SA2 afferents, like SA1 afferents, are continuously sending pulses under indentation. SA2 afferents are six times less sensitive to the indentation [88] and their role in roughness perception is

not clear. These afferents have the lowest innervation density which is only  $10/cm^2$ . However, these afferents are responsible in detecting stretch of the skin, the tangential force [90], hand shape, and the direction of the motion.

(c) RA Afferents

Due to the shallow position of their receptors, the RA afferents can detect soft indentation and minute motion [88]. RA afferents are about four times more sensitive to the skin deformation than are the SA1 afferents. RA system will stop sending pulse even the skin is still under indentation. However, not like SA receptors, RA receptors will evoke detection signals spontaneously. These afferents are most sensitive to the vibratory stimuli with the frequency range from  $40Hz$  to  $60Hz$  and the amplitude range from  $2$  to  $20\mu m$ . Bensmaïa and Hollins [91] showed that RA channel supports discrimination of complex waveforms of vibratory stimuli. These waveforms were discriminated on the basis of uniformity or nonuniformity of the sequences of perceived amplitudes within stimulus cycles.

(d) PC Afferents

A Pacinian is a large onion-like corpuscle which comprises corpuscles within corpuscles separated from one another by fluid. This cascade structure of corpuscles prevent PC afferents from detecting the low frequency vibratory stimuli. Each PC corpuscle is connected to a single afferent. These very sensitive afferents will respond vigorously to the transient deformation of the skin over an extensive area, the sensitivity can be demonstrated by blowing gently on the palm [27].

The Pacinian corpuscles, although extremely sensitive to stimuli with small amplitudes of vibration, are not spontaneously excited [92]. The PC afferents will start sending pulses when the compression pressure inside the corpuscles reaches its static level [93]. At room temperature of  $21 - 26^{\circ}C$  the Pacinian corpuscles detect the vibratory stimuli with the frequency range from  $150Hz$  to  $200Hz$  [94].

The role of the PC afferents in roughness perception is still in debate. Katz [95] believed that the sense of vibration is the basis of the roughness perception. Bensmaïa and Hollins [96] suggested that sliding the fingerpad over the surface with fine textures will generate high frequencies which can be detected and discriminated by PC afferents. On the other hand, Lederman et al. [97] and Johnson [88] reported that strong vibratory sensitivity of PC



afferents has no effect on perceiving the roughness due to the absence of gradation in the spatial or temporal response.

In psychophysical studies, the entities which mediate the mechanosensory information are called channels. Although neurophysiological experiments have identified four afferent fiber types (SA I, SA II, RA, and PC) in glabrous skin of the human, early psychophysical experiments detect only three channels have been shown to mediate mechanoreceptive perception [98]. They are P channel, NP I (non-Pacinian I) channel, and NP II (non-Pacinian II) channel. According to the model, each of these channels is associated with one afferent system, P channel with PC afferents, NP I channel with RA afferents, NP II channel with SA2 afferents. The role of these channels in sensing and perceiving the tactual stimuli has been studied mostly using vibration.

From the threshold measurements, the P channel have been shown to detect the vibratory stimuli with the frequency from 40 – 800  $Hz$  with maximum sensitivity near 300  $Hz$  [99, Page 4]. This channel is able to perform spatial summation from the stimuli presented in adjacent and temporal summation from the stimuli presented in consecutive. P channel will not detect the vibratory stimuli when the the contactor area is less than 0.02  $cm^2$  [98].

The NP I channel operates over the vibratory-frequency range of 10 – 100  $Hz$ . The threshold sensitivity of the NP I channel is relatively flat across its operating frequency. The sensitivity of this channel does not depend on the total area of the stimulation and does not show either temporal or spatial summation [98].

The NP II channel is responsible to detect the vibratory stimuli with small contactor area (less than 0.02  $cm^2$ ). The range of the operating frequency of this channel is from 15  $Hz$  to 400  $Hz$  [100]. The threshold sensitivity of the NP II channel will increase as the exposure of the stimulus duration increases [98]. This channel does not exhibit temporal and spatial summation [101].

By masking various channels and modifying the skin-surface temperature, Bolanowski Jr et al. [100] reported to find the fourth channel, namely NP III channel, which is sensitive to very-low vibratory frequency (0.8  $Hz$ ) and is mediated by SA1 afferents. This channel does not show spatial and temporal summation.

Bolanowski Jr et al. [100] reported that although each of these channels has sensitivity for a specific range of frequency, their absolute sensitivities are partially overlap. Thus, it is likely that the suprathreshold stimuli, i.e. the stimuli that exceed the sensitivity threshold, will activate two or more channels at the same

time and the central nervous system may perceive a stimuli by integrating all the signals from those triggered channels [101, Page 39].

The initial support for this hypothesis came from the two phenomena which arise when two vibrotactile stimuli were presented simultaneously called enhancement and summation [102, Page 3]. Enhancement is an increment in the perceived magnitude of second stimulus due to the presentation of a first stimulus and summation is an overall increment of perceived magnitude of the two stimuli. In contrast, when the two stimuli activated the same channel together, the perceived sensation of the pair was determined by the total energy of the two stimuli, not by the sum of individual sensation of the stimuli [101]. Enhancement effects are negligible when the first and second stimulus of the pair are the same intensity regardless of the stimulus frequency. The sensation increment happens when the first stimulus is more intense than the second stimulus, otherwise the sensation decrement happens.

The second support to the hypothesis that two or more channels contribute in tactile perceptions is the temporal summation phenomena that happens in vibrotactile stimuli perception. The bigger the frequency of the stimulus applies the lower the threshold of the tactile sensitivity [103]. Another support came from the spatial summation phenomena. For the same frequency, the threshold detection of the vibrotactile stimuli will decrease as the area of the contactor increase. Although the identification and the characterization of each channel have been well established, the fundamental questions remain concerning how they contribute together in the tactile perception.

### **2.2.2 Un-myelinated mechanoreceptive afferents**

The skin is commonly believed as having only four sub-modalities that convey tactile, temperature, and itch signals to the central nervous system. However, there is strong indication that the affective property becomes the fifth sub-modality. Affective property of a surface refers to the emotional sensations which is more difficult to be quantified than roughness sensation [104]. The pleasantness is the earliest affective tactile sensation being investigated.

Pleasantness sensing is relayed by low-threshold unmyelinated mechanof-ferents (C tactile,CT) [105–107]. McGlone et al. [108] reported that pleasant sense by hairy skin is processed by posterior insular cortex and mid-anterior orbitofrontal cortex. These limbic-related cortex represents an innate non-cognitive process.

Although CT afferents are not innervated in the glabrous skin of the hand, it is observed that glabrous skin is able to sense pleasantness of a surface [108]. Touch perception by glabrous skin is mediated by A-beta afferents and processed by somatosensory cortex which works analytically. However, the contribution and or the ability of primary somatosensory cortex to perceive the affective roughness is still debatable. Case et al. [109] reported that somatosensory cortex (S1) is not responsible for perceiving the pleasantness of a texture. Therefore, for evaluating the emotional perception of a fabric touch it might be better using hairy skin such as forearm [110].

Other researches reported that primary somatosensory cortex (S1) contribute to the emotional sensation. In a caressing experiment Gazzola et al. [111] reported that heterosexual males were sensually caressed by either a man or woman. This experiment have shown that glabrous skin may evoke emotional sensation. The top-down cognitive factors at the abstract level of words may contribute to the affective touch perception by S1 [112]. It means that the pleasantness perception by glabrous skin is affected by noticed pre-experience. In sensing by using fingerpad, it is reported that the pleasant feel is related with soft and smooth surface, while unpleasant sensation is related to harsh, rough, and coarse.

### 2.2.3 Tactile spatial acuity

The pattern and the intensity of the distribution of the receptors being activated depend on the surface topography. The roughness level and the curvature of a surface are detected and discriminated based on their pressure distribution. However, the relationship between the pattern of receptors being activated and the sensation of surface topography remains unclear [101]. This is one of the reasons to study the characteristics of the neural codes which build the sensitivity of the fingerpad. The psychophysical method to characterise the sensitivity of the fingerpad is by measuring its spatial acuity, i.e. the ability to resolve the spatial structure of surfaces pressed upon the skin [113].

The early and the most common measure of the spatial acuity is two-point threshold. However, this measure has been doubted to be the measure of the actual spatial acuity [114]. Several new measures have been proposed, such as gap detection, grating resolution, and grating orientation [31]. By using the grating orientation as a measure of tactile spatial acuity, Craig [115] reported that grating orientation sensitivity varies as a function of location on the fingerpad which is consistent with the changes in the receptors' density. Also, there is no evidence

that subjects perceive gratings differently when presented in the proximal-distal (PD) direction than gratings presented in lateral-medial (LM) direction. This result shows that subjects perceived the roughness of gratings on the basis of spatial rather than intensive cues [116].

There are evidences which provide strong argument that SAI system is the critical afferents in detecting spatial acuity in which RA system is three times poorer [116]. The slowly adapting were found to be very sensitive to spatial discontinuities and fine detail within the stimulus. RA afferents' response are about proportional to the indentation depth but they detect only the gross spatial details. Those evidence are derived from studies in which three modes of stimulation are performed: static touch, scanned touch, and the Optacon [117].

1. Static touch

Psychophysical studies using gratings show that subjects can discriminate gaps of 0.5 *mm* [31]. Studies with other patterns show a similar result. In grating stimuli experiments, SAI afferents resolve the spatial cues of all gratings. In contrast RA afferents only begin to discern structure of gratings with 1.5 *mm* gaps and bars and some even fail with 3 *mm* gaps and bars. So, in static touch the limit of spatial acuity is accounted by SAI.

2. Scanned touch

If compared to static touch, a 10 to 20% improvement in spatial acuity happens in scanned touch. SAI afferents are still considered as the critical system for two reasons: first, the responses of SAI afferents to scanned stimuli with its dimension near the acuity limit are sufficiently acute for discerning the gaps and second, SA preserve spatiotemporal information more effectively than RA.

3. Optacon

The optacon is a tactual simulator which is digitally-based controlled comprising 144 pins in 6×24 array with spacing  $2.2 \times 1.2$  *mm*. The pins are normally submerged and some will rise when they are actuated to make certain patterns and indent the skin in normal direction for 43 *ms*. Gardner and Palmer [118] shown that Optacon only activates RA and PC afferents. A 3.6 *mm* gap is required to produce 50% different of signal mean rate. That is why, compared to when SAI stimulated which can recognize 1 – 2 *mm*, gap discerning ability using Optacon is three times poorer.

Tactile acuity of the skins are different across the body; for the hand's skin, the fingertip is the most acute [119]. Peters et al. [113] reported that tactile spatial acuity depends on the finger size; the smaller the finger size the better the acuity. In some cases it was found that the threshold detection of spatial structure is less than 0.5 mm. Loomis [120] reported that the threshold of misalignment in a three-dot pattern could be less than 0.1 mm. This tactile hyperacuity threshold can reach the resolution of 10-30 times smaller than the resolution of a two-point threshold for the respective body part [121].

It is believed that RA and SA1 afferents are used together in sensing tactile hyperacuity. Even though the innervation density of SA1 receptors is lower than the hyperacuity threshold, SA1 afferents share big portion in hyperacuity perception [122]. Tactile hyperacuity is determined by the cortical representation of the fingers in *primary somatosensory cortex* (S1) [123]. There is no different hyperacuity performance between the blind and sighted [124]. Although the tactile spatial sensitivity has been well studied, it is still not clear when the mechanoreceptors sense two separated stimuli as two different asperities or as one asperity by summing both stimuli (unconsciously).

#### 2.2.4 Perception of roughness magnitude

The neural mechanisms of roughness perception have been studied through psychophysical and neurophysiological experiments. In nature, a roughness stimulus will likely activate more than two or more afferents. Researchers have been devoting to investigate what afferents are responsible in perceiving the roughness and how their firing patterns correlate to the roughness sensation.

According to Johnson et al. [28] each of four afferents which innervate glabrous skin of the hand has different function in touch perception. SAI system is a major spatial system primarily responsible for tactual *form* and roughness perception of coarse surfaces [35, 125]. RA system which has a lower spatial acuity than SAI but higher sensitivity to local vibration provides signal about minute skin motion and, thereby, has a critical role in grip control. The PC system is responsible for the perception of external events that are manifested through transmitted high-frequency vibration. Therefore, Pacinian channel is central to the perception of fine roughness [125]. The SA2 afferents have poor spatial-resolution which means they do not contribute to the roughness perception [35]. They are mainly sensitive to tangential skin stretch that assume responsible to the perception of hand conformation and to the perception of forces acting on the hand [28].

The correlation between firing pattern of the mechanoreceptors being activated and the roughness sensation have been explored through four types of neural codes which become possible bases for roughness perception: intensive, modal, temporal, and spatial [126]. *Intensive codes* are measures of neural activity such as mean impulse rate. *Modal code* is based on the relative magnitudes of response intensity between neuronal population with different transducer properties. *Temporal codes* depend on the temporal structure of firing in afferent fibres. *Spatial codes* depend on the spatial structure of impulse rate across a population.

Connor et al. [35] and Connor and Johnson [36] reported that the correlations between mean impulse firing rate of the SA, RA, and PC afferents with the perceived magnitude of the roughness are low. This is why dot patterns with different spacing will always be detected as having different roughness even though their firing rates are the same. So, the roughness perception can be predicted using mere mean firing rate. However, the firing rate still contribute to the subjective roughness judgement. The firing rate variation, especially from SA afferents, correlate with the roughness judgement [35].

Modal codes have been suggested to be useful to predict the perceived roughness magnitude. Although some evidences were presented that the different proportion of channels being activated will produce the different perceived roughness, there is no simple linear combination of rates across channels that could account for perceived roughness magnitude [117].

The measure of the temporal variation indicates the change in total number of afferents being activated at each time in sequential activations. Using two different structures of dot patterns Connor and Johnson [36] showed that roughness perception is not based on local temporal variation. On the other hand, The correlation between spatial firing rate variations of both SA and RA afferents with roughness perception is high [36]. Spatial variation is a measure of the amount of areal fluctuation in firing rate.

However, it is found that subjective roughness is not always based on SAI spatial mechanism [117]. The surfaces with microscopic roughness are not likely to be sensed by SAI and also the textured surface can be discriminated through a rigid probe by crossing it on the surface. The pioneer of the touch research, David Katz [95], in early 20th century argued that the perception of surface roughness relies on *spatial* cues for coarse textures and on *temporal* cues for the fine ones [127]. This conception is commonly called duplex theory and some experiments have been done to prove it [30, 128]. Hollins and Risner [128] conducted three

experiments to prove the evidence of that theory. In the *first* experiment the subjects were performing 2IFC (two-interval force choice, see [129, page 42-44]) tasks to discriminate two fine surfaces (9 and  $15\mu m$ ) and coarse ones (141 and  $192\mu m$ ). The results showed that performance in discriminating two fine textures by using movement or static touching is significantly different and in the same way those performances for differentiating two coarse surfaces are almost the same. The hand lateral movement is needed to sense and discriminate the roughness of fine surfaces even though the sliding speed has no influence in perceiving roughness as long as the skin deforms fast enough to prevent adaptation [17].

Most of the studies of the roughness perception were using coarse surfaces (such as using gratings and raised dots). In such experiments it was found that the activation of SA1 afferents to be more correlated to the roughness perception. Lederman [130] argued that perceived roughness is related to skin deformation and not to the vibrational cues. Sathian et al. [40] reported that roughness increased with an increase in groove-width and decreased with an increase in ridge-width and at the same time SAs and RA afferents increase in response when the perceived roughness increased. Another report from Dépeault et al. [131] shown that in the perception of coarse-roughness surfaces the perceived roughness increased with the increase of the distance of each particles. All this reports imply that skin deformation and SAs afferents determine the roughness perception of surfaces with coarse particles.

Although it is well known that human can perceive fine-roughness textures better by touch than by vision [32], for example, human can discriminate roughness of sandpapers with  $5\mu m$  particles from  $9\mu m$  particles using touch but not vision, only few of researches focused on the roughness perception of fine-surface textures [132]. Libouton et al. [30] reported that the discrimination threshold for the fine surfaces ( $<46\mu m$ ) is ( $14.7\pm 8.5\mu m$ ) and for the rough surfaces ( $>46\mu m$ ) is ( $43.5\pm 32.5\mu m$ ). In the *second* experiment the subjects had to assign a magnitude for each of twelve samples with their roughness ranging from  $9\mu m$  to  $350\mu m$ . The result showed that the absent of lateral movement declines the roughness perceived and reduces the slope of the psychophysical function, i.e. particle size vs roughness perceived. In the *third* experiment the subject was asked to assign the properties arbitrarily for the surfaces. The result showed that perceived roughness increases as the particle size gets bigger and reciprocally for the smoothness. Also from those experiments it is known that the pattern of perceived roughness before and after  $100\mu m$  is different. So, the particle size less than that is considered smooth and greater than that is coarse.



Surface roughness perception has been studied under active and passive touch. In the active touch the hand is allowed to move when exploring the surface texture of a static object, whereas passive touch the finger is at the static position and the surface of the object is moved. Compared to passive touch, active exploration elicited greater and more distributed activated neurons outside the somatosensory cortex. However, the roughness of a surface that is perceived either by passive touch or by active touch will have the equivalent sensation magnitude [33, 133].

### 2.2.5 Tactual perceptual field

Perceptual field refers to the spatial array of perceptual contents which have spatial properties and functions which derive from the spatial properties and functions of corresponding stimuli [134]. In the visual perception, the field of the perceptual content contains the image of the two-dimensional (2D) view which reserves 2D spatial properties and relations of the object being seen such as lateral angle and outline form that enables humans to predict not only the identity but also the size of the object within the image.

In the visual perception theory, the image is perceived not merely based on the information from visual sensory receptors but also on the informative percepts [135]; for example, two identical ellipses may be perceived differently as seen in Figure 2.5. This is called principles of perceptual organization [136]. There are three major views to this theory: structuralism, Gestalt, and Helmholtzian [135]. Gestalt theory is the most studied. Based on the Gestalt view, the visual pattern can be perceived and discriminated by: area, proximity, similarity, closure, good continuation, convexity, and symmetry [135].

Some researches have investigated whether touch sensing generates a perceptual field analogous to the visual field [31]. The firing intensities pattern of the receptive field (RF) on the skin which reflects the asperities of a stimulus's surface is analogous to the signals of black-and white image in retina. Most of tactile field studies were using large size stimuli which were applied on the large area of skin such as palm or some fingers. Haggard and Giovagnoli [137] reported that tactile patterns applied over relatively large skin regions are sensed as a tactile field analogous to the visual field. Serino et al. [134] have showed that a spatial arrangement of multiple tactile stimuli will be perceived as a unique, complex, spatial percept. Moreover, Lappin and Foulke [138] reported that one finger may be added to the tactual field. Two fingers from different hands perform better than two fingers from the same hand in recognizing tactile stimuli.



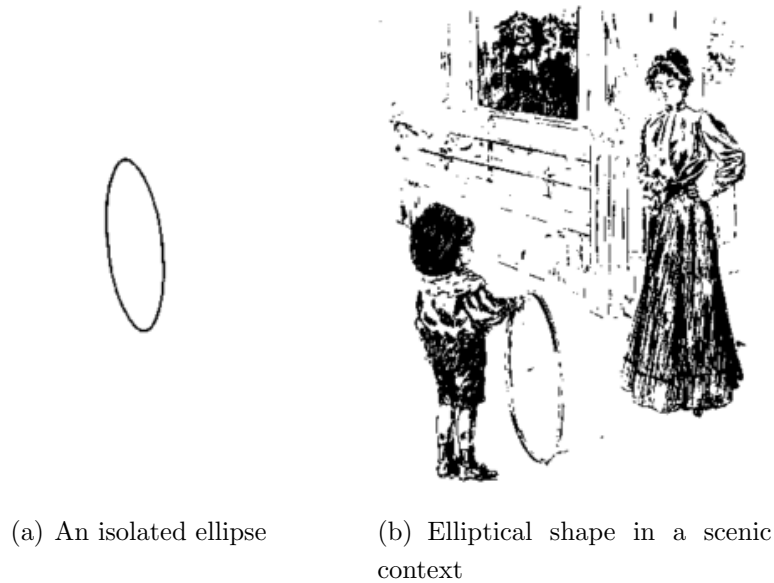


Figure 2.5: For a variety of factors, the elliptical shape (b) is perceived as round hoop [135]

Whitaker et al. [139] and Harrar and Harris [140] argued that despite having perceptual fields which are analogous, vision and touch contribute information to the perception of texture in an independent but complementary manner. Better recognition in touching the objects with familiar form or texture is believed to be due to the cognitive influences, not due to integration of basic visual and tactile sensory encodings. However, some researches have reported that principles of visual perception prevail in tactile perception. The applicability of Gestalt theory, in tactile perception has been investigated [141]. Gestalt law of proximity applies to contour haptic detection [142]. It has been reported that good continuation principle operates in the haptic task [143–146]. These findings are useful to investigate how discriminative tactile response correlates with parameters of surface topography such as roughness and waviness.

### 2.2.6 Human perception on tactual patterns

While the perception of regular roughness patterns (dots and gratings) is much studied, the perceived roughness evoked by surfaces with irregular roughness which are common in nature is less understood. The perceived roughness for this surface is difficult to predict because the shape, the size, and the arrangement of each roughness element on a non-homogeneous surface may not be able to be definitely determined. In particular, while there is a general correlation between measured and perceived roughness, the correspondence is not one-to-one, and

textures that have same physical roughness can have very different perceived roughness. One of the reason is despite being random, roughness elements always form a specific pattern on the surface.

Humans should be able to not only perceive roughness but also discriminate its pattern to a certain degree because it is convincing that humans fingers have the field of tactual perception which is useful to recognize the pattern on a surface. Early studies in the perception of tactile patterns were intended to convert sound and images to the tactile pattern to help the deaf and blind communicate [147]. The pattern was generated using Optacon, a regular array of pins placed below a perforated surface. They are controlled and actuated so that some of them appear on the surface to form a pattern, such as a letter or Braille, or others. The array size normally fits the finger pad area. Bliss [148] showed that subjects were successfully able to read letter shape patterns using Optacon. The reading performance is influenced by pattern size [149], display time [150], and the presentation mode [151]. Those factors are underlaid by tactile aspects such as spatial acuity, temporal resolution, cutaneous masking, perceptual integration, and limited attention [147].

Researches in the discrimination of tactual textures using non-regular pattern are very limited. Culbert and Stellwagen [43] were among the first who used non-regular patterns to investigated the human ability in discriminating tactile patterns. They created forty tactual stimuli by converting images to embossed patterns. A hundred and fifty subjects were ordered to perform 200 discrimination judgements on those embossed patterns. They reported that eleven out of forty patterns were well discriminated. However, the variables of importance in mediating the tactual pattern discrimination failed to be figured out in this research. Heller [152] reported that sighted, congenitally blind, and late blind individuals have the similar performance in an matching experiment of embossed shapes. Elkharraz et al. [44], Elkharraz [153] made twenty four different tactile textures to investigate a set of visual features which correlate to affective responses of the touch. Although they did not investigate specifically the pattern discrimination, it showed clearly that subjects were able to discriminate those textures. All of these results indicate that tactual pattern can be perceived by touching.

### 2.2.7 Cross-modal interactions between visual perception and touch perception

The primary sense modalities such as visual, auditory, and touch are generally considered to be separated as each sensory cortices to be fixed or "hardwired" to process special task [154]. Many researches suggested that each sensory system has distinct encoding path. For example, roughness perception is processed in somatosensory cortex while distance spacing is primarily perceived by occipital lobe [155]. Whitaker et al. [139] suggested that vision and touch contribute different information to the perception of texture. Vision is more related to recognize texture boundary while touch is responsible to assess roughness and compliance of the surface. Baumgartner et al. [156] shown that the tactile sense can work well independently from the visual sense in the material perception experiment. Heller [152] reported that sighted and late blind individuals performed no better than early blind in recognizing and matching tactile patterns which means haptic and visual systems have different channels. Therefore, haptic and visual systems have different roles in perceiving the world. Haptics is more related to substance and spatial frequency rather than shape [157].

However, some researches had shown evidences that the brain has some degree of plasticity so that it can rewire or adjust itself to accommodate or enhance certain sensory perception [158]. This cross-modal plasticity can be found in tactile perception which some time is involving both somatosensory cortex and visual cortex. Merabet et al. [159] investigated the extent of involvement of early visual cortical areas in tactile perception. They reported that even simple tactile discrimination tasks induced significant activation in primary visual cortex. The similar finding also reported by Burton et al. [160]. In the normal tactile perception of some object properties such as pattern orientation, shape, and size the visual cortex will be activated [161, 162]. Sathian and Zangaladze [163], Sun et al. [164] had shown that visual cortex was active and even was necessary for tactile discrimination of orientation. Although the role of the visual cortex can be influenced by late-onset blindness or by short-brief interruption of visual input, the neural plasticity of visual cortex seems strong in normal sighted and early blindness [165]. Those findings indicate that in relatively coarse textures it is possible to recognize tactile patterns by touch which is mediated by SA1 channel. The roughness pattern recognition might be similar to image pattern identification due to in both processes the visual cortex is active.

The tactual pattern in texture with fine roughness is more likely cannot be recognized let alone be discriminated. The discrimination of fine texture relies on vibration cues to which Pacinian afferents are sensitive. SA1 systems which are sensitive to spatial arrangement of coarse particles will not recognize any particular continuation of fine particles which may form a shape or a pattern. However, discrimination of fine texture is still possible not based on pattern but on the roughness level that is related to vibrational level of cues.

## 2.3 Relationship between Physical Roughness and Perceived Roughness

A function which relates the surface texture parameters with human touch sensation is essential for manufacturers to be able to create materials with surface properties that would elicit emotions supporting the product's brand [166]. Among tactile sensations, roughness is the most studied. However, most of the studies were using relatively homogeneous stimuli such as gratings or dot patterns. The perceived roughness were correlated with the particles' size, the ridges' width and the groves' width. The objectives of these studies were to analyse the patterns and the roles of the mechanoreceptive afferents in perceiving the roughness of the stimuli.

Some studies, mostly psychophysical ones, have used stimuli with more natural roughness that were intended to investigate human tactile perceptions which are not only roughness. There are two approaches of the studies: *first*, the studies which investigated the relationship between the features of vibrations evoked by the surface and the touching responses, and *second*, the studies which directly tried to correlate the physical parameters of the surface to the tactile perceptions. In the first studies it is not needed to measure the surface topography; the stimuli were chosen based on the prediction that they will generate different pattern of vibrations. A vibration sensor or an artificial finger were used to detect and record the pattern of the vibration. While in the second studies it is needed to measure the physical parameters of the surface's properties such as average roughness, thermal conductivity, and compliance.

### 2.3.1 Vibratory cues approach

When asked to feel the roughness, humans will automatically scan their finger across the surface. The fingerpads' skin will vibrate and the mechanoreceptors

will be activated accordingly so that the brain can feel certain level of roughness judgement for the surface. Furthermore, it is reported that fingerprint might help in sensing fine textures [167]. This mechanism has inspired researchers to use vibration sensors to record the vibratory signals generated by the fingerpads' skin during scanning a surface texture. The commonly used transduction method is piezoelectric [168]. The sensors are commonly configured in three different ways: first, mounted on the frame of the stimulus holder in some places [169, 170]; second, attached on the scanning finger [171–173]; third, embedded in an artificial finger [174].

Some features of the signals' profile are then extracted and correlated with the touching sensations. Ye et al. [175] reported that the mean and standard deviation of the vibration amplitude correlate with the roughness perception. De Boissieu et al. [176] selected the power spectrum density (*PSD*) of the recorded vibration signals as the basis of the tactile texture recognition. They used a three-axial microelectromechanical systems (MEMS)-based force sensor which is packed in an artificial finger to scan ten kinds of paper. Two types of classification algorithms were used to analyse the *PSD* values so that each type of paper can be recognized. The similar method can be found in [177].

Chen et al. [174] proposed five computational features of the vibration signals which were calculated using roughness parameters formulas, *Peak Average*, *Peak Ratio*, *Spectral Centroid*, *Average power*, and *Shannon Entropy* to correlate with tactile touch sensations. The coefficient of friction of each fabric was also used in the analysis. The result showed that only *Average power* matches well with Roughness-Smooth dimension while other features do not. *Average power* is the average value of the vibration energy, larger P will likely produce rougher hand feel. Tang et al. [178] reported that among four vibration features (*arithmetic average*, *root mean square*, *maximum height of peaks*, *peak ratio*), only the arithmetic average was reported to correlate with perceived roughness; the lower the values of  $R_a$  the smoother the surface feels.

Kikuuwe et al. [171] used a signal processing program based on the FFT (*fast Fourier transform*) to analyse the vibration signals recorded from a finger-mounted tactile sensor during scanning nine different fabrics. They reported that the system could distinguish each of these fabrics. Hu et al. [179] reported that a FFT-based technique they developed can be used to classify five fabrics with different textures accurately.

Although these methods were reported to work effectively in modelling the relationship between the vibration signals generated and the tactile touch re-

sponses, these methods are irreversible. It means that these methods can predict the tactile responses of a surface texture but they can not be used to create the desired surface texture which can evoke certain values of the perceived roughness. In order to be reversible, a method must put the measure of surface textures in the relationship model between the textures and the perceived roughness.

### 2.3.2 Physical properties approach

Most of the studies of roughness perceptions used stimuli with homogeneous textures and quantified the roughness simply by measuring the size of particles and the width of ridges and groves of the grating stimuli. The result of the previous studies are not enough to predict the roughness sensation of non-homogeneous textures which are more common in nature because; first, perception of touch has a complex mechanism [20] as discussed in Subsection 2.2.1 and second, the topography of surfaces with non-homogeneous textures can not be simplified as dots or gratings. The surface textures have been quantified in the standard 2D and 3D roughness parameters. However, only few studies investigated and reported the correlation between these parameters and the perceived roughness.

Akay et al. [180] and Liu et al. [181] have reported that *arithmetic average roughness* correlates with perceived roughness, the bigger the values of  $R_a$  the rougher the surface feels. Barnes et al. [182] investigated eight roughness parameters ( $R_a$ ,  $R_p$ ,  $R_{sk}$ ,  $R_{ku}$ ,  $\Delta_q$ ,  $\lambda_q$ ) to affect touch sensations. Two parameters, i.e.  $R_p$  (*maximum height of peaks*) and  $R_z$  (*ten-point height*), are better descriptors to relate the perceived roughness.  $R_q$  is believed to correlate with roughness perception too. However, the dependence of roughness sensation on  $R_a$  and  $R_q$  can be inferred as a dependence on asperity radius of curvature which is equivalent of the particle size in sandpaper and dots experiments [17, page 4] that showed that the bigger the particle diameter the bigger the subjective magnitude of the roughness [33]. In other word,  $R_a$  and  $R_q$  values represent the particle size of a texture. They are not detected as a unique feature which affects roughness perception. Liu et al. [181] showed that surface's kurtosis has a negative correlation with the perceived roughness which means the fingertip is able to detect the ridges but not to detect the narrow deep grooves. Tiest and Kappers [84] used three roughness parameters ( $R_a$ ,  $R_q$ ,  $R_z$ ) to make correlations with the perceived roughness and they suggested that there is no strong correlation between physical roughness and perceived roughness.

The aforementioned studies used amplitude-based roughness parameters which take into account the amplitude of the asperities without considering their spatial spread despite that roughness perception is affected by the spatial distance between peaks that equivalents to the groove width [40]. Moreover, there is no research so far which studies the roughness perception based on the 3D roughness parameters. Most of the recent studies do not focus on roughness perception itself but rather on affective touch sensations. Less attention to physical and perceived roughness relationship is likely due to the difficulties in designing the stimuli with predefined roughness parameters.

Elkharraz et al. [44] have demonstrated how to design and manufacture tactile textures by converting images to the surfaces' topographies. A surface topography was formed by an array of boxels. A boxel is a regular tetragonal prism with its height determined by a pixel's value in the respective matrix cell of an image. The generated topography is 2.5-D printed version of the image being used. This image-to-topography transformation method makes it possible to design and evaluate the surface roughness in the image processing domain. A similar transformation method has been used by Ikei et al. [183] to show that an image data is compatible with geometry data which has direct relation to the tactile stimulus. Thus, an image data is suitable for representing a tactile texture.

## 2.4 Image Textures

The most recent analysis of tactile texture in the image domain has been performed by extracting and evaluating the image textures which correlate with affective touch sensations [44, 52]. Texture which can be observed in the patterns of various synthetic and natural surfaces [184] is an important property for analysing images [49]. Despite its importance, a formal or complete definition of texture does not exist [47, 49, 184]. Within an image pattern, the texture may be seen and described subjectively using terms such as coarse, fine, smooth, granulated, rippled, regular, irregular, and linear [184]. Haralick [49] considered an image texture as an organized area phenomena which has two dimensions. First dimension depicts the tonal primitives or local properties while the second dimension relates to spatial organization or arrangement of those tonal primitives. A pixel or a groups of pixels connected with each other can be counted as a tonal primitive. Haralick [49] referred it as the elementary component of texture but Whelan and Molloy [184] used pixel itself as basic element of texture. When a small-area patch of an image has a large intensity variation then the patch has

texture as dominant feature. When a small-patch area has little intensity variation then the dominant feature in the area is tone [184]. Haralick [49] described tone and texture based on the variation of tonal primitives not pixel intensity.

### 2.4.1 Extraction methods of image features

There are various approaches and methods for extracting and analysing textural features. Bharati et al. [47] proposed four categories of methods: (1) statistical methods, (2) structural methods, (3) model-based methods, and (4) spectral-based methods. The quite similar categories also made by Tuceryan and Jain [53].

*Statistical texture analysis* techniques are primarily based on grayscale histograms to describe texture of patch area in images. Haralick [49] mentioned eight approaches within this statistical methods: autocorrelation function, optical transforms, digital transforms, textural edgeness, structural elements, spatial gray tone cooccurrence probabilities, gray tone run length, and autoregressive models. The first three approaches are related with spatial frequency. Fine textures are rich in high spatial frequencies while coarse textures are rich in low frequencies. Elkharraz et al. [52] made three categories for statistical methods: (a) first order statistics, (b) second order statistics, and (c) higher order statistics. First-order statistics describe the likelihood of observing a grey value at a randomly-chosen pixel. The average, median, variance, and percentile are among the first-order statistics. Second-order statistics are mainly based on cooccurrence matrix. Higher-order statistics includes grey run length and absolute gradient. Szczypiński et al. [185] developed MaZda software to compute texture features based on image histogram, co-occurrence, run-length and gradient matrices, auto-regressive model, and wavelet transform. In the histogram-based methods there are five parameters: mean, variance, skewness, kurtosis, and percentile. In the gradient-based methods there are four parameters: GrMean, GrVariance, GrSkewness, and GrKurtosis. In the run-length matrix based method there are five parameters: ShrtREmph, LngREmph, GLevNonUni, RLNonUni, and Fraction. In the last three methods there is only one parameter for each of them.

*Structural texture analysis* techniques assume that textures are structured by primitives (basic patterns). These methods describe texture as the composition and orientation of texton (texture element) such as regularly spaced dots or parallel lines. Two main steps that must be performed to create structural textures are



extraction of texture elements and inference of the placement rule. This method is rarely used since they can only describe very regular texture [47]. Moreover, extracting structural features which is commonly called as primitives from data is difficult [186].

*Model-based texture analysis* techniques are intended to construct an image model that can be used to describe texture and synthesize it [53]. A probability models or a linear combinations of a set of basis functions are commonly used as the model of an image [187]. The probability models generate an empirical approximation of each pixel in the image based on a weighted average of pixel values in its neighbourhood. Examples of the model-based methods are auto-regressive model, Markov random fields, and fractal models [47, 53].

*Spectral-based texture analysis* techniques convert the image into new form using the spatial frequency through some function transformation methods such as wavelet and FFT transform. Evidence from the psychophysical researches has shown that human brain does frequency analysis [188, 189]. Those findings suggest that frequency-based features will be promising to model image textures which are related to surface roughness. In this method the image is transformed into distribution of spatial frequencies which describe global periodicity of grey levels of an image. There are two common types of transformation used in the texture analysis: first, wavelet transform and, second Fourier transform. The method of standard wavelet transform has been well presented in [190] and [191]. Although wavelet methods have been reported successfully to be used for classifying textures, they only are suitable for analysing non-stationary transient signals [192]. Fourier transform is the best method to represent frequency cues of images [53]. It has been used as texture descriptors in considerably many researches.

## 2.5 The Importance of Magnitude and Phase in Signal

The Fourier transformation of any signal such as an image will always consist of two parts: the magnitude part and the phase part. For example, the Fourier transform of an image  $f(x, y)$  –where  $f(x, y)$  is the pixel’s value of the image at a spatial point with coordinates  $(x, y)$ , is  $F(u, v) = |F(u, v)| \times e^{-j\phi(u, v)}$  where  $|F(u, v)|$  is the magnitude spectra and  $e^{-j\phi(u, v)}$  is the phase spectra. The original image can be recovered by performing the inverse of that Fourier transform.

### 2.5.1 Justifications of the argument that phase is more important than magnitude

The phase part of Fourier transform of an image, or in general any signal irrespective of its dimensionality, preserves the essential features and a lot of structural contents of the image. The inverse transform of the phase part will usually retain the texture of the image, while the inverse transform of the magnitude part will mostly bear no resemblance to the image [193, 194]. In other example if a Fourier transform was formed from a combination of the phase and the magnitude of two different images, the inverse of that Fourier transform will usually resemble the image which shared the phase part of its Fourier transform [195]. In other words, the phase is more important than the magnitude. Researchers have been exploring the justification of the relative importance of phase from signal processing stand-point in a number of contexts such as image coding and compression, designs of digital filter, speech recognition and enhancement, image features detection, and image recovery [193, 195–197].

In the data compression techniques that use the discrete Fourier transform (DFT), both the magnitude and the phase information are encoded using a lower number of bits to optimize the amount of the data. It has been reported that the phase needs more bits (higher resolution) than the magnitude so that the compressed image is not severely distorted. Pearlman and Gray [198] proposed that the phase must be contained in 1.37 times more bits rate than the magnitude to achieve the lowest distortion for each compression rate. Tescher [199, page 63] showed that at the lower level of quantization (less than eight) the RMS error due to phase quantization is around ten times larger than the RMS error due to magnitude quantization. Piotrowski and Campbell [194] tried to measure the effect of the quantization of phase's values on visual recognition. They reported that even two levels of quantization still produce a retrieved image which is recognizable. However, some quantization levels of phase can hinder the retrieved image to be recognized and the how it happens has not been explained.

The phase has also been reported to be relatively more important than magnitude in the digital filter applications although most of the past researches on recursive digital filters, whether in first- or two-dimensional domain, utilized only the magnitude part, such as in Upadhyay and Karmakar [200], Ekstrom and Woods [201], Friedlander [202]. That the phase was usually ignored in the design of image filters is unexpected as the importance of the phase has been known for a long time. Huang et al. [196] argued that phase is extremely important to

be included in the filter design, as excluding the phase may lead to unsatisfactory design. Horner and Gianino [197] concluded that the phase-only filter has better performance in terms of all three measures they used (e.g.: criteria of discrimination, correlation peak, and optical efficiency) than the performance of the magnitude-only filter and the classical match filter. They also reported even in matched filtering the phase information is considerably more important than the magnitude information. A similar conclusion has been reported by [203]. They found that by performing single-frequency filtering in the phase only in speech signals will preserve the information being conveyed.

Although initially the phase was considered as unimportant in speech enhancement [204, 205], many researches have argued otherwise. Paliwal and Alsteris [206] showed that short-time speech signals which were synthesized from phase spectra only can be as intelligible as the signals recovered from magnitude spectra only although the common view argues that the phase has less contribution in speech recovery. They showed that the phase even becomes more important than magnitude in longer windows of speech signals. A similar conclusion has been reported by Paliwal et al. [207]. They opposed the believe that short-time phase is unimportant. They conducted a series of objective and subjective experiments on four different methods of speech enhancement and they concluded that the phase spectrum compensation method achieves better speech quality improvements than the rest of the methods. After that, phase-based speech enhancement techniques become more popular and are considered to perform better than the magnitude-based methods [208].

A quite different approach was made by Ni and Huo [209]. They proposed a series of statistical derivations of the DFT to support the idea that phase is more important than magnitude. They demonstrated that the inverse Fourier transform of a set of complex numbers with random values will produce a set of random numbers with suppression only when all the phases are zero. The first element (the DC component) of this suppressed set of numbers is too large compared to the rest of the elements. This will not happen when the values of the magnitude is constant. They also made some statistical derivations showing that a reconstruction with distorted phase in a set of random numbers will be unlikely to be close to the original. A similar approach which also provide the same conclusion had been made by [210]. However, those results seem only valid for signals with random values because in some cases it is clear that the phase can be less important than the magnitude. Moreover, they did not make any

confirmation from visual tests to prove that the image from distorted phase will be perceived as different to the original one.

Based on the belief that the phase is more important than the magnitude, many researchers developed techniques to recover signals using phase only. Those methods are useful in certain applications in which only the phase information is available [195]. However, because a signal cannot in general be uniquely defined by its phase only, some additional constraints must be available to recover signals from their phase [211]. For example, if a sequence of signal has no zeros in reciprocal pairs or on the unit circle then it will have minimum phase and thus can be uniquely defined to within a scaling factor by its phase [212]. Ma [213] derived a matrix from the constants of the Fourier transform to define the uniqueness of a finite length real sequence which is reconstructed from its phase. Ma [213] concluded that if the matrix is non-singular then that sequence can be uniquely recovered.

Although the exact set of constraints has not yet been confirmed, many researches have proposed algorithms that can recover an image uniquely from its phase only. Among the early methods are the iterative schemes and the closed form solution [195, 211, 212, 212, 214]. In the iterative methods the sequence will be transformed at least twice in each iteration. It has been reported that if the FFT length of the sequence is at least twice the length of the sequence the iterative algorithms will always converge [215, 216]. Some modifications had been made to improve the convergence speed and the quality of the image being recovered [217]. The second method is the closed form solution which is very different from the iterative scheme. In this method the FFT of the sequence was derived into a set of matrices multiplication and then by solving a matrix inversion the target sequence can be achieved [212]. Compared to the iterative methods, the close form solution guarantees the desired sequence without iterations [211, 212].

Not only from the signal processing point of view, justifications which support that the phase is more important than the magnitude also come from the result of psychophysics experiments that involve subjects to perceive images visually. There is much evidence reported for the importance of this. The first observed visual evidence of the phase dominance over magnitude is from the field of X-ray crystallography where phase determines the shape of the electron density [218]. Piotrowski and Campbell [194] and Oppenheim and Lim [195] performed simple experiments which shows a similar result. They swapped the phase of two common different images and the resulted image will clearly resemble the image which share its phase. Using the same method Skottun [219] showed that

phase also dominate the influence in the perception of the Muller-Lyer illusion. More vigorous investigations have been made by other researchers. Victor and Conte [220] have shown that the discrimination of iso-dipole textures (textures with identical one-dimensional second order statistics [221]) is based on relative spatial phase and not on global Fourier amplitudes. Patterns with the same amplitudes spectra but different in phase spectra will be discriminated. Even small perturbation such as randomization and quantization on phase will create salience of the statistical differences between the original image and the phase-perturbed image [222].

### 2.5.2 Magnitude can be more important than phase

In spite of so much evidence and proofs, there is still no clear explanation on how exactly the phase spectra become more important than the magnitude spectra. From the signal processing stand-point, there are many researches suggested that the phase is not always important. Lohmann et al. [223] made two quantitative measurements to know which one between the phases-based hybrid image and the magnitude-based hybrid image that will be more similar to the original image. The first measure was called the test in isolation method where the correlation of phase-based image and the original image was compared to the correlation of the magnitude-based image and the original image. The second method was the test of robustness method. A comparison between the phase-based hybrid image and the magnitude-based image was made in this method. However, in the second method, the phase and the magnitude were each combined with its conjugate pair. They concluded that they believe that the phase is more important than the magnitude cannot be confirmed.

If the importance of the phase or the magnitude is based on the possibility to reconstruct an image using the inverse Fourier transform of the phase only or the magnitude only, it will be difficult to decide convincingly which one is more important than the other because both of them have received mathematical supports in terms of the solution availability and its stability [213, 224–227]. Moreover, both the magnitude and the phase have been used as the bases to develop a large number of algorithms which have been implemented in various applications. The review of each method can be found in [205] for the phase-based algorithms and in [228, 229] for the magnitude-based algorithms. The main reason of the development of the phase-based methods is the belief that phase is more important than magnitude, whereas most of the magnitude-based

algorithms for signal reconstructions have been developed due to the absence of the phase information, so that only the magnitude spectra is available. Only small portion of those methods were developed based on the believe that the magnitude has more influence to the result than the phases has. It happened especially in the field of speech enhancement and recognition in which since Wang and Lim [204] concluded that the phase is unimportant, many algorithms of speech recognition and enhancement have been adopting magnitude-based methods [230–232].

Although it seems to be true that the magnitude is more dominant over the phase, as has it has been reported by Wang and Lim [204], that happened most likely due to the length of the signals were relatively short so that the magnitude’s influence tends to be more significant [233, 234]. There are at least three cases that have been reported which make the magnitude becomes more important than the phase. The first case is when the phase information is not available, the magnitude becomes important. This case happens in some applications [212, 235–237]. However, this reason will be irrelevant to measure the dominance of the phase over magnitude. The second case is when some distortion or some noise are presence in the original data, the magnitude become more important than the phase because signal reconstructions from the phase will be more difficult than from the magnitude [204]. Therefore, in some applications where the phase spectra are noisy, such as in speech recognition, the phase will be ignored completely and leave only the magnitude information to be used to develop the algorithm of image recovery so that the optimal solution can be achieved [238]. The third case is when the data of the phase is incomplete, to recover an image using such data will produce an unreliable result [239]. Meanwhile, reconstructing an image from its distorted magnitude spectra will resemble the original image [210]. Therefore, in this case the magnitude is more needed than the phase.

In the ideal case, i.e., when the data is relatively free from noise, the phase usually will be more important than the magnitude. Despite it is still possible to recover signals from their magnitudes, it will normally be more difficult [237]. Moreover, the constraints that must be provided for the magnitude-based algorithms will be more restrictive than those for the phase-based methods [212]. Therefore, from the signal processing stand-point, it seems that the phase is still more important than the magnitude.

However, from the visual perception point of view, it has been reported that the magnitude spectra can be more important than the phase spectra. As the phase contains topological information about image edges whereas amplitude encodes image intensity, it will be possible that in certain cases, the perception of

images will be more influenced by the image intensity than the edges. Therefore, visually, the magnitude can be more dominant than the phase. Moreover, it has been reported that magnitudes seems to bear some main textures' characteristics. Julesz [240], from his early works on texture discrimination, concluded that textures which have the same second-order statistics would not be discriminated. This result implies that images with identical magnitude spectra and therefore have the same texture will be perceived to be as the same category of images regardless the phase spectra they have. This believe is supported by Guyader et al. [241] who also argued that the shape of the magnitude spectra determine the texture of the image. Therefore, images will be perceived to be more similar if the shape of their magnitude spectra is the same. Juvells et al. [242] also reported that magnitudes appear to be more dominant in natural images because the shapes of the magnitude spectra of those images are basically similar. However, when their magnitude spectra have substantially different shapes, the phases will be unimportant.

Although some counterexamples to that argument exist, Julesz [243] had been vigorously re-examining the importance of the magnitudes and reported that the discrimination of two different textures is independent of phase. In other word, magnitudes have bigger influence in the texture discrimination. A report by Tang and Stewart [190] also suggested that magnitude spectra contain enough texture information which is useful in the algorithm of the image classification. The images with relatively similar magnitude spectra will tend to be perceived as similar images. Other than the shape, the orientation of distribution energy of the magnitude spectra is believed to also influence the dominance of magnitudes over phases in the appearance of the hybrid images [244]. The size of the magnitude spectra is also reported as determining the dominance of the magnitudes. Morgan et al. [233] conducted an experiment by swapping magnitude patches and phase patches of two images. The result shown that the smaller the patches the less the dominance of the phases and therefore the bigger the influence of the magnitudes. This result shown that the smaller the size of the magnitude spectra the stronger the dominance of the intensity over the image edges.

### 2.5.3 Quantitative measurements on phase dominance

Although there have been huge number of researches in the phase and the magnitude dominance, there are only few attempts have been made to measure quantitatively the influence or the dominance of the magnitude or the phase using



the Fourier spectra of the image itself. The earlier uses of the Fourier spectra in relation with the dominance of the phase are to measure the effect of the phase and magnitude distortion. Hsiao et al. [245] derived a set of error metrics from the spectral magnitude and phase to measure the intelligibility of images reconstructed from distorted amplitude and phase spectra. Those metrics seems not to give an effective result as the effects of amplitude and phase errors appear to be similar. Another further rigorous elaboration on error metrics was then made [246]. The error was calculated from the euclidean distance of each corresponding elements of the original and the distorted Fourier transforms. However, that proposed error metrics was again not effective to depict the effect of the magnitude distortion, especially when the distortion is relatively large.

A quite similar method to measure the effect of the phase and the magnitude distortion was proposed by Lattman and DeRosier [247]. They derived two parameters, i.e.: the R.M.S. error and the correlation coefficient, from the Fourier transform of the hybrid image and the source images. Their method seems to work well as the hybrid image will always has bigger correlation and small error with the source image which shares the phase than the one which contributes the magnitude. However, they reported that when the sources image have a high correlation, the methods will give a poor result. As initially intended to measure the distortion effect on phases and magnitudes only, the method therefore can not be used to predict in what measure the magnitude will dominate the phase.

An attempt that was intended to measure the dominance of the phase had been made by Millane and Hsiao [218]. They proposed a ratio between two error-distances of the circular power spectra of the images to determine the dominance of the phase. The maximum value of the ratio is 2.2 which will happen if the power spectra of the two images are the same and the minimum one is 1.2 if the power spectra of the two images are very different. They argued that the phase will always be dominance for the ratio greater than 1.0 although if the ratio less than 1.5, the phase dominance is getting weaker. There are at least two things to be concerned with that proposed function of ratio. The first, although they provided two sets of images which exhibit as predicted by the ratio function, more sets of images are needed to verify the validity of the function along the curve within more convincing spaces of values. The second, that ratio function can not allow the ratio value which represents the sets of images which have dominant magnitude although that kind of sets of images can be easily found even in the set of natural images. Therefore, this function ratio still needs further investigation.



There are at least two reasons why the above statistical approaches of the phase dominance are not effective. The first reason is that the magnitude spectrum itself is not the representation of the image. The phase spectrum is also important, even in most cases the phase is more dominant so that two images with exactly similar magnitude spectra but different phases will be perceived differently. The second reason is that merely element-wise measurement of statistics of the magnitude spectra does not convey spatial information of the image's pixels. Therefore, measuring the dominance of the phase using statistical properties of the magnitude spectra will not always provide the correct result. As shown by Gluckman [248], Mashhadi et al. [249], the images with different pattern can have magnitude spectra which share the same statistics. They reported that images with same frequencies (magnitude spectra) but different phases can have same statistical moments.

#### 2.5.4 Fourier transform-based features

Although the use of the magnitude spectra did not seem to give promising result, it does not mean that the magnitude spectra will not be useful to predict the dominance of the phase. As it has been reported by [233] that the smaller the size of the image patches the weaker the dominance of the phase. In other perspective, the higher the frequency of the images' texture, the weaker the influence of its phase. At some point, the magnitude will be more dominant than the phase. Beyond that point the magnitude will even become more dominant. It also means that the image with high frequency of texture will have dominant magnitude.

As each element of the magnitude spectra of an image represents a spatial frequency, the measurement in that domain can be used to measure the phase dominance. By definition, the the stronger the phase, the more similar the hybrid image to the source image which contributes phase. Therefore, the texture features which have been used to discriminate images' textures can be used to measure the phase dominance of images. Weszka et al. [250] proposed two types of features, they are the ring-shaped and the wedge-shaped regions of the summation of the power-spectra (the square of the magnitude spectra). The rings' sizes and the wedges' angles were varied into four values. Liu and Jernigan [54] proposed twenty eight texture features which were extracted in the spatial frequency domain to classify images under additive noise. Although they reported that not all of the twenty eight features were useful, at least four of them gave accuracy of at least 92%. Based on those twenty eight features, Tsai et al. [251] selected

five of them and made some modifications in them to assess surface roughness. They showed that among five features only one of them that did not correlate with the roughness. The similar features were used by Lee et al. [252] to develop an automatic system of roughness inspection by a computer vision. They used two power spectra-based features and one spatial domain-based feature.

Although all of them reported that the use of those magnitude spectra-based features were successful, they could not show that each feature has a high correlation with the image's textures. They incorporated non-linear methods and used those features as the input variables so that the successful result could be achieved. Some researchers utilized some filters to get features that provide better results for texture discrimination. Maani et al. [253] proposed a set of features which based on the circular band-pass filters. Zhang et al. [254] applied the wedge and Gaussian filters into the magnitude spectra. Despite so many features have been developed, it is still difficult to discriminate the textures merely by the use of linear combination of them. Therefore, some of those researchers did not hesitate to use neural networks instead of regression methods.

Beside the magnitude spectra, again, based on the belief that the phase is more important than the magnitude, some researchers have made attempts to extract a set of features from the phase spectra. Eklundh [255] proposed the ring-shaped and the wedge-shaped regions of the phase features which are similar to Weszka et al. [250] but calculated in the phase spectra domain. He reported that those phase features were not useful for texture discrimination. Dong et al. [256] applied a set of fifty one features which have been listed in Dong et al. [257] into phase spectra to measure the similarity between images. However, to make a comparison of their performances, they also applied those features calculation into the magnitude spectra. They reported that the result was not as initially expected. Eventually, those features worked better for the magnitude than for the phase. Ojansivu and Heikkilä [258] proposed a local phase-feature to classify textures under blur condition. Four elements of the phases are selected based on the certain criteria. They reported that the performance of the method was much better than other used methods. When the radius of the blur is two pixels, this methods still gave the accuracy of more than 90% while the other used methods provided the accuracy below than 40%. This method has been adopted in other applications such as identification of face expression [259], signature verification[260], and fingerprint recognition [261].

## 2.6 Summary

In this chapter, the term roughness was defined in two different meanings: first, physical roughness which represents the surfaces' asperities that can be measured and quantified using standard parameters; and second, perceived roughness which is a sensation felt by touching or sliding the skin across a rough surface. Both roughness terms are used to characterize surfaces' textures. Physical roughness is more studied and well understood. Many measurement techniques have been established. The 2D and 3D standard roughness parameters have been defined to describe the surface topographies in the better representations. Roughness perception has different situation. Despite having been studied for decades by many researchers, it is still not well understood how humans perceive and discriminate the roughness of surfaces. Early psychophysical and neurophysiological studies were devoted mostly to investigate the correlation between particles' size and the subjective magnitude of roughness and to understand how neural-codes that underlie the roughness perception work. The stimuli used had relatively simple and homogeneous textures. The more recent researches have studied the roughness perception not only by direct touching but also by using sensors that record the vibrations evoked when they slide across the surfaces. Some features of the vibration profiles were extracted and correlated with the touching perception. However, most of them were using available materials as the stimuli such as fabrics and sandpapers. In 2009, Elkharraz et al. [52] proposed a method to design and manufacture stimuli with predefined textures. In this method, the surfaces' topography can be represented using images instead of roughness parameters. Therefore, the image's features can be used to model the perception of the roughness. One of the image's feature types is the Fourier transform-based features. They convey spatial frequency information of the textures and therefore they are most likely to correlate with roughness which also implies vibration. The features may be extracted from the magnitude or the phase spectra. Due to there is still no agreed conclusion so far either the magnitudes or the phases that is more important to represent the image, further investigation is needed both in the visual and touch perception.

# Chapter 3

## Magnitude Estimation of Roughness

### 3.1 Experiment Rationale

The present study aims to investigate human ability in perceiving and discriminating irregular roughness patterns on surfaces. This series of experiments were intended to determine, for both vision and touch:

1. How people perceive roughness of the irregular patterns on the tactile textures and the images;
2. The relationship between  $R_a$  values and the perceived roughness of first-order tactile textures;
3. The relationship between visual and tactile perception for irregular patterns.

While the perception of regular roughness patterns (dots and gratings) is already much studied, the perceived roughness evoked by surfaces with irregular roughness which are common in nature is less understood. The perceived roughness for this surface is difficult to predict because the shape, the size, and the arrangement of each roughness element on a non-homogeneous surface may not be able to be definitely determined. In particular, while there is a general correlation between measured and perceived roughness, the correspondence is not one-to-one, and textures that feel very different can have the same measured roughness.

Despite being random, roughness elements always form a pattern on the surface. Cutaneous mechanoreceptors are spread across two-dimensional receptive

fields [134] just like vision [31]. Therefore, humans should be able to not only perceive roughness but also discriminate its pattern to a certain degree.

Early studies in tactile patterns were intended to convert sound and images to the tactile pattern to help the deaf and blind communicate [147]. The pattern was generated using Optacon, a regular array of pins placed below a perforated surface. They are controlled and actuated so that some of them appear on the surface to form a pattern, such as a letter or Braille, or others. The array size normally fits the finger pad area. Bliss [148] showed that subjects were successfully able to read letter-shaped patterns using Optacon. The reading performance is influenced by pattern size [149], display time [150], and the presentation mode [151]. Those factors are underlaid by tactile aspects such as spatial acuity, temporal resolution, cutaneous masking, perceptual integration, and limited attention [147]. Whereas those aspects are well studied in regular patterns, there is no study which has investigated their role in perceiving irregular roughness patterns.

In this study the irregular roughness pattern will be created by transforming a binary image pattern into the boxels formation. A boxel is a regular tetragonal prism with its height determined by a value in the respective matrix cell. All values in the matrix are regarded as grayscale values of an image. The surface topography was formed by boxels. The designed surface textures were, then, engraved on the top of stimuli plaques. The *.stl* file of the stimuli were created using a customized computer program. The plaques were then manufactured using a 3D printer. This technique is adopted from [52].

The boxels's size is determined so that it is touched and perceived either individually or in group as a feature. Its cross section area is therefore smaller than the spatial acuity of the finger skin which is around 0.87 mm [117]. Because the position and orientation of the texture elements are random, the skin will likely be detecting vernier alignments on it. As shown by Loomis [120], the human fingerpad can detect alignments which are one-fifth shorter than two point threshold acuity, i.e. approximately 0.17 mm. A detectable alignment will consist of at least two boxels. In this experiment the cross section size of a boxel is  $0.8mm \times 0.8mm$ . The maximum height of the boxels should be at least more than just noticeable difference (JND) for the smooth surface which is  $(15 \pm 8.5\mu m)$  [30].

This study emulates Julesz's work on the discrimination of visual patterns. Visual texture perception theories are well-established compared to those of tactile texture perception. An image is perceived not merely based on the information from visual sensory but also on the informative percepts [136]. There are

three major views to this theory: structuralism, Gestalt, and Helmholtzian views [135]. Based on the Gestalt views, the visual pattern can be perceived and discriminated by the following properties: area, proximity, similarity, closure, good continuation, convexity, and symmetry.

Stepping from the Gestalt theory Julesz investigated the discriminability of the visual texture from Markovian generated patterns [240]. In this type of pattern, the colour of each pixel is determined by a probability rule (it is commonly called as *transition probability*) which take into account the colours of its neighbouring pixels. The number of the neighbouring pixels affecting the transition probability is called order. For example, in a second-order pattern, the transition probability of the pattern is determined by two pixels, first the corresponding pixel itself and second, an adjacent pixel on left side ( $i - 1^{th}$  cell of an array).

Julesz conjectured that visual patterns can be discriminated if they have differences in the first- and second-order probability (i.e. in which the probability of a pixel having a particular value is affected to different degrees by those of its first, second and third nearest neighbours). The difference in the third- and higher-order statistics will not be visually discriminable. His generated patterns showed the relevance of the theory. However, Julesz did not perform quantitative experiments; his conclusions were apparently self-evident from the images he used in his papers.

## 3.2 Method

### 3.2.1 Participants

The number of subjects in the experiments of magnitude estimation vary among the studies [33, 38, 262–264]. There is no explicit rule has been reported to effectively determine the number of subjects. Rather, trials' number is preferable instead of subjects' number. Kingdom and Prins [129, page 57] mentioned that 400 trials is a reasonable number to estimate both the threshold and the slope of a *psychometric function* (PF). Thus, at least two responses have been obtained from each subject, and an average response over subjects is taken as the magnitude scale [265]. The averaging over subjects is preferred due to the need for central tendencies, not individual differences. To obtain more than 400 trials for each texture which consisted of nine stimuli with two repetitions, at least twenty three subjects are needed in this study. However, in this study there were thirty participants which result in 540 trials for every experiment with

one texture. The participants were recruited from undergraduate and graduate students at the University of Leeds. All subjects were interviewed to make sure they were free from diseases or injury that could affect the tactile sensitivity of their hands. They were naive to the hypothesis. Ethics approval was granted by the University of Leeds ethics committee.

### 3.2.2 Stimuli

The image patterns were created by adopting Julesz's three markovian visual textures: first-, second-, and third-order statistical images. The textures were composed from black and white pixels. A computer program written in Java™ was used to generate the images (Appendix A.1). Thus, the probability distribution was generated from a pseudo-random generator.

In the first type of textures, the probability for being black for each dot is independent from the colours of the neighbouring pixels. However, the probability of white dots in each pattern of the nine images was set to be 10%, 20%, 30%, 40%, 50%, 60%, 70%, 80%, and 90% (Figure 3.1).

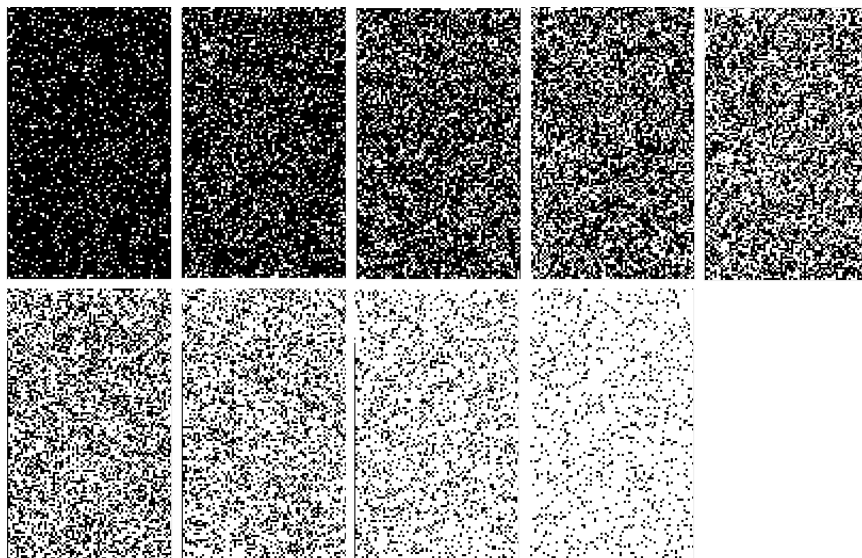


Figure 3.1: First-order textures with transition probabilities from 10% to 50% in the upper row, and 60% to 90% in the lower row.

The second type of textures have identical first-order distribution (black and white dots of equal probability) but differ in their second order probability distribution. The colour of each dot depends on the colour of the left-side dot following



a Markov process having the transition probabilities:

$$P(\mu_{i-1}, \mu_i) = \begin{cases} \frac{a}{100}, & \text{if } \mu_{i-1} = \mu_i \\ \frac{100-a}{100}, & \text{if } \mu_{i-1} \neq \mu_i \end{cases} \quad \mu_i = 0 \text{ or } 1 \quad (3.1)$$

where  $\mu_i$  is the colour value of the  $i^{\text{th}}$  dot,  $i-1$  refers to the left adjacent dot, zero means black and one means white. The colour of the first dot of a horizontal line is independent of the last dot colour of the previous line. There are nine different patterns by setting the values of  $a$ : 10, 20, 30, 40, 50, 60, 70, 80 and 90 (Figure 3.2).

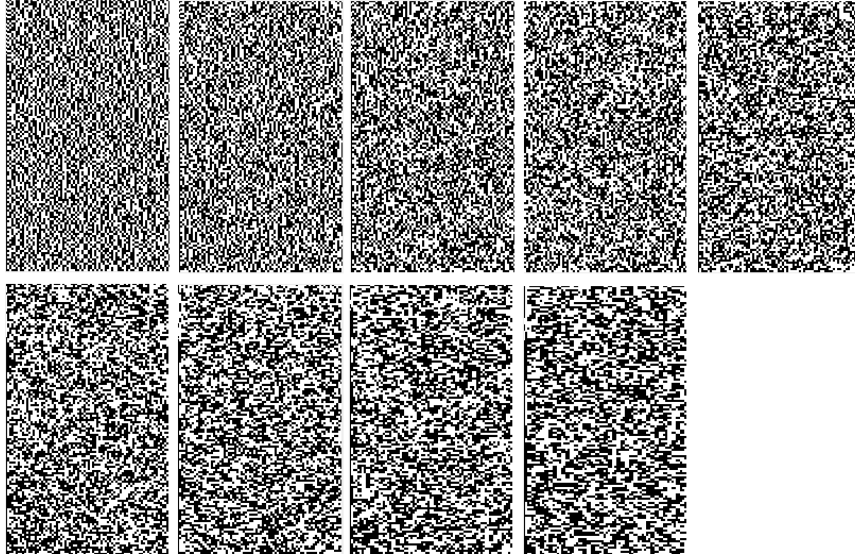


Figure 3.2: Second-order textures with transition probabilities from 10% to 50% in the upper row, and 60% to 90% in the lower row.

The third-order textures have identical first-order distribution (each colour has the equal probability) and second-order probability distribution (the colours of two adjacent dots are independent) but differ in their third-order probability distribution which was defined by the following transition probabilities:

$$P(k|ij) = P[2k - i - j = s(\text{mod}2)] = P(s) \quad (3.2)$$

where  $i$ ,  $j$  and  $k$  are the values (which may be zero or one) of successive samples along the horizontal line from left to right,  $s$  is zero or one which refers to black or white. The values of the transition probabilities ( $P(s)$ ) were set: 10%, 20%, 30%, 40%, 50%, 60%, 70%, 80%, and 90% (Figure 3.3).

Julesz created two different patterns for each  $n^{\text{th}}$ -order statistical textures by setting two contrast values of transition probabilities. These two patterns



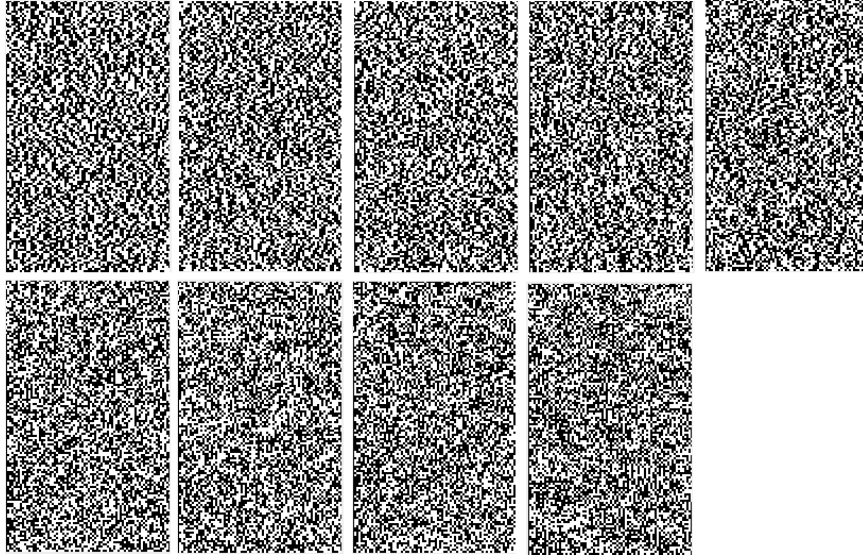


Figure 3.3: Third-order textures with transition probabilities from 10% to 50% in the upper row, and 60% to 90% in the lower row.

were presented in pair side-by-side or one contained in the other. The tasks in his experiment were to discriminate both patterns in each pair. In the current experiment, the transition probability of each statistical-order was varied from 10% to 90%; thus, there were nine different patterns for each  $n^{\text{th}}$ -order statistical textures or 27 patterns in total. The subjects' tasks were to estimate and report the roughness for each pattern. If two different patterns were perceived to have the similar roughness it means both patterns were indistinguishable, otherwise if both patterns have different perceived roughness it means both patterns were likely to be discriminable.

In the visual experiment, these textures were used directly as stimuli which were displayed on an lcd monitor. While, in the tactile experiment, the textures were transformed into 3-D surfaces by converting the dots to the boxels (Figure 3.4). The white dots become boxels with 0.5 *mm* height and the black dots become boxels with 0 *mm* height. The size of each stimulus is 51 *mm*  $\times$  25 *mm*  $\times$  3 *mm*, so there are 102  $\times$  50 boxels for each surface. The tactile stimulus were printed using *Perfactory 3 Mini Multi Lens*<sup>®</sup> with printing resolution up to 30  $\mu\text{m}$ . The material used was resin.

### 3.2.3 The computer codes for creating textures

As mentioned in the previous section, there are three types of textures: first-, second-, and third-order textures. Each texture was composed by white and black

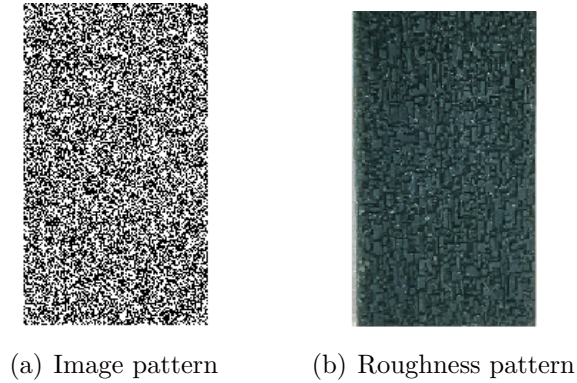


Figure 3.4: Image (a) to roughness pattern (b) transformation

pixels in an 512 array. In the first-order type of textures, the probability for being white for each dot is independent from the colours of the neighbouring pixels. Algorithm 1 shows how the first-order textures were created. The probability of white pixels ( $a$ ) is used to determine the transition-probability of the first-order textures.

---

#### Algorithm 1 First-order textures

---

```

1: procedure FIRST-ORDER MARKOV
2: SET:
3:   fill array with 0
4:   get the probability threshold of white pixel ( $a$ )
5: loop:
6:   for each row in array do
7:     for each element in a row do
8:       generate random number ( $r$ )
9:       if  $r \leq a$  then
10:        set the element's value: 255
11:       else
12:        set the element's value: 0

```

---

In the second-order textures, the colour of each dot depends on the colour of the left-side dot following a Markov process having the transition probabilities in equation 3.1. Algorithm 2 is used to implement this equation. The position of an element in the array is notated as  $(i, j)$ , where  $i$  is for a column number and  $j$  for a row number. The probability of being white for the first pixel of each row is set to be 50%.

In the third-order textures, the probability of each dot to be white depends on the colour of two previous adjacent pixels following equation 3.2. This equation implies that if the two previous pixels have the same colour, the probability of being white is equal to the transition probability being set. Otherwise, the probability of the third pixel to be white is one minus the transition probability.

---

**Algorithm 2** Second-order textures
 

---

```

1: procedure SECOND-ORDER MARKOV
2: SET:
3:   fill array with 0
4:   get the transition-probability ( $a$ )
5: loop:
6:   for each row in array do
7:     for each element in a row do
8:       if  $i = 0$  then
9:         generate random number ( $r$ )
10:        if  $r \leq 50$  then
11:          set the element's value: 255
12:        else
13:          set the element's value: 0
14:      else
15:        generate random number ( $r$ )
16:        if  $r \leq a$  then
17:          ( $i^{th}$ ) element's value = ( $i - 1^{th}$ ) element's value
18:        else
19:          ( $i^{th}$ ) element's value =  $255 - (i - 1^{th})$  element's value

```

---

Algorithm 3 is used to implement this procedure. Again, the position of an element in the array is notated as  $(i, j)$ , where  $i$  is for a column number and  $j$  for a row number. The probability of being white for the first and the second pixels of each row are set to be 50%.

All the algorithms were implemented in Java™ language to generate the image textures (Appendix A.1). Another Java™ code was written to convert all image textures into ASCII *.stl* files (Appendix A.2). A sample of CAD model of the tactile stimuli is in Figure 3.5. The size of the stimuli's base is  $50mm \times 25mm \times 2mm$ . The size of each boxel is  $0.3mm \times 0.3mm \times 1.0mm$ . The ASCII formatted *.stl* files were then converted into binary *.stl* files using Netfab™. This software was also used to repair any error in the files such as duplicated lines or meshes. The files were then brought to the *Perfactory 3 Mini Multi Lens*® to print the textures.

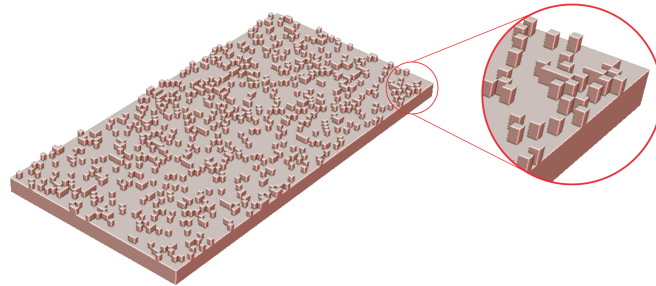


Figure 3.5: A sample of CAD model of the tactile stimulus.

---

**Algorithm 3** Third-order textures
 

---

```

1: procedure THIRD-ORDER MARKOV
2: SET:
3:   fill array with 0
4:   get the transition-probability ( $a$ )
5: loop:
6:   for each row in array do
7:     for each element in a row do
8:       if  $i = 0$  or  $i = 1$  then
9:         generate random number ( $r$ )
10:        if  $r \leq 50$  then
11:          set the element's value: 255
12:        else
13:          set the element's value: 0
14:        else
15:          generate random number ( $r$ )
16:          if  $(i - 1^{th})$  element's value =  $(i - 2^{th})$  element's value then
17:            if  $r \leq a$  then
18:               $(i^{th})$  element's value = 255
19:            else
20:               $(i^{th})$  element's value = 0
21:            else
22:              if  $r \leq a$  then
23:                 $(i^{th})$  element's value = 0
24:              else
25:                 $(i^{th})$  element's value = 255

```

---

### 3.2.4 Procedure

There were two sessions of experiments. *The first session* was a tactile experiment, i.e. touching and estimating the roughness magnitude of the plaques, and *the second session* was a visual experiment by seeing the image texture stimuli on an LCD monitor and estimating the roughness perceived. Each subject completed a session of visual experiment and a session of tactile experiment. Both experiments had an identical set-up. The order of the sessions was counter-balanced. Among thirty subjects, fifteen of them started the experiment from the visual session and then followed by the tactile session and then another fifteen started in otherwise order of sessions.

Each session consisted of three blocks which were labelled F for the experiment using first-order textures, S for the experiment using second-order textures, and T for the experiment using third-order textures. The order of the blocks was counter-balanced too. There were six combinations for ordering these blocks: F-S-T, F-T-S, S-F-T, S-T-F, T-F-S, and T-S-F. Each subject completed a block of visual experiment session and a block of tactile experiment session. There were five subjects for one combination.

A magnitude estimation (ME) method was adopted in the current experiment.

Two stimuli were presented side-by-side. In the tactile experiment, to avoid confusion, the left side stimulus was the reference and the right-side stimulus was the test. The reference stimuli for each type of texture was using a texture with transition probabilities 50% of the same type. For example, the experiment using third-order textures would use a reference stimulus having third-order texture with transition probabilities 50%. In the visual experiment, both reference and test stimuli were randomized (Figure 3.6). The subjects were asked to sense and assign a roughness value for each test stimulus by comparing to the reference one (the value of which was allocated 50).

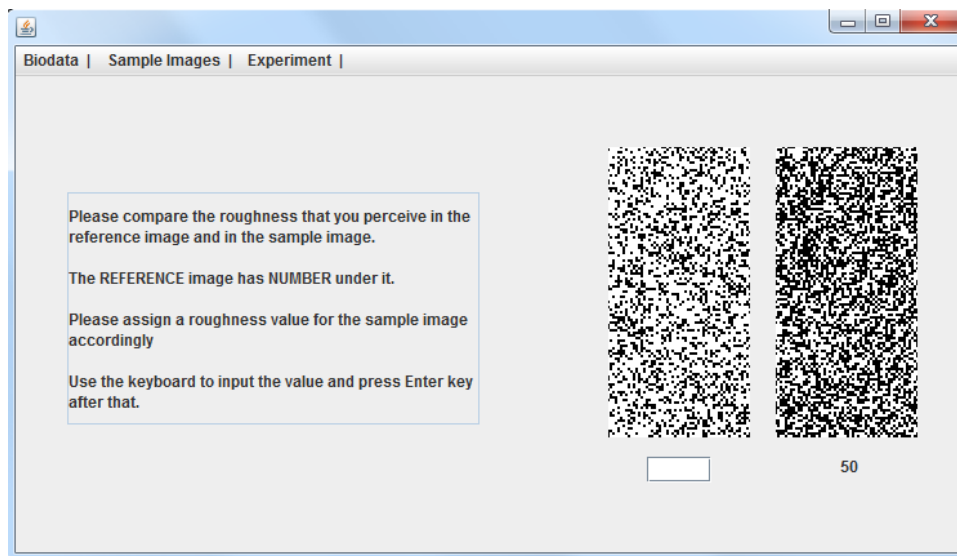


Figure 3.6: Image textures in the visual experiment. The subjects were asked to assign a roughness value for the test stimulus by referring to the reference images.

An exercise to show the subjects how to work with ME method was given prior to the experiment session. In the exercise, each subject was given a magnitude estimation training sheet presenting twelve lines with different lengths. The first line (at the top) is used as the reference (the value is 50). The participants were asked to estimate and assign a value of each line by referring to the reference line.

In the tactile experiment, the subjects were asked to use the dominant hand and the same finger during exploring the stimuli's surfaces. A handedness questionnaire was given to the participant to know which hand is his/her dominant one. Before exploring the stimuli's surfaces, the condition of the fingerpad's skin was standardized by washing it using a sanitary wet wipe. The subjects were asked to wear a sound defender to prevent the ear from listening to any sound evoked by fingerpad when sliding on a stimulus's surface.

### 3.2.5 Analysis

The actual arithmetic average roughness ( $R_a$ ) of the pattern is calculated based on formula 3.3:

$$R_a = \frac{1}{n} \sum_{i=1}^n |y_i - \bar{y}| \quad (3.3)$$

where  $n$  is the number of boxels,  $y_i$  is the height of the boxel. As there are only two pixels value (0 and 255), there are also only two heights of boxel, i.e.  $y_1 = 0$  and  $y_2 = 255$ . If the proportion of  $y_1$  value is  $p$ , then the actual  $R_a$  is:

$$R_a = 2(p - p^2)|y_2 - y_1| \quad (3.4)$$

Based on formula 3.4, the actual roughness of the first order is increasing from  $p$  equals to 0% to 50% and then is decreasing symmetrically from 50% to 100% order as shown in Figure 3.7. So, a pattern with the probability of  $y_1 = p$  will have the same actual  $R_a$  with a pattern with the probability of  $y_1 = 1 - p$ .

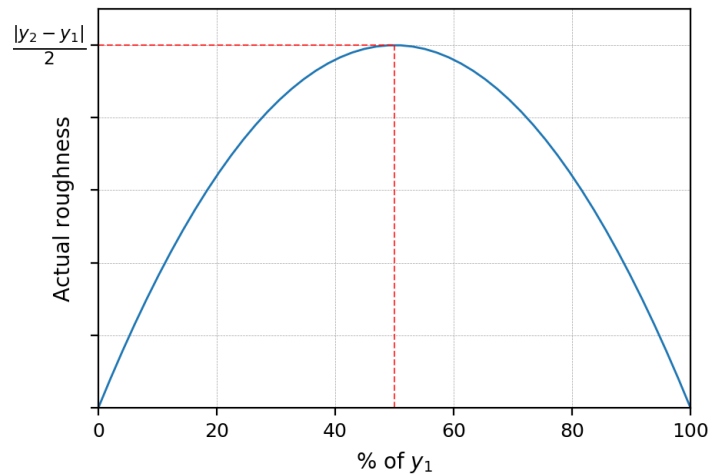


Figure 3.7: Percent of Markov Order vs Actual Roughness.

However, both patterns have contrasting topographies, the first one has a flat surface with a number of hills and the second one has a flat surface with that number of holes.

Since all the tactile stimuli with second- and third-order statistics textures have the same  $p$  values (50%) and the boxels' height is 0.5 mm, their  $R_a$  values are identical i.e. 0.25 mm. These stimuli differ only in the spread pattern of the boxels across their surfaces.

## 3.3 Result and Discussion

### 3.3.1 Visual experiment

The result shown that each type of textures was perceived differently (Figure 3.8). The mean of the scales of the perceived roughness is generally decreasing in the first-order textures, monotonically increasing in the second-order textures, and relatively constant in the third-order textures. Their plot lines meet at the middle point which indicates that the textures with 50% transition probabilities were perceived to have an equal roughness regardless their type of textures. For simplicity, each texture will be called as texture-10, texture-20, and so-forth to indicate their percentage of transition probabilities.

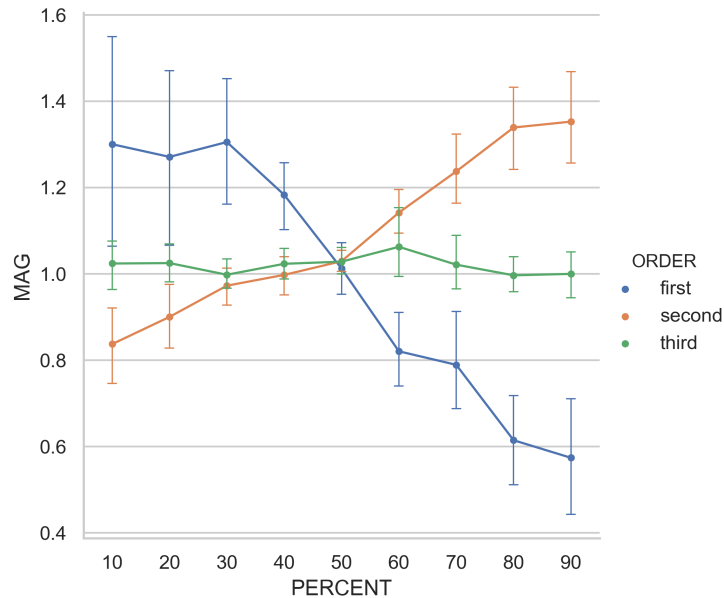


Figure 3.8: Scales of the perceived roughness of the visual textures with first-, second-, and third-order statistics. The horizontal axis is the category of textures with each point indicates the percentage of the transient probabilities of the corresponding texture. The vertical axis is the scales of the perceived magnitude of the textures.

To measure the difference between the perception patterns of each visual texture, the correlations of the perceived roughness between texture types were used as the indication. Shepherd's pi correlation method ([266]) was used to calculate the correlation. This method was selected due to its robustness to the influential outliers [267]. The result is presented in Table 3.1. It is seen that the correlation magnitude between texture types ( $r$  value) is less than 0.305. The ranges of correlations between the textures (CI-95%) are also not too far different from the

Table 3.1: Shepherd's Pi Correlation between the Visual Texture Types

Order	n	r	CI.95%	r2	adj_r2	p-val	power
first - second	540	-0.305	[-0.38, -0.23]	0.093	0.089	.000	.970
first - third	540	0.182	[0.1, 0.26]	0.033	0.03	.000	.990
second - third	540	-0.12	[-0.2, -0.04]	0.014	0.011	.007	.796

measured correlation ( $r$ ). A correlation value which is below than 0.30 is considered as negligible [268]. Therefore, it is more acceptable to consider that each type of textures was perceived differently than to accept that they were perceived similarly.

Although it is negligible, the correlation between texture types can give a glimpse of the relationship between them. As shown in Table 3.1, the correlation between the first-order and the second-order statistical textures is negative. It indicates that both of them have trends of subjective roughness with opposite direction. The first-order and the third-order textures have positive correlation and, therefore, they have the same direction of roughness pattern. Finally, the second-order and the third-order textures have negative correlation which means they have different pattern of subjective roughness. As seen in Figure 3.8 that the roughness scale of the third-order textures is relatively constant, they will always give a low correlation with other types of texture as can be seen from the  $r$  values in Table 3.1).

### First-order visual textures

In the first-order visual textures, subjects were able to recognize and to discriminate all test textures from the reference one (texture-50) as shown by Table 3.2. This table is the output of the ANOVA analysis and it shows whether there is a statistically significant difference between groups of the textures in the mean of scales of the perceived roughness. It is seen in the table that the value of  $F(8, 531)$  equals to 15.933 and it refers to a significance value ( $p$ ) of .000 which is significantly smaller than .05 and, therefore, the null hypothesis that there is no difference between group means is rejected. The variance of the texture contributes 19.4%, which is large (Table 3.3), to the total variance ( $EtaSq$ ). This result supports the conclusion that the scale of the perceived roughness for each texture is different.

Furthermore, the difference of the scales for all of the first-order statistical textures can be investigated in more detail from the multi-comparisons of the mean of scales between all texture groups. A pairwise comparisons test based



Table 3.2: ANOVA Test for First-Order Visual Textures: Between Textures

Source	SS	DF	MS	F	Pr(>F)	EtaSq
TEXTURE	41.709	8	5.214	15.933	.000	0.194
Within	173.751	531	0.327			

Table 3.3: The Criteria of Eta Squared [269–271]

Effect Size	EtaSq
Small	.01
Medium	.06
Large	.14

on Tukey’s *honestly significant difference* (Tukey-HSD [272]) method was used to analyse the means’ difference of the subjective scale between the texture groups. The result is shown in Table D.1. To have more clarity, the means’ differences are plotted in Figure 3.9. It can be seen that the mean difference between the scales of perceived roughness for every adjacent pair of textures is not significantly different. At a glance, it gives an impression that the subjective roughness of all textures is the same.

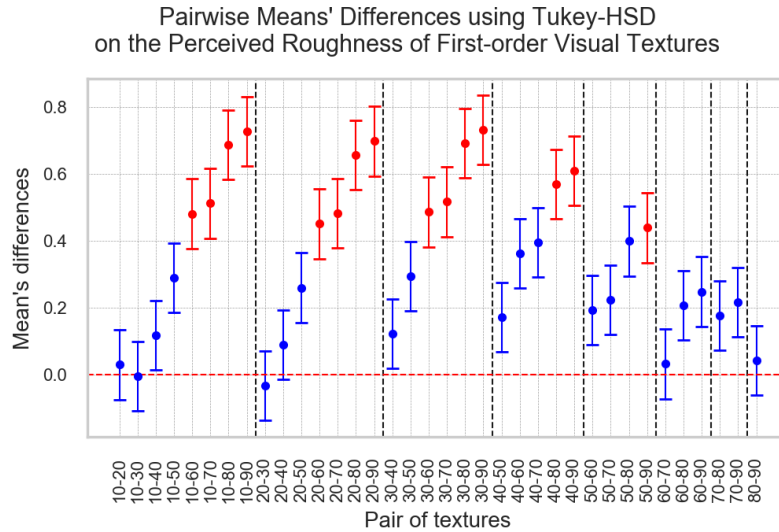


Figure 3.9: Multiple comparisons of the scales’ means of the perceived roughness between all pairs of the first-order visual textures. The blue error bars indicate that the difference of scales’ means for the corresponding pair is not statistically significant ( $p\text{-Tukey} \geq .05$ ). If the error bar is red, the scales’ means for the corresponding pairs is statistically significant ( $p\text{-Tukey} \leq .05$ ).

However, textures with a large difference in transition probability will be likely to have significantly different perceived roughness (Figure 3.9). For example, the first texture was perceived to be considerably rougher than texture-60 (their

means' difference is around 0.5). In general, the left side textures (their position in the plots are in the left of the texture-50), were perceived to be rougher than the right side ones (their position in the plots are in the right of the texture-50). Therefore, it gives a different impression than the previous one. In here, the scale of the perceived roughness of the first-order statistical visual textures is seen to decrease.

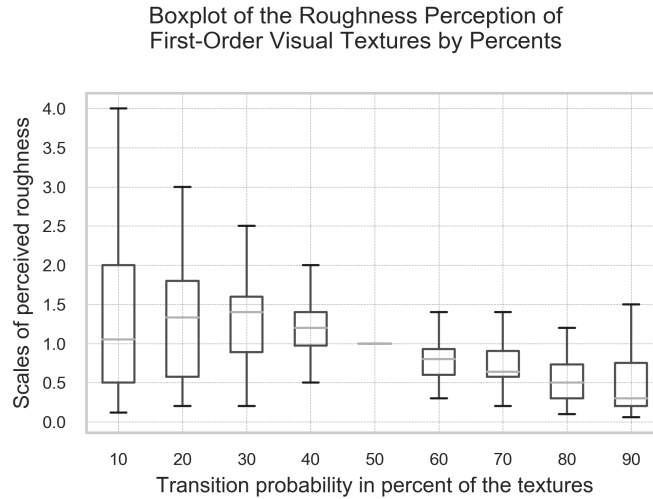


Figure 3.10: Boxplot of subjective scale for each of first-order visual texture. The horizontal axis is the category of textures with each point indicating the percentage of the transient probabilities of the corresponding texture. The vertical axis is the scales of the perceived roughness of the textures.

The decreasing pattern of the roughness' scales can also be seen from Figure 3.10. The figure shows that the median value (the segment line in the middle of each boxplot) of the subjective scales initially increases until reaches its peak at texture-30 and then decrease until reaching the lowest point (at texture-90) which is also lower than the initial value (at texture-10).

Figure 3.10 also shows that the variance of the subjective scale of roughness varies significantly. The first three textures share a significantly large variance. It can explain why they have a similar subjective roughness although they have different median values as shown in Table D.1. Furthermore, the similarity of subjective roughness of every two neighbouring textures can also be indicated from their variance boxes which share the same wide portion.

From Figure 3.10, it can be seen that the further the distance of the texture from the reference, the larger the variance. This result implies that the bigger the difference between roughness sensation, the wider the spread of the subjects'

response. Texture-50 has the narrowest variance because it actually has the same texture as the reference, which therefore would give a small difference in roughness sensation to subjects.

The first two textures have wide variances which have around 2/3 of their part above the scale of 1.0 (rougher than the reference texture) and around 1/3 of their part below the scale of 1.0 (smoother than the reference texture). It can also be seen from Figure 3.11 which shows more obviously that some subjects perceived the first two textures to be rougher and some subjects perceived those textures to be less rough than the reference texture. This result indicates that not all subjects agree that those textures have a rougher sensation than the reference texture.

Moreover, the average scale of subjective roughness of texture-10 was perceived to be higher than the reference's roughness, its median value (the line segments in the centre of the boxplots) is lower than the mean value (the centre of the boxplots) which, therefore, indicates that the proportion of the number of subjects who perceived texture-10 to be smoother than the reference texture is bigger than the number of subjects who perceived otherwise (Figure 3.10). These opposite perceptions in the same texture will be called as different perspectives of roughness.

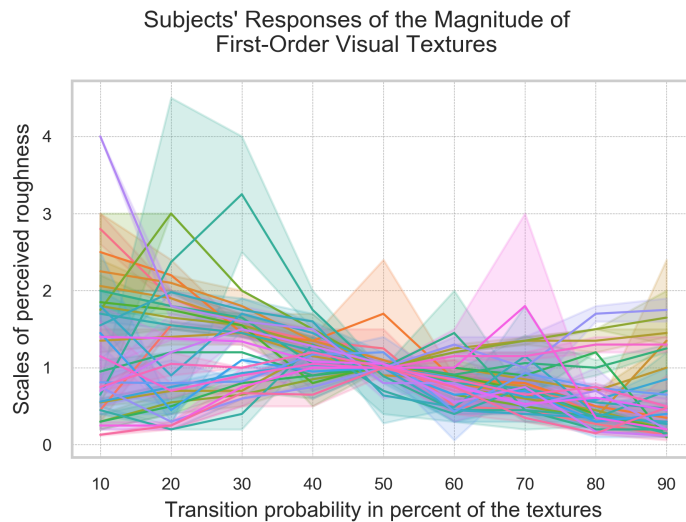


Figure 3.11: Subjects' roughness sensation on the visual textures with first-order statistics. The horizontal axis is the category of textures with each point indicates the percentage of the transient probabilities of the corresponding texture. The vertical axis is the scales of the perceived roughness of the textures.

This indication of different perspectives of roughness perception can also be

seen in Figure 3.11. This figure shows the response's plots with different directions (slopes). The direction of these lines can be estimated using the correlation between the transition-probability of the textures and the roughness responses of each subject as shown in Figure 3.12. From this image it can be seen that 60% of the subjects have high negative correlations ( $-0.75$  to  $-1.0$ ) for their responses. It means that the line plots of their roughness responses have negative slopes. This also means that the roughness of the first-order statistical visual textures were perceived mostly to get lower as the percentage of the transition probability increases.

Ten percent of the subjects perceived these textures oppositely as seen also from Figure 3.12. They felt that the roughness of the first-order statistical visual textures increases as the percentage of the transition probability increases. Other subjects (30% of them) have a relatively small correlation value ( $-0.5$  to  $+0.5$ ) which indicates three possibilities of different perception patterns. The first, subjects may have perceived all the textures as relatively the same rough. The second, the roughness may be perceived as increasing and then decreasing again at some point. The third possibility is opposite to the second, the roughness sensation decreased and then at some point increased.

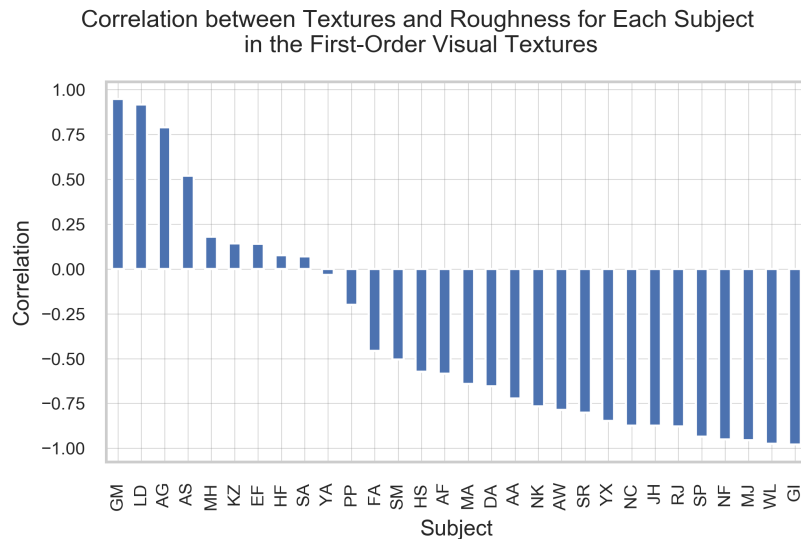


Figure 3.12: The correlation between transition probabilities of the first-order visual textures and the scales of perceived roughness for each subject. The subject with positive correlation means that he/she perceived the scale of roughness to increase as the transition probability increases. Zero correlation indicates the roughness perception is either constant, concave or convex. Negative correlation indicates that the scales of perceived roughness decreases.

To measure the effect of the roughness variance by the subjects to the to-

tal roughness variance, an ANOVA analysis was performed. The output of the analysis is presented in Table 3.4. From this table, it is seen that the value of  $F(29, 510)$  equals to 1.909 which, therefore, will refer to a significance value ( $p$ ) of .003 which indicates that each texture has different roughness scales. The variance of the scales of perceived roughness which comes from subjects contributes 9.8% which is relatively medium (Table 3.3), to the total variance of the data. However, compared to the variance contribution by the textures which is 19.4% (Table 3.2), the variance by subjects is considerably smaller. This indicates that the textures themselves give more effect to the pattern of the roughness response than the subjects which, therefore, supports an indication that each texture has a different roughness scale.

Table 3.4: ANOVA Test for First-Order Visual Textures: Between Subjects

Source	SS	DF	MS	F	Pr(>F)	EtaSq
SUBJECT	21.098	29	0.728	1.909	.003	0.098
Within	194.362	510	0.381			

Despite the evidence that there are different perspectives of visual roughness among subjects, as shown in Figure 3.13, the scales of the perceived roughness of the first-order statistical visual textures generally decrease. Although, in this figure, the responses of the roughness scales are represented only by their mean value for each texture (red dots), to fit the polynomial functions, all response values were used in the calculation. Four polynomial functions that were used to fit their roughness responses show that it is sufficient to use the third degree of polynomial function. Higher than that degree, the  $R^2$  values will not improve. The plot of the subjective roughness is seen to be sigmoid. The third-degree polynomial plot shows that at the beginning, the roughness scale does not really change, then it changes sharply at texture-40, and then finally starts to be constant again at texture-80.

### Second-order visual textures

In the second-order textures, subjects were also able to recognize and to discriminate all the test textures from the reference one. Table 3.5 shows the result of the ANOVA analysis with the value of  $F(8, 531)$  equals to 25.718 which, therefore, refers to a significance value ( $p$ ) of .00 which is significantly smaller than .05 and this indicates that the means of the scales of perceived roughness of each texture are different. The variance of the textures contributes 27.9% which is

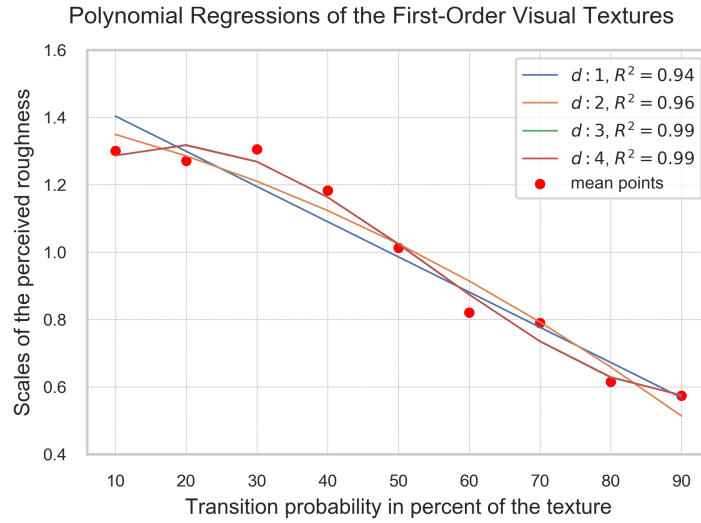


Figure 3.13: Polynomial regressions of the perceived roughness of the visual textures with first-order statistics. The red scattered-dots are the mean of the scales of perceived roughness of each texture. There are four polynomial functions with different degrees to fit.

very large (Table 3.3) to the total variance (*EtaSq*). This result implies that all the second-order visual textures could be discriminated.

Table 3.5: ANOVA Test for Second-Order Visual Textures: Between Textures

Source	SS	DF	MS	F	Pr(>F)	EtaSq
TEXTURE	16.872	8	2.109	25.718	.000	0.279
Within	43.543	531	0.082			

Furthermore, the difference of the scales of perceived roughness for all of the second-order statistical textures can be investigated in more detail from the means comparison of the scales of perceived roughness for each texture group. A pairwise comparisons test based on Tukey-HSD method was used to analyse the means' difference of the subjective scale between the texture groups. The result is presented in Table D.2 and in Figure 3.14. From this figure, it can be seen that the mean difference between the scales of perceived roughness for every adjacent pair of textures is not significantly different. At a glance, it gives an impression that the subjective roughness of all textures is the same.

However, as the difference of the transition probability becomes larger, the texture will be more likely to have different scales of perceived roughness. For example, texture-10 and texture-20 were able to be discriminated from initially texture-60 (Figure 3.14). Then, texture-30 starts to be significantly discriminated from texture-70. In general, the subjective scale of the roughness magnitude of

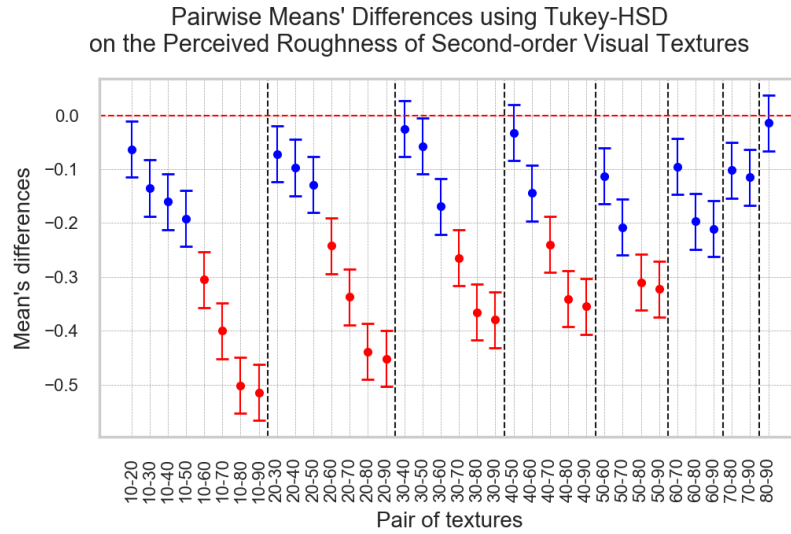


Figure 3.14: Multiple comparisons of the scales' means of the perceived roughness between all pairs of the second-order visual textures. The blue error bars indicate that the difference of scales' means for the corresponding pair is not statistically significant ( $p\text{-Tukey} \geq .05$ ). If the error bar is red, the scales' means for the corresponding pairs is statistically significant ( $p\text{-Tukey} \leq .05$ ).

the second-order statistical visual textures is monotonically increasing as shown in Figure 3.8.

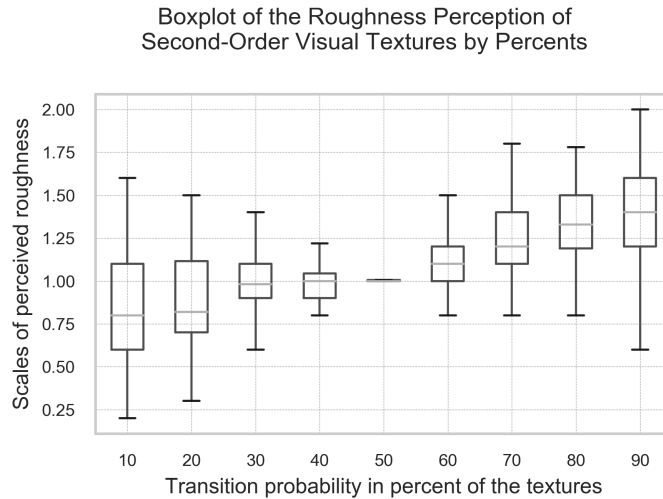


Figure 3.15: The boxplot of subjective scale for each of second-order visual texture. The horizontal axis is the category of textures with each point indicates the percentage of the transient probabilities of the corresponding texture. The vertical axis is the scale of the perceived roughness of the textures.

The pattern of an increasing scale can also be seen from the boxplot of the scales of perceived roughness as shown in Figure 3.15. The figure shows that the median value of the scales becomes higher when the transition probability of the textures increases. However, the variances of the scales for each texture are different. The further the distance of the texture from the reference, the larger the variance. The pattern of the variance can also be seen from the plot of subjects' response in Figure 3.16. This figure shows that the line plots of the subjects' responses indicates that the at the beginning, the spread of the response is wide, then becomes narrower until it reaches texture-50, and finally start becoming wider again.

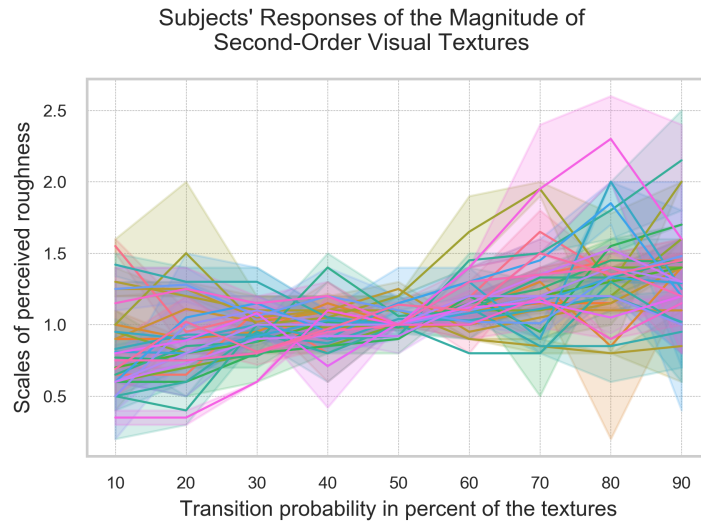


Figure 3.16: Subjects' roughness sensation on the visual textures with second-order statistics. The horizontal axis is the category of textures with each point indicates the percentage of the transient probabilities of the corresponding texture. The vertical axis is the scales of the perceived roughness of the textures.

Figure 3.16 also indicates that each subject may have a different pattern of perception. This indication can be seen in the line plots in Figure 3.16 which shows the response's plots with different directions. The direction of these lines can be estimated using the correlation between the transition-probability of the textures and the roughness responses of each subject as shown in Figure 3.17. From this image it can be seen that most of the subjects (70% of them) have positive correlations for their responses. It means that the line plots of their roughness responses have positive directions. This also means that the scales of roughness of the second-order statistical visual textures were perceived by most subjects to get higher as the percentage of the transition probability increases.



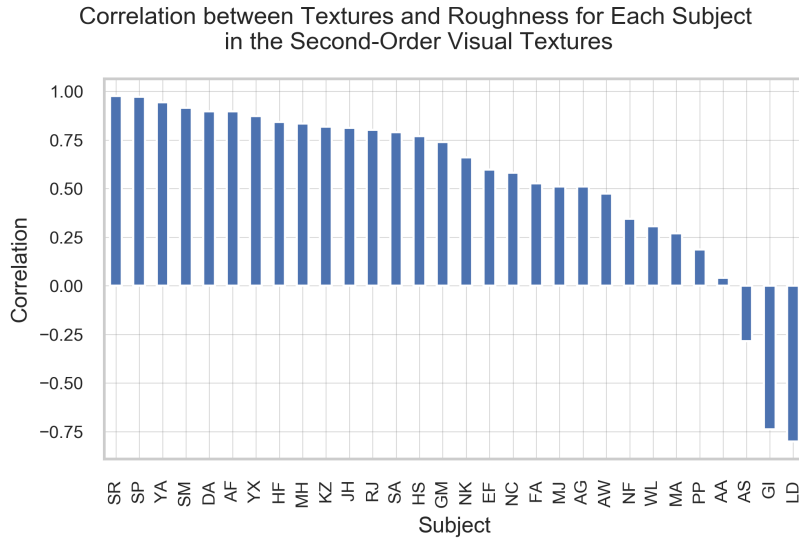


Figure 3.17: The correlation between transition probabilities of the second-order visual textures and the perceived scales of their roughness for each subject. The subject with positive correlation means he/she perceived the the roughness scale to increase as the transition probability increases. Zero correlation indicates the roughness perception is either constant, concave or convex. Negative correlations indicate that the scales of perceived roughness decreases

Only less than 7% of the subjects perceived these textures differently as can be seen also from Figure 3.12. They felt that the scales of roughness of the second-order statistical visual textures decreases as the percentage of the transition probability increases. A subject has a relatively small correlation value. To know whether the responses variance came from the responses' noise or from the different subjects' perspective of the second-order visual textures, an ANOVA analysis was, then, performed. The output is shown in Table 3.6. From this table it is seen that subjects have a different pattern of roughness perception as the significant value ( $p$ ) is .033 which is a little smaller than the confidence level (.05). Moreover, the variance of the subjects contributes 8.2% which is medium (Table 3.3), to the total variance. However, compared to the variance contribution by the textures which is 27.9% (Table 3.5), the variance by subjects is smaller. This indicates that the textures give more effect to the pattern of the roughness response than the subjects themselves.

Table 3.6: ANOVA Test for Second-Order Visual Textures: Between Subjects

Source	SS	DF	MS	F	Pr(>F)	EtaSq
SUBJECT	4.929	29	0.170	1.562	.033	0.082
Within	55.486	510	0.109			

As shown in Figure 3.18, the subjective scale of the roughness of the second-order statistical visual textures generally increases. Although, in this figure, the responses of the roughness scales are represented by their mean value for each texture (red dots), to fit the polynomial functions, all response values were used. Four polynomial functions that were used to fit their roughness responses show that it is sufficient to use the first degree of polynomial function. Higher than that degree, beside the  $R^2$  values do not improve significantly, the function may also tend to overfit the roughness data. As it is seen in the figure, the subjective roughness tends to increase linearly as the transition of the probability increases.

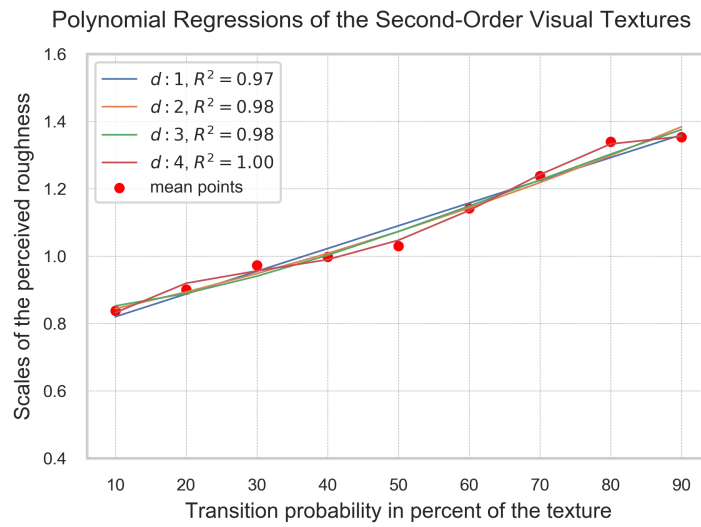


Figure 3.18: Polynomial regressions of the perceived roughness of the visual textures with second-order statistics. The red scattered dots are the scales' mean of the perceived roughness of each texture. There are four polynomial functions with different degrees to fit.

### Third-order visual textures

In the third-order textures, subjects were not able to recognize and to discriminate all the test textures from the reference one. As it can be seen in Figure 3.8, the plot of the subjects' responses is flat. It means that all textures were perceived to be the same. To know whether this statement is true or not an ANOVA analysis was performed and the result is presented in Table 3.7. This table shows that the value of  $F(8, 531)$  equals to .061 which, therefore, will give a significance value ( $p$ ) of .777 which is larger than .05 and it indicates that the means of the subjective scales of each texture are the same. The variance of the textures contributes 0.9% to the total variance ( $EtaSq$ ) which is small (Table 3.3). It implies that all the third-order visual textures could not be discriminated.

Table 3.7: ANOVA Test for Third-Order Visual Textures: Between Textures

Source	SS	DF	MS	F	Pr(>F)	EtaSq
TEXTURE	0.202	8	0.025	0.061	.777	.009
Within	22.329	531	0.042			

Furthermore, the similarity of the scales of perceived roughness for all the third-order statistical textures can be investigated in more detail from the means comparison of the subjective roughness scales of each texture group. A pairwise comparisons test based on Tukey-HSD method was used to serve that purpose. The output is presented in Table D.3 and in Figure 3.19. The differences between group means (diff) are mostly less than 0.06 which are relatively small compared to the means themselves which are around 1.0 (Table D.3). Then, it can be seen that all  $p$ -*tukey* values are equal to or more than .05 which means that the difference between means of subjective scales for all the textures is not significant.

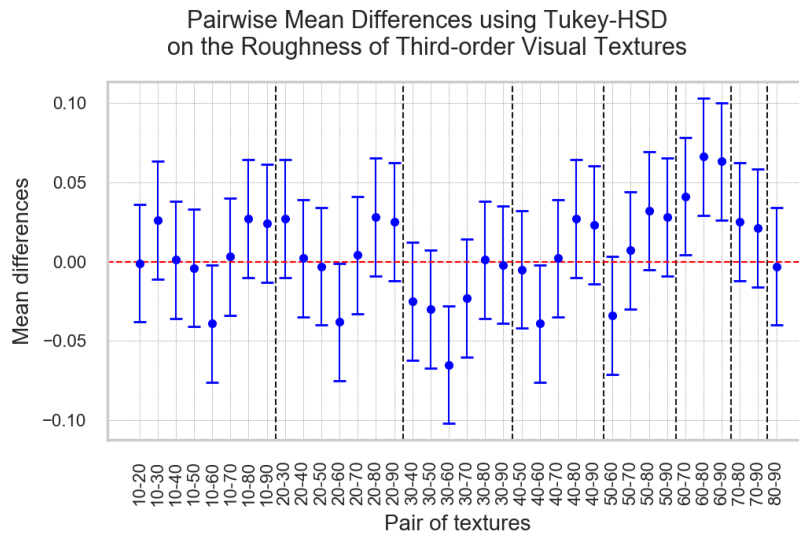


Figure 3.19: Multiple comparisons of the scales' means of the perceived roughness between all pairs of the third-order visual textures. The blue error bars indicate that the difference of scales' means for the corresponding pair is not statistically significant ( $p$ -Tukey  $\geq .05$ ). If the error bar is red, the scales' means for the corresponding pairs is statistically significant ( $p$ -Tukey  $\leq .05$ ).

The boxplot in Figure 3.20 shows that the medians of each texture's scale are at the same level which also indicates that the subjective magnitude scales of all textures are relatively similar. From this figure, it can be seen that the first four textures have different variances while the last four textures have relatively the same medians and variances. It indicates that the first four textures gave more

diverse sensation to the subjects than the last four textures which have almost the homogeneous roughness sensation.

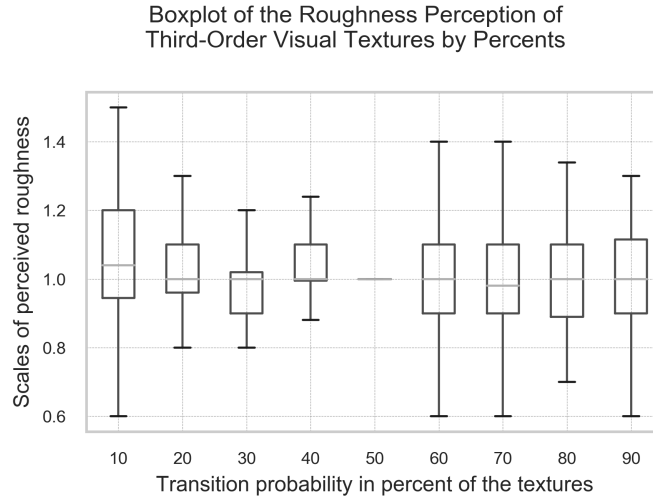


Figure 3.20: The boxplot of subjective scale for each of third-order visual texture. The horizontal axis is the category of textures with each point indicates the percentage of the transient probabilities of the corresponding texture. The vertical axis is the scales of the perceived roughness of the textures.

The line plot of the roughness responses itself shows a similar pattern (Figure 3.21). In this figure, it is seen that all lines form a relatively horizontal band which, therefore, indicates that all textures have arguably no different roughness. However, it is still possible that each individual line has slightly different slope and position (some parallel lines are above or below others). As each line represents the subjective roughness from each subject, the information of the line direction will depict the pattern of his/her subjective roughness.

The direction of these lines can be estimated using the correlation between the transition-probability of the textures and the roughness responses of each subject as shown in Figure 3.22. From this image it can be seen that almost a half of the subjects have positive correlations and another half of the subjects have negative correlations for their responses. It means that there is a different pattern of perception among subjects. It seems at a glance that a half of the subjects perceived the third-order statistical visual textures to have lower roughness as the transition probability increases, and another half of subjects perceived in opposite direction.

However, there are 80% of the magnitudes of those correlation that are less than 0.5 which is considerably low [268]. This results indicates that 80% of the

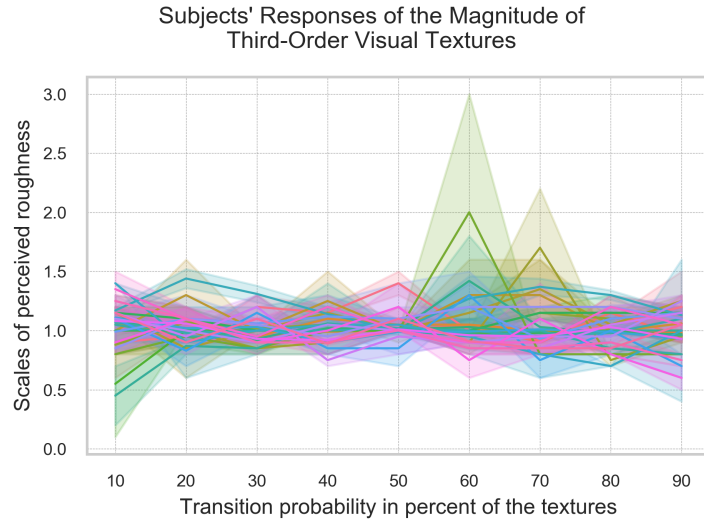


Figure 3.21: Subjects' roughness sensation on the visual textures with third-order statistics. The horizontal axis is the category of textures with each point indicates the percentage of the transient probabilities of the corresponding texture. The vertical axis is the scales of the perceived roughness of the textures.

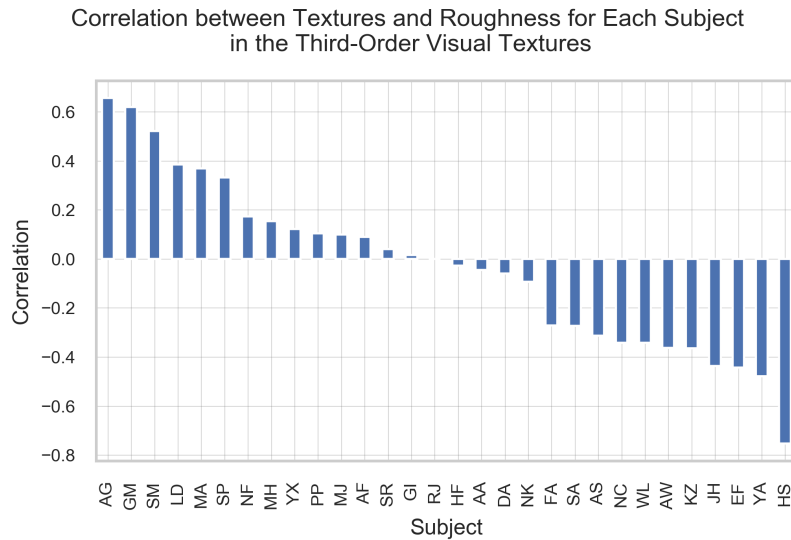


Figure 3.22: The correlation between transition probabilities of the third-order visual textures and the perceived scales of their roughness for each subject. The subject with positive correlation means he/she perceived the the roughness scale to increase as the transition probability increases. Zero correlation indicates the roughness perception is either constant, concave or convex. Negative correlation indicates that the scales of perceived roughness decreases.

subjects' responses of the roughness have negligible correlation with the texture types. In other words, this result support the statement that the roughness scale of the third-order visual textures does not depend on the textures themselves.

To know whether this different subjects' perspective of the roughness is statistically present or not in the third-order visual textures, an ANOVA analysis was performed. The output is shown in Table 3.8. This table shows that the value of  $F(29, 510)$  equals to 2.137 which, therefore, will give a significance value ( $p$ ) of .001 which is significantly smaller than 0.05 and it indicates that subjects have a different pattern of roughness perception (Figure 3.22).

The variance of the roughness scales from each subject contributes 10.8% to the total variance (*EtaSq*) which is quite large (Table 3.3). However, compared to the variance contribution by the textures which is 0.9% (Table 3.7), the variance by subject is significantly larger. This indicates that the textures give considerably little effect to the pattern of the roughness response than the subjects themselves.

Table 3.8: ANOVA Test for Third-Order Visual Textures: Between Subjects

Source	SS	DF	MS	F	Pr(>F)	EtaSq
SUBJECT	2.441	29	0.084	2.137	.001	0.108
Within	20.090	510	0.039			

Four polynomial functions were used to fit the relationship between the textures and the roughness responses. The plot of those functions is presented in Figure 3.23. Although, in this figure, the responses of the roughness scales are represented by their mean value for each texture (red dots), to fit the polynomial functions, all response values were used. Four polynomial functions that were used to fit their roughness responses show that it is sufficient to use the third degree of polynomial function (line plot). Higher than that degree, beside the  $R^2$  values does not improve significantly, the function may also tend to overfit the roughness data. The third-degree polynomial accommodates the concave trend for the lower percentage of textures and the convex trend for the higher percentage of the textures. This can not be done by the lower degree polynomials. Therefore, its  $R^2$  value increases significantly.

However, this  $R^2$  value is only 0.43 which means that only 43% of the perceived roughness was correctly predicted by the third degree of polynomial function. Moreover, as it is seen in the figure, all lines seem to be similar and linear even though they have different degrees. This shows that responses can be considered as constant, meaning that the subjects could not discriminate visual textures with third-order statistics as has been shown by Table 3.7 and Figure 3.19.

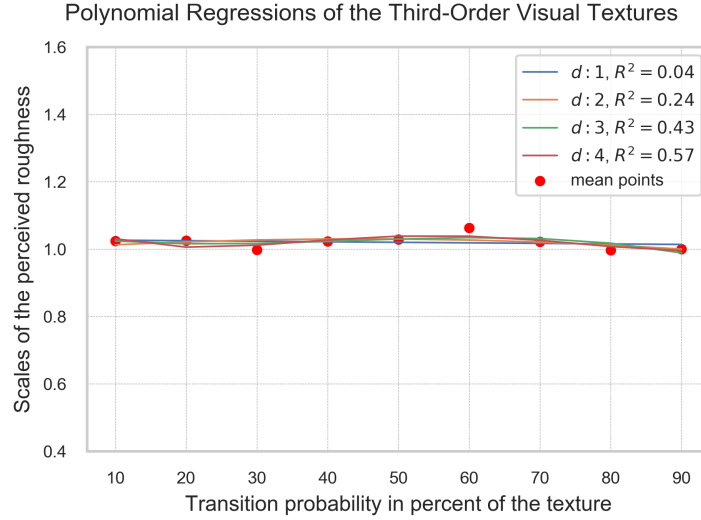


Figure 3.23: Polynomial regressions of the perceived roughness of the visual textures with third-order statistics. The red scattered dots are the mean of the roughness of each texture. There are four polynomial functions with different degrees to fit.

Table 3.9: Sepherd's Pi Correlation between the Types of Tactile Textures

Order	n	r	CI.95%	r2	adj_r2	p-val	power
first - second	540	-0.342	[-0.41, -0.27]	0.117	0.114	.000	1.0
first - third	540	0.384	[ 0.31, 0.45]	0.147	0.144	.000	1.0
second - third	540	-0.104	[-0.19, -0.02]	0.011	0.007	.000	0.677

### 3.3.2 Tactile experiment

The results show that each type of tactile texture was perceived differently, especially the first-order texture (Figure 3.24). The mean of the scales of the perceived roughness significantly decreases in the first-order textures, slightly increasing in the second-order textures, and slightly decreasing in the third-order textures. Their plot lines meet at the middle point which indicates that the textures-50 were perceived to have an equal roughness regardless their type of textures.

The correlation analysis which has been performed also indicates that each type of texture was perceived differently. The output of the analysis is presented in Table 3.9. It can be seen that the magnitude of the correlation between texture types ( $r$ ) ranges between 0.104 and 0.384 which is considerably low. Therefore, it is more acceptable to consider that each texture type is uncorrelated and, therefore, the patterns of their roughness are different.

Although it is low, the correlation between texture types can give a glimpse of the relationship between them. As shown in Table 3.9, the correlation between the first-order and the second-order statistical tactile textures is negative. It in-

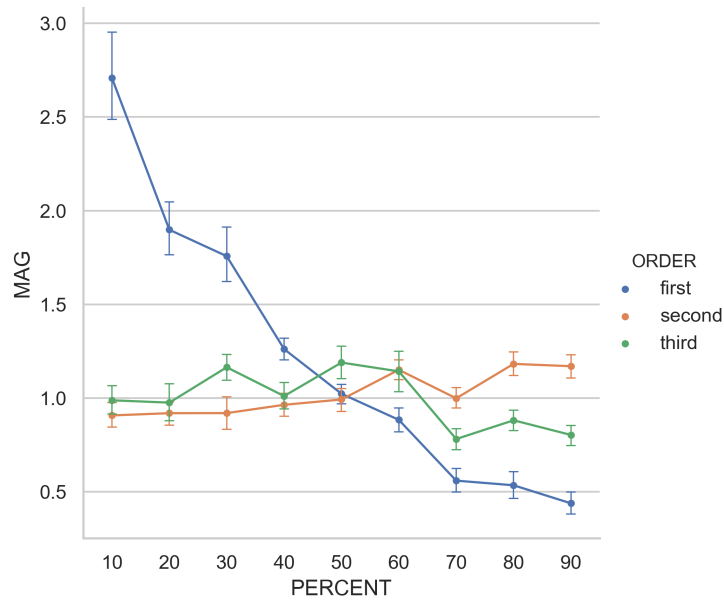


Figure 3.24: Perceived magnitude-scales of the roughness of the tactile textures with first-, second-, and third-order statistics. The horizontal axis is the category of textures with each point indicates the percentage of the transient probabilities of the corresponding texture. The vertical axis is the scales of the perceived magnitude of the textures.

indicates that both of them have patterns of subjective roughness with opposite direction. The first-order and the third-order textures have positive correlation and, therefore, they have the same direction of roughness pattern. Finally, the second-order and the third-order textures have negative correlation which means they have different pattern of subjective roughness. The roughness scales of the second- and the third-order textures have the same pattern but in opposite directions (Figure 3.24). That is why they have almost the same value of correlation with the first-order textures despite having the opposite signs as can be seen from the  $r$  values in Table 3.9.

### First-order tactile textures

In the first-order tactile textures, subjects were able to recognize and to discriminate all the test textures from the reference texture (texture-50) as shown by Table 3.10. This table is the output of the ANOVA analysis and it shows whether there is a statistically significant difference between groups of the textures in the mean of subjective scale. It is seen in the table that the value of  $F(8, 531)$  equals to 34.727 and it will refer to a significance value ( $p$ ) of .000 which is significantly smaller than .05 and, therefore, the null hypothesis that there is no difference



Table 3.10: ANOVA Test for First-Order Tactile Textures: Between Textures

Source	SS	DF	MS	F	Pr(>F)	EtaSq
TEXTURE	277.815	8	34.727	167.74	.000	0.716
Within	109.932	531	0.207	-	-	-

between group means is rejected. The variance of the texture contributes 71.6% to the total variance (*EtaSq*) which is very large (Table 3.3). This result suggests that the subjective scales of the roughness is different for each texture.

Furthermore, the difference of the subjective scales for all the first-order statistical tactile textures can be investigated in more detail from the means comparison of the subjective scales of each texture group. A pairwise comparisons test based on Tukey-HSD method was used to analyse the means' difference of the subjective scale between the texture groups. The result is shown in Table D.4 and in Figure 3.25. It can be seen that the mean difference (diff) between the roughness scales of every neighbouring textures is mostly significantly different as their respective significant value (p-Tukey) equals to or more than .05 (null hypothesis is accepted), except between texture-10 and texture-20 and between texture-30 and texture-40.

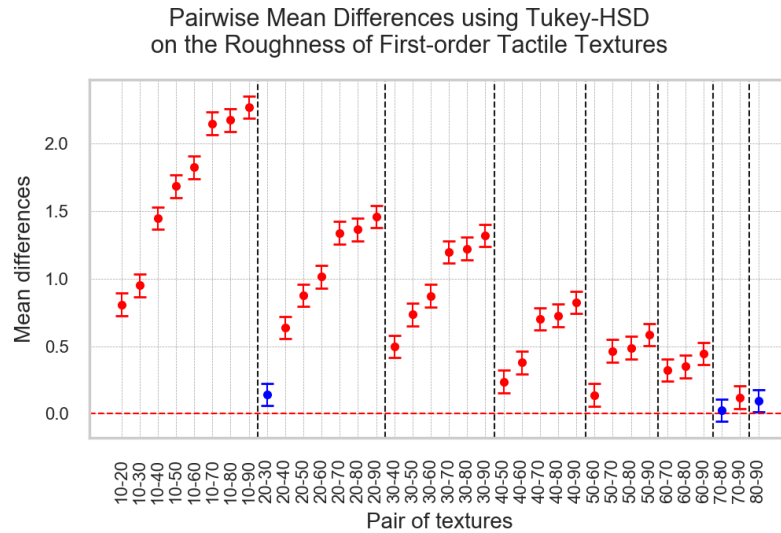


Figure 3.25: Multiple comparisons of the scales' means of the perceived roughness between all pairs of the first-order tactile textures. The blue error bars indicate that the difference of scales' means for the corresponding pair is not statistically significant ( $p\text{-Tukey} \geq .05$ ). If the error bar is red, the scales' means for the corresponding pairs is statistically significant ( $p\text{-Tukey} \leq .05$ ).

Texture-10 is seen to have the widest variance (Figure 3.26). It implies that when the roughness ratio between texture-10 and the reference (texture-50) is

too large, despite being easier to discriminate, it is difficult for subjects to assign a fix scale of the roughness sensation. It will also happen to other textures with a large gap of roughness intensity. Although texture-10 has a considerably wide variance, it has the highest median which is significantly higher than the medians of the following textures (Figure 3.26). Therefore, this texture was perceived to be different from other textures (Table D.4). Furthermore, almost all textures that are separated by at least one texture have significantly different roughness. Only the last three textures were perceived to have the same roughness. Therefore, as it can also be seen in Figure 3.26, all the textures seems to have different roughness.

The boxplot in Figure 3.26 also shows that the level of medians of each texture's scale decreases. At the beginning, the roughness descent looks steep. Start from the middle, the descent becomes less steep. The last three textures, however, are seen to have relatively the same median and the same variance which indicates that the subjects perceived them indifferently. From Figure 3.26 it is seen that the wide of the variance becomes larger when the distance of the texture gets further from the reference texture. It is also seen that when the two textures have a relatively the same median (level of roughness), the wide of their variances looks similar.

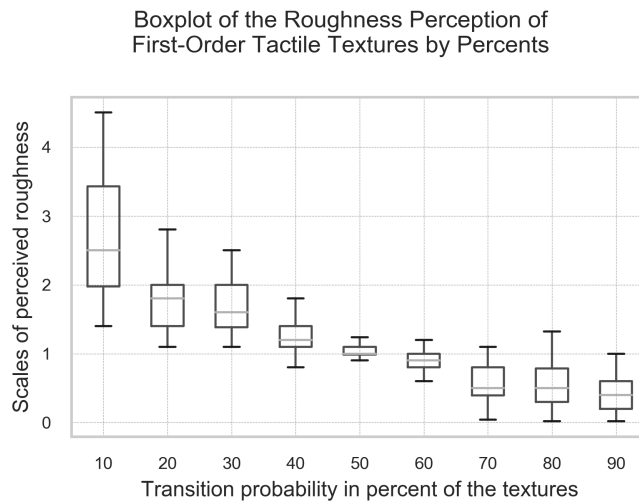


Figure 3.26: The boxplot of subjective scale for each of first-order tactile texture. The horizontal axis is the category of textures with each point indicates the percentage of the transient probabilities of the corresponding texture. The vertical axis is the scales of the perceived magnitude of the textures.

The decreasing pattern of subjective scales can also be seen from the plot of

the subjects' response itself as shown in Figure 3.27. Despite having different start points, all line plots of the subjects' responses looks to have the same decreasing pattern. From this figure, it can be seen that the spread of the response of texture-10 is the largest. Then, the response' spread becomes narrower as the transition probability of the textures increases. In other perspective, the bigger the roughness difference from the texture, the wider the spread of the response. It indicates that subjects had more difficulties to assign the specific scale for the texture which has a big roughness different from the reference.

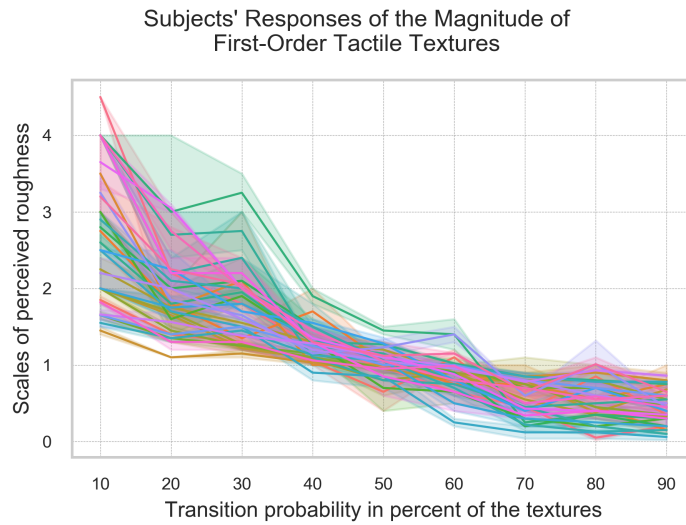


Figure 3.27: Subjects' roughness sensation on the tactile textures with first-order statistics. The horizontal axis is the category of textures with each point indicates the percentage of the transient probabilities of the corresponding texture. The vertical axis is the scales of the perceived magnitude of the textures.

Although it relatively obvious that all lines in Figure 3.27 have the same direction which is decreasing, it is still important to check whether there is any line with different orientation such as horizontal. This type of line can show the presence of different perspective of roughness perception by the subjects. The direction of those plotted lines in Figure 3.27 can be estimated using the correlation between the transition-probability of the textures and the roughness responses of each subject as shown in Figure 3.28. From this image it can be seen that all subjects have high negative correlations ( $-0.75$  to  $-1.0$ ) for their responses. It means that the line plots of all subjects' responses have negative slopes. This also means that the roughness of the first-order statistical visual textures were perceived to get lower as the percentage of the transition probability increases.

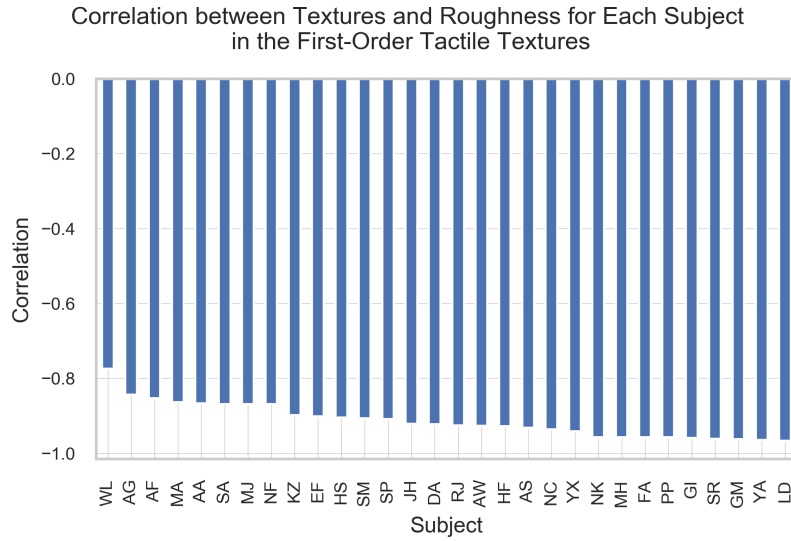


Figure 3.28: The correlation between transition probabilities of the first-order tactile textures and the perceived scales of their roughness for each subject. The subject with positive correlation means he/she perceived the the roughness scale to increase as the transition probability increases. Zero correlation indicates the roughness perception is either constant, concave or convex. Negative correlation indicate the roughness perception decreases

Table 3.11: ANOVA Test for First-Order Tactile Textures: Between Subjects

Source	SS	DF	MS	F	Pr(>F)	EtaSq
SUBJECT	22.343	29	0.770	1.075	.363	0.058
Within	365.404	510	0.716	-	-	-

To identify more thoroughly whether there is any difference of subjects' perspective of the first-order tactile textures or not, an ANOVA analysis was then performed. The output is shown in Table 3.11. This table shows that the value of  $F(29, 510)$  equals to 1.075 which, therefore, refers to a significance value ( $p$ ) of .363 which is significantly larger than .05 and it indicates that subjects have no different pattern of roughness perception even though the variance of the roughness scales from each subject contributes 5.8% to the total variance (*EtaSq*) which is medium (Table 3.3). However, compared to the variance contribution by the textures which is 71.6% (Table 3.10), the variance by subjects is significantly smaller. This indicates that the textures them self give more effect to the pattern of the roughness response than the subjects which, therefore, supports an indication that each texture has a different roughness scale.

To fit the relationship between the textures and the roughness responses, four polynomial functions were used. The plot of those functions is presented in Figure 3.29. All of the response data were used get the best fit. However, in

this figure, the responses of the roughness scales are represented by their mean value for each texture (red dots). Four polynomial functions that were used to fit their roughness responses show that it is sufficient to use the second degree of polynomial function. Higher than that degree, beside the  $R^2$  values does not improve significantly, the function may also tend to overfit the roughness data. The roughness scale decreases significantly especially at the beginning. This result is in line with the correlation between the roughness and the textures of most of the subjects which are highly negative (Figure 3.27).

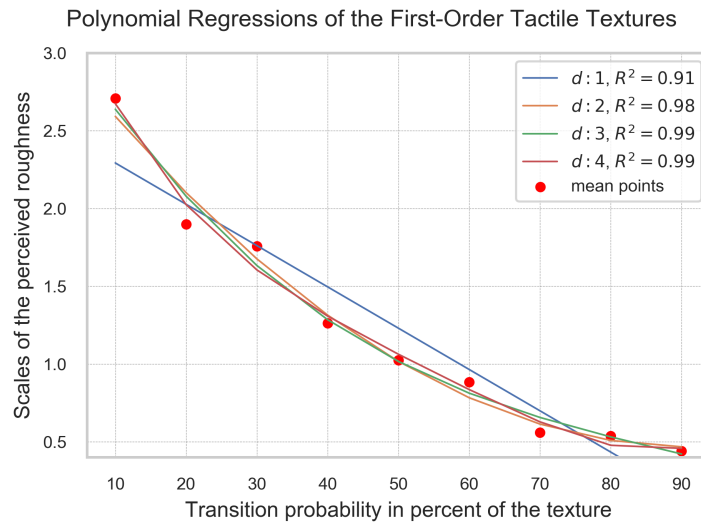


Figure 3.29: Polynomial regressions of the perceived roughness of the tactile textures with first-order statistics. The red scattered dots are the mean of the roughness of each texture. There are four polynomial functions with different degrees to fit.

## Second-order tactile textures

In the second-order tactile textures, subjects were able to recognize and to discriminate all the test textures from the reference texture (texture-50) as shown by Table 3.12. This table presents the output of the ANOVA analysis. It shows whether there is a statistically significant difference between texture groups in their mean of subjective scales. It is seen in the table that the value of  $F(8, 531)$  equals to 11.708 which will give a significance value ( $p$ ) of .000 that is significantly smaller than .05 and, therefore, the null hypothesis that there is no difference between group means is rejected. The variance of the texture contributes 15% to the total variance ( $EtaSq$ ) which is large. This result suggests that the subjective scales of the roughness magnitude is different for each texture.

Table 3.12: ANOVA Test for Second-Order Tactile Textures: Between Textures

Source	SS	DF	MS	F	Pr(>F)	EtaSq
TEXTURE	6.187	8	0.773	11.708	.000	0.15
Within	35.075	531	0.066	-	-	-

Furthermore, the difference of the subjective scales for all the second-order statistical tactile textures can be investigated in more detail from the means comparison of the subjective scales of each texture group. A pairwise comparisons test based on Tukey-HSD method was used to analyse the means' difference of the subjective scale between the texture groups. The result is shown in Table D.5 and in Figure 3.30. It can be seen that the difference (diff) between the means of the roughness scales of neighbouring textures is not significant as their respective significant value (p-Tukey) equals to or more than .05 (null hypothesis is accepted). It is seen that the first five textures have no significant different in the scales' mean. The jump of the roughness scale happens at texture-60 which has the mean of roughness significantly different from its four preceding textures. Texture-80 and texture-90 were perceived to be very similar to texture-60 as the significance value (p-Tukey) of their mean differences is 0.9. However, at texture-70, the roughness scale decreases again as seen from the its negative mean difference (diff) with its neighbouring textures (Table D.5). It gives an impression that the roughness scale is constant at the beginning and then increases suddenly from texture-60.

The more obvious pattern of the roughness perception can be seen from the boxplot in Figure 3.31. It shows that the level of medians of the roughness scale for texture-10 to texture-60 slightly increases. The median decreases at texture-70. For the last two textures, however, the roughness scale slightly increases again and reach at the same level as texture-60's level. Therefore, it seems that texture-60, texture-80, and texture-90 have the same roughness. Figure 3.31 also shows that the variance of the first five textures are relatively the same. This usually happens in the textures whose the roughness gaps is not significant. The variance of the roughness scales of texture-60, texture-80, and texture-90 are seen to be the widest. This usually happens when the roughness of the texture has a significant difference from the reference's roughness.

The increasing pattern of subjective scales can also be seen from the plot of the subjects' response as shown in Figure 3.32. From this figure, it can be seen that the spread of the responses for each texture is the same. In general, the pattern of the response increases even though at texture-70 it is seen that the

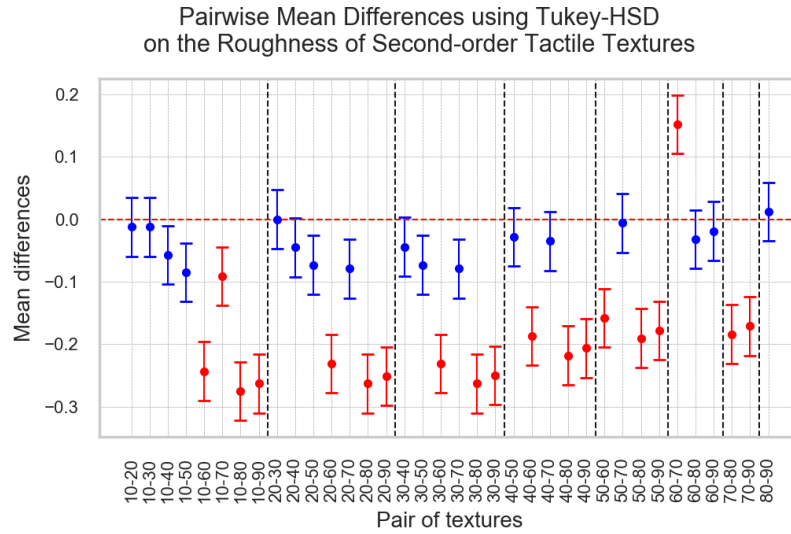


Figure 3.30: Multiple comparisons of the scales' means of the perceived roughness between all pairs of the second-order tactile textures. The blue error bars indicate that the difference of scales' means for the corresponding pair is not statistically significant ( $p\text{-Tukey} \geq .05$ ). If the error bar is red, the scales' means for the corresponding pairs is statistically significant ( $p\text{-Tukey} \leq .05$ ).

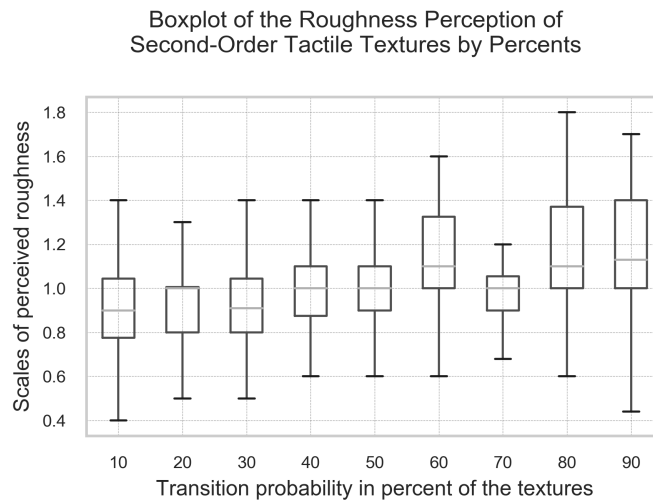


Figure 3.31: The boxplot of subjective scale for each of second-order tactile texture. The horizontal axis is the category of textures with each point indicates the percentage of the transient probabilities of the corresponding texture. The vertical axis is the scales of the perceived magnitude of the textures.

pattern decreases. However, the line plot of each subject's responses is seen to cross each other. It makes difficult to know whether each subject has different pattern of perception or not.

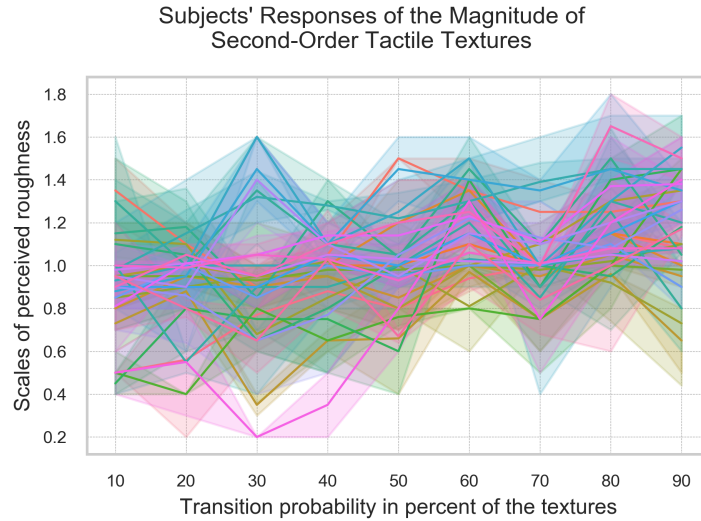


Figure 3.32: Subjects' roughness sensation on the tactile textures with second-order statistics. The horizontal axis is the category of textures with each point indicates the percentage of the transient probabilities of the corresponding texture. The vertical axis is the scales of the perceived magnitude of the textures.

However, the direction of those plotted lines in Figure 3.32 can be estimated using the correlation between the transition-probability of the textures and the roughness responses of each subject as shown in Figure 3.33. From this image it can be seen that 30% of subjects have high positive correlations (ranges from 0.75 to 1.0) for their responses. It means that the line plots of those subjects' responses have positive slopes which indicates that their roughness perception increases as the percentage of the transition probability increases. Furthermore, more than 50% of subjects also have positive correlations although they are lower than 0.5. Only 10% of subjects (three peoples) have negative correlations. However, those correlation is very low (less than 0.3).

An ANOVA analysis was then performed to identify thoroughly whether the difference between subjects' responses of the second-order tactile textures is significant or not. The output is shown in Table 3.13. This table shows that the value of  $F(29, 510)$  equals to 6.008 which, therefore, will give a significance value ( $p$ ) of .000 which is significantly smaller than .05 and it indicates that subjects have different patterns of the roughness perception. However, as the correlations between textures and the roughness scales are mostly positive (Figure 3.33), the identified difference of the subjects' responses comes from the difference slopes of each subject's response.

The variance of the roughness scales from each subject contributes 25.5% to



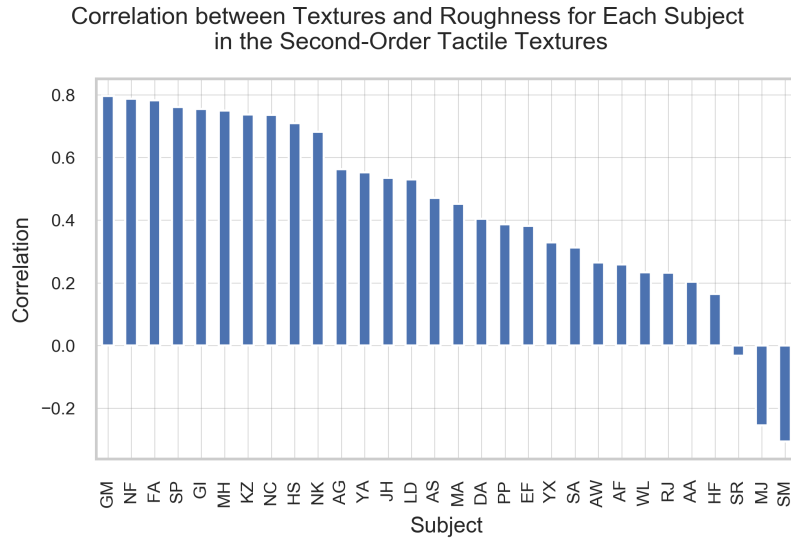


Figure 3.33: The correlation between transition probabilities of the second-order tactile textures and the perceived scales of their roughness for each subject. The subject with positive correlation means he/she perceived the the roughness scale to increase as the transition probability increases. Zero correlation indicates the roughness perception is either constant, concave or convex. Negative correlation indicate the roughness perception decreases

Table 3.13: ANOVA Test for Second-Order Tactile Textures: Between Subjects

Source	SS	DF	MS	F	Pr(>F)	EtaSq
SUBJECT	10.507	29	0.362	6.008	.000	0.255
Within	30.754	510	0.060	-	-	-

the total variance (*EtaSq*) which is considerably large (Table 3.3). Compared to the variance contribution by the textures which is 15.0% (Table 3.10), the variance by subjects is also significantly larger. It indicates that the subjects' variance give more effect to the pattern of the roughness response than the textures' variance. This usually will happen when the roughness gap between textures is not too contrast.

To predict the relationship between the second-order statistical tactile textures and the roughness responses, four polynomial functions were used to fit the roughness data. The plot of those functions is presented in Figure 3.34. All of the response data were used get the best fit. However, in this figure, the responses of the roughness scales are represented by their mean value for each texture (red dots). Four polynomial functions that were used to fit their roughness responses show that it is sufficient to use the first degree of polynomial function (linear plot). Higher than that degree, beside the  $R^2$  values does not improve significantly, the function may also tend to overfit the roughness data. As it is seen

in the figure, the subjective roughness tends to slightly increase linearly as the transition of the probability increases. This result is in line with the correlation between the roughness and the textures of most of the subjects which are positive (Figure 3.32).

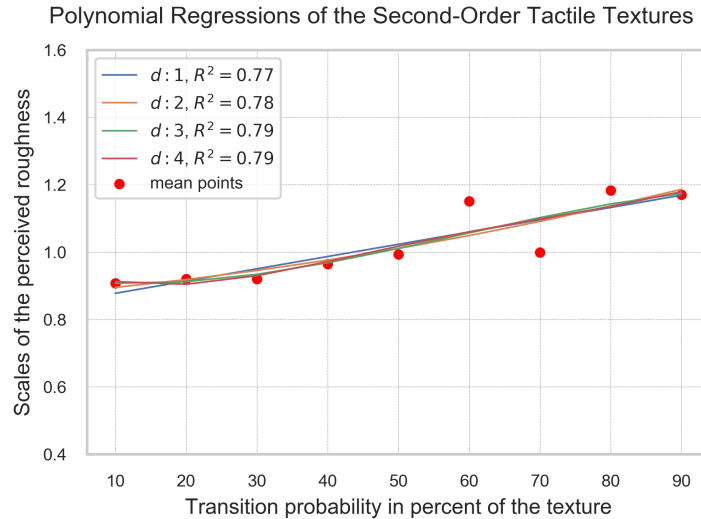


Figure 3.34: Polynomial regressions of the perceived roughness of the tactile textures with second-order statistics. The red scattered dots are the mean of the roughness of each texture. There are four polynomial functions with different degrees to fit.

### Third-order tactile textures

In the third-order statistical tactile textures, subjects seem to be able to recognize and to discriminate all the test textures from the reference one. As it can be seen in Figure 3.8, the plot of the subjects' responses of the third-order textures slightly increases until it reaches the peak point at texture-50 and then decreases. To identify whether the responses for each texture are different or not an ANOVA analysis was performed. The result is presented in Table 3.7. This table shows that the value of  $F(8, 531)$  equals to 14.933 which, therefore, will give a significance value ( $p$ ) of .000 which is significantly smaller than .05. This result indicates that the means of the subjective scales of each texture are not the same. The variance of the textures contributes 18.4% to the total variance ( $EtaSq$ ) which is large (Table 3.3). This result implies that the third-order tactile textures were perceived to be different.

The difference of the roughness scales for all the third-order statistical tactile textures can be investigated in more detail from the means comparison of the

Table 3.14: ANOVA Test for Third-Order Tactile Textures: Between Textures

Source	SS	DF	MS	F	Pr(>F)	EtaSq
TEXTURE	11.045	8	1.381	14.933	.000	0.184
Within	49.095	531	0.092	-	-	-

subjective scales of each texture group. A pairwise comparisons test based on Tukey-HSD method was used to analyse the means' difference of the subjective scale between the texture groups. The result is shown in Table D.6 and in Figure 3.35. It can be seen that the difference (diff) between the means of the roughness scales of neighbouring textures is not significant except between the response mean of texture-60 and the response mean of texture-70. The roughness scales of texture-10 to texture-60 are not significantly different. All p-Tukey values of the means difference (diff) among those textures is more than .50. The response decreases considerably from texture-60 to texture-70 as it can be seen from its significant p-Tukey value in Table D.6. It is also seen that the last three textures have significantly similar roughness. This result gives an impression that the roughness scale is constant and then suddenly decreases at texture-70.

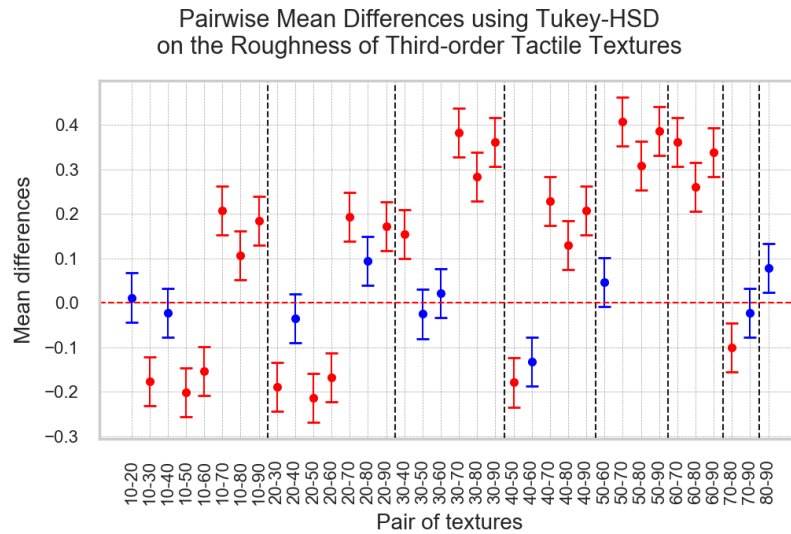


Figure 3.35: Multiple comparisons of the scales' means of the perceived roughness between all pairs of the third-order tactile textures. The blue error bars indicate that the difference of scales' means for the corresponding pair is not statistically significant ( $p\text{-Tukey} \geq .05$ ). If the error bar is red, the scales' means for the corresponding pairs is statistically significant ( $p\text{-Tukey} \leq .05$ ).

The roughness pattern can be seen more clearly from the boxplot in Figure 3.36. This plot shows that the level of medians of the roughness scale slightly in-

creases along texture-10 to texture-50. The median decreases slightly at texture-60 and significantly decreases at texture-70. For the last three textures, however, the roughness scale is the same. It is seen in Figure 3.36 that the variance of the roughness scales of all textures is not significantly different. This will usually happen when the roughness difference is not too large.

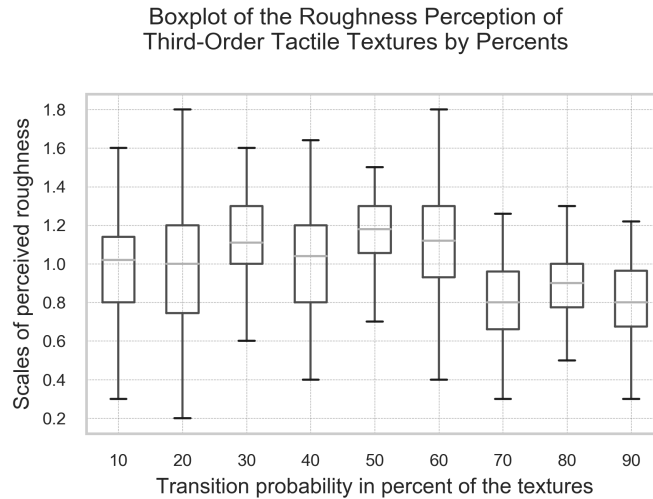


Figure 3.36: The boxplot of subjective scale for each of third-order tactile texture. The horizontal axis is the category of textures with each point indicates the percentage of the transient probabilities of the corresponding texture. The vertical axis is the scales of the perceived magnitude of the textures.

The pattern of the roughness perception of the third-order statistical tactile textures can also be seen from the plot of the subjects' response as shown in Figure 3.37. From this figure it is seen that the line plots of the subjects' response form a constant from pattern. The response looks slightly decreasing from texture-60 to texture-70 and then is constant again. Two considerably high response roughness appear at texture-50 and texture-60. These responses make the mean of the roughness scale of both textures increase significantly. However, in general, from this figure, it can also be seen that the spread of the responses for each texture is relatively the constant.

Because the line plots of some subject's responses in Figure 3.37 are seen to cross each other and are not always linear, it suggests that there are different patterns of perception among subjects. The direction of those plotted lines in Figure 3.37 can be estimated using the correlation between the transition-probability of the textures and the roughness responses of each subject as shown in Figure 3.38. From this image it can be seen that 90% of the subjects have negative correlations

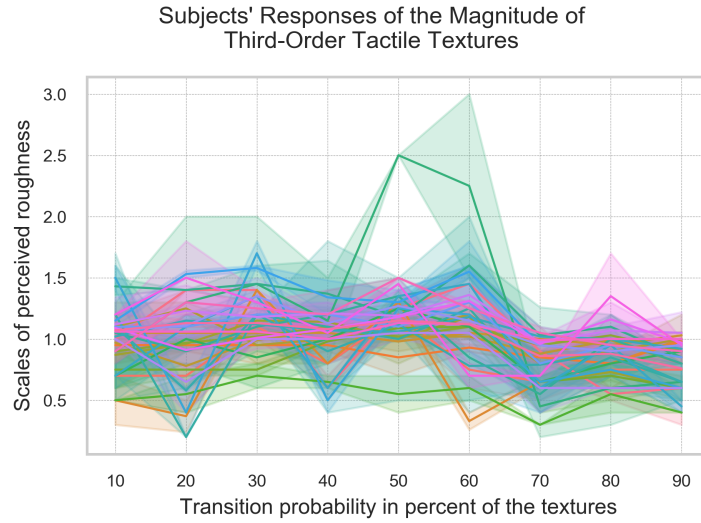


Figure 3.37: Subjects' roughness sensation on the tactile textures with third-order statistics. The horizontal axis is the category of textures with each point indicates the percentage of the transient probabilities of the corresponding texture. The vertical axis is the scales of the perceived magnitude of the textures.

Table 3.15: ANOVA Test for Third-Order Tactile Textures: Between Subjects

Source	SS	DF	MS	F	Pr(>F)	EtaSq
SUBJECT	12.379	29	0.427	4.558	.000	0.206
Within	47.761	510	0.094	-	-	-

for their responses. It means that the line plots of those subjects' responses have negative slopes which indicates that their roughness perception decreases as the percentage of the transition probability increases. However, only less than 14% of the subjects have moderate negative correlations. More than 86% of the subjects have low to negligible correlations. This result indicates that the roughness is independent of textures in almost all subjects. However, as seen in Figure 3.37 that the correlation between roughness and textures in every subject is different, each subjects will be identified as to have a unique pattern of roughness perception.

To identify more thoroughly whether there is any difference of subjects' perspective of the first-order tactile textures or not, an ANOVA analysis was then performed. The output is presented in Table 3.15. This table shows that the value of  $F(29, 510)$  equals to 4.558 which, therefore, will give a significance value ( $p$ ) of .000 which is significantly smaller than .05 and it indicates that subjects have different patterns of the roughness perception.

The variance of the roughness scales from each subject contributes 20.6% to the total variance ( $EtaSq$ ) which is considerably large (Table 3.3). Compared

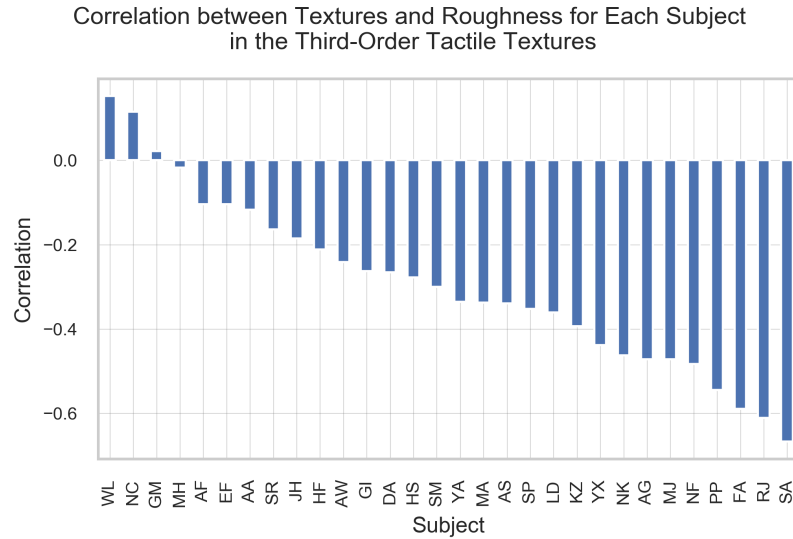


Figure 3.38: The correlation between transition probabilities of the third-order tactile textures and the perceived scales of their roughness for each subject. The subject with positive correlation means he/she perceived the the roughness scale to increase as the transition probability increases. Zero correlation indicates the roughness perception is either constant, concave or convex. Negative correlation indicate the roughness perception decreases

to the variance contribution by the textures which is 18.4% (Table 3.14), the variance by subjects is also larger. It indicates that the subjects' variance give more effect to the pattern of the roughness response than the textures' variance. This usually will happen when the roughness gap between textures is not too contrast.

To predict the relationship between the third-order statistical tactile textures and the roughness responses, four polynomial functions were used to fit the roughness data. The plot of those functions is presented in Figure 3.39. All of the response data were used get the best fit. However, in this figure, the responses of the roughness scales are represented by their mean value for each texture (red dots). Four polynomial functions that were used to fit their roughness responses show that it is sufficient to use the second degree of polynomial function. Higher than that degree, beside the  $R^2$  values does not improve significantly, the function may also tend to overfit the roughness data.

However, its  $R^2$  value which is 0.57 indicates that only 57% perceived roughness can be correctly predicted by the model. This result shows that the perceived roughness of third-order statistical tactile textures is difficult to predict. As the arithmetic average roughness ( $R_a$ ) of this type of textures are the same and the surface of specimens is similar, it is most likely that the friction between the

surfaces and the fingerpad determined the perceived roughness. In this case, the friction is influenced by the pressure of the finger applied on the surface. When two surfaces seem similar, some subjects tried to explore their roughness by applying higher pressure onto the surfaces. This may result in different friction and distinctive perceived roughness although they have similar surfaces.

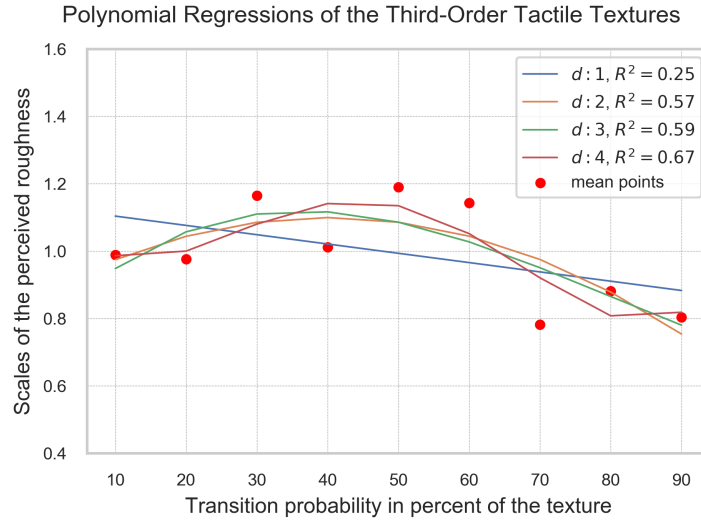


Figure 3.39: Polynomial regressions of the perceived roughness of the tactile textures with third-order statistics. The red scattered dots are the mean of the roughness of each texture. There are four polynomial functions with different degrees to fit.

### 3.3.3 Comparison between the roughness scales of the visual and the tactile textures

As it has been discussed in the previous section, the result of the experiment shows that there are some similarities between the roughness perception of the visual and the tactile textures. Each texture in the first-order statistical visual and tactile groups can be discriminated. Moreover, the roughness scales of the first-order statistical visual and tactile textures are relatively the same. They decrease as the transition probability of the texture increases. In the second-order groups, each texture is still can be discriminated. However, the subjects could discriminate the visual textures better than the tactile textures. The roughness scales in both type of textures increase, although in the visual textures, the increase is sharp while in the tactile textures is not. In third-order groups, the visual textures could not be discriminated while the tactile textures seems to be discriminated slightly.

Table 3.16: Correlation between Roughness and Textures of the Visual and Tactile First-Order Textures

Experiment	level_1	textures
visual	roughness	-0.427
tactile	roughness	-0.809

### First-order statistical textures

The correlation between the transition probability of the textures (textures) and the roughness scales (roughness) of the first-order visual textures is lower than the same correlation of the first-order tactile textures (Table 3.16). The roughness perception of the first-order visual textures has different perspective. In this group, each particular texture can be perceived oppositely, some subjects assigned lower roughness scales than the reference ( $< 1.0$ ) and some subjects assign higher scales ( $> 1.0$ ). As the effect, the mean of the roughness scales of the first-order visual textures become not far to one which indicates that they were not significantly different from the reference (see Figure 3.40) despite the fact that subjects could easily discriminated the textures and assigned significant scales to them. This result also makes the variance of the roughness response become relatively high and as a consequence, the correlation between the roughness and the textures becomes low ( $-0.43$ ).

This kind of different perspectives did not happen in the tactile textures. There was no ambiguity of roughness sensation when it comes from tactile textures. The roughness of each texture was perceived consistently and significantly different from the roughness of the reference texture as seen in Figure 3.40. For example, the roughness mean of the first tactile texture (the first blue dot) is 2.5 which is almost a double of the roughness mean of the first visual texture (the first red dot). Therefore, the correlation between the roughness and the texture of these tactile textures becomes relatively high ( $-0.809444$ ).

The roughness responses of the tactile textures decrease sharply at the beginning (Figure 3.40). They can be best fitted by the second degree of polynomial function (the blue line). Meanwhile, the roughness responses of the visual texture decrease slowly at the beginning. A third degree polynomial is the best fit for these responses (the red line).

Although the roughness responses of both texture types are different, they have at least two similarities. The first, both of the could be discriminated relatively easily by the subjects. The second, the roughness perception of both types of textures has the same decreasing pattern as it can be seen from the roughness



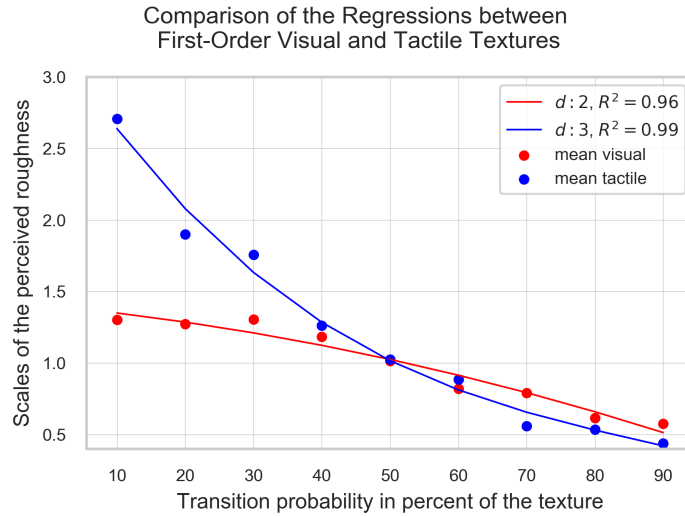


Figure 3.40: Polynomial regressions of the perceived roughness of the first-order statistical visual and tactile textures. The red scattered dots are the mean of the roughness of the visual textures and the blue scattered dots are the mean of the roughness of the tactile textures.

Table 3.17: Sepherd's Pi Correlation between Visual and Tactile Textures with First-Order Textures

n	r	CI 95%	r2	adj_r2	p-val	power
540	0.407	[0.33, 0.47]	0.165	0.162	.000	1.0

correlation between both textures (Table 3.17). This correlation, although it is considerably low, has a positive value which indicates that both texture have patterns of the roughness perception with the same direction (they decrease).

### Second-order statistical textures

There was no ambiguity of roughness sensation for second-order statistical textures in both the visual and the tactile perceptions. Each particular texture was perceived consistently. The textures with transition probability which is lower than 50% were perceived to have a relatively lower scale of roughness (less than 1.0). Meanwhile, the textures with higher transition probability were perceived to be rougher.

Table 3.18: Correlation between Roughness and Textures of the Visual and Tactile Second-Order Textures

Experiment	level_1	textures
visual	roughness	0.521183
tactile	roughness	0.340053

Table 3.19: Sepherd's Pi Correlation between Visual and Tactile Textures with Second-Order Textures

n	r	CI 95%	r2	adj_r2	p-val	power
540	0.175	[0.09, 0.26]	0.031	0.027	.000	0.984

However, the second-order visual textures were more discriminable than the tactile textures as the correlation between the roughness and the textures of the visual textures is higher (Table 3.18). The correlation is 0.52 which is moderate positive. This value is higher than the same correlation of the tactile textures (0.34). The correlation value is also related to the increase rate of the roughness perception as it can be seen in Figure 3.41. This figure shows that the increase of the roughness perception in visual textures is higher (the red line) than the increase in tactile textures (the blue line).

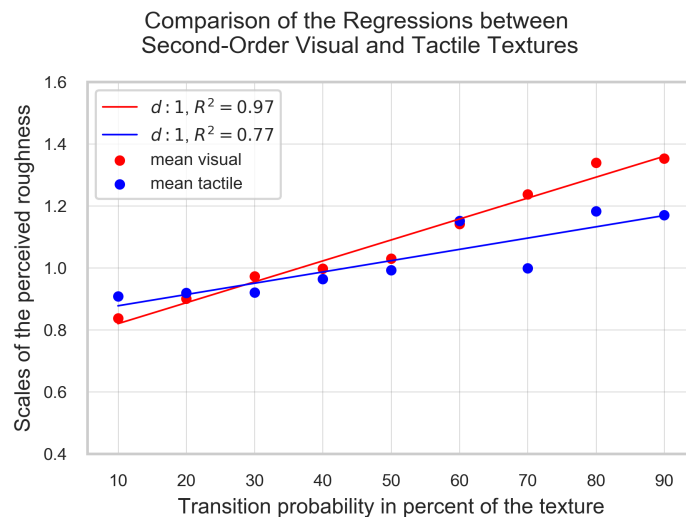


Figure 3.41: Polynomial regressions of the perceived roughness of the second-order statistical visual and tactile textures. The red scattered dots are the mean of the roughness of the visual textures and the blue scattered dots are the mean of the roughness of the tactile textures.

The obvious similarity between the visual and tactile textures which have second-order statistical pattern is that their roughness scale increases and can be fitted well by using linear functions (Figure 3.41). Although the roughness' correlation between the visual and the tactile textures is low (Table 3.19), it still can give an indication that both types of textures have the same direction of roughness perception as the value is positive.

Table 3.20: Correlation between Roughness and Textures of the Visual and Tactile Third-Order Textures

Experiment	level_1	textures
visual	roughness	-0.020
tactile	roughness	-0.214

### Third-order statistical textures

The correlation between the textures and the perceived roughness of the third-order visual textures is very low (Table 3.20). It is only  $-0.020$  which, therefore, is negligible. As it can also be seen from Figure 3.42, the regression plot of the perceived roughness of the visual textures is a relatively horizontal line although it is a third degree of polynomial and its  $R^2$  value is small. These results indicate that all second-order visual textures have a similar roughness. In other words, these visual textures were not discriminated.

The same correlation in the second order-tactile textures is ten times larger (Table 3.20). However, it is still considerably low which indicates that the relationship between textures and their perceived roughness is weak. The regression which best to describe this relationship is a second degree of polynomial function (Figure 3.42). However, the  $R^2$  value is only 0.57 which indicates that only 57% of the perceived roughness is correctly predicted by the function.

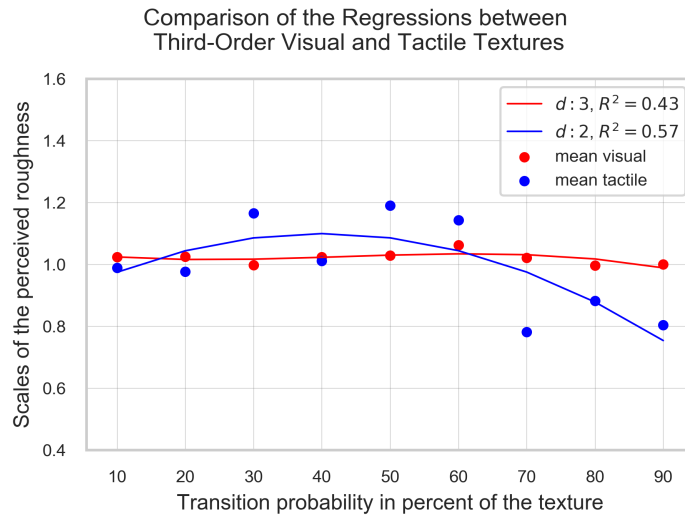


Figure 3.42: Polynomial regressions of the perceived roughness of the third-order statistical visual and tactile textures. The red scattered dots are the mean of the roughness of the visual textures and the blue scattered dots are the mean of the roughness of the tactile textures.

Although the perceived roughness of the third-order visual and tactile textures

Table 3.21: Sepherd’s Pi Correlation between Visual and Tactile Textures with Third-Order Textures

n	r	CI 95%	r2	adj_r2	p-val	power
540	0.042	[-0.04, 0.13]	0.002	-0.002	.344	0.163

seems to have different patterns, each of them have a relatively low correlation with the textures which indicates that the perceived roughness of the third-order visual and tactile textures cannot be discriminated.

### 3.4 Conclusion

The first-order textures are discriminable. However, the perception is quite ambiguous; subjects perceived differently for the roughness of each particular texture. The second-order image textures are also discriminable. This result shows that the images with coarser dots pattern are perceived to have higher roughness although they have the same proportion of the black and white dots. This result aligns with Julesz’s finding Julesz [240, page 86] which mentioned that the subjective impression of second-order textures might be regarded as a difference in granularity which make this type of textures are easy to be discriminated. The third-order image textures are not distinguishable. This result conforms with Julesz’s conjecture [240].

The first-order tactile texture are very well discriminable. As opposed to the visual perception, the roughness perception of the tactile textures is not ambiguous. The subjective magnitudes are convincingly to be monotonically decreasing. The textures with sparse particles are perceived to have rougher surfaces than the textures with sparse grooves. Furthermore, narrow grooves are not detectable by the fingerpads.  $R_a$  values can not describe the perceived roughness although some researches reported otherwise. These results indicate that the perceptions of roughness on image and tactile stimuli that have first-order statistical pattern have different mechanism. The roughness perception of tactile stimuli is more straightforward and less ambiguous than the roughness perception of visual stimuli.

Unlike the second-order visual textures, the corresponding tactile textures were barely discriminable. Here, the visual perceptions seems better in discriminating the textures. However, the textures with coarse fibres were perceived to be rougher in both visual and tactile roughness perceptions. This result conform with the report that sandpapers with coarser particles are perceived to be rougher

than sandpapers with finer particles. In this case, the Gestalt connectivity theory prevails in tactile texture perception. The textures with more connected boxels (fibrous textures) are discriminable from the textures with less connected boxels (non-fibrous textures).

The third-order tactile textures were not discriminable just like the corresponding image textures. This is may due to the fact that these textures are almost identical because they have the same actual roughness and indistinguishable boxels's patterns. However, the third-order visual textures were even more indistinguishable. The visual perception here is sharper in recognizing the textures. Textures which have a similar pattern will be perceived to have the same roughness. Meanwhile, the roughness perception is not as sharp as visual perception in recognizing such a similar textures.

The overall result suggests that both roughness perceptions on the visual and the tactile stimuli have different mechanisms. However, they have a similar pattern in perceiving the size of the grains or particles. The surface with coarse grains have rougher sensation in both visual and tactile perceptions. The perceived roughness of the tactile textures depends more on the spread and the size of particles rather than particle orientation.

# Chapter 4

## The Influence of Magnitude and Phase Spectra in the Discrimination of Images

### 4.1 Experiment Rationale

Scientists have been investigating for centuries of how humans perceive visual stimuli [273]. One of the main goals of such studies is to build a machine which can see. As machines only understand mathematical languages, researchers have been trying to relate computational models of images with the corresponding human perceptions.

In the spatial domain, a greyscale image can be represented by a two-dimensional (2D) matrix  $A[m, n]$  with size  $M \times N$ , where  $m \in [0, M - 1]$  and  $n \in [0, N - 1]$ . Each element at row  $m$  and column  $n$  in  $A_{m,n}$  represents a pixel's value  $f[m, n]$  of the image which is an integer between 0 to 255.

In studies of visual perception, it is common and acceptable to represent an image  $A[m, n]$  in the domain of spatial frequency  $\alpha_{u,v}$  in which  $u \in [0, N - 1]$  and  $v \in [0, M - 1]$  [274]. Each element in 2D matrix  $\alpha_{u,v}$  is a complex number  $F[m, n]$  which is the Fourier Transform (FT) of the image  $f[m, n]$ .

$$F[u, v] = \frac{1}{NM} \sum_{m=0}^{M-1} \sum_{n=0}^{N-1} f[m, n] e^{-2\pi j(\frac{um}{N} + \frac{vn}{M})} \quad (4.1)$$

The final result of this equation will be in the form:

$$F[u, v] = |F[u, v]| \times e^{-j\phi[u, v]} \quad (4.2)$$

where  $|F[u, v]|$  is the magnitude and  $\phi[u, v]$  is the phase of  $F[u, v]$ . The original image can be retrieved from each element of its FT matrix  $\alpha_{u,v}$  using the inverse

transform operation as follow:

$$f[m, n] = \frac{1}{NM} \sum_{m=0}^{M-1} \sum_{n=0}^{N-1} |F[u, v]| \times e^{j[\phi[u, v] + 2\pi(\frac{um}{N} + \frac{vn}{M})]} \quad (4.3)$$

Using combinations of the magnitudes and the phases of Fourier Transforms of any of two images  $f_1(x, y)$  and  $f_2(x, y)$  other two child images can be generated. Firstly, determine the Fourier Transform of both parent images (Equation 4.4).

$$\begin{aligned} \mathcal{F}(f_1(x, y)) &= F_1(u, v) = R_1(u, v) \times e^{-j\phi_1(u, v)} \\ \mathcal{F}(f_2(x, y)) &= F_2(u, v) = R_2(u, v) \times e^{-j\phi_2(u, v)} \end{aligned} \quad (4.4)$$

From both parent images, then two derivative images which are represented by  $f_{12}(x, y)$  and  $f_{21}(x, y)$  can be created by swapping either the magnitudes or the phases of their parents as follows:

$$\begin{aligned} f_{12}(x, y) &= \mathcal{F}^{-1}[R_1(u, v) \times e^{-j\phi_2(u, v)}] \\ f_{21}(x, y) &= \mathcal{F}^{-1}[R_2(u, v) \times e^{-j\phi_1(u, v)}] \end{aligned} \quad (4.5)$$

Many researches had reported that the phase is more important than the magnitude in image reconstruction. It means that the image  $f_{12}$  will be more likely to be perceived as similar to image  $f_2$ , and image  $f_{21}$  will be more similar to image  $f_1$  (Figure 4.1). Kermisch [275] and Oppenheim and Lim [195] argued that it is possible to retrieve an image from its phase component. Huang et al. [196] showed that phase is very important in image processing filter. From a statistical point of view, Ni and Huo [209] showed that small changes in phase will distort the retrieved image significantly while small difference in magnitude will not. Piotrowski and Campbell [194] tried to measure the effect of the quantization of the phase's values to the visual recognition. They reported that even two levels of quantization still produce a retrieved image which is recognizable. However, surprisingly, some quantization levels of phase can hinder the retrieved image to be recognized and how it happens has not been explained.

Although most of works have shown that phase is more important than magnitude, some of them reported otherwise. In some cases, the magnitude is more dominant than the phase (Figure 4.2). Some argued that there is no clear explanation of how phase is more important than magnitude [223]. Gladilin and Eils [274] argued that phase is not the only cognitive features of visual stimuli. Zhang et al. [276] suggested that only the phase that discriminates coarse orientations is essential in image recognition.

Despite a huge number of researches in the phase and the magnitude dominance, only a few attempts have been made to measure quantitatively the influence or the dominance of the magnitude or the phase using the Fourier spectra

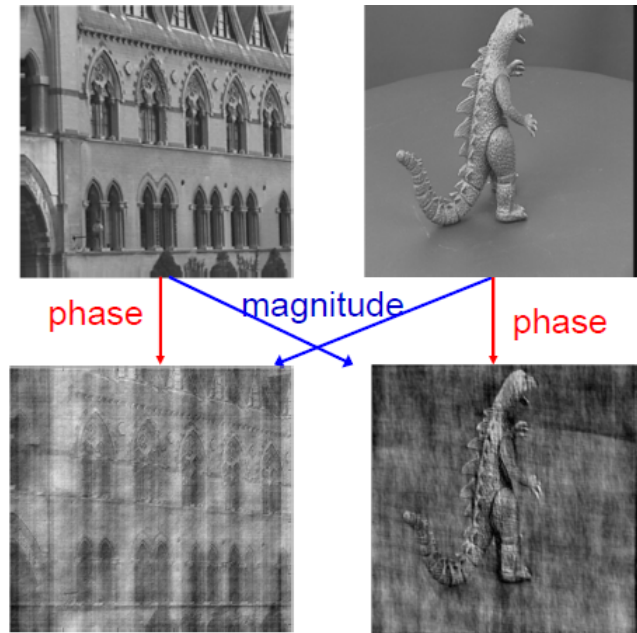


Figure 4.1: Phase components have more influence to image recognition (Zisserman, 2014).

of the image itself. The present study aims to investigate the influence of each Fast Fourier Transformation (FFT) component of images to the visual object recognition. In this experiment, the circumstances in which the two components dominate each other will be determined. This experiment is intended to

1. measure and compare the contribution of phase and magnitude components to the phase's and magnitude's dominance,
2. determine the relationship between phase and magnitude components on visual perception.

## 4.2 Method

### 4.2.1 Stimuli

There were four types of stimuli used in this experiment. They were sawtooth, sinusoidal, square, and triangle which are coded as saw, sin, squ, and tri respectively (Figure 4.3). There are three reasons of why these types of basic signal were chosen. The first, signals are relatively unusual to the subjects; therefore they will not have any pre-conception about the image similarity. These types of signals make all subjects naive to the images and reduce the subjectivity bias.



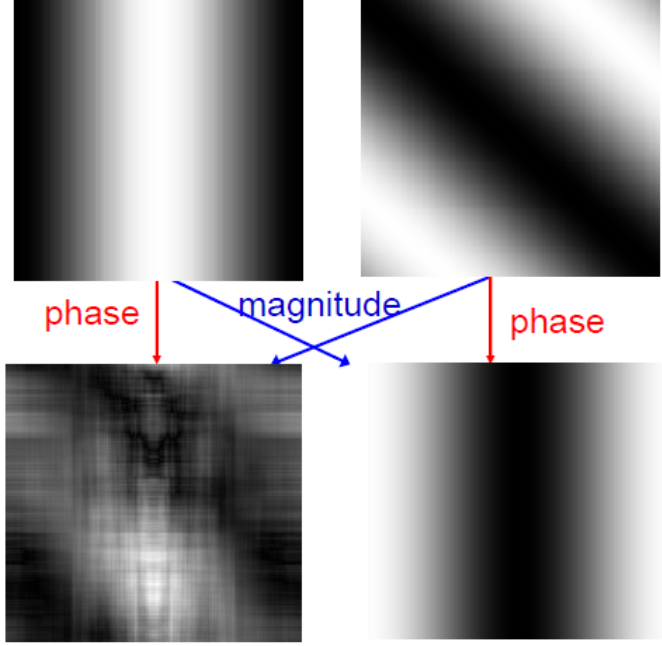


Figure 4.2: Magnitude component seems to have more influence to image recognition.

Table 4.1: Two-Dimensional Functions of each Type of the Image Stimuli

No	Type	$f(x, y) \mid x, y \in [0, N]$
1	Sin	$f(x, y) = A \cdot \sin\left(\frac{2\pi f}{N}(x \cos \Phi + y \sin \Phi)\right)$
2	Triangle	$f(x, y) = 2A \cdot \left  \frac{f(x \cos \Phi + y \sin \Phi)}{N} - \left\lfloor \frac{f(x \cos \Phi + y \sin \Phi)}{N} - \frac{1}{2} \right\rfloor \right $
3	Square	$f(x, y) = \frac{A}{2} + \frac{A}{2} \cdot \text{sign}\left(\sin\left(\frac{2\pi f(x \cos \Phi + y \sin \Phi)}{N}\right)\right)$
4	Sawtooth	$f(x, y) = A \cdot \left( \frac{f(x \cos \Phi + y \sin \Phi)}{N} - \left\lfloor \frac{f(x \cos \Phi + y \sin \Phi)}{N} \right\rfloor \right)$

Note:

In this case  $A = 255$ ,  $N = 420$ ,  $f = 1, 3, 9$  and  $\Phi = 0, 0.25\pi, 0.5\pi$ .

However, the sketchy pattern of the parent images still allow the subjects to recognize them pre-attentively. Second, as they are basic signals, their characteristic will be more easy to measure. Third, the parameters of these types of signals are easy to adjust.

The mathematical functions of these image stimuli are listed in Table 4.1. The size ( $M \times N$ ) of the images is 420 pixels  $\times$  420 pixels. Each type of image was varied in term of frequency ( $f$ ) and rotation angle ( $\Phi$ ). There are three different frequencies for each images: one wave, three waves, and nine waves. There are three rotations for each pattern:  $0^\circ$ ,  $45^\circ$ , and  $90^\circ$  of rotation. In total, there will be thirty six parent images.

All images were transformed using 2-D FFT to get their phase and magnitude components. Then, the phase of each image was combined with the magnitude of

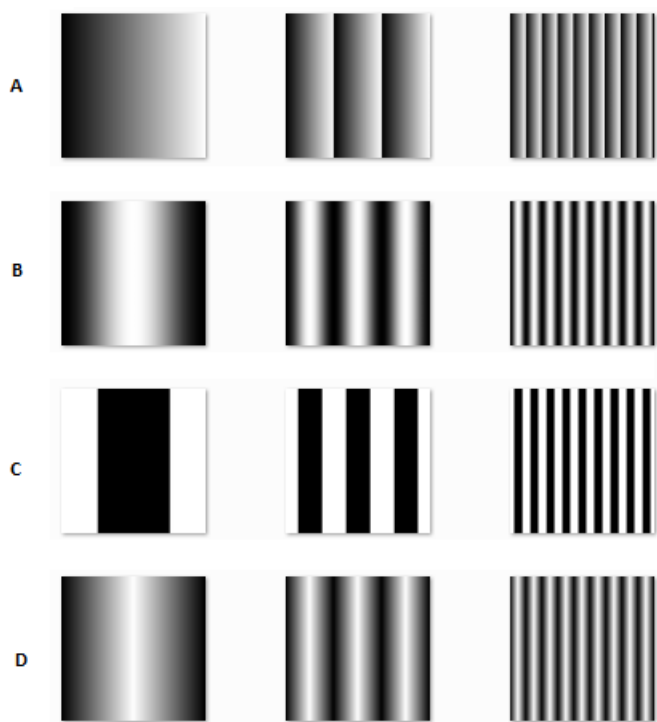


Figure 4.3: A sample of twelve images selected from thirty six parent images that were used as stimuli in this experiment. The complete set of the parent images can be found in Appendix (B). Here, their sizes are adjusted for sake of clarity. Their actual size is  $420 \times 420$ . Images in row A have sawtooth type of signal with their frequency from left is 1, 3, and 9 respectively. In row B, the signal type is sinusoidal, in row C is square, and in row D is triangle and their frequencies follow the pattern of row A.

another pattern to create a child pattern using a Two-Dimensional Inverse Fast Fourier Transform (2-D IFFT). From the combination of those thirty six images resulted 1,260 hybrid images. To compare the strength of the influence of the magnitude and the phase of parent images, each hybrid image was put in a pair with two related parent images. For simplicity purpose, the parent image which contributes its magnitude is labelled as MP and the parent image which shares its phase is coded as PP.

### 4.2.2 Participants

Twenty eight volunteers were the subjects in this experiment and each of them performed 1260 tasks. They were students and staff at the University of Leeds. All participants were interviewed to ensure they are free from impairments that could affect their ability to perceive the visual patterns. Participants were naïve to the hypotheses. In all experiments the duration of the stimuli exposure was not specified to allow subjects to make thorough explorations of the patterns.

### 4.2.3 Procedure

The experiment used a full-factorial design method. Therefore, from four types of image, three different frequencies, and three angle variations, would generate thirty six different parent images. To form a set of hybrid images, all the magnitudes and the phases of these parent images were swapped. The swapped of magnitudes and phases from the same images were not used because they will form the hybrid images which are similar to their parent images. The combination of the swapped magnitudes and phases produced 1260 ( $36 \times 35$ ) hybrid images.

All pairs were displayed one by one on a computer screen (Figure 4.4). Each pair consists of a test image which is the hybrid image and two related parent images. The position of the test image was always at the top and the position of the parent images are at the bottom. However, the relative position of each parent images was randomized for each pair at every presentation. It means that sometimes the left side was the parent image which contributes its magnitude and the right side was the parent image which contributes its phase and sometimes this position's order was reversed.

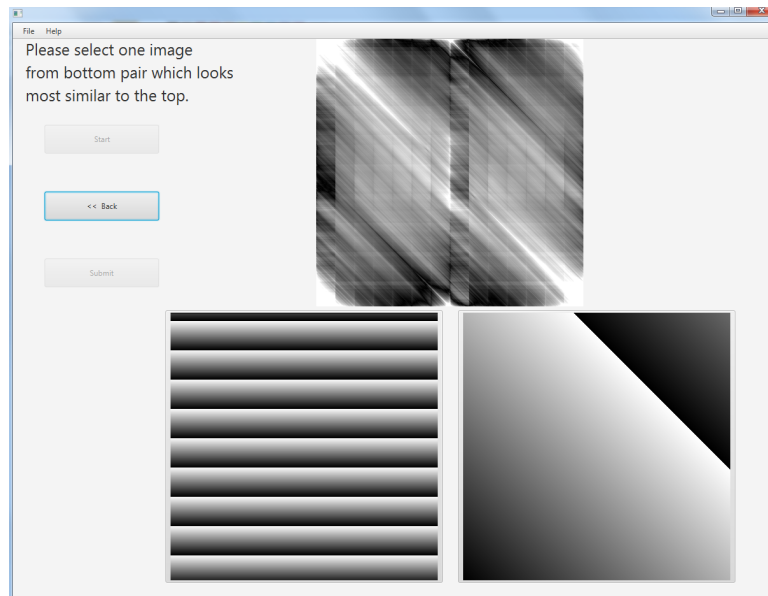


Figure 4.4: The scheme of a pair of images displayed on computer screen. Here, the sizes of the image stimuli are reduced for sake of clarity. The actual size of each image is  $420 \times 420$ .

The order of the pair presentation was randomized. Therefore, each subject would see a different order of image pairs. The subject were asked to choose the parent image which looks most similar to the test (hybrid) image in each

pair using two alternative-forced choice (2AFC) Match-to-Sample method [277]. There was no special instruction and guidance for the subjects about the criteria and the degree of similarity. They were free to interpret the definition of similarity between images. However, all subjects were given a preliminary experiment using fifteen pairs which were randomly selected from the actual pair of images. This exercise experiment was not included in the analysis. There was no break during the session. It took around forty minutes for each subject to complete this visual experiment.

#### 4.2.4 Analysis

The data recorded were used to analyse the effect of three different parameters of the periodic images on the phase dominance. Those parameters are the type, the frequency, and the rotation angle of the signals. Some supplementary analyses were performed to investigate the influence of some features from the power spectra of the periodic images to the dominance of the magnitude.

Each image has a particular power spectra which bears the unique information of the image's texture (Figure 4.5). The first segment line at point zero is the DC component. It is equivalent to the average of all the pixels' intensity. All signals have this line in their power spectrum. Other segment lines in the power spectrum represent the frequency components of the image. The abscissa of the line shows the frequency and the length of the segment indicates the strength of that frequency component. The number of the segment lines indicates the number of the frequency components which builds the texture of the image.

The profile of the power spectrum of each signal is different. In Figure 4.5, the sinusoidal signal has only one line segment of the frequency component at abscissa 1.0 that cannot be seen clearly because it is too close to the line of the DC component. The number of the line of frequency components increases from the sinusoidal to the sawtooth image. Therefore, it may potentially be used as one of the features to characterize the image's texture.

The power spectrum of the same type of periodic signal will also change when their frequency is changed. The segment lines of the frequency component look to shift their position horizontally as their frequency increases (Figure 4.6). The distance of this shift may also become another feature to define the textures. It is also seen that the space between each segment lines becomes wider which, therefore, can be used to create some features from it such as: the distance between

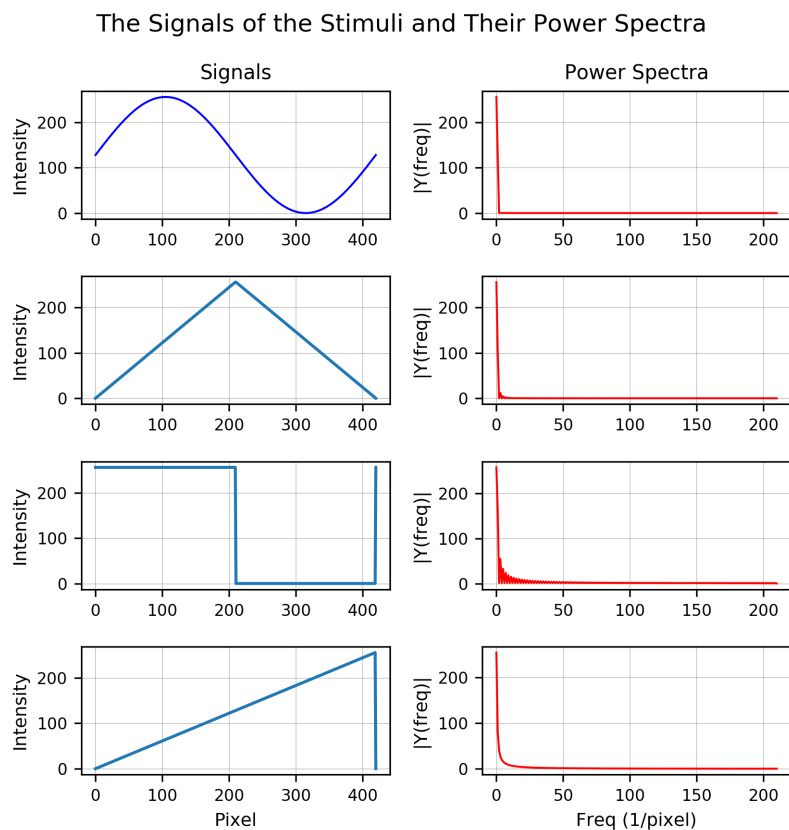


Figure 4.5: Four periodic signals which were used to generate the parent images and their power spectra. The left side plots are the periodic signals. From the top to the bottom is: sinusoidal, triangle, square, and sawtooth signal. The right side plots are the power spectra of each corresponding signal at the left side.

two major frequency components, the density of the power spectra, and the total moment of the spectra. These power spectra-based features were extracted from the power spectra of the parent images which contribute their magnitude data. Based on these features, the possibility to construct a measure of the phase dominance was investigated.

A third of the parent images have  $45^\circ$  rotated signals, and another third have  $90^\circ$  rotated signals. Based on the property of Fourier transform that rotation of a signal in time (space) domain corresponds to a rotation in frequency domain, the power spectra of the rotated signals are expected to be the same power spectra of the corresponding unrotated signals. This happens in the parent images with  $90^\circ$  signal's rotation. Their spectra profile is exactly the same with the spectra profile of the corresponding unrotated images. Unexpected profiles of the power spectra appear in the images with  $45^\circ$  signal's rotation. Instead of the

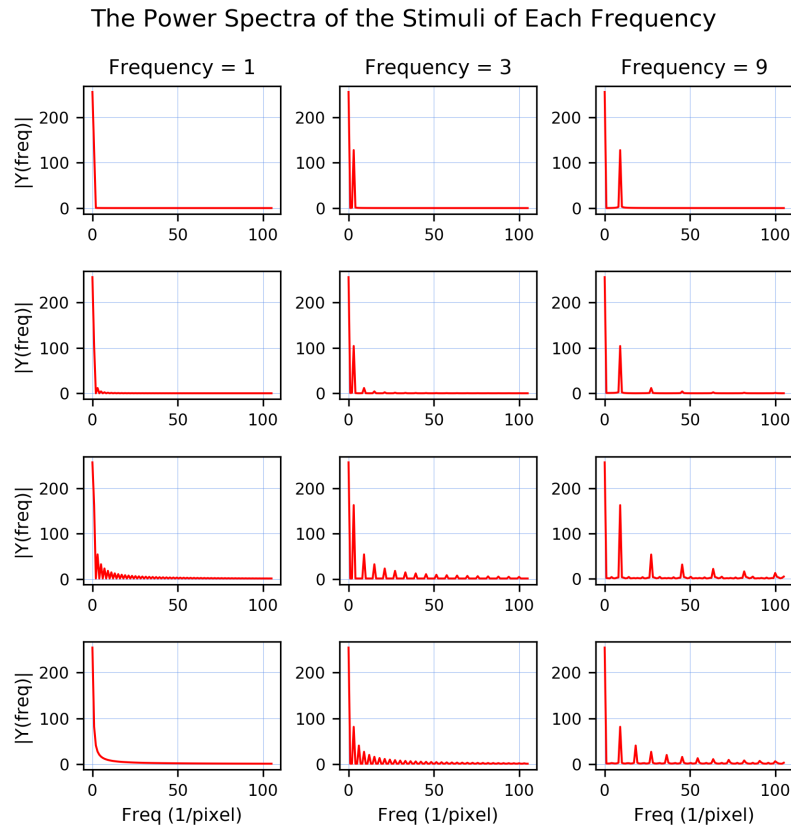


Figure 4.6: The power spectra of each periodic signals in three different frequencies. From the top to the bottom is the spectrum of the: sinusoidal, triangle, square, and sawtooth signal.

original power spectra rotated for  $45^\circ$ , the spectra changed completely. It happens because instead of a specific local texture that is rotated, a whole image changes completely due to the rotation of its signal. However, some characteristics of the power spectra still remain. Therefore, a similar set of power spectra-based features can be applied.

To extract the features, the profile of the power spectra is preferred to the phase spectra because the former has a more regular pattern than the latter. Moreover, because the phase spectrum is angular data in radians (within the range  $-\pi$  and  $\pi$ ), it will not provide a direct information to the image's texture. So, in this experiment, the power spectra were used to characterize the texture of the images. One hundred and seven features were extracted from the profile of the power spectra of the image textures. Twenty eight of them were adopted from Liu and Jernigan [54] and five features were from Tsai et al. [251]. The rest of the features were modified from Liu and Jernigan [54]. The details of all those features can be found in Appendix C.

Table 4.2: Response Summary

	Frequency	Percent	Valid Percent	Cumulative Percent
Valid 0	4092	11.6	11.6	11.6
1	31188	88.4	88.4	100.0
Total	35280	100.0	100.0	

### Evaluation and selection of the most important features

A feature is an individual property or parameter which can be measured [278]. This term is usually used in the machine learning field. In statistics, feature is commonly called as predictor or dependent variable. A set of features which consists of tens to hundreds individual feature is commonly generated to build a machine learning or a statistical model. However, initially, the effectiveness of each feature within the set is not known in most of the time. An evaluation and a selection of a subset of features become important [279]. The irrelevant features which do not provide any information to the model will be removed [279, 280].

The techniques to eliminate irrelevant features can be grouped based on the labels' availability and the search strategy [281]. In terms of availability of the label's information, the feature selection technique can be roughly classified into three groups: supervised methods, semi-supervised methods, and unsupervised methods. Meanwhile, based on the search strategies, the feature selection can be divided into three techniques: filter, wrappers, and embedded methods [278, 279]. By using these methods, it is expected to get a set of the most relevant features in a smaller number as possible. The fewer the related features, the faster the calculation and the clearer the model.

## 4.3 Result and Discussion

For every presented pair, the responses gathered from the subjects were coded as 1 if MP was selected and 0 if PP was chosen to be more similar to the test image. Each subject generated 1260 binary responses for all the sets of image pairs. In total, 35280 binary responses were collected from twenty eight individuals. The result shows that response 1 gets 31188 picks (88.4%) while response 0 gets just 4092 picks (11.6%) with no missing data (Table 4.2). This result indicates that the magnitude is more dominant than the phase and, therefore, contradicts to many reports which suggested that the phase is more dominant than the magnitude.

Furthermore, all types of MP are magnitude dominant. The sawtooth MPs with frequency 1 are the least magnitude dominant (Figure 4.7. However they

Table 4.3: Chi-square Analysis of Magnitude's Dominance of the MP

Number of observations	DOF	Critical ( $P > 95\%$ )	$\tilde{\chi}^2$	P-value	Cramer's V
35280	35	49.802	3152.06	.000	.30

still obtained more than 60% of response 1s (600 picks out of 980 of the total responses). The sinusoidal MPs with frequency 3 and 9 are the most magnitude dominant with more than 95% of response 1s.

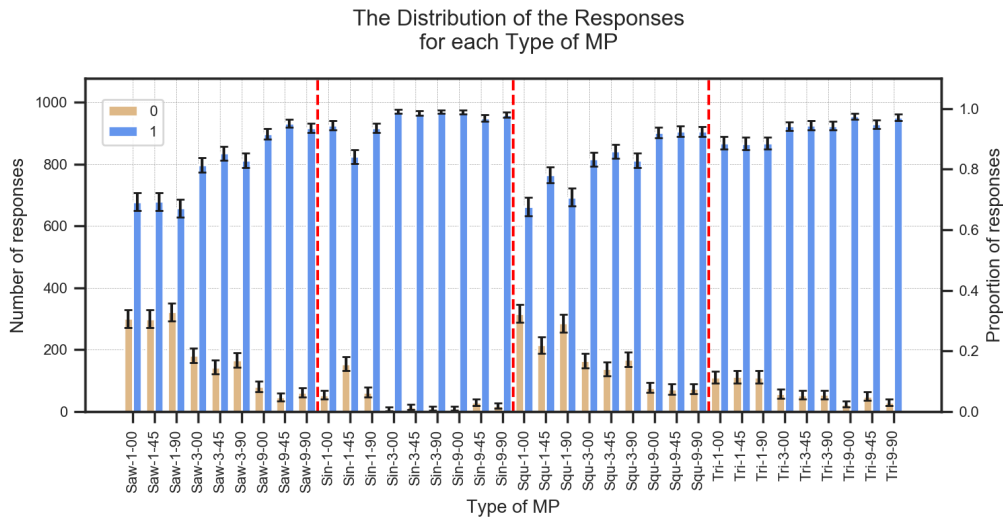


Figure 4.7: Frequency distribution of the responses for each the type of MP. Each x-axis label indicates the type, the frequency, and the rotation angle of the signal. The signal's types are coded as Saw, Sin, Squ, and Too which stands for Sawtooth, Sinusoidal, Square, and Square-wave respectively. Each type of MP were paired with 980 of PP. Therefore, this number also indicates the total number of responses for each type of the stimuli. The error bar represents the corresponding standard deviation value.

It seems that the magnitude's dominance among MPs is different. The Chi-square test supports the indication that there is a significant difference of the magnitude's dominance between MPs (Table 4.3). This result also indicates that there is a relationship between the signal of MP and the magnitude's dominance. In other words, the magnitude's dominance depends on the type of MP. The level of this relationship can be seen from the Cramer's V value which is .30 that according to Cohen [271, page 227] is medium.

However, not all MPs seems to have a different magnitude's dominance (Figure 4.7). Some of them share a relatively similar one. For example, Saw-1-00 and Saw-1-45 have the same proportion of responses. Furthermore, the post-hoc analysis shows that there are 110 pairs of MPs which have an insignificant difference of



the magnitude's dominance between them (Table D.1). This result indicates that the magnitude's dominance may be influenced by either the type, the frequency, the rotation angle, or the combination between them of the signals.

### 4.3.1 The effect of the type of the signals to the magnitude's dominance

The magnitude's dominance seems to depend on the type of MP and to decrease from the sinusoidal MPs to the sawtooth Mps (Figure 4.8, the left chart). From the total of 8820 responses, there are 8453 (96%) responses selected MP with sinusoidal texture to be more similar to the hybrid images. The triangle MPs obtained 8215 of 1s (93%) which becomes the second in the rank order of the magnitude's dominance. The decrease of the number of 1s from the sinusoidal MP to the triangle MP is 238 (3%). The square-wave MPs acquired 7307 of 1s which is 908 (11%) less than the to the triangle MPs. Having the least magnitude's dominance, the sawtooth MP still received 7213 of 1s (82%). Furthermore, the difference of the number of 1s between the sawtooth MPs and the triangle MPs is only 1% which may indicate that both types of MP have a similar magnitude's dominance.

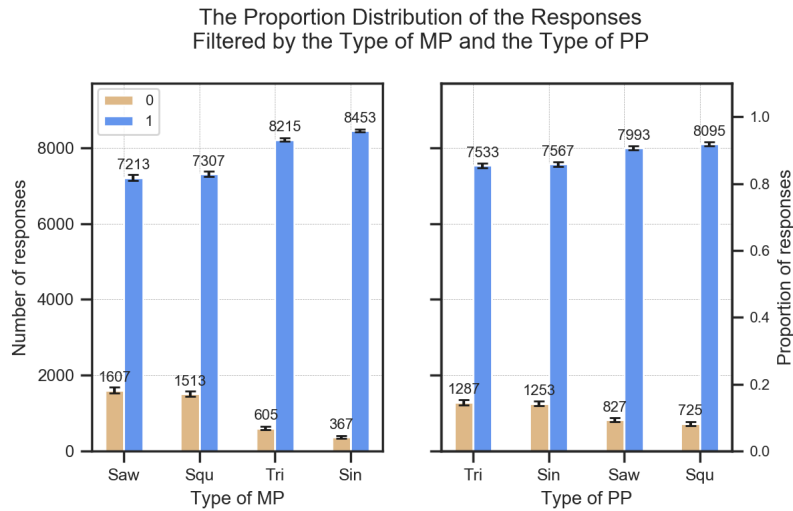


Figure 4.8: Frequency distribution of the responses filtered by the type of MP (left) and filtered by the type of PP (right). Each of the x-axis label stands for Sinusoidal (Sin), Triangle (Tri), Square-wave (Squ), and Sawtooth (Saw). They indicate the signal's type. Every type of MP (PP) were paired with 8820 of PP (MP) of all types. Therefore, this number also indicates the total number of responses for each type of the stimuli.

Table 4.4: Chi-square Test on the Prevalence of Different Magnitude's Dominance among the Types of MP

Signal	Observed frequency			Expected frequency		
	0	1	Total	0	1	Total
Saw	1607	7213	8820	1023	7797	8820
Sin	367	8453	8820	1023	7797	8820
Squ	1513	7307	8820	1023	7797	8820
Tri	605	8215	8820	1023	7797	8820
Total no. of observations (n_obs)						35280
Degree of freedom (dof)			3	$\chi^2$	1311.68	
P-value			.000	Reject $H_0$	true	
Effect size (Cramer's V)			.20			

Table 4.5: Post-hoc Pairwise Comparison of Chi-squared Test between the Types of MP

Pair of		P-value	P-value Corrected	Significant?	Reject $H_0$ ?	Cramer's Value
MP 1	MP2					
Saw	Squ	.0665	.0665	(ns)	false	.0138

The Chi-square test supports the indication that the types of MP affect the magnitude's dominance (Table 4.4). The p-value which is close to zero means that there is a significant difference of the responses' proportion among the types of MP. It also means that each type of MP has a particular value of the magnitude's dominance. Based on the Cramer's V value which is .20, the strength of the relationship between the type of MP and the magnitude's dominance is medium.

However, not all types of MP seems to have a different magnitude's dominance. For example, the difference of the number of response 1s between the sinusoidal and the triangle MP is 3% and between the square-wave and the sawtooth MP is 1% which gives an indication that both pairs of MP has a similar magnitude's dominance. The post-hoc pairwise comparison of Chi-squared test shows that within the types of MP, only the sawtooth MPs and the square-wave MPs which have no significant difference of the responses proportion between them (Table 4.5). Despite only 3% different, the sinusoidal MPs and the triangle MPs have a significant difference of responses proportion or magnitude dominance.

The order of the signal's type, starting from the most to the least magnitude dominant (Figure 4.8), is the same with the order of the signal's types based on the number of the frequency components in their power spectra (Figure 4.5). In other words, the fewer the number of frequency components, the stronger the magnitude's dominance; hence, the weaker the phase's dominance. It also indicates that the fewer the number of the frequency components of an image, the more the informations contained by its power spectrum and the fewer the

features conveyed by its phase spectrum. Otherwise, the more the number of the frequency components of an image, the fewer the features conveyed by its power spectrum and the more information brought by its phase spectrum.

In term of the number of response 0s, the sinusoidal MP has the smallest number. Only in 367 (4%) cases, the sinusoidal MP was perceived to be less similar to the test image than the PP. The number of response 0s increases almost double for the triangle MP and more than four times for the square-wave MP. There is no significant increase of the number of response 0s between the square-wave MP and the sawtooth MP.

Compared to the decrease of the number of response 1s, it is obvious that the increase of the number of response 0s is more obvious in all types of MP. Therefore, instead of the decrease of the response 1, the increase of the response 0 seems to be more related to the number of frequency components of MP (Figure 4.5 and Figure 4.6). The bigger the number of frequency components, the stronger the phase dominance of the stimulus.

The type of signal which has a stronger magnitude seems to have a more dominant of phase too. Figure 4.8 (right) shows that when each type of signal contributes its phase (PP), the sinusoidal and the tooth of PP also have the higher number of 0s despite having a higher number of 1s when they contribute their magnitudes (MP). The square-wave and the sawtooth signals even though they have relatively stronger phase dominance, their phase contributions are still weaker than the phase dominance of the sinusoidal and the triangle signals. Thus, it gives an counter-intuitive indication that a signal which is magnitude dominant is also phase dominant.

The same indication can also be seen from the distribution of responses' proportion that is filtered by the pair of signal's types (Figure 4.9). The magnitude's dominance of each type of MP is always high when paired with the same type of PP or to the type of PP with weaker magnitude's dominance. Having the strongest magnitude's dominance, the sinusoidal MP always obtains a high proportion of 1s when paired with any type of PP. The triangle MP decrease its magnitude's dominance only when paired with the sinusoidal PP. In fact, all types of MP will decrease its magnitude's dominance when paired with the PP which has stronger magnitude's dominance.

From the perspective of phase's dominance, any tipe of MP with a higher phase's dominance will also increase its proportion of 0s when paired with the type of PP with a stronger phase's dominance. For example, the sawtooth MP and the square-wave MP which both of them have the strongest phase's dominance

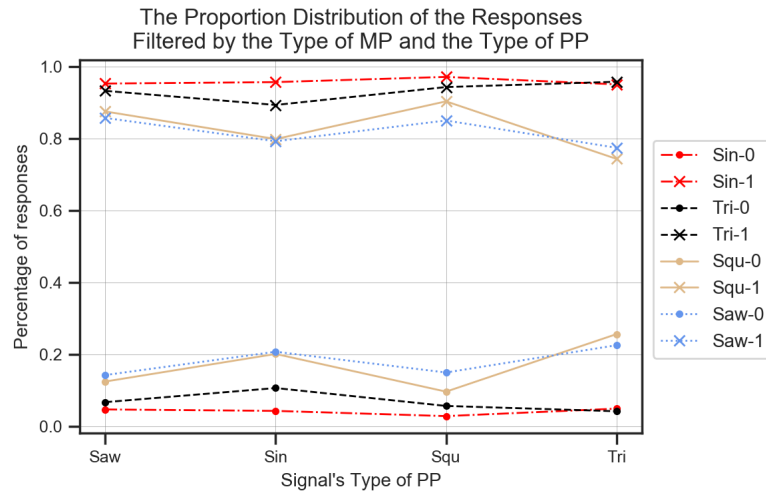


Figure 4.9: The percentage of the number of the response 0 and the response 1 for each type of MP when they are paired with each type of PP. The total responses for each pair is 2268 if the signal type is different and 2016 for the pair with the same type of signal. The upper lines are the plot of the percentage of 1s, and the bottom ones are the plot of the percentage of 0s.

(Figure 4.8), obtained a higher proportion of 0s when paired with the sinusoidal PP (20%) and to the triangle PP (> 20%). This result aligns with the previous finding that the stronger the magnitude's dominance of an image, the weaker the phase's dominance.

### 4.3.2 The effect of the frequency of MP to the magnitude's dominance

The magnitude's dominance considerably rises when the frequency of the MP increases (Figure 4.10:left). At frequency 1, MP obtained the lowest proportion of response 1s (80%) which is 8% lower than the overall percentage of response 1s (Table 4.2). Therefore, the dominance of the phase mostly appears in MP with frequency 1. The magnitude's dominance rises to 90% at frequency 3 and reaches 95% at frequency 9.

The Chi-square test supports the indication that the magnitude's dominance is influenced by the frequency of MP (Table 4.6). The p-value which is closed to zero means that there is a significant difference of the responses' proportion among the frequencies of MP. It also means that each frequency of MP has a particular value of the magnitude's dominance. Based on the Cramer's V value which is .20, the strength of the relationship between the frequency of MP and

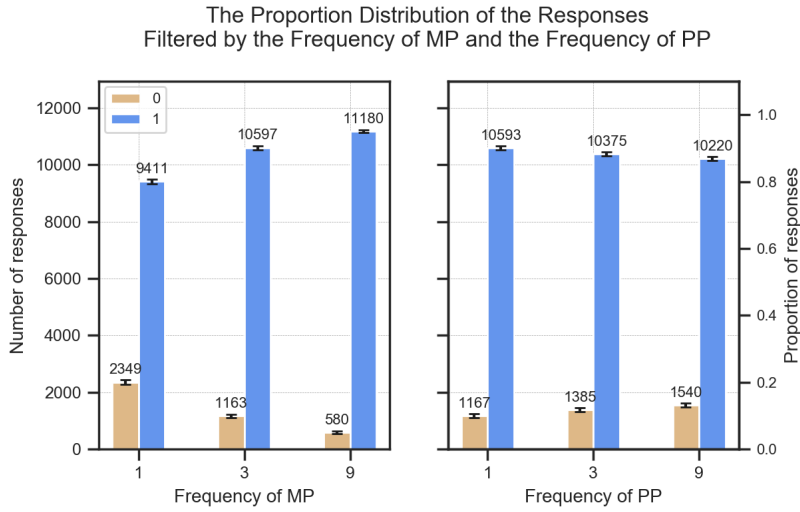


Figure 4.10: Frequency distribution of the responses filtered by the signal's frequency of MP (left) and by the signal's frequency of PP (right). Each MP (PP) with a particular signal's frequency were paired with 11760 of PP (MP) of all types.

Table 4.6: Chi-square Test on the Prevalence of Different Magnitude's Dominance among MPs at Different Frequencies

Signal's Frequencies	Observed frequency			Expected frequency		
	0	1	Total	0	1	Total
1	2349	9411	11760	1364	10396	11760
3	1163	10597	11760	1364	10396	11760
9	580	11180	11760	1364	10396	11760
Total no. of observations (n_obs)						35280
Degree of freedom (dof)			2	$\bar{\chi}^2$	1347.89	
P-value			.000	Reject $H_0$	true	
Effect size (Cramer's V)			.20			

their magnitude's dominance is medium.

Furthermore, the post-hoc of pairwise Chi-square analysis shows that all pairs of frequencies of MP have a significant difference of the magnitude's dominance (Table 4.7). This result, therefore, supports the indication that the magnitude's dominance rises when the frequency of MP increases. Referred to the profile of the power spectrum in Figure 4.6, this result shows that the further the distance of frequency components from the DC component of the stimulus, the stronger the magnitude's dominance. In other words, the further the frequency component from the centre of the power spectrum, the more the features being conveyed.

Although it is not obvious, the texture with higher frequency tends to have a larger phase's dominance too (Figure 4.10: right). At frequency 1, PPs obtained

Table 4.7: Post-hoc Pairwise Comparison of Chi-squared Test between the Frequencies of MP

MP Pairs with		P-value	P-value Corrected	Significant?	Reject $H_0$ ?	Cramer's Value
Freq1	Freq2					
1	3	.0000	.0000	true	true	.1414
1	9	.0000	.0000	true	true	.2276
3	9	.0000	.0000	true	true	.0944

Table 4.8: Post-hoc Pairwise Comparison of Chi-squared Test between the Frequencies of PP

PP Pairs with		P-value	P-value Corrected	Significant?	Reject $H_0$ ?	Cramer's Value
Freq1	Freq2					
1	3	.0000	.0000	true	true	.0296
1	9	.0000	.0000	true	true	.0496
3	9	.0000	.0000	true	true	.0198

10% 0s. The phase's dominance of PPs rises to 12% at frequency 3 and reaches 13% at frequency 9. Despite having a relatively low difference, the Chi-square test shows that in general, there is a significant difference of the phase's dominance among frequencies of PP (the p-value is .000). However, the Cramer's value is low (.0406) and it indicates that the relationship between the frequencies of PP and their phase's dominance is low. In other words, this value agrees with the fact that the increase of the phase's dominance is low. The post-hoc pairwise comparison shows that any pair between two different frequencies of PP will have a significant difference of the phase's dominance (Table 4.8).

Each type of MP seems to have the different characteristics of the magnitude's dominance under the varying frequency (Figure 4.11:left). Both the sinusoidal MPs and the triangle MPs have a similar pattern of the magnitude dominance. At frequency 1, both the sinusoidal and the triangle MPs have around 90% magnitude dominance and even higher at frequency 3 and 9 (close to 100%). Meanwhile, the magnitude dominance of the square-wave and the sawtooth MPs is only around 78% and 65% at frequency 1 which is considerably lower than magnitude dominance of the sinusoidal MPs and the triangle MPs. However, it always increases and reaches at around 90% at frequency 3 and around 100% at frequency 9.

The phase's dominance of each type of PP under varying frequency is even more contrast (Figure 4.11:right). Both the sinusoidal PPs and the triangle PPs have a similar pattern of the phase dominance. Although it is not easily noticeable, both types of PP tend to have a weaker phase dominance as the frequency increases. Meanwhile, for the square-wave PPs and the sawtooth PPs, the phase dominance rises significantly as their frequency increase. The later finding

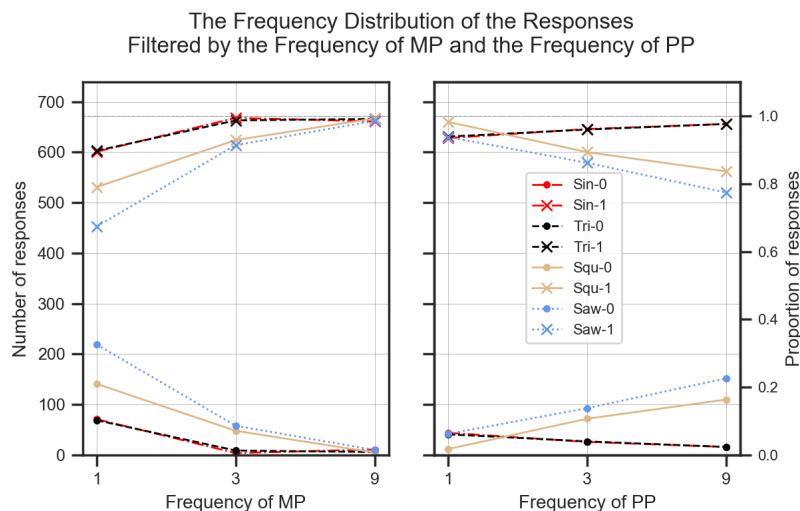


Figure 4.11: The number of 0s and 1s for each type of signal in every frequency of MP (left), and in every frequency of PP (right). Each type of MP is paired with the same type of PP. Therefore, the effect of pairing of different signals can be suppressed. The total number of response for each frequency is 672 responses.

seems to be counter-intuitive because, normally, the magnitude dominance and the phase dominance of an image's texture can not increase together.

However, these results eventually suggest that within the frequency measure, there is no relationship between the magnitude's dominance and the phase's dominance. The type of signal confound with the frequency to influence both the magnitude and the phase dominances. An image with a high frequency of texture can have a phase dominance which is either relatively low or high depends on the type of the texture.

Each type of MP has a different characteristics of the magnitude's dominance (Figure 4.12). For all types of MP, the magnitude's dominance tends to be weaker when the frequency of MP is the same with the frequency of PP. However, when there is a difference between the frequency of MP and the frequency of PP, each type of MP has a different pattern of magnitude dominance. The sinusoidal MP and the triangle MP tends to have higher magnitude's dominance when they are paired with PP with higher frequency. Meanwhile, there is no noticeable increase in the magnitude's dominance when the square-wave MP and the sawtooth MP are paired with PP with higher frequency.

Figure 4.12 also shows that the low magnitude dominance at almost all frequencies is mostly contributed by the low magnitude's dominance of the square-wave and the sawtooth MPs. Moreover, at frequency 1, the magnitude's domi-

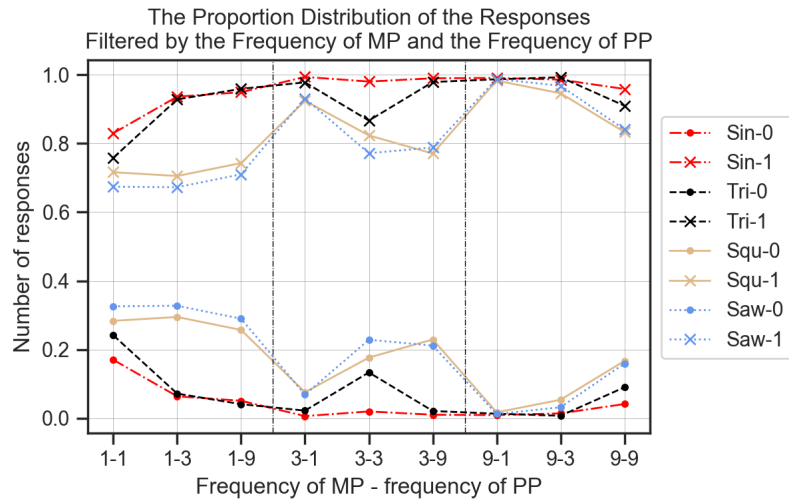


Figure 4.12: The percentage of the number of the response 0 and the response 1 for each type of MP when they are paired with each frequency of PP. The total number of responses for each frequency of MP at each frequency of PP is 1008 responses for the pair with different frequencies, and is 924 responses for the pair with the same frequency.

nance of these textures is still low even when they are paired with PP with higher frequency. This result indicates that the type of MP has more influence to the magnitude's and phase's dominance than the frequency. In term of power spectrum, the number of the frequency component have more informations than its distance from the DC component (the centre of the power spectrum).

### 4.3.3 The effect of the rotation angle of MPs to the magnitude dominance

The rotation of signal seems to not influence the magnitude dominance of the MP (Figure 4.13: left). The magnitude dominance of MP for each rotation angle is the same at around 88% which is the same with the overall magnitude dominance of all MPs (Table 4.2). The slight variation of the responses' proportion among MPs for each rotation angle is more likely by chance. The result of the Chi-square test supports this indication. The p-value is .516 which means that there is no significant difference of the response's proportions among the groups of rotation angle. The Cramer's V value is also very small .006 which, therefore, indicates that there is no significant relationship between the rotation angle and the magnitude dominance.

The post-hoc pairwise Chi-square analysis shows that all pairs of the rotation



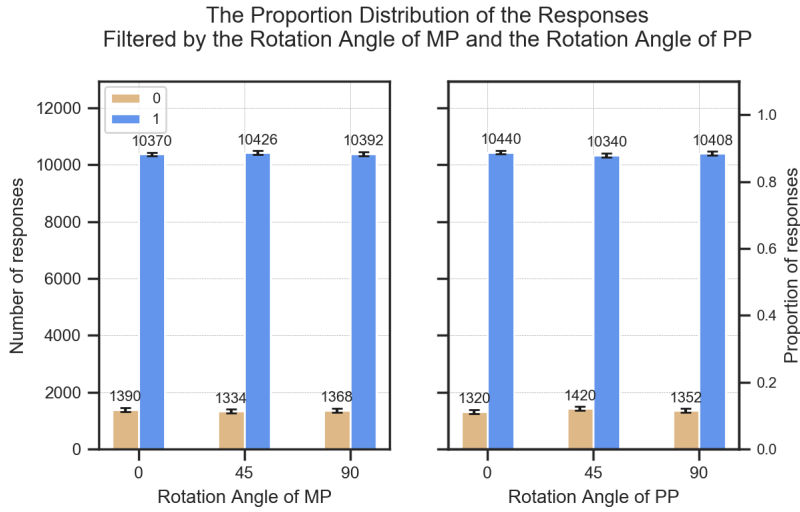


Figure 4.13: Frequency distribution of the responses filtered by the rotation angle of MP (left) and the rotation angle of PP (right). The total number of responses is 1760 for each rotation angle.

Table 4.9: Chi-square Test on the Prevalence of Different Magnitude's Dominance among MPs with Different Rotation Angle

Rotation Angle	Observed frequency			Expected frequency		
	0	1	Total	0	1	Total
0	1390	10370	11760	1364	10396	11760
45	1334	10426	11760	1364	10396	11760
90	1368	10392	11760	1364	10396	11760
Total no. of observations (n_obs)						35280
Degree of freedom (dof)			2	$\tilde{\chi}^2$		1.32
P-value			.516	Reject $H_0$		false
Effect size (Cramer's V)			.006			

angles of MP have no significant difference of the magnitude's dominance (Table 4.10). All p-values are significantly bigger than .05 and the Cramer's value is very small. It indicates that each rotation angle of MP has statistically the same magnitude dominance.

The rotation angle of the phase spectra of PP also seems not to influence the phase dominance (Figure 4.13: right). The Chi-square analysis shows that the p-value is .1150 which indicates that there is no significant difference of proportion of response 0s among PPs for each rotation angle. Furthermore, the Cramer's value which is .0111 indicates that there is no significant relationship between the rotation angle and the phase dominance. Any pair of rotation angles among PPs has no significant difference of the response's proportion which, therefore, means

Table 4.10: Post-hoc Pairwise Comparison of Chi-squared Test between the Rotation Angles of MP

PP Pairs with		P-value	P-value Corrected	Significant?	Reject $H_0$ ?	Cramer's Value
Freq1	Freq2					
0	45	.2624	.6704	true	false	.0073
0	90	.6704	.6704	true	false	.0028
45	90	.4998	.6704	true	false	.0044

Table 4.11: Post-hoc Pairwise Comparison of Chi-squared Test between the Rotation Angles of PP

PP Pairs with		P-value	P-value Corrected	Significant?	Reject $H_0$ ?	Cramer's Value
Freq1	Freq2					
0	45	.0442	.1326	true	false	.0131
0	90	.5241	.5241	true	false	.0042
45	90	.1754	.2631	true	false	.0088

that for each rotation angle, the phase's dominance of PP is the same. All results above agree with there being no change in the profile of power spectra for the rotated texture and, therefore, its magnitude dominance will not change under rotation.

However, the difference of the rotation angles between MP and PP influences the magnitude's dominance. When MP and PP have a different the rotation angle, the magnitude dominance of MP is high (Figure 4.14). Meanwhile, when their rotation angles are the same, the magnitude dominance of MP decreases at a different rate according the type of the signal. This, again, indicates that the type of MP has a considerable influence to the magnitude's dominance. The sinusoidal and the triangle MPs, again, have the higher magnitude's dominance while, the square-wave and the sawtooth MPs appear to have a lower magnitude's dominance. The square-wave and the sawtooth MPs have a proportion of response 1s that is even lower than 60% in this case. However, it shows that both signals have a relatively strong phase dominance which is already known from the previous result.

When the rotation angle is different, the magnitude dominance improves significantly. It means that the angular texture of the hybrid image looks more similar to the angular texture of MP(Figure 4.14). Thus, the magnitude spectrum shared by MP conveys not only global frequency of the image texture but also the angular pattern of the image.

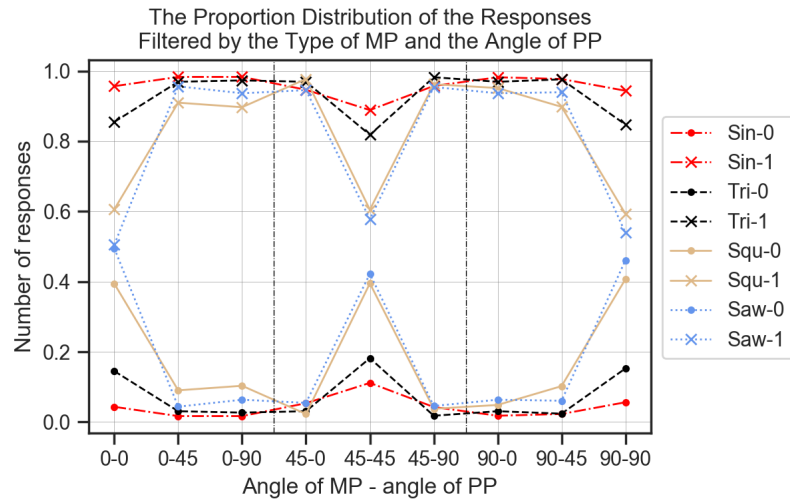


Figure 4.14: The percentage of the number of the response 0 and the response 1 for each type of MP when they are paired with each angle of PP. The total number of responses is 1008 when the rotation angles of MP and PP are different, and it is 924 when the rotation angles are the same.

#### 4.3.4 The effect of the combination between the type and the frequency of MPs to the magnitude's dominance

From the previous section, it was found that the type and the frequency of signal are the only parameters which influence the magnitude's dominance. The combination of both factors seems to have a higher effect to the magnitude's dominance than the influence from each of them individually. By selecting only the responses of pairs with the same rotation angle, the effect of the type and the frequency of signal becomes more obvious (Figure 4.15). Eventually, not all MPs are magnitude dominant. The sawtooth MP and the square-wave MP have a considerably dominant phase at frequency 1. Although in the previous section it was found that they have the same level of magnitude's dominance, here it is seen more obviously that the square-wave MP has a higher magnitude dominance. The sinusoidal MP still appears to have the highest magnitude dominance.

The magnitude dominance of each frequency in every type of MP is significantly different. This indication is supported by the Chi-square test which shows that all the p-values are zero (Table 4.12). The relationship between the frequency and the magnitude dominance can be estimated from the Cramer's value. The higher the value, the stronger the relationship. Furthermore, the Cramer's value also indicates the rate of the increase of the the magnitude dominance. As all the Cramer's values are positive, the correlation between the frequency and the

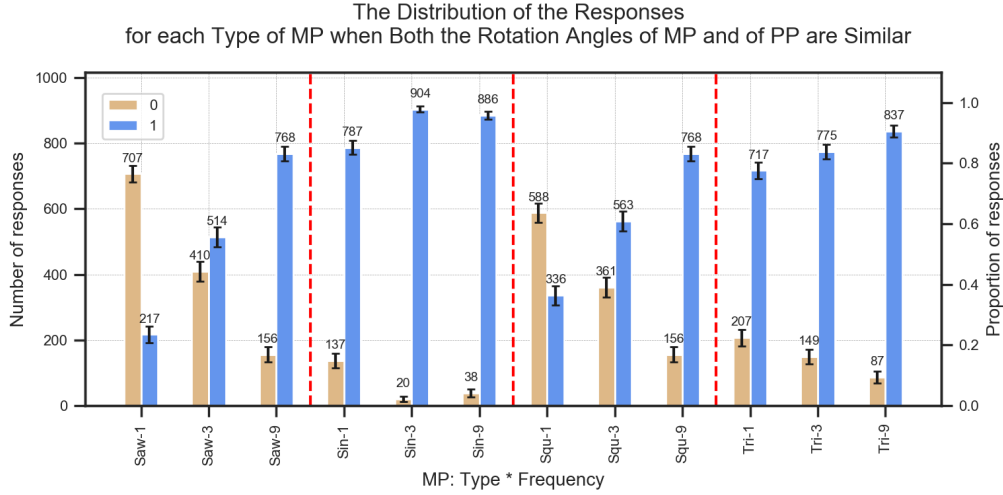


Figure 4.15: The percentage of response 1s and the response 0s for each type of MP when they are paired with PP which has the same rotation angle.

Table 4.12: The Chi-square Test on the Prevalence of Magnitude's Difference within the Combination of the Types and the Frequency of the MP's Signals

Type of MP	$\chi^2$	P-value	Significant?	Reject $H_0$ ?	Cramer's Value
Saw	662.88	.0000	true	true	.4890
Sin	131.36	.0000	true	true	.2177
Squ	421.62	.0000	true	true	.3900
Tri	58.05	.0000	true	true	.1447

magnitude's dominance also positive. Therefore, when the frequency increases, the magnitude's dominance also raises. The larger the Cramer's value, the higher the increase rate.

Thus, it can be concluded that the sawtooth MP has the highest increasing rate of the magnitude dominance under the increase of frequency (Table 4.12). The square-wave MP has the second highest rate. The sinusoidal MP has a relatively low rate despite having the strongest magnitude dominance. However, at frequency 3, its magnitude dominance has reached 98% which is considerably strong and it practically stops increasing at this point. The lowest Cramer's value belongs to the triangle-wave MP which, therefore, means that it has the least rate of the increase of the magnitude dominance.

Table 4.13: The Structure of the Variables and Their Data Types

Features					MP			PP			Response
$f_0$	$f_1$	$f_2$	...	$f_{107}$	ms	mf	ma	ps	pf	pa	
$x_0^0$	$x_0^1$	$x_0^2$		$x_0^{107}$	$ms_0$	$mf_0$	$ma_0$	$ps_0$	$pf_0$	$pa_0$	$r_0$
$x_1^0$	$x_1^1$	$x_1^2$		$x_1^{107}$	$ms_1$	$mf_1$	$ma_1$	$ps_1$	$pf_1$	$pa_1$	$r_1$
$x_2^0$	$x_2^1$	$x_2^2$		$x_2^{107}$	$ms_2$	$mf_2$	$ma_2$	$ps_2$	$pf_2$	$pa_2$	
$\vdots$	$\vdots$	$\vdots$		$\vdots$	$ms_3$			$ps_3$			
$x_{36}^0$	$x_{36}^1$	$x_{36}^2$		$x_{36}^{107}$							
*continuous data					*nominal data						

### 4.3.5 Power spectra-based features to measure the magnitude's dominance

From the previous sections, it was found that the power spectra is related to the type and the frequency of signal and, hence, to the magnitude dominance. The number of their non-zero frequency components is associated with the type of signal. The less the number of the frequency components, the stronger the magnitude dominance. The distance of their frequency components from the DC component has a positive correlation with the frequency of signal. The further the distance, the larger the frequency and also the stronger the magnitude dominance.

One hundred and seven features (Appendix C) were intended to measure the number and the distance of frequency components of the power spectra. For each feature there will be thirty six values which were calculated from thirty six different power spectra. The values of each feature can be put in a column vector (Table 4.13). In total, there are one hundred and seven column vectors ( $f_0$  to  $f_{107}$ ). These values are all continuous data. The parameters of MP which consist of four types of signal ( $ms$ ), three different values of frequency ( $mf$ ) and three distinctive rotation angle ( $ma$ ) were considered to be nominal data. The same treatment was also applied to the parameter of PP. Because the rotation angle itself is found to not contribute to the magnitude's dominance, its correlation with the feature will not be investigated. Finally, the binary responses were coded as response 0 ( $r_0$ ) and response 1 ( $r_1$ ) and they are categorical data.

#### The features that are most correlated with the type of signal

To find the correlation between each feature and the type of signal, an Anova analysis was performed with that feature as the dependent variable and the type of signal as the independent variable. The p-value obtained from the analysis

indicates the correlation between that feature and the type of signal. If the p-value is less than .05, there is a significant different of means among the type of signal which, therefore, that feature is more likely to correlate with the type of signal. Because p-value does not indicate the size of correlation, the  $\eta^2$ , which is equivalent to correlation, was used to measure the strength of the relationship between that feature and the type of signal. The larger the value of  $\eta^2$ , the stronger the correlation. As there are one hundred and seven features, there were also one hundred and seven Anova analyses.

The most correlated features were selected based on their Anova analysis's result. A feature is considered to have a relatively high correlation with the type of signal if it passed the filter which based on two criteria—i.e., the p-value must be less than .01 and the  $\eta^2$  must be greater than .10 [282, 283]. As the  $\eta^2$  value is equivalent to correlation, eliminating the value which is less than .10 is reasonable [268]. Among one hundred and seven features, only thirty of them passed the filter (Figure 4.16). The pcm and rd\_m2 have the largest  $\eta^2$ . However, the calculation of both features are based on the distance of frequency component of the power spectra which, therefore, is more related with the frequency than with the type of signal. Among the features which are calculated based on the number of frequency component, only area\_h2 which appear to have a medium  $\eta^2$  (.20).

### **The features that are most correlated with the frequency of signal**

A similar method using a series of Anova analyses was used to find the features which have the highest correlation with the frequency of signal. The features were set as the dependent variables and the frequency type was set as the independent variables. The result was also filtered using the same criteria to select the most correlated features. Finally, forty three features meet the criteria (Figure 4.17). Six of them have a perfect  $\eta^2$  (1.0), four features have high  $\eta^2$  values (.70 to .90), and other four features have moderate  $\eta^2$  values (.50 to .70). The features which have a perfect  $\eta^2$  value, —i.e., smf, pts\_r2, area\_r, pts\_r, and rad\_m are calculated based on the distance of the largest frequency component of the power spectra which, therefore, is not unpredictable to have a strong relationship with the frequency of signal.

There are ten features which meet both criteria from the type's (Figure 4.16) and the frequency's filter (Figure 4.17). They are emp, fro\_m, lmp, lsp, mass\_p, mo\_, mom1, pcm, r\_cog1, and rd\_m1. However, most of them do not have a high correlation with either the type of the frequency of the signal.

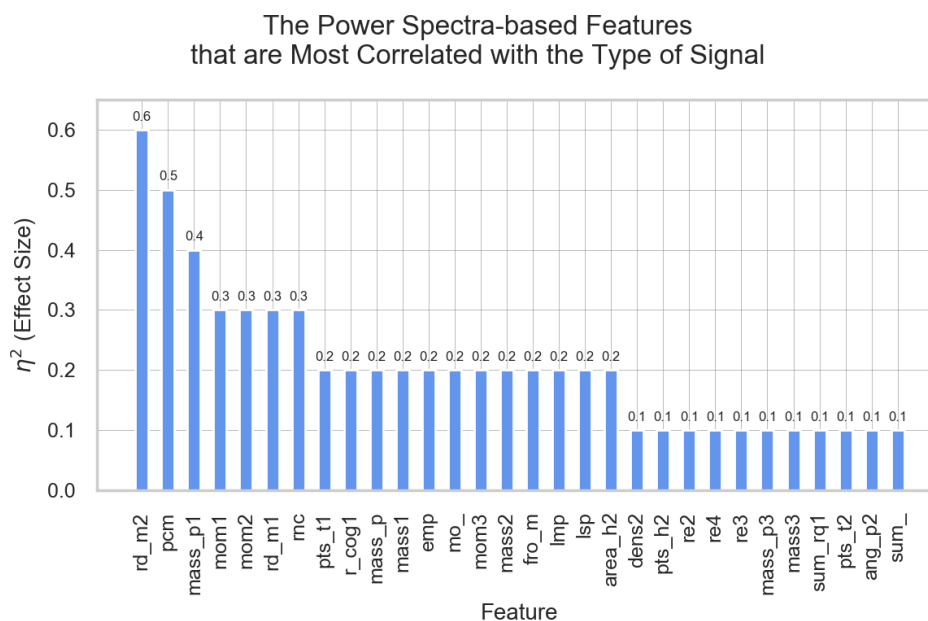


Figure 4.16: A set of power spectra-based features that are most correlated with the type of signal

### **The features that are most correlated with the combination of the type and the frequency of signal**

The combination of the type and the frequency of signal contributes the most significant influence to the magnitude dominance. Therefore, the feature which correlates with this combination of parameters is highly likely to give the most accurate prediction to the responses. From a series of two-way Anova analyses to one hundred and seven features, thirty three of them have the  $\eta^2$  greater than .10 (Figure 4.18). Three of features have a large  $\eta^2$  ( $> .60$ )—i.e., rd\_m1, pcm, and mom1. These features also pass the correlation filters for the type and the frequency of signal. The first feature was calculated based on the distance of the frequency component and the other features were calculated based on the multiplication between the distance and the value of frequency component which is equivalent to moment in physics.

Despite having a strong relationship with the frequency and the type of signal, there is no guarantee that these features will also have a high correlation with the response. This may happens because each MP was combined with PP which of course will influence the magnitude's dominance of the hybrid (child) image. A certain interaction between two values of feature which belong to MP and PP will determine the magnitude's dominance of MP in each hybrid image. A measure

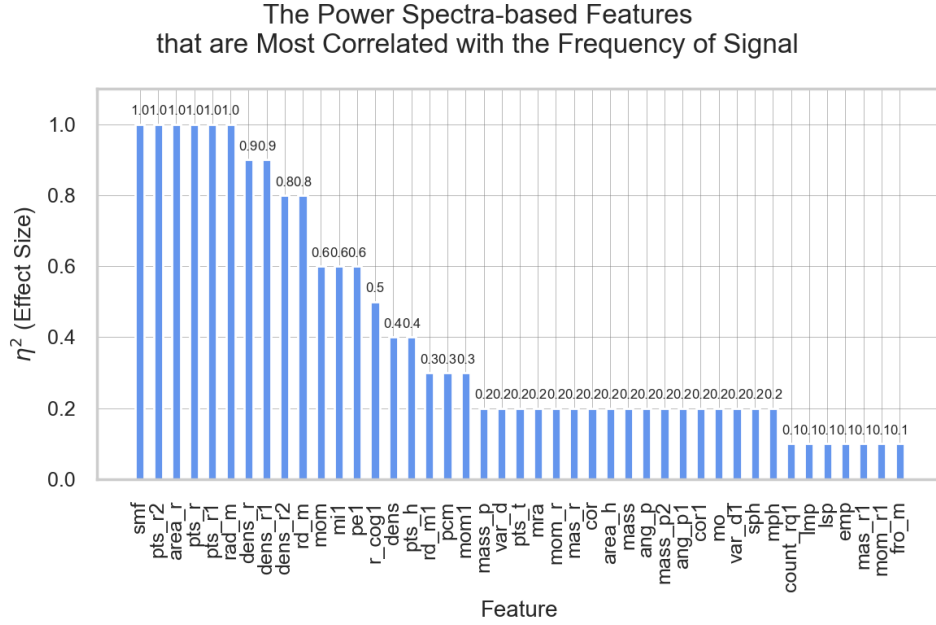


Figure 4.17: A set of power spectra-based features that are most correlated with the frequency of signal.

on this interaction must be established so that the probability of the response can be predicted.

### The logistic regression model using the features to predict the responses

As any level of the magnitude's dominance implies the opposite level of the phase dominance, their summation can be limited as 1.0. By assuming that the value of each feature follows the normal distribution, the contribution conveyed by the feature to the magnitude dominance can be modelled in the *cumulative distribution function* (cdf) of the normal distribution (Equation 4.6).

$$\text{mag}_f(x) = 0.5 \left( 1 + \text{erf} \left( \frac{x - \bar{x}}{\sigma\sqrt{2}} \right) \right), 0.0 \leq \text{mag}_f(x) \leq 1.0 \quad (4.6)$$

Where  $f$  is the feature,  $\bar{x}$  is the mean value of the feature, and  $\sigma$  is the standard deviation of the feature. The corresponding phase dominance is  $1.0 - \text{mag}_f(x)$  and can be simplified as in Equation 4.7.

$$\text{pha}_f(x) = 0.5 \left( 1 - \text{erf} \left( \frac{x - \bar{x}}{\sigma\sqrt{2}} \right) \right), 0.0 \leq \text{pha}_f(x) \leq 1.0 \quad (4.7)$$

The interaction between two values of a certain feature which belong to MP and PP in the hybrid image can be estimated by subtracting the magnitude's



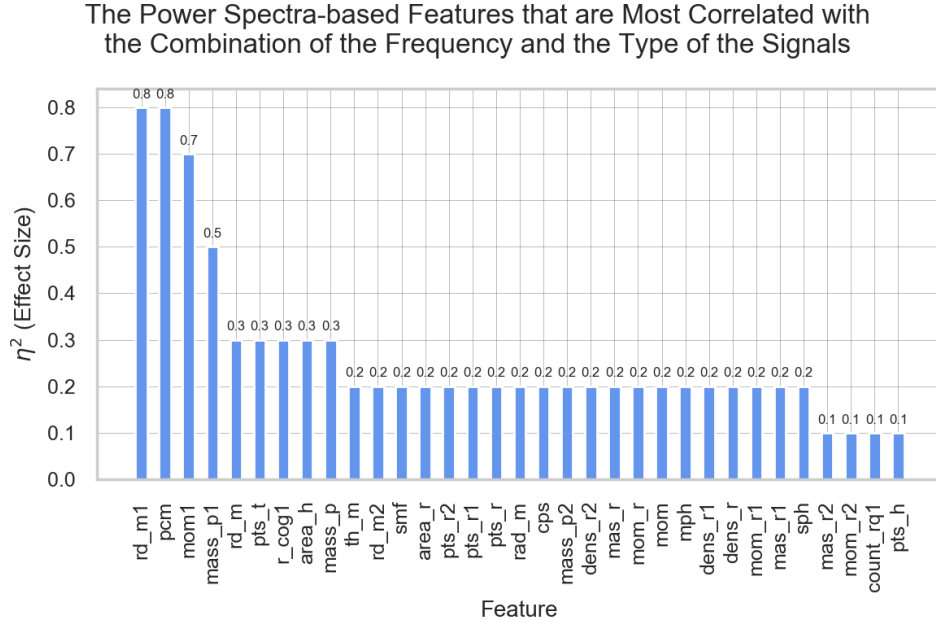


Figure 4.18: A set of power spectra-based features that are most correlated to the combination of the type and the frequencies of signal of MP

dominance of MP and the magnitude's dominance of PP at their values of feature. If the value is positive then the response will tend to be 1. The higher the difference between them, the more likely for the response to be 1. Otherwise, if the difference is negative, the response will tend to be 0. For example, if the magnitude's dominance of MP is lower than PP has, the hybrid image will tend to have less dominance of magnitude as the subtraction between  $mag_{MP}$  and  $mag_{PP}$  is significantly negative (Figure 4.19).

A set of thirty three features which significantly correlate with the type and the frequency of signal (Figure 4.18) were selected. A further reduction on this number of features was performed by removing the features which are highly correlated with each other. The threshold was set at .95 and, eventually, the number of selected features was reduced to nineteen. Each of these selected features was, then, standardized and was transformed to include the strength of the magnitude's dominance of PP using Equation 4.8.

$$\text{mag}_{f'}(x) = 0.5 \left( \text{erf} \left( \frac{x_{MP} - \bar{x}}{\sigma\sqrt{2}} \right) - \text{erf} \left( \frac{x_{PP} - \bar{x}}{\sigma\sqrt{2}} \right) \right), -1.0 \leq \text{mag}_{f'}(x) \leq 1.0 \quad (4.8)$$

Where  $\text{mag}_{f'}$  is the transformed feature,  $x_{MP}$  is the value of the feature of MP, and  $x_{PP}$  is the values of the feature of the corresponding PP. The values of feature in MP and the values of feature in PP are combined to calculate the mean value and the standard deviation of the feature. All features undergo the same treatment.

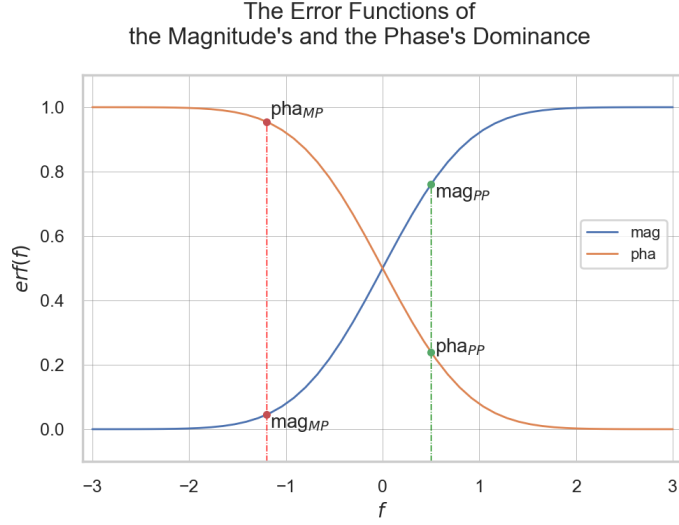


Figure 4.19: The error function used to estimate the relationship between the magnitude's dominance and the phase's dominance. The sum of their values at any point along the feature axis is always 1.0. For example, a value of the feature which corresponds to an image with 80% magnitude's dominance will imply that the phase's dominance of that image can also be known directly from that value which, therefore is 20%. It is assumed that as the value of the feature increases, the magnitude's dominance also increases.

A binary logistic regression is used to model the relationship between the features and the response (Equation 4.9).

$$h_{\beta}(\mathbf{x}) = \frac{1}{1 + e^{-\mathbf{x}\beta}} \quad (4.9)$$

where

$$\mathbf{x}\beta = \begin{bmatrix} 1 & x_1^1 & x_1^2 & \cdots & x_1^n \\ 1 & x_2^1 & x_2^2 & \cdots & x_2^n \\ \vdots & \vdots & & \vdots & \\ 1 & x_m^1 & x_m^2 & \cdots & x_m^n \end{bmatrix} \begin{bmatrix} \beta_0 \\ \beta_1 \\ \beta_2 \\ \vdots \\ \beta_n \end{bmatrix} \quad (4.10)$$

and  $\mathbf{x}$  is the column vectors of the feature,  $\beta$  is the column vector of the coefficients of the features, except for  $\beta_0$  which is the intercept,  $m$  is the number of the training samples, and  $n$  is the number of the features. By assuming that those  $m$  samples are independent, the likelihood function of the coefficients  $\beta$  for the logistic regression can be written as in Equation 4.11.

$$L(\beta) = \prod_i^m h_{\beta}(\mathbf{x}_i)^{y_i} (1 - h_{\beta}(\mathbf{x}_i))^{1-y_i} \quad (4.11)$$

A Lasso regularization (Equation 4.12) method was implemented to the log of Equation 4.11 in order to avoid overfitting by reducing the number and the values of coefficient  $\beta$ s [284, 285].

$$\ell_1(\boldsymbol{\beta}) = \sum_{i=1}^m \left( y_i \log h_{\boldsymbol{\beta}}(\mathbf{x}_i) + (1 - y_i) \log (1 - h_{\boldsymbol{\beta}}(\mathbf{x}_i)) \right) - \lambda \sum_{j=0}^n |\beta_j| \quad (4.12)$$

By implementing a grid search cross validation (GridSearch-CV) method [286, 287] in the data, it was found that the best value of  $C$  for the  $\ell_1$  penalty is 5.46 (Figure 4.20). This  $\ell_1$  regularization helps removing the least important features by making their coefficient to zero which, therefore, aligns with the goal to find a set of most useful features.

The ordinate value of the point where the vertical line (at  $C = 5.46$ ) crosses the curve of the feature becomes the coefficient of that feature ( $\beta_j$ ) in the logistic regression model. The maximum value of the coefficient is 5.7 which belongs to feature *mom* and the minimum value is  $-6.1$  which belongs to feature *pts.t* (Figure 4.21). The intercept ( $\beta_0$ ) is 1.30.

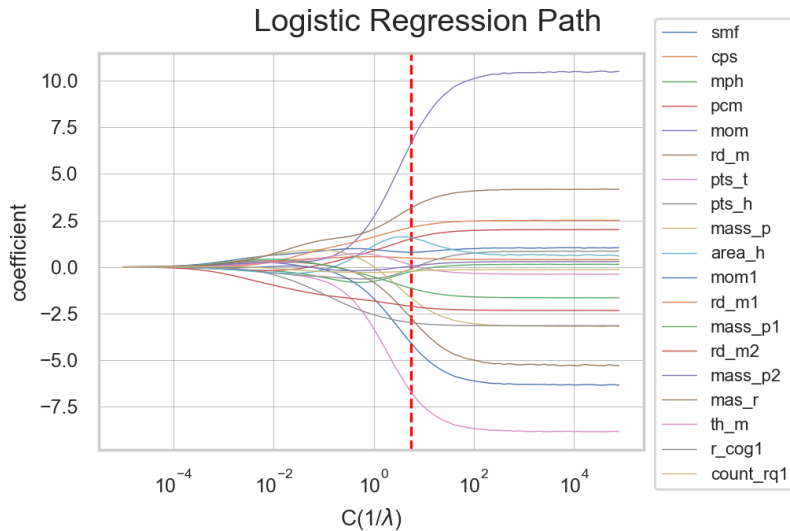


Figure 4.20: Constant  $C$  is the inverse of  $\lambda$  (the penalty term's constant). The larger the  $C$  value, the logistic regression becomes more similar to the ordinary logistic regression. The coefficients become large. To shrink the coefficient, the  $C$  value must be adjusted to the smaller level. The closer the value of  $C$  to the zero, the bigger the penalty applied to the loss-function which eventually makes the logistic regression's coefficients shrink.

The features with a positive coefficient indicate that their contribution to the probability of getting response 1 is positive. In other words, this feature has a

Table 4.14: The Classification Report of the Logistic Regression

	Precision	Recall	f1-score	Support
0	.66	.45	.54	905
1	.82	.91	.86	2422
accuracy			.79	3327

positive correlation with the magnitude dominance. Otherwise, if their coefficient is negative, the features contribute in increasing the chance of obtaining response 0. The larger the coefficient, the bigger the contribution of the feature to the logistic function.

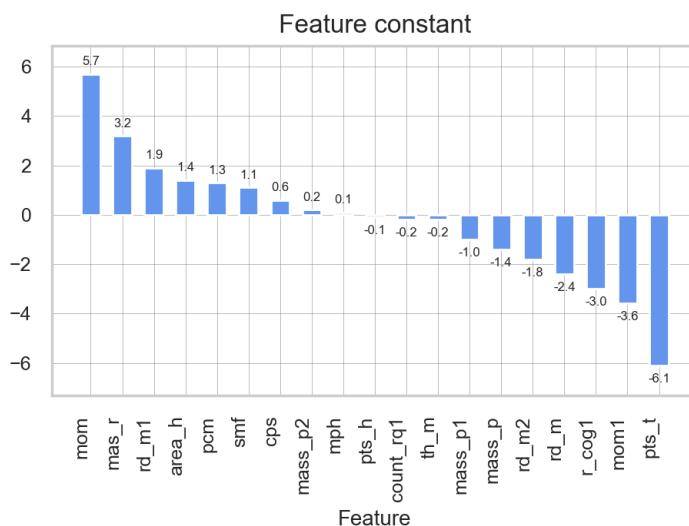


Figure 4.21: The coefficients of each feature ( $\beta$ ) of the logistic regression which is supposed to give the best performance (See Equation 4.9).

By using those features and coefficients, the logistic regression achieved the accuracy of 79% (Table 4.14). It means that 79% of the responses were correctly predicted. The performance in predicting the response 1 (82% correct) is better than in predicting the response 0 (66% correct). Only 45% (recall) were correctly predicted from the total number of predictions of response 0. Meanwhile, 91% of the total of response 1s predicted are correct.

## 4.4 Conclusion

Images with one-dimensional (1-D) periodic signal are magnitude dominant. This type of image has a power spectrum with a few frequency components that being arranged in one line for the signal with  $0^\circ$  and  $90^\circ$  rotation angle, and in two

lines for the signal with  $45^\circ$  rotation angle. The fewer the number of frequency component, the stronger the magnitude dominance which, therefore, the weaker the phase dominance. Having only a single frequency component, the image with sinusoidal signal becomes the most magnitude dominant. In other words, the fewer the frequency components, the more the texture's information conveyed by the power spectra, and, hence, the less the information contained in the phase spectra.

The second parameter of 1-D periodic signal which also influence the magnitude dominance is the frequency. The higher the frequency of signal, the stronger the magnitude dominance. The frequency is related with the distance of the largest frequency component and the distance of arrangement between the frequency components of the power spectra. The larger these distance, the stronger the magnitude dominance.

The rotation angle of signal has no effect to the magnitude dominance of its power spectra. The magnitude dominance of an hybrid image composed from two parent images with the same rotation angle is determined only by the type and the frequency of both of parent images. Only when the parent images have different rotation angle, the hybrid image will have the higher magnitude dominance. This, however, is caused by the appearance of directional textures which again is more related to the type and the frequency of signal than the rotation angle of signal itself. Therefore, the magnitude dominance of an image with a 1-D periodic signal is influenced only by the type and the frequency of signal.

Based on these evidences, the power spectra can be used to measure the magnitude dominance of images. Some features can be generated to extract the information about the effective number and the distance of the frequency components so that the magnitude dominance of an image can be measured. As the level of magnitude dominance implies the opposite level of phase dominance, the total of these potentials can be limited as 1.0. Therefore, an image with 0.8 of magnitude dominance will have 0.2 of phase dominance. The magnitude dominance of an hybrid image can be estimated by the difference of the magnitude dominances of its parent images.

# Chapter 5

## The Influence of Scaling Transformation to the Magnitude Dominance of Images

### 5.1 Experiment Rationale

From Chapter 4, it was found that the magnitude dominance of an image can be estimated from its power spectrum. Moreover, instead of using the phase spectrum itself, the phase dominance of an image can also be measured from its power spectrum because the phase dominance is just the opposite level of magnitude dominance. In the image with a periodic texture, the magnitude dominance can be determined by the number and the distance of the arrangement of frequency components in the power spectrum. The bigger the number of frequency components, the weaker the magnitude dominance. Meanwhile, the further the distance between non-zero frequency components, the stronger the magnitude dominance.

In this experiment, those evidences would be examined again. It was hypothesized that by changing the frequency of its texture, any image can be modified from being phase dominant to become magnitude dominant or vice versa following a pattern shown in Figure 5.1. To test this hypothesis, a set of images with natural textures were used as the stimuli. Because most of natural images have aperiodic textures, it is common for them to have a low frequency [256] and, hence, become phase dominant. However, this condition makes these textures even more suitable to become the stimuli.

To change a natural image from being phase dominant to become magnitude dominant, one of the possible methods is to increase the frequency of its texture

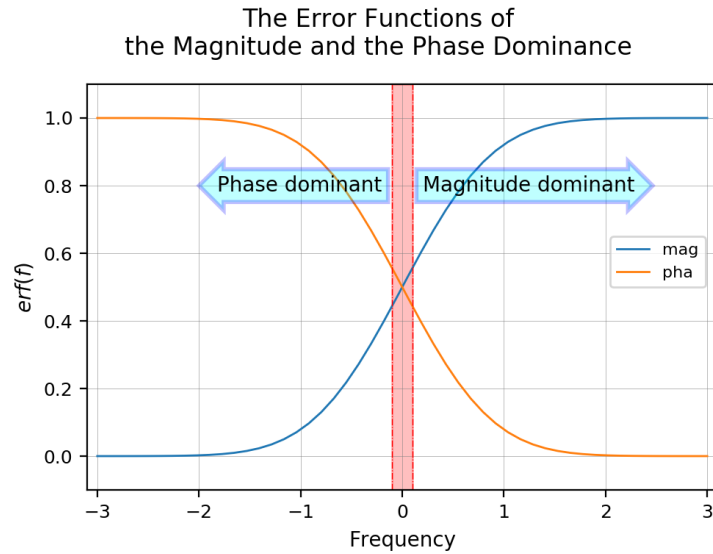


Figure 5.1: The error function can be used to estimate the magnitude dominance of an image based on its features. An image cannot be both magnitude dominant and phase dominant at the same time. However, by changing the frequency of its texture, the magnitude dominance of an image can be modified. Increasing the frequency will improve the magnitude dominance of the image and therefore, a phase dominant image can become magnitude dominant. Reducing the frequency will result the contrary effect.

which can be done by scaling down their size and, then using its replications to fill the vacant space. The result is a new image with a more periodic texture for which, therefore, the magnitude dominance becomes higher than the original image.

However, as the profile of the power spectrum of an image with natural texture is not regular, the number of non-zero frequency components will not directly reflect its magnitude dominance. Not only the number and the distance, but the weight of frequency components will also influence the magnitude dominance. Besides, as the arrangement of the non-zero frequency components is irregular, their spacing distance will be difficult to determine and, hence, the frequency of the image's texture will not be possible to calculate. Based on this evidence, the power spectra-based features become even more preferred to characterize the power spectrum and to measure its magnitude dominance.

The present study aims to investigate the influence of the scaling method to the magnitude dominance of images. The power spectra of the scaled images would be characterized using a set of features to predict when the scaled image shifted from being magnitude dominant to become phase dominant and vice versa.

This experiment was intended to determine the ratio of the scaled images at these two shifting points and to determine a number of power spectra-based features to characterize the magnitude dominance of images.

## 5.2 Method

Although it would not be exactly known, the magnitude dominance of a common image was assumed to be lower than its phase dominance. The magnitude dominance of an image can be modified using a scaling method, i.e. the image is shrunk and then the emptied space is filled by the shrinking pattern so that the original size is kept intact. The new texture of the image becomes filled by a number of tiles of shrunk patterns. The smaller the shrunk image the higher the frequency of its texture and the stronger the magnitude dominance. At some point, the texture will shift from being phase dominant to become magnitude dominant.

To observe and to measure the magnitude dominance of the scaled image, another image is needed. The magnitude spectrum of the scaled image is combined with the phase spectrum of the other image to form a hybrid image. A visual observation is needed to compare these images and to determine whether the hybrid image is more similar to the scaled one or the other one. The scaled image is considered as magnitude dominant if it is perceived to be more similar to the hybrid image. Otherwise, it will be phase dominant.

### 5.2.1 Stimuli

Fourteen images were used in the experiment. Five of them were used as the parent images which contribute the power spectra. This kind of parent image was then coded as MP to shorten its mention. They were set to have different levels of magnitude dominance. However, as it is difficult to find and to collect a set of natural images which can be sorted in a regular order according to the type or the frequency, five different images were chosen carefully from Brodatz dataset so that they would have different frequencies of texture (Figure 5.2). During the experiment, their texture was modified from the natural one to the more regular and artificial one by scaling down their size. This transformation was intended to increase the frequency of the texture and, therefore, their magnitude was predicted to increase too.



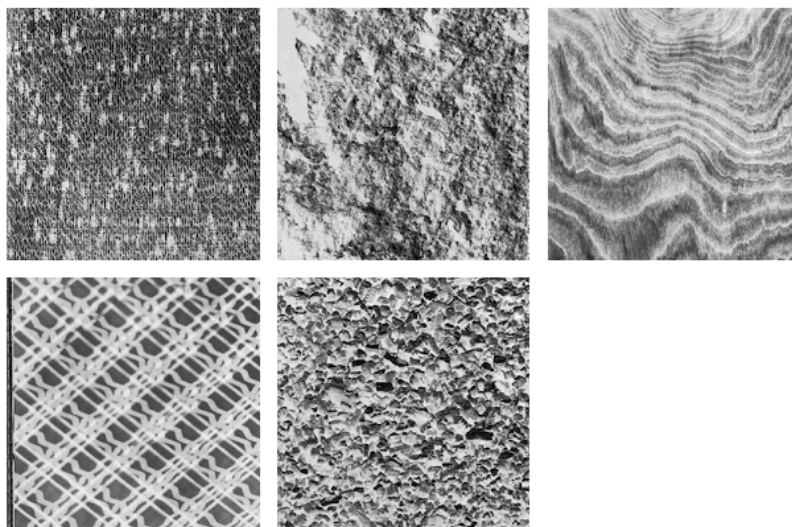


Figure 5.2: The set of parent images which were used as the source of the power spectra (MP). From the top left to the bottom right, the patterns are labelled as MP-1 to MP-5 respectively. Here, the sizes of the image stimuli are reduced for sake of clarity. The actual size of each image is  $256 \times 256$ .

Nine images were used as the parent images which contributed the phase spectra (Figure 5.3). This parent image was coded as PP. As modifying the phase spectra will result an unpredictable effect, they were kept fixed. However, these images were selected by putting the different levels of phase dominance into the consideration. Three groups of images with different phase dominances were collected. The first group consists of three images with no noticeable global frequency of texture (Figure 5.3: top row). This type of image was supposed to have a high phase dominance. Their texture were predicted to always appear in the hybrid image at some point within the range of the scale of MP. The second group of images were selected from Brodatz dataset (Figure 5.3: middle row). Three images within this groups were predicted to have a different level of phase dominance which are still lower than the first group, yet, higher than the third group of images which have the lowest phase dominance (Figure 5.3: bottom row). The third group of images have the lowest phase dominance. Therefore, their texture was predicted to will never appear in the hybrid image.

## 5.2.2 Participants

Eighteen volunteers were the subjects in this experiment and each of them performed ninety tasks. They were students at the University of Leeds. All participants were interviewed to ensure they are free from impairments that could

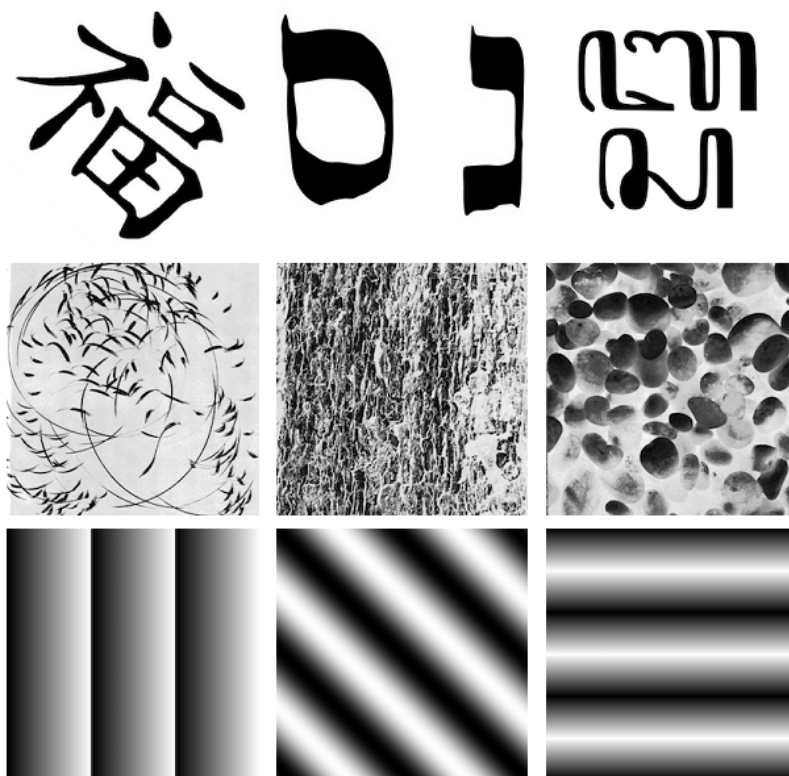


Figure 5.3: The set of parent images which were used as the source of the phase spectra (PP). From the top left to the bottom right, the image are labelled as PP-1 to PP-9 respectively. These images were displayed along with the hybrid image and their texture was not modified. Thus, their phase spectra did not change. Here, the sizes of the image stimuli are reduced for sake of clarity. The actual size of each image is  $256 \times 256$ .

affect their ability to perceive the visual patterns. Participants were naïve to the hypotheses. In all experiments the duration of the stimuli exposure was not specified to allow subjects to make thorough explorations of the patterns.

### 5.2.3 Procedure

Forty five hybrid images were created from five MPs and nine PPs. Each hybrid image was then paired with PP and was displayed on a computer screen (Figure 5.4 and 5.5). The scaled MP was not shown. However, its changing power spectrum affected the appearance of the hybrid image.

There were two setups of scaling activity. First, the left setup in which the MPs were initially set to the lowest ratio (0.07). In this condition, all of their textures became regular and periodic with a high frequency. Their power spectra became magnitude dominant so that even PP with a high phase dominant will

disappear from the hybrid image (Figure 5.4: right image). Hence, all PPs would not be seen on the hybrid image at the beginning. The maximum ratio was set at 1.0 and, therefore, the slider could not move beyond that limit.

The task given to the subjects was then to move the slider on the screen so that the texture of the left image (PP) starts appearing on the hybrid image and to press the button Yes if the left texture was seen. If the slider had been moved to the most right and the left texture still can not be seen, the subjects were instructed to press the button No (Figure 5.4). As the magnitude dominance of MP was decreasing, the first six PPs (in the first and the second rows in Figure 5.2) were predicted to be seen at some point when the slider was being moved to the right side. However, the bottom row PPs, which have a very low phase dominance, were predicted to be not seen at all.

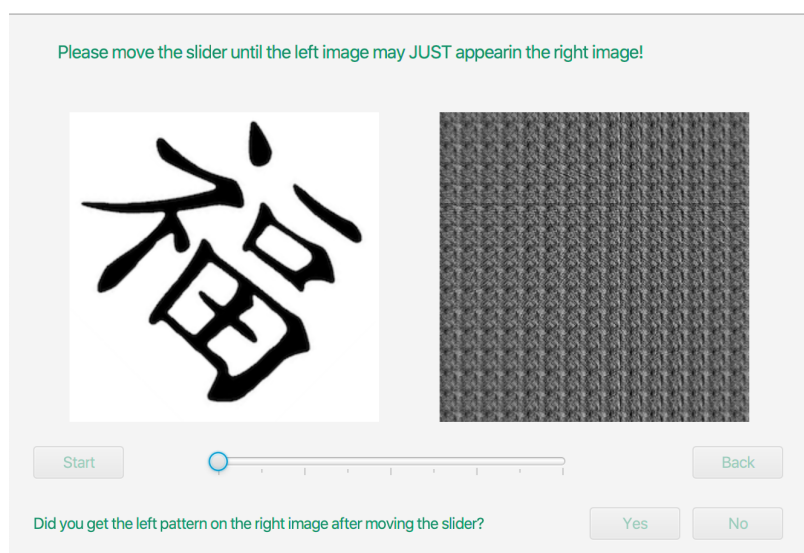


Figure 5.4: The scheme of a pair of images displayed on computer screen for the left-setup experiment. The left image is PP which contribute phase spectrum and was not transformed. The right image is the hybrid image which is changing if the slider is moved due to its power spectrum changing too. If the slider is move to the right, the texture of the left image (PP) will probably and slowly appear in the hybrid image. Here, the sizes of the image stimuli are reduced for sake of clarity. The actual size of each image is  $420 \times 420$  pixels.

Second, the right setup in which the ratio was set from 1.0 and the slider is initially at the right position (Figure 5.5). At this condition, the first six PPs were predicted to be seen and the rest to be not seen on the hybrid image. Then, the subjects were asked to move the slider from the right to the left so that the ratio decreases. At the position where PP starts disappearing, the subjects were asked to press button Next. If, from the beginning, the left pattern cannot be

seen in the right image, the subjects were instructed to press button No directly without moving the slider. If subjects mistakenly moved the slider despite PP not being seen in the hybrid image, the button Refresh was provided to restart the display of the stimuli.

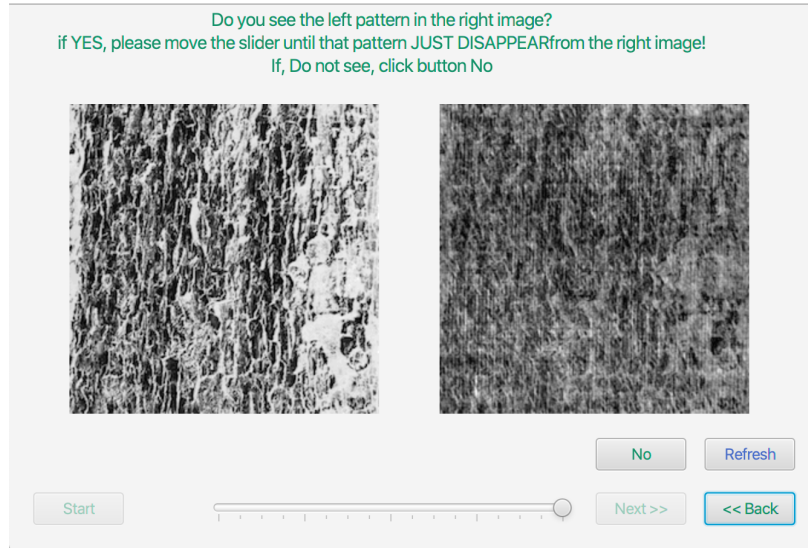


Figure 5.5: The scheme of a pair of images displayed on computer screen for the right-setup experiment. The slider was initially set the right side which indicates that the scaling ratio of MP is 1.0. At this condition, the texture of PP will probably appear in the hybrid image (right side). If the slider is moved to the left side, the texture will slowly disappear. Here, the sizes of the image stimuli are reduced for sake of clarity. The actual size of each image is  $420 \times 420$ .

All subjects performed both setups of experiment. In each setup, forty five pairs of stimuli were presented twice (in two rounds). Therefore, in both setups, each subject was conducting four rounds of trials (180 adjustment activities). To minimise the bias, the experiment's order was counterbalanced. Nine subjects performed the experiment from the left setup and then the right setup. The other nine subjects did the experiment in the opposite order of setups.

#### 5.2.4 Analysis

The data collected were used to analyse the effect of scaling transformation to the magnitude dominance of images. The position of the slider at which the texture of PP starts either appearing (in left-setup) or disappearing (in the right-setup) indicates the ratio of the shrinking MP. Ideally, the mean of scaling ratio is the same for each setup. However, the most likely to happen is the mean of scaling ratio in the left setup would be larger than the same mean in the right setup. A

paired t-test would be used to determine whether these means of scaling ratio are the same or not.

One hundred and seven features were extracted from the power spectra of the stimuli. The features that are most correlated with the magnitude dominance will be used in a binary logistic regression to model the magnitude dominance of the transformed images. As each feature has values from MP and PP, its relative value was then calculated using Equation 4.8 before being used in the regression model.

## 5.3 Result and Discussion

Two types of data were obtained from the collected responses. The first data are the informations of whether subjects noticed either the appearance or the disappearance of PP in the hybrid image. The data were coded as 1 if subjects noticed any one of them and as 0 if did not. In the left-setup experiment, code 1 means that subjects noticed the shift of the magnitude dominance of MP from being high to become low which was marked by the appearance of PP in the hybrid image. Meanwhile, in the right-setup experiment, code 1 means that subjects noticed the shift of the magnitude dominance MP from being low to become high which was marked by the disappearance of PP in the hybrid image.

The second information is the scaling ratio of the transformed MP. From the left-setup experiment, the collected scaling ratios indicate the size of transformed MPs at which their magnitude dominance start becoming lower than their phase dominance. Meanwhile, from the right-setup experiment, the scaling ratio indicates that the magnitude dominance of MPs was perceived to become higher than their phase dominance.

### 5.3.1 The appearance and disappearance of PPs in the hybrid image

A total of 3240 responses were collected from both setups of experiment with each of them contributing a half of that number (1620). In the left-setup experiment, it was predicted that subjects would notice the appearances of PP in two-thirds of 1620 occasions (1080) as two-thirds of the PPs are phase dominant (Figure 5.3). However, the result shows that PPs were perceived to appear in twenty nine more occasions than it was predicted (Table 5.1). A similar result was obtained from the right-setup experiment. In more than two-thirds occasions,

Table 5.1: The Summary of Responses on Appearance and Disappearance of PPs

Experiment Setup	Observed Number of Appearances (Predicted)	Observed Number of Disappearances (Predicted)
Left	1119 (1080)	501 (540)
Right	416 (540)	1204 (1080)

Table 5.2: The Summary of Responses on Appearance and Disappearance of PPs for Each PP in Both Experiment Setups

Setup	Response	PPs								
		1	2	3	4	5	6	7	8	9
left	0	0	1	0	11	98	2	119	170	100
	1	180	179	180	169	82	178	61	10	80
right	0	0	1	0	5	72	1	97	148	92
	1	180	179	180	175	108	179	83	32	88

subjects was seeing PP disappear from the hybrid image. Both results suggest that scaling down the size of images can systematically increase their magnitude dominance and scaling up their size will reduce it.

All presented stimuli were predicted to obtain response 1s except for PP-7, -8, and -9 which were predicted to obtain all 0s. These three PPs have a significantly low phase dominance so that they should never appear in the left-setup experiment and also never disappear in the right-setup one. However, eventually, the result came with the unpredicted responses instead of with the predicted ones. As an evidence, despite obtaining all 1s, PP-2, -4, -5, and -6 obtained a number of 0s in both the left- and the right-setup experiment respectively (Table 5.2). For PP-2 and PP-6, as their proportion of 0s is less than 5%, those unpredicted responses were most likely due to chance. However, for PP-4 and PP-5, the responses seems to not merely due to chance. Another evidence is found in PP-7, -8, and -9. Despite being predicted to obtain only 0s, they obtained a considerably number of 1s, especially for PP-7 and -9. This result shows the source of the discrepancy between the number of observed responses and the predicted ones (Table 5.1).

In general, from a total of 3240 responses, 545 (17%) of them are unpredicted (Table 5.3). Among them are 354 unpredicted 1s (predicted to be 0s, yet was found to be 1s). This number accounts for 33% of total predicted 0s. Thus, despite having a low phase dominance, PP-7, -8, and -9 were perceived to be phase dominant by appearing 354 times from 1080 corresponding pairs. Unpredicted 0s (predicted to be 1s, yet was found to be 0s) came from 191 (9%) pairs out of 2160 corresponding pairs. It means that PP-2, -4, -5 and -6 were perceived to be



Table 5.3: The Cross Tabulation of the Predicted and the Observed Responses

Observed \ Predicted	0	1
	0	726
1	354	1969

Table 5.4: Chi-Square Test of Independence of Responses

Difference between	$\lambda$ (Pearson)	Num. of Obs.	DoF	$\tilde{\chi}_{cr}^2$	$\tilde{\chi}^2$	P-val	Cramer's V
Observed and predicted	1.0	3240	1	3.81	1206.40	.000	.610
Left- and right-setups	1.0	3240	1	3.81	10.73	.001	.058
First- and second-round	1.0	3240	1	3.81	.49	.482	.012

less phase dominant by not appearing in the hybrid image for 191 times despite being phase dominant.

Those unpredicted responses, however, are eventually significantly different from the predicted ones (Table 5.4: first row). Both of the p-value and the Cramer's V value support this indication. This result, therefore, shows that those unpredicted responses were actually not really to be unpredicted ones. The responses' proportion of PP-5, -7, -8 and -9 were arguably not due to chance. In other words, the texture of those images influences the subjects' perception systematically.

Although the response's proportions for each PP in the left-setup and the right-setup experiments seems to be the same (Table 5.2: second row), the result from a Chi-square test shows that they are significantly different. This result indicates that these setups influence the responses, especially for PP-5, -7, and -9. However, as the Cramer's V value is small (.058), the relationship between the setups and the responses is relatively weak. In other words, the response's proportions between the left-setup and the right-setup is small yet significant. Meanwhile, between two rounds, the response's proportion shows no difference (Table 5.2: third row). The obtained p-value (.49) and the Cramer's V value (.012) support this indication. Thus, trial does not influence the response.

### 5.3.2 The ratio of the resized MPs

The scaling ratios of the resized MPs from both of the left- and the right-setup experiments are not normally distributed (Figure 5.6). Using a Shapiro-Wilk test, the obtained  $p$ -value is close to 0.00 which indicates that the assumption of both distributions are normal should be rejected. Both of them have a positive

skewness; they are 1.31 and 2.48 respectively although it seems that the tail of their distributions has different direction. The low frequencies spread across the segment line between ratio value of 0.5 and 1.0 make the skewness of the scaling ratios of the left-setup experiment becomes positive (the blue histogram). If those frequencies were removed, the skewness of this distribution becomes  $-1.37$ .

The scaling ratios of the left-setup experiment has a mean ( $\mu_l$ ) which equals to 0.44 and a median ( $\tilde{x}_l$ ) which equals to 0.40. The scaling ratios of the right-setup experiment has a mean ( $\mu_r$ ) which equals to 0.11 and a median ( $\tilde{x}_r$ ) which equals to 0.15. This result indicates that, in the left-setup experiment, the size of MPs have to be scaled up from initially 0.07 to 0.40 of their size on average so that PPs start appearing in the hybrid images and, in the right-setup experiment, MPs must be scaled down to 0.15 of their size on average so that PPs start disappearing from the hybrid images.

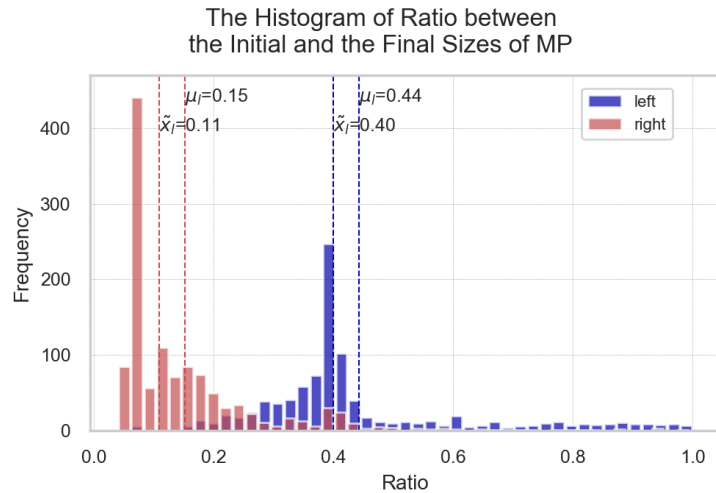


Figure 5.6: The histogram of the gathered scaling ratios of transformed MPs for the left-setup and the right-setup experiments. The frequency of scaling ratios is not normally distributed for both experiments.

The scaling ratio of resized MPs in the left-setup experiment is significantly larger than the same scaling ratio in the right-setup experiment. This indication is supported by the t-test results in Table 5.5. The obtained p-value and the effect-size value indicate a strong difference between  $\mu_l$  and  $\mu_r$ . Furthermore, it is seen that the scaling ratio of the resized MPs in the left-setup experiment is 0.28 higher than the same scaling ratio in the right-setup experiment with 95% confidence level.



Table 5.5: Paired T-tests on the Prevalence of Different Means of Scaling Ratio between Setups and between Rounds

Source	T	dof	Tail	P-value	CI (95% )	Cohen-d
setup (left-right)	41.77	986	greater	.000	[.28, $\infty$ ,]	1.86
round (first-second)	1.46	1096	two-sided	.140	[-.00, .01]	.02

Table 5.6: ANOVA tests on the Prevalence of Different Means of Scaling Ratio within MPs and PPs

Source	ddof1	ddof2	F	P-unc	$\eta p^2$
Subject	17	2182	20.938	.000	.140
MP	4	2195	4.197	.002	.008
PP	8	2191	10.483	.000	.037

The gap between  $\mu$  and  $\tilde{x}$  in each experiment setup is significantly smaller than the difference either between  $\mu$ 's or between  $\tilde{x}$ 's of both setups of experiment (Figure 5.6). As a result, either a parametric or a non-parametric test will provide the same result although the scaling ratio is not normally distributed. The paired t-test is preferred to the Wilcoxon signed-rank test because the former provides not only the same reliable results but also more information than the later.

Two rounds of experiment showed no different means of scaling ratio (Table 5.5: second row). The p-value is significantly larger than .025 and the effect size is also negligible (.02). Both parameters imply that rounds have no influence to the experiment's result. Meanwhile, different subjects gave significantly distinctive responses of scaling ratio (Table 5.6: first row). Moreover, subjects contributed 14% to the variance of the scaling ratio values which is considerably larger than the contribution of MPs and PPs. Two latter parameters also influence the scaling ratios although in the smaller portions (Table 5.6: second- and third rows). This, however, is not unpredictable as each MP and PP has a different texture which, therefore, has a different magnitude dominance too.

### 5.3.3 A Logistic regression to model the relationship between a set of power spectra-based features and the visual responses

Despite being related each other, the scaling ratio of the scaled image cannot be used to measure the magnitude dominance of that image by itself due to two reasons. First, for the same scaling ratio, two distinctive images will always have a different magnitude dominance. Second, the information of the scaling ratio is

only available when the image was scaled, whereas it is uncommon for an image to come from a scaling process. Besides, to measure the scaling ratio of this type of image is impossible and not useful. Therefore, instead of using scaling ratios to model the magnitude dominance, power spectra-based features were adopted here.

A set of one hundred and seven features which has been used in Chapter 4 were used again here. For PPs, as their size is fixed, the features were extracted from their power spectra at its original size. Meanwhile, for MPs, the features were extracted at each of their scaled sizes. Then, each feature was analysed using a Wilcoxon signed-rank test to know whether it is highly correlated with the magnitude dominance or not. In the test, the feature was set as the dependent variable and the binary response was used as the independent variable. The feature would be selected if the obtained p-value is less than .001 and the CLS value is larger than .56 (is equivalent to 10% of correlation) [288, 289]. From one hundred and seven features being tested, seventy six of them were found to pass those criteria.

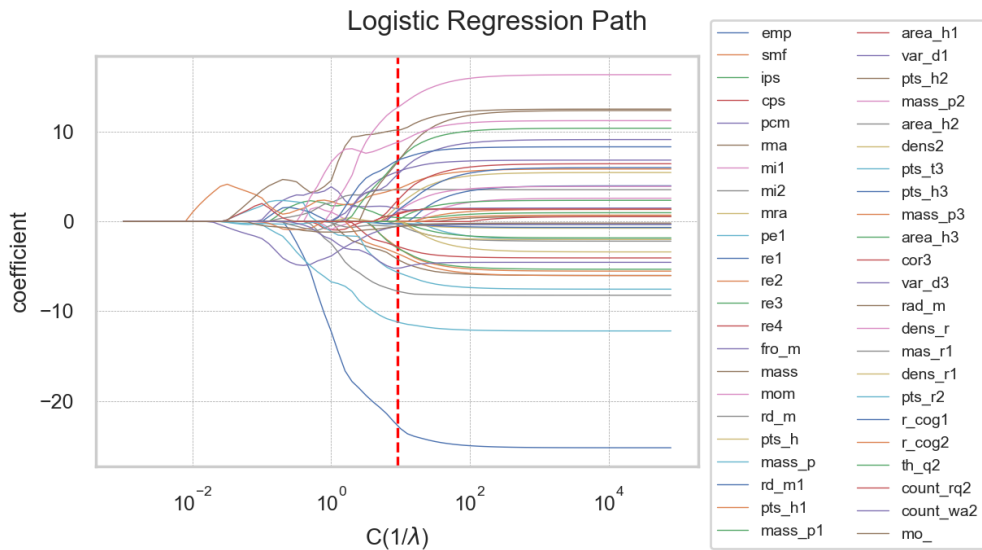


Figure 5.7: The optimal C value is shown by the vertical red dashed-line. The ordinate value of crossing points between this line and the feature paths become the coefficient value of each corresponding feature in the logistic regression model which can give the best prediction.

A further possible reduction on the number of features was investigated by measuring the correlation between themselves. The threshold was set at .95. Each number of features which are correlated to each other were removed except one. From this step, it was found that among seventy six of features, thirty one of

them have a correlation which is higher than .95 which were then being excluded from the list of useful features (Figure 5.8). Then, only forty six candidates of feature were selected to be used in the binary logistic regression model (Equation 4.9).

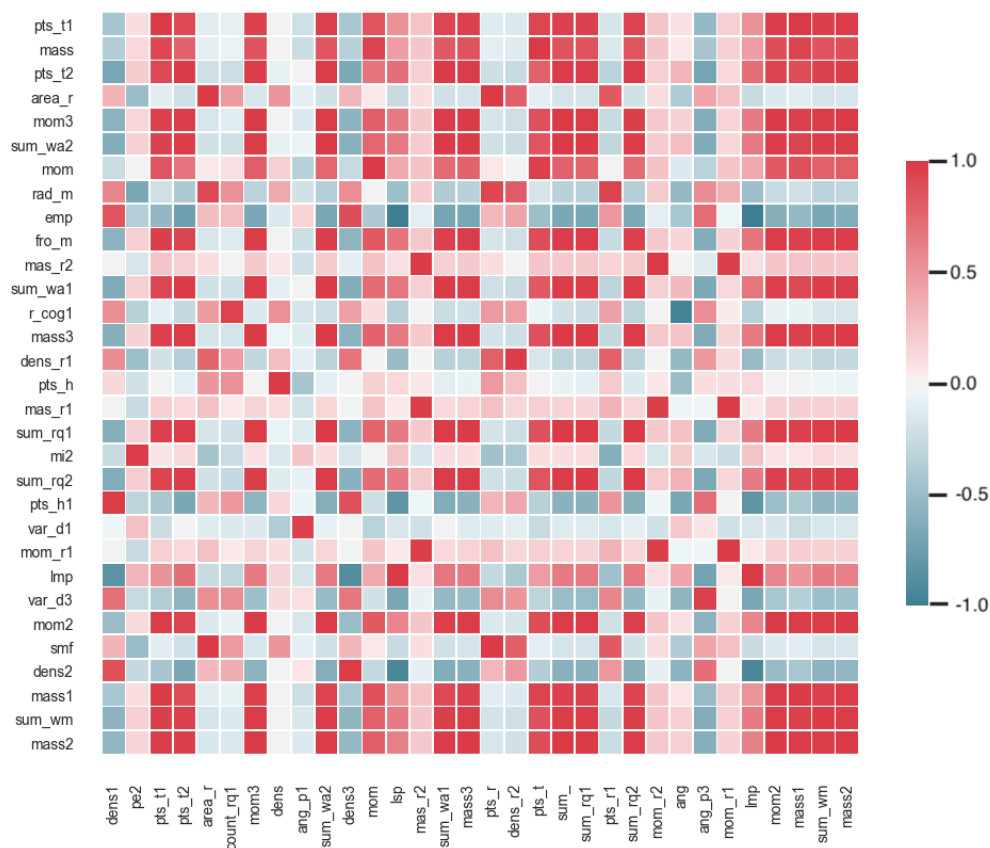


Figure 5.8: Features that are correlated each other above the threshold and would be excluded from the regression model.

To avoid overfitting and to shrink the values of  $\beta$ , a lasso regularization method ( $\ell_1$ -penalty) was implemented in the regression model (Equation 4.12). A GridSearch-CV method was used to find out the accuracy of the regression within a range of C values [286, 287]. The values of constant C ranged from  $10^{-3}$  to  $10^4$ . The result showed that the best C value is 13.26 which can provide an accuracy to the model at around 87% (Figure 5.9). Although the smaller value of C will reduce the value of  $\beta$ s (Figure 5.7), it will also make the accuracy of the model decrease (Figure 5.9). Meanwhile, the larger value of C will increase the value of  $\beta$ s, yet without improving the model's accuracy.

Based on this C value, the value of  $\beta$ s can be determined from the curves in the logistic regression path (Figure 5.7). The ordinate value of the point where

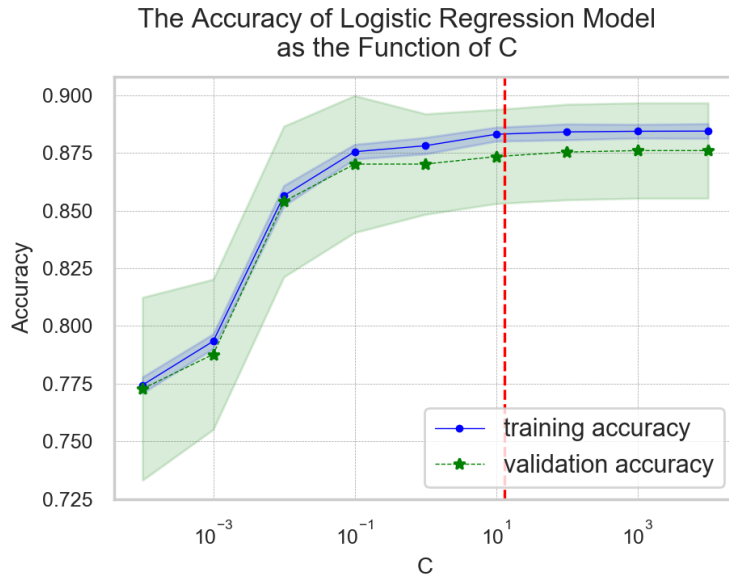


Figure 5.9: Using either training or validation data, the accuracy of the binary logistic regression model is seen to not improve for the  $C$  ( $1/\lambda$ ) value larger than 10. A GridSearch-CV method gave  $C$  equals to 28 to obtain the best accuracy.

the vertical line (at  $C = 13.26$ ) crosses the curve becomes the coefficient of the corresponding feature ( $\beta_j$ ) in the logistic regression model. However, as it seems that some features have a considerably smaller absolute value (magnitude) than the others, these features, therefore, can be removed from the model without affecting its accuracy significantly. There were seven features which have  $\beta$  of zero. The final list of thirty eight features and their coefficients ( $\beta$ ) is shown in Figure 5.10. The maximum value of coefficient is 13.6 which belongs to feature mass\_p2 and the minimum value is  $-23.7$  which belongs to feature emp. The intercept ( $\beta_0$ ) is  $-1.6$ .

Among those features, nineteen of them (50.0%) have a positive coefficient which means that if their value increases, their contribution to the magnitude dominance of the image also increases. The rest have a negative coefficient which indicates that if their value increases, their contribution to the magnitude dominance of the image decreases. However, these features will have a positive correlation with phase dominance.

By using those features and their coefficients, the binary logistic regression model achieved the accuracy of 87% (Table 5.7). It means that 87% of the responses were correctly predicted. The performance in predicting the appearance of PP (response 0: 83% correct) is lower than in predicting the disappearance of

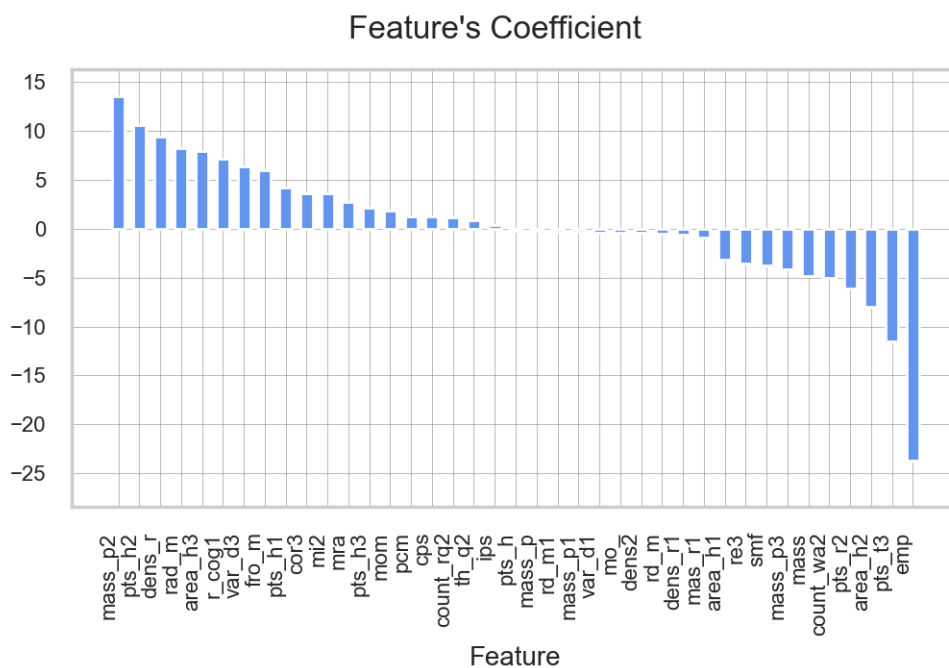


Figure 5.10: The coefficients of each feature ( $\beta_j$ ) of the logistic regression which is estimated to give the best performance.

Table 5.7: The Classification Report of the Binary Logistic Regression Model

	Precision	Recall	f1-score	Support
0	.83	.83	.83	258
1	.89	.89	.89	402
Accuracy			.87	660

PP (response 1: 89% correct). Furthermore, from the total number of prediction of response 0, 83% (recall) were correct. Meanwhile, 89% of the total number of response 1s being predicted were correct. This result indicates that the model is better in predicting the magnitude dominance than in predicting the phase dominance.

### Clustering performance of the binary logistic model

The scaling ratio correlates strongly with magnitude dominance. Simply by increasing or decreasing its scaling ratio, the magnitude dominance of an image will change accordingly. Meanwhile, for features, their correlation with magnitude dominance varies from strongly negative to highly positive. Therefore, the correlation between a set of one hundred and seven features and the magnitude dominance of images becomes obscure.

Since the beginning, it has been assumed that each feature has a non linear relationship with magnitude dominance (Figure 5.1). However, to investigate the performance of this assumption, three clustering techniques were implemented on the 3240 data points (rows) consisting of one hundred and eight columns (which are consisted of one hundred and seven features and the corresponding subject's response (either 0 or 1)).

The first technique was a K-means clustering method. It was intended to make two clusters of the subjects' responses from the 3240 data points using unsupervised classification processes. Prior to the process, each value of the features was transformed using Equation 5.1.

$$x' = 0.5 (\text{mag}_f(x) - \text{pha}_f(x)) \quad (5.1)$$

where,  $x'$  is the transformed value of the corresponding feature,  $\text{mag}_f(x)$  and  $\text{pha}_f(x)$  have been defined in Equation 4.6 and 4.7. In this transformation process, the features from both magnitude and phase spectra were taken into account. To visualize the result on a 2D chart, an MDS method was used to project one hundred and seven dimensions into two dimensions of data. The result (Figure 5.11: upper right) shows that the labels made by this method still differs significantly from actual observation (Figure 5.11: upper left).

The second technique was using a binary logistic regression to create two clusters of the responses. The data of features have also been transformed using Equation 5.1 prior to the process. A better result of classification was obtained as shown by the spread of the labels which is very similar to the distribution of responses (Figure 5.11: bottom left).

The third technique was also using a binary logistic regression to cluster responses into two groups. However, the data of features were not transformed as in the previous techniques. The data of features were taken solely from the images which contribute magnitude spectra. The performance seems to be better than the K-Means clustering method but worse than the binary logistic regression technique with transformed data (Figure 5.11: bottom right).

These results, therefore, indicate that the set of power spectra-based features are related non-linearly with the magnitude dominance. In this case, two error functions (Equation 4.6 and 4.7) (which are non-linear) were needed to transform the data of features from both images which contribute the magnitude and phase spectra. To accommodate the effect of the magnitude dominance of images MPs and PPs, Equation 5.1 was also used in this process of data transformation. This method has been shown to give a better result to the clustering process. Finally,

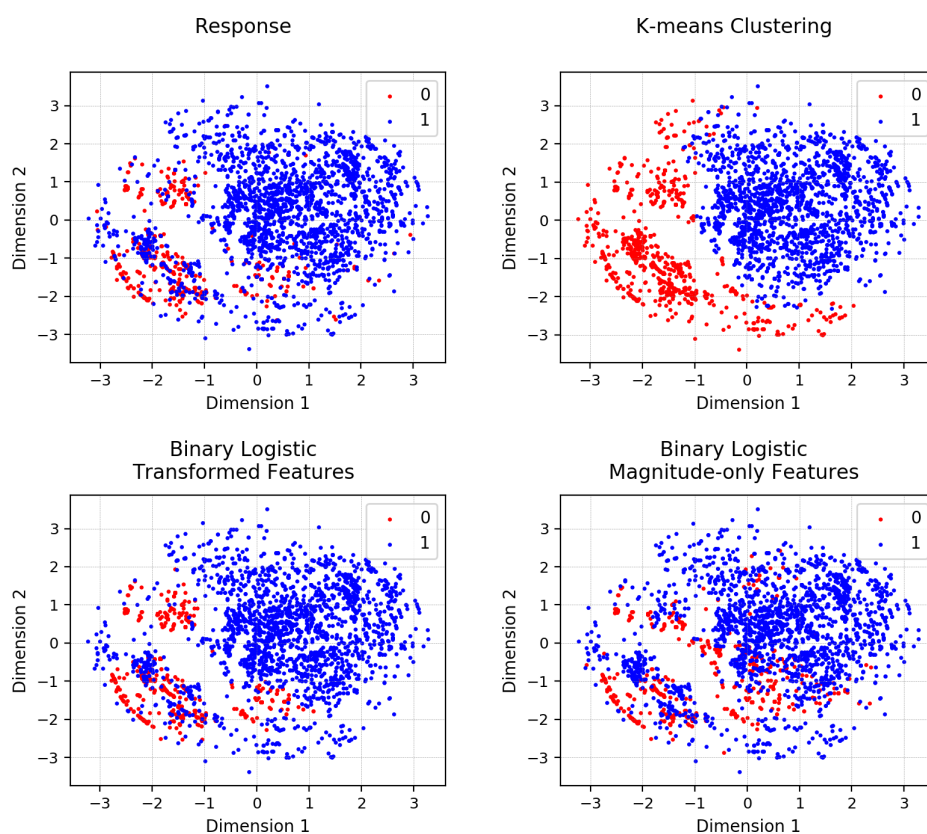


Figure 5.11: Scatter plots of 3240 responses. An MDS method was used to transform the dataset from one hundred and seven into two dimensions so that they can be visualized using scatter plots. The blue points indicates that the scaled images is magnitude dominant and the red ones for phase dominant images. Upper left is the plot of subjects' responses; upper right is the plot of clustered responses using K-means clustering method; bottom left is the plot of the clustered response from the binary logistic regression model using transformed-features (Equation 4.8); bottom right is the plot using the same binary logistic regression model but the features were from the MPs only.

a binary logistic regression technique is better to model the responses than using K-Means clustering method.

## 5.4 Conclusion

The magnitude dominance of images with natural texture can be adjusted by using the scaling method. This type of image will still be phase dominant even after being scaled down to around 44%. As the scaling ratio decreases, a high frequency of texture will appear in the scaled images. This type of texture will have a higher magnitude dominance. When the ratio scaling reaches at around 0.15,

the scaled images which were phase dominant will become magnitude dominant.

Having a scaling ratio lower than 0.15, most of images with natural textures which are originally phase dominant will turn to magnitude dominant. To recover their phase dominance, however, they need a scaling ratio higher than 0.15, i.e. around 0.44. This gap indicates that there is a hysteresis in the perception of image appearance.

Among one hundred and seven power spectra-based features being investigated, thirty eight of them were most correlated with the magnitude dominance of the scaled images. Four of them, i.e. `r_cog1`, `pcm`, `mass_p2`, `smf` have been used in Chapter 4 to model the magnitude dominance of images having texture with periodic signals. By using these selected features, the binary logistic regression model can achieve an accuracy of 86%.



## Chapter 6

# Magnitude Dominance of Natural Textures in the Visual and Tactile Perception

### 6.1 Experiment Rationale

Although it is widely believed that phase is more dominant than magnitude [193], especially in the images with a natural texture [256], the phase dominance of an image does not depend on whether it is natural or not. It has been found in Chapter 4 and 5 that the phase or the magnitude dominance of an image depends rather on the frequency components of its power spectrum. From the visual aspect, the magnitude dominance of an image is influenced by the frequency of its global texture. The higher the frequency, the stronger the magnitude dominance and, therefore, the less the phase dominance.

However, as the frequency of texture can not be easily measured, a set of one hundred and seven power spectra-based features are able to be used to represent it. They have been shown to perform well in the binary logistic regression model to predict the magnitude dominance of images. The present study aims to investigate the presence of natural textures which are magnitude dominant both in visual and tactile perception. Brodatz texture database was the source of the natural textures used in this study. The set of features were used to select a group of images which are magnitude dominant and another group of images which are phase dominant within the database. The magnitude and phase dominance of each image would be tested in both visual and touch experiment. Furthermore, these experiments were intended to

1. obtain some evidences of the presence of images with natural texture which are magnitude dominant,
2. show that the power spectra-based features can be used to cluster images with natural textures into a phase dominant and magnitude dominant group, and
3. to measure and compare the performance of visual and touch perception in discriminating textures with different levels of magnitude dominance.

## 6.2 Method

### 6.2.1 Stimuli

There were three steps to obtain the set of textures that would be used in this experiment. The first step is to collect a number of grayscale images that have natural texture. In the next step, only seven of them would be selected. As in Brodatz album all images are captured from natural objects, this album was chosen as the source of images. In total, there are one hundred and eleven images with different textures in that album. Two additional images were added to the collection; they are a sinusoidal image with frequency 1 Hz and an image of Chinese character. The former is the most magnitude dominant among other images in the collection and the later was known to have a relatively high phase dominant (Table 5.2). Based on those characteristics, both images were suitable as the reference images. The magnitude dominance of the other images can be estimated by referring their "distance" to both images. The natural texture of images which are magnitude dominant will surround the sinusoidal image. Meanwhile, the images which are phase dominant will stay close to the image of a Chinese letter. Then, all images were numbered from 1 to 113. The last two number for the images with sinusoidal texture (number 112) and the Chinese character (number 113).

The second step is to characterize each image in the collection using a set of one hundred and seven features which were extracted from its power spectrum. Those are the same features which have been used in chapter 4 and 5. A multidimensional scaling (MDS) method was then used to measure the distance between each image based on the collected values of features. This method was chosen because it preserves the similarities (closeness) of the data points in both low- and

high-dimensional space during optimization process [290]. The distance between images ( $D_{i,j}$ ) was calculated using Equation 6.1 (adopted from Buja et al. [291]).

$$\text{Stress}_D(\mathbf{x}_1, \dots, \mathbf{x}_N) = \left( \sum_{i \neq j=1}^N (D_{i,j} - \|\mathbf{x}_i - \mathbf{x}_j\|)^2 \right)^{1/2} \quad (6.1)$$

where  $\text{Stress}_D$  is a loss function to be minimized and  $\mathbf{x}_i$  is a column vector of features' values of image  $i$ .  $D_{i,j}$  is a two-dimensional matrix which was obtained by minimizing  $\text{Stress}_D$ . Based on this matrix, the relative position of each image represented by its label was then visualized in 2D plot (Figure 6.1).

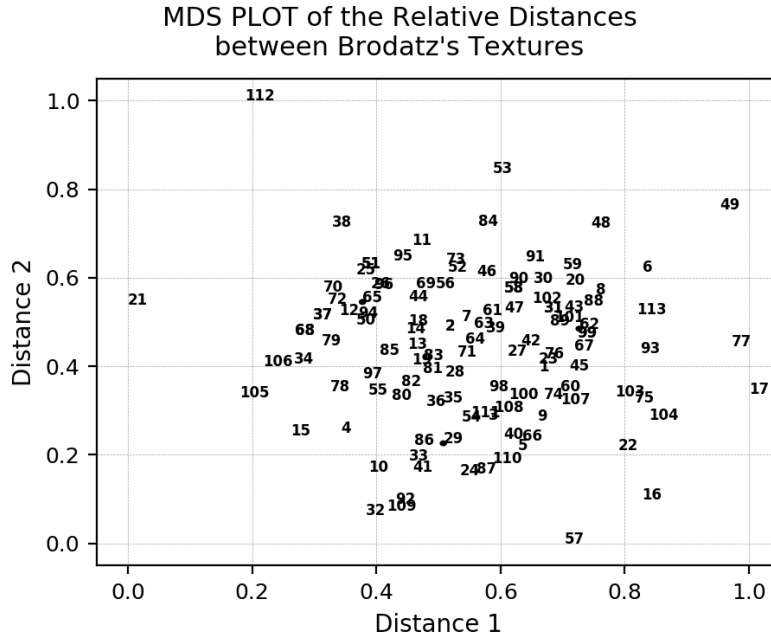


Figure 6.1: One hundred and thirteen labels of images are arranged based on their relative closeness. Image 112 has sinusoidal texture and here, it is the most magnitude dominant. Image 113 is a Chinese letter and it is most likely to have the most phase dominant.

The third step is to put the images in Figure 6.1 into several clusters. The two-dimensional matrix representing the relative position of each image that was obtained from the MDS method was used as the input data for the clustering process. As there was no initial labels, K-means clustering method was chosen to determine and obtain a reasonable number of clusters through unsupervised clustering process [292, 293]. The objective function is given by Equation 6.2.

$$J = \sum_{n=1}^N \sum_{k=1}^K w_{nk} \|\mathbf{x}_n - \boldsymbol{\mu}_k\|^2 \quad (6.2)$$

where  $J$  represents the sum of the square of the distances between each data point ( $\mathbf{x}_n$ ) and its centre of corresponding cluster ( $\mu_k$ ),  $w_{nk} = 1$  for data point  $x_n$  if it belongs to cluster  $k$ ; otherwise,  $w_{nk} = 0$ ,  $N$  represents the number of observations, and  $K$  is the number of clusters. By minimizing the value of  $J$  for a given value of  $K$ , the clusters and their members of data points can be determined.

The number of clusters assigned in the clustering process influences the value of  $J$ . Theoretically, the possible  $k$  ranges from 1 to  $N$ . However, it is uncommon to have either  $k = 1$  or  $k$  closes to  $N$ . The reasonable  $k$  can be determined by comparing the values of  $J$  for a range of  $k$ 's. Commonly, the value of  $J$  reaches its peak at  $k = 1$  and then drops significantly at a certain value of  $k$ . At this point, the value of  $J$  starts to flatten out and forming an elbow which means that the increase in  $k$  values does not improve the distance error  $J$ . Therefore, it is common and reasonable to pick this  $k$  as the chosen number of clusters.

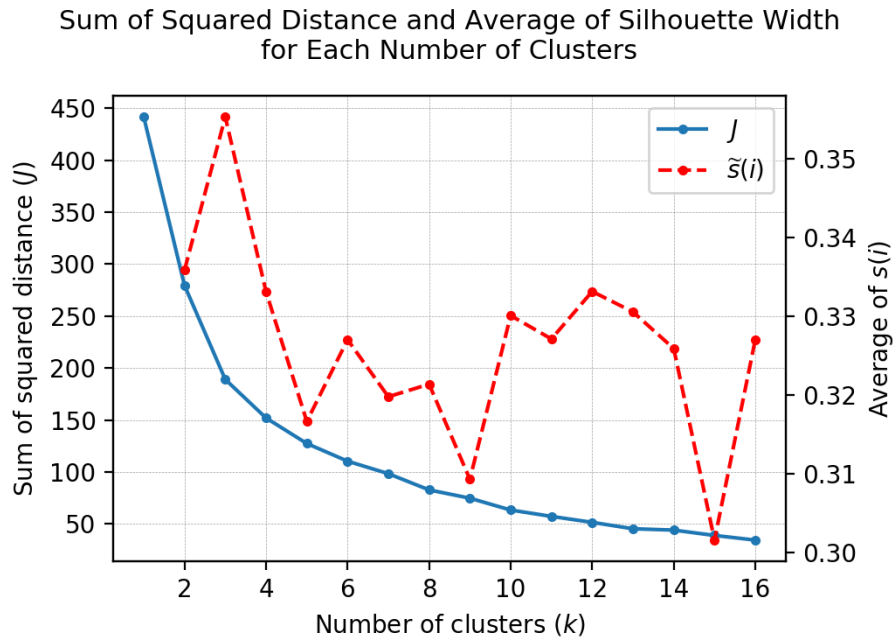


Figure 6.2: The blue curve shows the total sum of squared distance between two data points ( $J$ ) within each cluster for every  $k$  number of clusters in range of  $[1, 16]$ . The lower value of  $J$  the better. The red line indicates the average width of the silhouettes ( $\tilde{s}(i)$ ) at each  $k$  number of cluster. The higher value of  $\tilde{s}(i)$  indicates the better degree of cluster separation.

However, sometimes, the value of  $J$  decreases monotonically as  $k$  increases as it happens here (Figure 6.2). In this case, selecting the best value of  $k$  becomes difficult. A method called silhouette analysis was used to overcome this

problem [294]. In short, this method measures the degree of separation between clusters. Each cluster is represented by a silhouette that is formed by a collection of horizontal lines representing the silhouette width  $s(i)$  of each data point within the cluster. For each data point  $i$  within a cluster, the silhouette width  $s(i)$  is calculated using Equation 6.3.

$$s(i) = \frac{b(i) - a(i)}{\max(a(i), b(i))} \quad (6.3)$$

where  $a(i)$  is the average dissimilarity or distance of data point  $i$  to its neighbouring data points within its cluster and  $b(i)$  is the average dissimilarity of data point  $i$  to all other data points within the closest cluster.

The silhouette width  $s(i)$  has a range of  $[-1, 1]$ . Data points with  $s(i)$  close to  $+1$  indicate that they are far away from neighbouring clusters. A data point with  $s(i)$  equals to  $0$  means that it is very close to the boundary of the closest cluster. Some data points may have negative values of  $s(i)$  which means that they might have been assigned to the wrong cluster. By averaging all  $s(i)$  values, the degree of separation between clusters can be measured. If the average value of all  $s(i)$ 's near to  $+1$ , all clusters are well separated. In contrast, if the average value closes to  $0$ , the clusters may close each other.

Based on the silhouette method, the best value of  $k$  is  $3$  with the average width of silhouettes  $\tilde{s}(i)$  equals to  $3.55$  (Figure 6.2). Although this value indicates that the separation made for three clusters is still weak [295], the value of  $\tilde{s}(i)$  already reaches its peak which means that other choices of  $k$  will result weaker split of clusters. Therefore, in this experiment, the number of clusters for the images was selected to be three (Figure 6.3).

It was initially expected that the centres of all clusters form a relatively straight line which means that their magnitude dominance were well ordered. However, it is not the case here as all three clusters are radially positioned (Figure 6.3). The first cluster contains image 112 that is strongly magnitude dominant and therefore, this cluster was considered to comprise images with magnitude dominant. The second cluster which is next to the first one was regarded as phase dominant cluster as it contains image 113, i.e., the reference of phase dominant images. The last cluster consists of images that are relatively distant from image 112 and image 113. This condition makes the dominance of their phase or magnitude become not easily estimated in an intuitive way although it does not mean to be impossible to measure. Here, it was assumed that the phase or magnitude dominance of the image depends on the difference between its distance to image 112 and its gap with image 113.

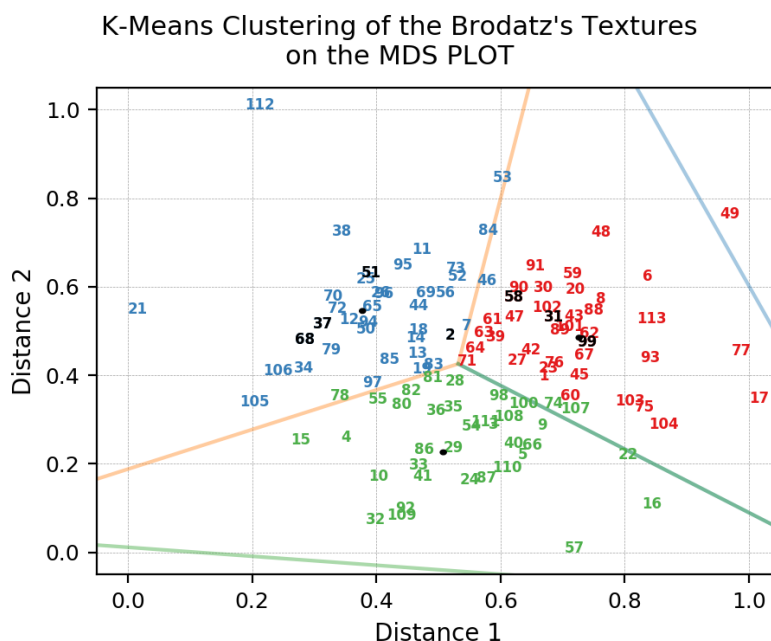


Figure 6.3: Three clusters were then generated using K-means clustering method. Each cluster is surrounded by line segments and their member of images have the same colour. All points in black colour are the centre of gravity of the corresponding cluster. The black numbers were the image chosen as the stimuli.

## Visual stimuli

The number of stimuli determines the cost to manufacture them and the time spent by the subjects in the experiment. The larger the number of the stimuli, the higher the production cost and the longer the time needed for subjects to explore and assess the stimuli which would affect their focus and performance. To avoid these issues, seven images were considered to be sufficient in this experiment; three of them to be phase dominant, another three images to be magnitude dominant, and one image as a dummy was selected from a point at about the middle position of those six images. It was expected that this dummy image is neutral, meaning that its phase and magnitude dominance are in balance.

All phase dominant images were picked from the cluster in which image 113 is inside; they are images 58, 31, and 99 (Figure 6.3). They were then labelled as P1, P2, and P3 respectively. The phase dominance of these images was expected to vary as they have different distances from image 113; P3 should be the most phase dominant, P1 to be the least, and P2 is in between. For the magnitude dominant images, one of them came from the cluster in which image 112 is inside and other two images came from the cluster beside it; they are image 37, 51, and

68. Those images were labelled as M1, M2, and M3 respectively. Their magnitude dominance was expected not to vary widely as their distances to image 112 are not significantly different. Finally, image 2 was chosen as the dummy image and it was given label D1. All selected images are displayed in Figure 6.4.

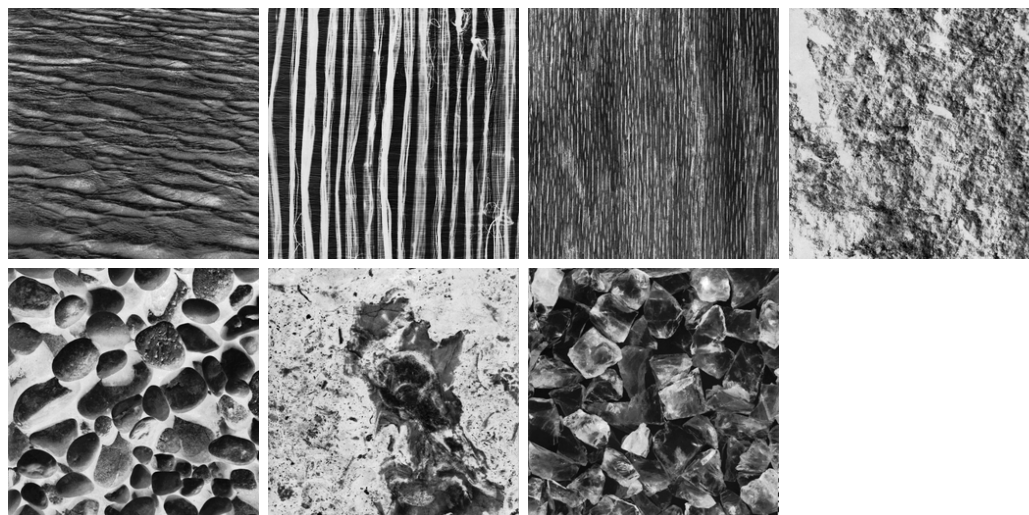


Figure 6.4: In the top row from left to right are M1, M2, M3, and D1. In the middle row from left to right are P1, P2, and P3. The actual size of each image is  $256 \times 256$  pixels. Here, their size is reduced for sake of the space.

By using those images, six hybrid images were created (Figure 6.5). First three hybrid images were created by combining the power spectrum of each image  $M$  with the magnitude spectrum of D1 and then performing the inverse Fourier transform to each combination of spectra. These hybrid images were used to test the magnitude dominance of image  $M_s$ . Another set of hybrid images were created by combining the phase spectra of P1, P2, and P3 and the magnitude spectra of D1 and then performing inverse Fourier transform to those combinations of spectra too. These images were used to test the phase dominance of image  $P_s$ . In total, therefore, thirteen visual stimuli were created; six of them are parent images, the other six are hybrid images, and the last one is the dummy image.

### Tactile stimuli

Thirteen grayscale images which were all used as the visual stimuli were adopted as the blueprints of the surfaces' contour of the tactile stimuli. Each image was converted into a 3D-CAD model in stereolithography (.*stl*) file format (Figure 6.6). Each pixel of the image represents the point in  $Z$ -axis of the corresponding vertex in the 3D model. Therefore, the height of asperities of the 3D model's



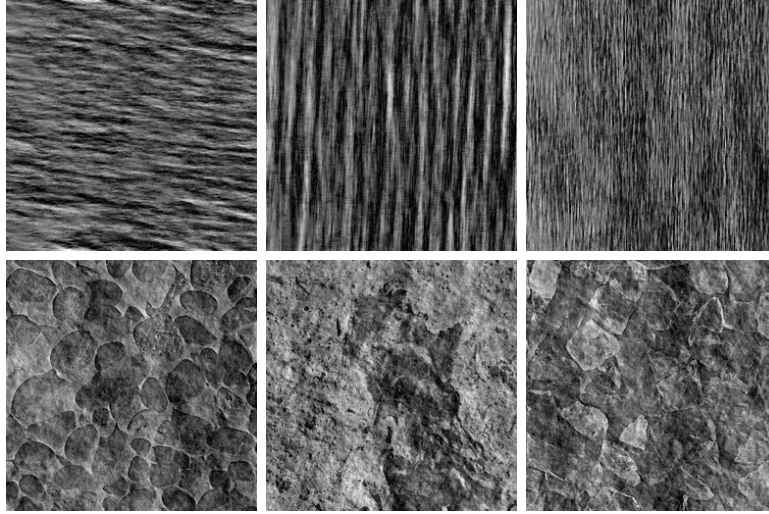


Figure 6.5: The hybrid images in the first row from left to right was created using the combination of the phase spectrum of D1 and the power spectra of M1, M2, and M3 respectively. In the second row from left to right, the hybrid images were created using the power spectrum of D1 and the phase spectra of P1, P2, and P3 respectively. Their actual size is  $256 \times 256$  pixels. Here, its size is reduced for sake of the space.

surfaces is defined by the value of its corresponding pixel of the blueprint image. The white pixels (255) were set as the valleys (0 mm from the base's surface) and the black pixels (0) were set as the peaks of the surface's contour (0.5 mm). The resolution of the asperities is  $30 \mu\text{m}$  which the highest resolution of the 3D printer being used can reach. By using this method, the surface of the tactile stimuli will look similar to their source images.

Thirteen 3D models of the tactile stimuli were 3D-printed by using polymeric-based material in *Perfactory 3 Mini Multi Lens*<sup>®</sup>. The size of each tactile stimulus is  $50 \text{ mm} \times 50 \text{ mm} \times 2.5 \text{ mm}$ . As there are 256 pixels for each texture, the horizontal resolution of each touch stimulus equals to five pixels per  $\text{mm}^2$ . With the total thickness of 2.5 mm, 2 mm of it is the base thickness and 0.5 mm of it is for the asperities. The base thickness was determined based on the consideration on the strength of the stimuli. Meanwhile, the high of the asperities was determined by considering the just noticeable difference (JND) for the smooth surface which is  $(15 \pm 8.5 \mu\text{m})$  [30]. So, in this experiment, the peak of asperities is around three times of the JND which therefore the asperities would be easily explored and perceived by the subjects.



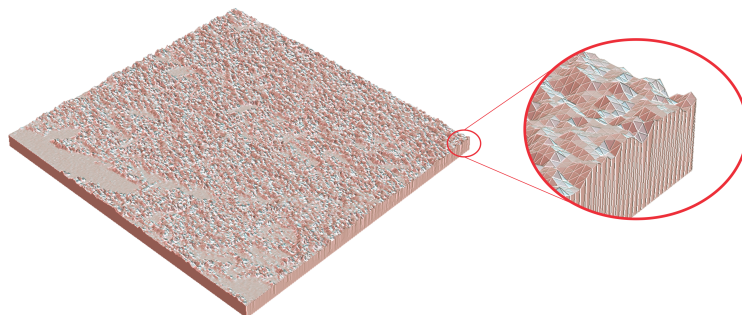


Figure 6.6: A sample of CAD model of the tactile stimulus with texture of D1. All CAD models of the stimuli were created using a computer code written in Python™ programming language (Appendix A.3).

## 6.2.2 Participants

Fifteen volunteers became the subjects of this experiment and each of subject performed eighteen trials in each experiment. They were students at the University of Leeds. All participants were interviewed to ensure they are free from impairments that could affect their ability to perceive the visual and the tactile patterns. Participants were naïve to the hypotheses. In all experiments the duration of the stimuli exposure was not specified to allow subjects to make thorough explorations of the patterns.

## 6.2.3 Procedure

There were two sessions of experiments. The first one was visual experiment in which six pairs of images were displayed on an LCD monitor one by one (Figure 6.7). Subjects used only a mouse to give their responses. The second experiment was tactile experiment in which six pairs of tactile stimuli were presented one by one inside a curtained box so that subject could not see the surfaces of the stimuli. Subjects were asked to touch and slide their fingers across the surface so that they can make comparisons. A form was provided to each subject for recording the responses.

Both experiments used 2AFC Match-to-Sample method [277]. The hybrid texture was used as the "sample" stimulus, and the parent textures were used as the "match" stimuli. In every presentation, subjects were asked to select which one between two "match" stimuli that is most similar to the "sample" stimulus.



Figure 6.7: The presentation of a pair of visual stimuli. The upper image is the "sample" stimulus and two lower images are the "match" stimuli. The actual size of each stimulus is  $256 \times 256$  pixels. Here, their size is reduced for sake of clarity.

The presentation order of the pair of stimuli was randomized. Each subject repeated the comparison activities three times.

There was no special instruction and guidance for the subjects about the criteria and the degree of similarity on both types of stimuli. They were free to interpret the definition of similarity between image in the visual experiment and between surfaces in the tactile experiment. However, all subjects were given a preliminary experiment using three pairs of stimuli which were randomly selected from the actual pairs in both experiment. The purpose of this experiment is to allow subjects to understand and become familiar with the instructions. There was no feedback given to the subjects after completing their preliminary experiment. This exercise experiment was not included in the analysis.

In the tactile experiment, the subjects were asked to use the dominant hand and the same finger during exploring the stimuli's surfaces. A handedness questionnaire was given to the participant to know which hand is his/her dominant one. Before exploring the stimuli's surfaces, the condition of the fingerpad's skin was standardized by washing it using a wet wipe. The subjects were asked to wear an ear defender to prevent the ear from listening any sound evoked by fingerpad when sliding on a stimulus's surface.

#### 6.2.4 Analysis

The data collected from the visual experiment was used to find an evidence of the presence of images with natural textures which are "unusually" magnitude

dominant. The responses were coded as 1 if the parent image with label either M or P was selected to be more similar to the corresponding hybrid image and otherwise was coded as 0 if D1 was selected to be more similar to the hybrid image. The number of response 1s obtained by M labelled images indicates the strength of the evidence.

Beside that, the visual responses joined with the touch responses were used to find an evidence that the touch perception would be able to detect the magnitude dominance of tactile textures in a similar mechanism that the visual perception has. Therefore, it was predicted that the magnitude dominant images will be still magnitude dominant when they are transformed into tactile stimuli. Likewise, the phase dominance of images will not change in the tactile perception.

As the visual and the touch perception do not have an exactly similar mechanism (Section 3.4), a further analysis on the influence of the roughness textures to the surface recognition was made. The topography of the stimuli was characterized by using seven parameters of areal surface texture; they are *arithmetic average height* ( $s_a$ ), *root-mean square deviation* ( $s_q$ ), *skewness of topography height distribution* ( $s_{sk}$ ), *kurtosis of topography height distribution* ( $s_{ku}$ ), *density of summits* ( $s_{ds}$ ), *the fastest decay auto-correlation length* ( $s_{al}$ ), and *texture aspect ratio* ( $s_{tr}$ ). These are 3D parameters and are extensions from those which have been used in the 2D characterization method [69, 82]. They were selected here because their measurement is based on 2D array of points which, therefore, is identical to image. Their corresponding 2D roughness parameters have been used to characterize perceptual roughness [84, 180–182].

The roughness of the tactile stimuli was estimated by performing the calculation on the images instead of the physical surfaces. If an image is represented by Equation 6.4,

$$f(m, n), 1 \leq m \leq M \text{ and } 1 \leq n \leq N \quad (6.4)$$

where  $M$  is the number of rows of the image's pixels and  $N$  is their number of columns, the asperities ( $y_i$ ) of the tactile stimuli can be defined as the value of the corresponding pixel subtracted by the total average of the pixel (Equation 6.5).

$$y_{m,n} = f(m, n) - \sum_{m=1}^M \sum_{n=1}^N f(m, n) \quad (6.5)$$

Based on Equation 6.5, the following formulae of areal surface textures can be defined.

- a.  $s_a$  is the average of absolute deviation of the asperities from the mean line. This parameter is easy to define and to measure, however it is not suitable to represent surfaces with regular asperities as they will have a similar value.

$$s_a = \frac{1}{MN} \sum_{m=1}^M \sum_{n=1}^N |y(m, n)| \quad (6.6)$$

- b.  $s_q$  represents the standard deviation of the surface asperities. This parameter depicts variation of the asperities dispersed across the surface.

$$s_q = \sqrt{\frac{1}{MN} \sum_{m=1}^M \sum_{n=1}^N y^2(m, n)} \quad (6.7)$$

- c.  $s_{sk}$  represents the asymmetry of the asperities' distribution. It indicates the common height of asperities. If the distribution is left skewed, most of asperities are higher than the mean. Otherwise, for the right skewed distribution, most of asperities are lower than the mean.

$$s_{sk} = \frac{1}{MN s_q^3} y^3(m, n) \quad (6.8)$$

- d.  $s_{ku}$  is a measure of the sharpness of the asperities' distribution. The higher the value, the sharper the distribution which indicates that the heights of asperities are closed to the mean.

$$s_{ku} = \frac{1}{MN s_q^4} y^4(m, n) \quad (6.9)$$

- e.  $s_{ds}$  represents the density of asperities' peaks across the surface. It belongs to the category of spacing parameters which means that it takes into account on not only the height of asperities itself but also the spatial domain. All following parameters also belong to this category. They were adopted from Blunt and Jiang [82].

$$s_{ds} = \frac{\text{number of summits}}{(M-1) \cdot (N-1) \cdot dx \cdot dy} \quad (6.10)$$

- f.  $s_{al}$  is calculated based on the *auto-correlation function* (ACF)'s value of the surface. It represents the shortest distance that the ACF decays to 0.2 in either  $X$ - or  $Y$ -axis direction.

$$s_{al} = \min_{(\tau_m, \tau_n \in R)} \left( \sqrt{\tau_m^2 + \tau_n^2} \right), R = \{(\tau_m, \tau_n) : \text{ACF}(\tau_m, \tau_n) \leq 0.2\} \quad (6.11)$$

g.  $s_{tr}$  represents the uniformity of the surface. The larger the value the more uniform the surface asperities.

$$s_{tr} = \frac{\min \left( \sqrt{\tau_m^2 + \tau_n^2} \right)}{\max \left( \sqrt{\tau_m^2 + \tau_n^2} \right)} \Bigg|_{R(\tau_m, \tau_n) \leq 0.2} \quad (6.12)$$

To investigate the relationship between each roughness parameter and the similarity of roughness texture, the value of each parameter for every image would be compared (Equation 6.13).

$$r_p = \frac{s_I - s_H}{s_D - s_H} \quad (6.13)$$

where  $r_p$  is the ratio of roughness' differences,  $s$  indicates to the roughness parameter, and its subscripts indicate to the image:  $I$  is for the parent image with label M and P,  $H$  is for the corresponding hybrid image, and  $D$  is for the image with label D. From these comparisons, it was expected that the smaller the ratio, the more similar the hybrid image to the stimuli M or P. Otherwise, the larger the ratio, the more similar the hybrid image to the stimuli D. Paired t-test would be used to measure the correlation between the ratio of each roughness parameter and the responses of similarity between stimuli.

### 6.3 Result and Discussion

A total of 540 responses were collected from both visual and tactile experiment with each of them contributes a half of that number (270). In the visual experiment, all images with label M obtained 45 of 1s which means that they were perfectly perceived to be magnitude dominant as has been predicted (Table 6.1). In the tactile experiment, the result is not really different. In one occasion, M2 was perceived to be less similar to the hybrid image than D1 (which contributed its phase spectrum). This result gives an evidence that natural textures can be magnitude dominant which means that their phase spectra are less important than their magnitude spectra.

In the visual experiment, P1 and P3 obtained 45 of 0s which means that they were perfectly perceived to be phase dominant as has been predicted. P2 was perceived five times (11%) not to be more similar to the hybrid image than D1 (which contributed its magnitude spectrum). In the tactile experiment, only P3 which obtained 45 of 0s. P1 received 40 of 0s which is five less than it received

Table 6.1: Response Summary

Setup	Response	Parent Images						
		M1	M2	M3	P1	P2	P3	D1
Visual	0	0	0	0	45	40	45	0
	1	45	45	45	0	5	0	5
Tactile	0	0	1	0	40	13	45	1
	1	45	44	45	5	32	0	37

Table 6.2: Chi-square Analyses of Responses' Difference within Round and Mode for P1, P2, and P3

Source	Num. of Obs.	DOF	Critical ( $P > 95\%$ )	$\tilde{\chi}^2$	P-value	Cramer's V
Round (1-3)	540	2	5.991	0.015	.992	.005
Mode (vis-tac)	540	1	3.841	6.824	.009	.112

from the visual experiment. P2 was perceived differently in the tactile experiment. Most subjects (71%) felt that P2 was less similar to the hybrid stimulus than D1.

When its phase spectrum was being used, D1 was never been perceived as phase dominant in the visual experiment, but once in the tactile experiment. It means that its phase is less dominant than the magnitudes of M1, M2, and M3. Meanwhile, when its magnitude spectrum being used, D1 was perceived to be magnitude dominant five times (4%) in the visual experiment and thirty seven times (27%) in the tactile experiment.

In general, responses are found to not be influenced by trial's repetition (Table 6.2: top row). It means that in each repetition, the stimuli were perceived independently. The previous presentation of stimuli did not influence the perception of the following presentation. However, the mode of experiment is found to influence the subjects' perception which is indicated by the significantly different responses obtained from the visual and the tactile experiment (Table 6.2: bottom row). In this case, by using those six stimuli, the influence is weak (the Cramer's V value = .112). Moreover, for M1, M2, M3, and P3, the influence is not seen; their responses are the same in both visual and tactile experiment. Meanwhile, for P1, the influence is noticeable and for P3, it changed the perception –i.e., from being strongly phase dominant in the visual experiment to become less phase dominant in the tactile experiment.

### The influence of the distance between parent images to the perception of surfaces' similarity

The relative distance of the parent images to D1 on the MDS plot was determined using Equation 6.14.

$$d = \sqrt{\Delta D_1^2 + \Delta D_2^2} \quad (6.14)$$

The result indicates that the distance between two parent images determines their degree of similarity with their hybrid image. Having the longest distances, M1, M3, and P3 were perceived to be most similar to the hybrid image (Figure 6.8). All subjects in both experiments could perceive their texture in the corresponding hybrid images (Table 6.1). Having the shortest distance, P2 was perceived to be less similar to its hybrid image. It was perceived to be not similar with the hybrid image five times in the visual experiment and thirty two times in the tactile one.

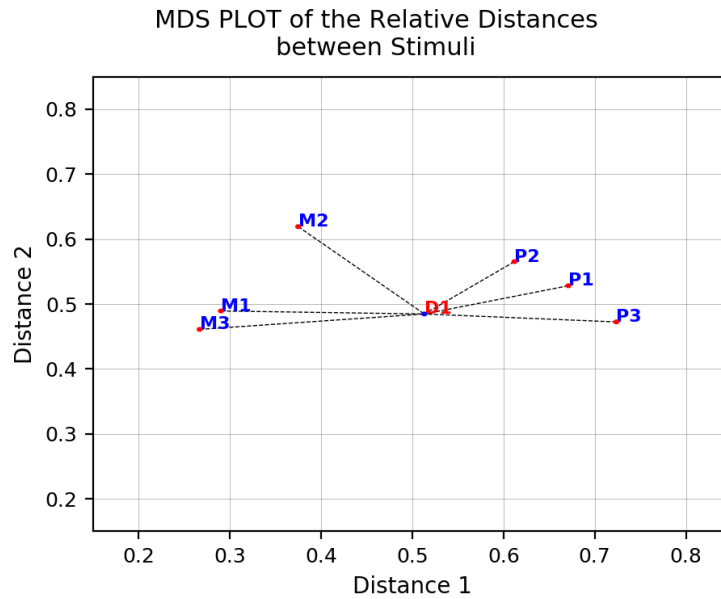


Figure 6.8: The relative distance between texture of the stimuli. Textures with labels M are magnitude dominant and the ones with labels P are phase dominant. D1 is the intermediate texture.

In other words, the further the distance from D1, the stimuli with either M or P label are more similar to the hybrid image. Otherwise, the closer the distance, either M, P, or D1 will obtain more responses in the same proportion which indicates that the confusion in perceiving the texture's similarity increases. In both experiments, the influence of this distance to the degree of similarity is significant (Table 6.3). This evidence, therefore, supports the indication that

Table 6.3: T-test on the Prevalence of Different Means of Distance between the Similar and Dissimilar Stimuli

Source	T	DoF	Tail	P-value	CI (95%)	Cohen-d
Visual (same-diff.)	6.917	264	two-sided	.000	[.01, .02]	.428
Tactile (same-diff.)	-20.921	100	two-sided	.000	[-.08, -.06]	2.257

the magnitude dominance of an image is influenced by its complementary image (Equation 4.8).

However, in each experiment, the influence of the distance to the similarity responses is different as shown by the Cohen-d values. The distance has a smaller influence in the visual experiment than in the tactile one which means that to have the same level of influence, the larger difference of distance is needed in the visual stimuli. Meanwhile, the smaller difference of distance between tactile stimuli will be more noticeable. Beside that, there is a possibility that in a certain cases the subjects had different perspective of roughness as there are two modes of tactile perception, i.e. duplex theory (Subsection 2.2.4). For the rough surface, the pressure from the surface's asperities is the main source of the roughness perception. The tactile field of perception may appear here.

However, for the smooth surface (the particle size on it is less than 100  $\mu$  m), the vibration that occurs on the fingerpad becomes the main source of the roughness perception. Beside that, in the activity of surface comparison, vibration will be evoked to provide more information about the surfaces although they are relatively rough. The more similar the surfaces, the more vibrational cues are needed. In this process, subjects will press the surface strongly and slide the finger quickly and frequently. This may be the reason of why P2 was perceived differently in the tactile experiment (Table 6.1).

### **Influence of the physical roughness to the perceived roughness**

To analyse whether the physical roughness influences the perceived roughness, the surface of the tactile stimuli was characterized using seven parameters of areal texture and the measured roughness (Table D.8) was then correlated with the responses of similarity. As there were only thirteen data of roughness collected for each parameter, the mean of surface roughness between stimuli was compared using Wilcoxon signed-rank tests. The first test is to measure the difference of the roughness mean between the parents stimuli with label M or P and the hybrid stimuli. The result shows that there is no significant difference between their



Table 6.4: T-test on the Prevalence of Different Means of Roughness between the Similar and Dissimilar Tactile Stimuli

Roughness Parameters	Between Ms, Ps and Hybrid Images			Between D1 and Hybrid Images		
	W-val	P-val	RBC	W-val	P-val	RBC
s.a	1.0	.059	.91	0.0	.036	-1.00
s.q	1.0	.059	.91	0.0	.036	-1.00
s.sk	7.0	.529	.33	0.0	.036	1.00
s.ku	5.0	.295	-.52	0.0	.036	1.00
s.ds	0.0	.036	1.00	2.0	.093	-.81
s.al	4.0	.854	.20	0.0	1.000	1.00
s.tr	4.0	.855	.20	6.0	.396	-.43

Table 6.5: T-test on the Prevalence of Different Means of Roughness between the Similar and Dissimilar Tactile Stimuli

Roughness Parameters	T	P-Value	Cohen-d	Power
s.a	7.940	0.0	0.613	0.937
s.q	8.145	0.0	0.623	0.944
s.sk	13.526	0.0	3.064	1.000
s.ku	6.708	0.0	0.553	0.882
s.ds	8.682	0.0	0.682	0.973
s.tr	-8.484	0.0	0.601	0.928

roughness mean (Table 6.4). The second test which compared between the roughness mean of the hybrid and D1 stimuli also shows no significant difference. Both results, thus, show that there is no significant difference of roughness between parent stimuli and the hybrid ones. These results also indicate that the tactile perception was not influenced by the physical roughness as reported by Tiest and Kappers [84].

However, a different indication appeared from comparison tests for the ratio of roughness' difference (Equation 6.13). The result shows that this ratio in the parent stimuli which were perceived to be similar is different from the same ratio in the parent stimuli which were perceived to be dissimilar. In short, the ratio of roughness' difference correlates with the responses of similarity (Table 6.5). All roughness parameters shows medium correlation, except for s.k which has a high correlation (its Cohen-d value equals to 3.1 which is high according to Cohen [271]). Beside that, between P2 and its hybrid image (D1\_P2), the values gap of s.k parameter is much larger compared to the values gap of s.k parameter between D1 and D1\_P2. These results may explain of why P2 was perceived mostly to be not similar to the hybrid stimuli compared to D1 (Table 6.1).

## 6.4 Conclusion

The magnitude dominance of images has been shown not to depend on whether their texture is natural or not. Any image can be magnitude or phase dominant depends on the frequency of its global texture. However, it is not easy to determine and select images which are magnitude or phase dominant using a mere visual inspection.

The results provide an evidence that the set of 107 power spectra-based features can be used to characterize and to cluster natural textures into a phase dominant and magnitude dominant group. The selected images from each group have been shown to be visually perceived in accordance with their group. For example, in the visual experiment, the images in the magnitude dominant group were perceived to be magnitude dominant too. The level of the magnitude and phase dominance of the textures are influenced by their "relative distance" from D1 (Figure 6.8). The larger the "distance", the stronger the magnitude or phase dominance of the image.

The result of the tactile experiment shows that, in general, the textures were perceived in accordance with their group too. This evidence indicates that tactile perception can perceive irregular textures in the same way the visual perception can. However, in the visual experiment, the subjects' performance in detecting the textures' similarity is better than in the tactile experiment. To have the same level of magnitude or phase dominance, the tactile texture needs a bigger "relative distance" to D1 than the visual texture.

# Chapter 7

## General Discussion and Conclusion

### 7.1 Overview

This study was aimed to measure the magnitude and phase dominance of image textures in both visual and tactile perception. To achieve this, several objectives were made; the relationship between visual and tactile perception on irregular patterns was investigated, the contribution of phase and power spectra to the magnitude's dominance of images was measured and compared using four types of standard signals, the prominent and potential features of power spectra which influence the magnitude dominance were re-examined using a set of images with natural textures, the selected features were used to cluster the images into a magnitude dominant and a phase dominant group of images.

To carry out these objectives, four sets of experiments were performed. The first set consists of a visual and tactile experiment using irregular patterns that are generated using the formulae of first-, second-, and third-order probability. This experiment was intended to determine whether the tactile perception has a similar mechanism with the visual perception. The evidences obtained from this experiment are important to determine the usefulness of the effort to model the surface's asperities and the roughness perception using images. The second set consists of a visual experiment only and was intended to find the parameters from the standard test signals which influence their magnitude dominance. Having found that the type and the frequency of these signals are the most influential parameters, the third set of experiments was intended to test both parameters using a scaling method in which the size of five different images with natural textures was being modified so that their frequency changes. The results show that

both type and frequency of images strongly influence their magnitude dominance. However, as these parameters in most cases can not be determined, a set of power spectra-based features were used to represent them. The relationship between these features and the magnitude dominance of the scaled images was made by putting them as the independent variables along with the subjects' responses as the dependent variable in a logistic regression model. The results show that this model could achieve an accuracy of more than 80% in predicting the magnitude dominance of the images. The fourth set of experiments were performed to get some evidences that by using these features, any image with natural texture can be determined whether it is magnitude or phase dominant. The experiments were also intended to obtain some evidences showing that the magnitude dominance of any image also prevails in its corresponding tactile texture.

This study may benefit to the affective surface engineering by providing some evidences showing that: first, surfaces can be well represented using images which makes it, therefore, possible to use image features that are abundant and relatively easier to be extracted and analysed than to use the actual roughness parameters for describing surface textures; second, magnitude-based image features can be used to characterize, especially, the frequency of image's textures and therefore, potentially, can be used to represent both image and surface textures in general; third, in Fourier spectra the magnitude components are more important than the phase parts, thus, instead of using phases-based features, magnitudes-based ones are more recommended to describe either visual or tactile textures in the study of affective dimension of surfaces.

In short, this study showed a reasonable and potential opportunity to use magnitude-based features for describing surface textures and for developing models of the touch sensation of those textures. As has been shown in this study, one hundred and seven magnitude-based features used in the experiments could successfully discriminate between the magnitude and phase dominant textures in both of visual and tactile specimens. This successful effort in using those features may be extended to model other dimensions of affective surface other than roughness such as smoothness, pleasantness, and comfort. Besides that, the use of this type of features also gives a very useful advantage by making it possible to reverse the process from analysis to synthesis of surface textures which in this case is analogous to the image synthesis that has been already well studied. This reverse process will not be possible if the standard roughness parameters were used in describing the surfaces. This texture synthesis process will be useful in designing a product with affective aspects.

## 7.2 General Discussion

The topography of a surface is commonly described using a number of parameters of surface roughness. Based on how the roughness is calculated, the roughness parameters can be categorised into three groups; they are amplitude parameters, spacing parameters, and hybrid parameters. Based on how the asperities of the surface is measured, there are two groups of roughness parameters; 2D parameters and 3D parameters. The higher the number of the parameters used, the better the description can get. However, to provide a full description about it using a finite number of parameters is not possible [69].

A number of these roughness parameters have been used to model the roughness perception and it was reported that they do not have adequate correspondence to the magnitude of perceived roughness [84, 296]. Elkharraz et al. [44] used image textures to represent the topography of surfaces which therefore make it possible to use a set of image features instead of roughness parameters to characterize the surface roughness. They attempted to model the affective response of tactile perception using 115 features of image textures [52]. It was reported that four out of 115 features can be used to predict the tactile responses. That method motivated this study to investigate the roughness perception through image recognition. A number of images were used as the visual stimuli and the same images were used again as the blueprints of the tactile stimuli. By comparing the performance of the visual and the tactile perception, the effectiveness of using images as the surface representation can be determined.

Image features can be extracted using at least four types of techniques; statistical methods, structural methods, model-based methods, and spectral-based methods. However, in this study, the spectral method was selected because it is related with spatial frequency of the image textures [53] which, therefore, will be most likely to be correlated with the roughness perception too since one of the prominent cues of the roughness perception is the vibration exerted on the fingerpad [17, 24, 97]. For this method, FFT spectra were selected and used as the source for features extraction.

As there two parts for every FFT spectra (the magnitude and the phase part), the features can be extracted from both of them. However, there have been long debates about which one of these parts is the most important. Despite no clear explanation, it is commonly believed that phase part is more important than the magnitude part. Millane and Hsiao [218] proposed a series of formula to measure the phase dominance of an image, yet the result is not convincing. Therefore, to

investigate the magnitude and the phase dominance of images becomes the focus of this study. It was also hypothesized that the magnitude dominance of images is preserved in the tactile textures that were created from the related images.

To examine that hypothesis, four series of experiments were performed. The first experiment (Chapter 3) was used to investigate the similarity of how subjects perceive the visual and the tactile stimuli with irregular patterns. Julesz [240] conjectured that visual patterns can be discriminated if they have differences in the first- and second-order probability. Images which are different in the third- and higher-order statistics will not be visually discriminable. To examine this conjecture, three groups of images having first-, second-, and third-order of statistics were created. Each group consists of nine images with transition probability ranges from 10% to 90% (Sub Section 3.2.2). These patterns were used to create the tactile stimuli so that the scheme of both visual and the tactile experiment is identical. The results obtained from both experiments support Julesz' conjecture. Subjects could discriminate the first- and the second-order textures which have different values of transition probability. The third-order textures were undistinguishable. The results give an indication that surface roughness can be represented by image textures.

The second experiment (Chapter 4) was visual and was dedicated to investigate the component of power spectra of images with standard 1D signals which influence the magnitude dominance. Four types of signals were used; they are sinusoidal, triangle, square-wave, and sawtooth signals. Each type of signal were varied in terms of rotation angle and frequency. In total, thirty six parent images were created. The magnitude and the phase of each parent image was cross-combined to each other to create 1260 unique hybrid images. Each hybrid image along with its parents were presented in a monitor and subjects were asked to select which parent image is most similar to the hybrid image. The results shows that more than 88% responses selected the parent images which contributed their magnitude part to be most similar to the related hybrid images which means that the magnitude is more important than the phase. The number and the arrangement's distance of non-zero frequency components of the magnitude spectra are the parameters which influence the magnitude dominance. The larger the number the weaker the magnitude dominance. Meanwhile, the further the distance between non-zero frequency components the stronger the magnitude dominance. It was also found that this distance is related with the frequency of the standard signals. As the magnitude spectra appeared to be more important than the phase spectra, a set of one hundred and seven power spectra-based features was used as

the inputs of a logistic regression model to determine the magnitude dominance of the parent images. The results show that the model could achieve an accuracy of 79% in predicting the magnitude dominance of the images (Table 4.14).

The third experiment (Chapter 5) was also visual and was intended to get more evidences of the influence of the number and the arrangement's distance of the frequency components on the magnitude dominance. A group of five images with natural textures were used to test the influence of both parameters. To modify the texture's frequency of this type of images, a scaling method was used (Sub Section 5.2). Another group of nine images were used to test the influence of the frequency changes of the first group of images on their magnitude dominance. The results show that by scaling down the size of the image stimuli with natural texture, their frequency and magnitude dominance increase. Furthermore, the same set of power spectra-based features to predict the magnitude dominance of the scaled images could achieve an accuracy of 86%.

The fourth experiment (Chapter 6) was visual and tactile in which the same set of power spectra-based features was used to measure and to cluster the magnitude dominance of images with natural texture. Three phase dominant images and three magnitude dominant images were selected from Brodatz album which consists of one hundred and eleven different images with natural texture. One additional image was chosen to test the magnitude dominance of those six images. All of those images were used as the blueprints of the tactile stimuli so that the identical visual and tactile experiment can be made. The result show that the subjects' responses for each image were generally not different from the prediction. In the visual experiment, all magnitude dominant images were perceived to be perfectly magnitude dominant (Table 6.1). For the phase dominant images, two of them were also perceived to be perfectly phase dominant. One image (P2) was perceived to have weaker phase dominance. Those responses is correlated with the distance of those images to image D1 (Figure 6.8). In the tactile experiment, all magnitude dominant textures were also perceived to be magnitude dominant too. For the phase dominant textures, two of them were also perceived to be phase dominant. Only P2 was perceived to have low phase dominance. Seven physical roughness parameters were correlated with the perceived roughness, yet only  $s_{sk}$  which is significantly correlated to the perceived roughness. Moreover, as the  $s_{sk}$  value of D1 is closer to the  $s_{sk}$  value of D1\_P2 than to the  $s_{sk}$  value of P2 which may explain that P2 was perceived to be less similar to D1. However, in general, the results indicate that both visual and

tactile perception have a relatively similar pattern although the visual perception has the better performance in recognizing and discriminating textures.

## 7.3 Conclusions and Recommendations

This thesis has shown that magnitude spectra are more important than the phase spectra which opposes the common believe that phases are more important than magnitudes. The magnitude dominance of images can be reliably measured using the magnitude spectra, not the phase spectra. As the dominance of the magnitude and the phase can be summed up as 1.0, their values can be determined by calculating the value of one of them.

The magnitude dominance of images is retained in some degree in the corresponding tactile textures. For example, a surface texture which was created from a magnitude dominant image will be magnitude dominant too. This evidence indicates that tactile perception is similar to visual perception and this makes it possible to use image features, especially magnitude spectra-based features, for modelling and predicting roughness perception in particular and touch sensation in general.

### 7.3.1 Conclusions

The most important evidences shown in this study are two; first, the phase and magnitude dominance of images can be determined using their magnitude spectra, second the tactile perception is able to discriminate irregular patterns in a relatively similar way that the visual perception does. Furthermore, from the comprehensive study, the following conclusions were derived:

1. By examining the famous Julesz's conjecture in the visual and tactile experiment, some evidences were obtained which indicate that the visual and tactile perception can discriminate irregular patterns in a similar way.
2. The magnitude dominance of images with standard signals is influenced by the number and the arrangement's distance of the non-zero frequency components of their magnitude spectra.
3. The texture's frequency of any image can be modified by a scaling method in which the image is resized. This transformation will also change the magnitude dominance of the image being resized.



4. The dominance of magnitudes and phases can be summed up as 1.0 and can be modelled using error function.
5. Power spectra-based features together with a logistic regression model can be used to determine both the magnitude and the phase dominance of images.
6. The relative distance between the parent images and the hybrid image on the MDS plane can be used to estimate the magnitude dominance of each parent image.
7. The roughness perception can be studied through images by using surface textures which were created by transforming the grayscale pixels of the images into *.stl* files.
8. Although both visual and tactile perception have a similar pattern, their performances are different. The visual perception is superior in recognizing and discriminating patterns. Beside that, they also have different mechanisms. In the visual perception, the grayscale pixels are perceived based solely on their intensity. Meanwhile, in the tactile perception, the asperities may be perceived based on the pressure they exert or on the vibration they generate.

### **7.3.2 Recommendations for future work**

There are two methods used in this study to convert images into CAD models; first, boxelling method in which each pixel is converted into a prism; second, the simple method in which each pixel represent a vertex of asperity in the *.stl* data. The later is more suitable and robust for representing textures than the former, especially for surface textures with a fine resolution. The wear and breakage of the surface's asperities can be minimized if the second method was used.

The power spectra-based features were found to be powerful in predicting the magnitude dominance of images which, therefore, are recommended to be used to characterize textures. Although they have been tested using natural textures, it will be useful to test them using both anisotropic and isotropic homogeneous textures by varying the size and the arrangement's distance of the particles within the textures. This examination can also be used to characterize the duplex theory of roughness perception so that the more complete roughness characterization may be obtained.

The results from the last tactile experiment support the indication that tactile fields were present in the roughness perception. Subjects are most likely to use these fields to recognize and discriminates pairs of surfaces. Further investigations are needed to get a strong evidence about the presence of these fields during touching.

Although other dimensions of the tactile perception have not been explored, the results from this study suggest that the power spectra-based features can be used to model and predict the tactile perceptions beyond roughness. Further investigation needs to be performed for this matter.

# Appendix A

## Computer Codes to Create Image Textures and CAD Models

### A.1 Java™ code to create the first-, second-, and third-order patterns

The snippet of code to create the first-order patterns:

```
int[][] array = new int[row][col];
Double[][] dumArray = new Double[row][col];
int pw1 = 0;
pw1 = Integer.parseInt(setPw.getText());
double prob = 0.0;
for (int i = 0; i < row; i++) {
    for (int j = 0; j < col; j++) {
        Random rnd = new Random();
        int val = rnd.nextInt(100) + 1;
        if (val <= pw1) {
            array[i][j] = 255;
        } else {
            array[i][j] = 0;
        }
    }
}
```

The snippet of code to create the second-order patterns:

```
int pw3 = Integer.parseInt(setPw.getText());
// fill the matrix with 0;
for (int i = 0; i < row; i++) {
    for (int j = 0; j < col; j++) {
        array[i][j] = 0;
    }
}
for (int i = 0; i < row; i++) {
    for (int j = 0; j < col; j++) {
        Random rnd = new Random();
        int val = rnd.nextInt(100) + 1;
```

```

    if (i > 0) {
        if (val <= pw3) {
            array[i][j] = array[i - 1][j];
        } else {
            array[i][j] = 255 - array[i - 1][j];
        }
    }
}
if ((i == 0) & (j > 0)) {
    if (val <= pw3) {
        array[0][j] = array[0][j - 1];
    } else {
        array[0][j] = 255 - array[0][j - 1];
    }
}
}
}
}

```

The snippet of code to create the third-order patterns:

```

int pw = Integer.parseInt(setPw.getText());
// fill the matrix with 0;
for (int i = 0; i < row; i++) {
    for (int j = 0; j < col; j++) {
        array[i][j] = 0;
    }
}

for (int i = 0; i < row; i++) {
    for (int j = 0; j < col; j++) {
        Random rnd = new Random();
        int val = rnd.nextInt(100) + 1;
        int k = i % 3;
        if (k == 0) {
            if (i > 2) {
                int a = array[i - 2][j] + array[i - 1][j];
                if ((a == 0) || (a == 510)) {
                    if (val <= pw / 2) {
                        array[i][j] = array[i - 1][j];
                    } else if (val > pw / 2) {
                        array[i][j] = 255 - array[i - 1][j];
                    }
                }
            } else if (a == 255) {
                if (val <= 100 - pw) {
                    array[i][j] = array[i - 1][j];
                } else if (val > 100 - pw) {
                    array[i][j] = 255 - array[i - 1][j];
                }
            }
        }
    }
}

if (k != 0) {
    if (val <= 50) {
        array[i][j] = 255 - array[i - 1][j];
    } else if (val > 50) {
        array[i][j] = array[i - 1][j];
    }
}
}
}
}

```

```

    }
  }
  if ((i == 0) & (j > 0)) {
    if (val <= 50) {
      array[0][j] = array[0][j - 1];
    } else {
      array[0][j] = 255 - array[0][j - 1];
    }
  }
}
}
}

```

## A.2 Java™ codes to convert a 2D array into an image and an *.stl* file of boxels

The snippet of code to convert a 2D-array into an image:

```

BufferedImage img = new BufferedImage(row, col,
BufferedImage.TYPE_INT_RGB);
for (int i = 0; i < row; i++) {
  for (int j = 0; j < col; j++) {
    data = array[i][j];
    dumArray[i][j] = (double) data;
    Color nC = new Color(data, data, data);
    img.setRGB(i, j, nC.getRGB());
  }
}
}

```

The snippet of code to convert and save a 2D-array into an *.stl* file of boxels:

```

// ==START THE ITERATION=====
for (int j = 0; j < loopY; j++) {
  for (int i = 0; i < loopX; i++) {
    if (hMatrix[i][j] != null){ // i and j should be re-check again
      // first triangle of top=====
      height = setBaseThickness + hMatrix[i][j] / heightScale;
      if (j == 0) {
        iheighty = 0;
      } else if (j > 0) {
        iheighty = setBaseThickness + hMatrix[i][j - 1] / heightScale;
      }
      if (i == 0) {
        iheightx = 0;
      } else if (i > 0) {
        iheightx = setBaseThickness + hMatrix[i - 1][j] / heightScale;
      }
      X = startX + iter;
      Y = startY + iter;
      bytes.add(" facet normal 0.000000e+000 0.000000e
+000 1.000000e+000"+ "\n");
      bytes.add("   outer loop" + "\n");
      bytes.add("\tvertex " + startX + " " + startY
+ " " + height + "\n");
    }
  }
}
}

```

```

bytes.add("\tvertex " + X + " " + startY
+ " " + height + "\n");
bytes.add("\tvertex " + X + " " + Y
+ " " + height + "\n");
bytes.add("    endloop" + "\n");
bytes.add("  endfacet" + "\n");
// second triangle of top
bytes.add(" facet normal 0.000000e+000 0.000000e
+000 1.000000e+000" + "\n");
bytes.add("    outer loop" + "\n");
bytes.add("\tvertex " + startX + " " + startY +
" " + height + "\n");
bytes.add("\tvertex " + X + " " + Y + " "
+ height + "\n");
bytes.add("\tvertex " + startX + " " + Y + " "
+ height + "\n");
bytes.add("    endloop" + "\n");
bytes.add("  endfacet" + "\n");
// first triangle of bottom
bytes.add(" facet normal 0.000000e+000 0.000000e+000
-1.000000e+000" + "\n");
bytes.add("    outer loop" + "\n");
bytes.add("\tvertex " + startX + " " + startY + " "
+ 0 + "\n");
bytes.add("\tvertex " + (startX + iter) + " "
+ (startY + iter) + " " + 0 + "\n");
bytes.add("\tvertex " + (startX + iter) + " "
+ startY + " " + 0 + "\n");
bytes.add("    endloop" + "\n");
bytes.add("  endfacet" + "\n");
// second triangle of bottom
bytes.add(" facet normal 0.000000e+000 0.000000e+000
-1.000000e+000" + "\n");
bytes.add("    outer loop" + "\n");
bytes.add("\tvertex " + startX + " " + startY
+ " " + 0 + "\n");
bytes.add("\tvertex " + startX + " " + (startY + iter)
+ " " + 0 + "\n");
bytes.add("\tvertex " + (startX + iter) + " "
+ (startY + iter) + " " + 0 + "\n");
bytes.add("    endloop" + "\n");
bytes.add("  endfacet" + "\n");

if (iheighty != height) {
// XZ wall
bytes.add(" facet normal 0.000000e+000 -1.000000e+
000 0.000000e+000" + "\n");
bytes.add("    outer loop" + "\n");
bytes.add("\tvertex " + startX + " " + startY + " "
+ iheighty + "\n");
bytes.add("\tvertex " + X + " " + startY + " "
+ iheighty + "\n");
bytes.add("\tvertex " + X + " " + startY + " "
+ height + "\n");
bytes.add("    endloop" + "\n");
}

```

```
bytes.add(" endfacet" + "\n");
// second triangle of XZ wall
bytes.add(" facet normal 0.000000e+000 -1.000000e
+000 0.000000e+000"+ "\n");
bytes.add(" outer loop" + "\n");
bytes.add("\tvertex " + startX + " " + startY
+ " "+ iheighty + "\n");
bytes.add("\tvertex " + X + " " + startY
+ " " + height + "\n");
bytes.add("\tvertex " + startX + " " + startY
+ " "+ height + "\n");
bytes.add(" endloop" + "\n");
bytes.add(" endfacet" + "\n");
}
if (iheightx != height) {
// YZ wall
bytes.add(" facet normal 1.000000e+000 0.000000e+
000 0.000000e+000"+ "\n");
bytes.add(" outer loop" + "\n");
bytes.add("\tvertex " + startX + " " + startY
+ " "+ iheightx + "\n");
bytes.add("\tvertex " + startX + " " + Y
+ " " + height+ "\n");
bytes.add("\tvertex " + startX + " " + Y
+ " "+ iheightx + "\n");
bytes.add(" endloop" + "\n");
bytes.add(" endfacet" + "\n");
// second triangle of YZ wall
bytes.add(" facet normal 1.000000e+000 0.000000e+
000 0.000000e+000"+ "\n");
bytes.add(" outer loop" + "\n");
bytes.add("\tvertex " + startX + " " + startY
+ " "+ iheightx + "\n");
bytes.add("\tvertex " + startX + " " + startY
+ " "+ height + "\n");
bytes.add("\tvertex " + startX + " " + Y
+ " " + height+ "\n");
bytes.add(" endloop" + "\n");
bytes.add(" endfacet" + "\n");
}
if (j == loopY - 1) { // code of back side XZ
// first triangle of back side XZ
bytes.add(" facet normal 0.000000e+000 -1.000000e+
000 0.000000e+000"+ "\n");
bytes.add(" outer loop" + "\n");
bytes.add("\tvertex " + startX + " " + Y + " " + 0+ "\n");
bytes.add("\tvertex " + X + " " + Y + " " + height+ "\n");
bytes.add("\tvertex " + X + " " + Y + " " + 0 + "\n");
bytes.add(" endloop" + "\n");
bytes.add(" endfacet" + "\n");
// second triangle of back side XZ
bytes.add(" facet normal 0.000000e+000 -1.000000e+
000 0.000000e+000" + "\n");
bytes.add(" outer loop" + "\n");
bytes.add("\tvertex " + startX + " " + Y + " " + 0+ "\n");
```

```

        bytes.add("\tvertex " + startX + " " + Y + " " + height + "\n");
        bytes.add("\tvertex " + X + " " + Y + " " + height + "\n");
        bytes.add("    endloop" + "\n");
        bytes.add("  endfacet" + "\n");
    }
    if (i == loopX - 1) { // right side YZ
        // first triangle of right side YZ
        bytes.add("  facet normal 1.000000e+000 0.000000e+
            000 0.000000e+000" + "\n");
        bytes.add("    outer loop" + "\n");
        bytes.add("\tvertex " + X + " " + startY + " " + 0 + "\n");
        bytes.add("\tvertex " + X + " " + Y + " " + height + "\n");
        bytes.add("\tvertex " + X + " " + startY + " " + height + "\n");
        bytes.add("    endloop" + "\n");
        bytes.add("  endfacet" + "\n");
        // second triangle of right side YZ
        bytes.add("  facet normal 1.000000e+000 0.000000e+
            000 0.000000e+000" + "\n");
        bytes.add("    outer loop" + "\n");
        bytes.add("\tvertex " + X + " " + startY + " " + 0 + "\n");
        bytes.add("\tvertex " + X + " " + Y + " " + 0 + "\n");
        bytes.add("\tvertex " + X + " " + Y + " " + height + "\n");
        bytes.add("    endloop" + "\n");
        bytes.add("  endfacet" + "\n");
    }
}
startX += iter;
if (i == loopX - 1) { // maxX = startX;
    startX = 0.0;
}
// start iteration from left again
}
startY += iter;
// if (j == loopY-1){maxY = startY;}
try {
    for (String r : bytes) {
        bufWriter.write(r);
    }
} catch (IOException er) {
    JOptionPane.showMessageDialog(null, er.getMessage());
}
bytes.clear();
}
bytes.add("endsolid " + nmFile[0]);
try {
    for (String r : bytes) {
        bufWriter.write(r);
    }
} catch (IOException er) {
    JOptionPane.showMessageDialog(null, er.getMessage());
}
bytes.clear();
bufWriter.close();
writer.close();
}

```



## A.3 Python <sup>TM</sup> code to convert and save a 2D array into an *.stl* file

```

files = os.listdir(open_path)

def main():
    for ii in files:
        img = Image.open(open_path + ii).convert('LA')
        mtx = array(img.convert('L'))
        ii = ii.split('.')[0]
        ii = ii + '.stl'
        file_name = os.path.join(save_path, ii)
        mtx = 255 - mtx      # invert white to valley
        create_stl(mtx, 50, 50, 256, 2, file_name) # 50 mm, 50 mm, mesh number: 150

def create_stl(img_mtx, x_size, y_size, resolution, t_base, file_name):
    row, col = img_mtx.shape
    x_max = img_mtx.max()
    x_min = img_mtx.min()
    img_mtx = (img_mtx - x_min) / (x_max - x_min)
    points = []
    triangles = []
    # ----- writing file mode -----
    use_file = True
    stl_mode = True
    x_step = row / resolution # (resolution - 1)
    y_step = col / resolution # (resolution - 1)
    X = array(range(resolution)) * x_step - row / 2
    Y = array(range(resolution)) * y_step - col / 2
    x_scalar = x_size / row # step along X axis in mm
    y_scalar = y_size / col # step along Y axis in mm
    z_scalar = 1.0 # 1.5 mm

    for i, x in enumerate(X):
        for j, y in enumerate(Y):
            points.append(array([x * x_scalar, y * y_scalar, t_base + z_scalar * img_mtx[i][j]]))
            if i > 0 and j > 0:
                p1 = i + j * resolution
                p2 = p1 - 1
                p3 = p1 - resolution
                p4 = p3 - 1
                triangles.append([p1, p2, p4])
                triangles.append([p1, p4, p3])

    x_step = x_size / (resolution - 1)
    y_step = y_size / (resolution - 1)
    X = array(range(resolution)) * x_step - x_size / 2
    Y = array(range(resolution)) * y_step - y_size / 2

    for i, x in enumerate(X):
        points.append([x, -y_size / 2., 0])
        if i > 0:
            p1 = i * resolution
            p2 = p1 - resolution

```

```

    p3 = resolution ** 2 + i
    p4 = p3 - 1
    triangles.append([p1, p4, p2])
    triangles.append([p1, p3, p4])

for i, x in enumerate(X):
    points.append([x, y_size / 2., 0])
    if i > 0:
        p1 = i * resolution + resolution - 1
        p2 = p1 - resolution
        p3 = resolution ** 2 + resolution + i
        p4 = p3 - 1
        triangles.append([p1, p2, p4])
        triangles.append([p1, p4, p3])

for j, y in enumerate(Y):
    points.append([-x_size / 2., y, 0])
    if j > 0:
        p1 = j
        p2 = p1 - 1
        p3 = resolution ** 2 + 2 * resolution + j
        p4 = p3 - 1
        triangles.append([p1, p2, p4])
        triangles.append([p1, p4, p3])

for j, y in enumerate(Y):
    points.append([x_size / 2., y, 0])
    if j > 0:
        p1 = resolution ** 2 - resolution + j
        p2 = p1 - 1
        p3 = resolution ** 2 + 3 * resolution + j
        p4 = p3 - 1
        triangles.append([p1, p4, p2])
        triangles.append([p1, p3, p4])

points += map(array,
              [[0, 0, 0], [-x_size / 2., -y_size / 2., 0],
               [x_size / 2., -y_size / 2., 0],
               [x_size / 2., y_size / 2., 0],
               [-x_size / 2.0, y_size / 2.0, 0]])
triangles.append(list(array([0, 1, 2]) + 4 * resolution + resolution ** 2))
triangles.append(list(array([0, 2, 3]) + 4 * resolution + resolution ** 2))
triangles.append(list(array([0, 3, 4]) + 4 * resolution + resolution ** 2))
triangles.append(list(array([0, 4, 1]) + 4 * resolution + resolution ** 2))

data = ''
if stl_mode:
    t = time.localtime()
    name = 'object%s%s%s%s%s' % (t.tm_year, t.tm_mon, t.tm_mday, t.tm_hour, t.tm_min, t.tm_sec)
    data += 'solid %s\n' % name
    for facet in triangles:
        # try:
        p = [array(points[f]) for f in facet]
        # except IndexError:
        # sys.stderr.write(str(facet)+"\n")

```

---

```

    # point=unit(cross(p[1]-p[0],p[2]-p[0]))
    # point=unit(cross(p[0]-p[2],p[2]-p[1]))
    point = [0, 0, 0]
    data += 'facet normal %s\n' % ' '.join(map(str, point))
    data += '  outer loop\n'
    # if inward_wall:
    p = [p[0], p[2], p[1]]
    for point in p:
        data += '    vertex %s\n' % ' '.join(map(str, point))
    data += '  endloop\n'
    data += 'endfacet\n'
    data += 'endsolid %s\n' % name

else:
    def tos(f):
        return f

    def map_tos(a):
        return '[' + ', '.join(map(tos, a)) + ']'

    def map_map_tos(a):
        return '[' + ', '.join(map(map_tos, a)) + ']'

    data = "polyhedron(\n points=\n%s,\n triangles\n=%s);" % (map_map_tos(points), triangles)

if use_file:
    f = open(file_name, "w")
    f.write(data)
    f.close()
else:
    print(data)

def poly(theta, n=4, r=10):
    theta = (int(theta * 180 / pi) % (360 / n)) * pi / 180
    theta = theta - 0.5 * (360 / n) * pi / 180
    if theta < -pi / 2:
        theta = -pi / 2
    if theta > pi / 2:
        theta = pi / 2
    x = r / (0.001 + cos(theta))
    return x

def mag(a):
    return sqrt(sum(a * a))

def unit(a):
    return a / mag(a)

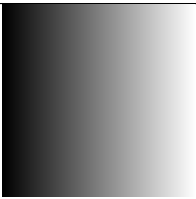
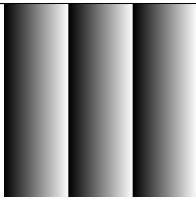
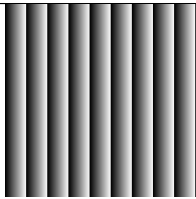

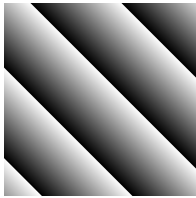
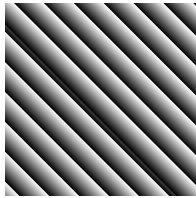
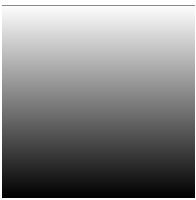
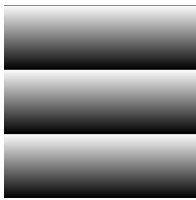
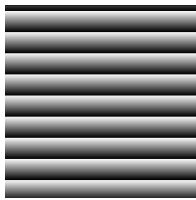
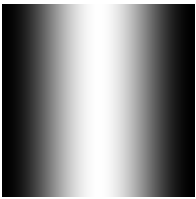
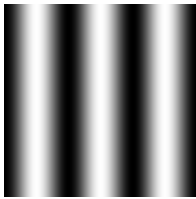
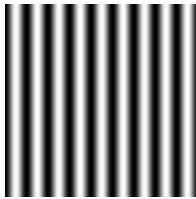
# -----
if __name__ == '__main__':
    main()

```

# Appendix B

## Parent Images with Standard Signals

All images' size is adjusted for the sake of clarity. Their actual size is  $420 \times 420$ .

Signal	Angle	Frequency		
		1	3	9
Sawtooth	0			
Sawtooth	45			
Sawtooth	90			
Sinusoidal	0			

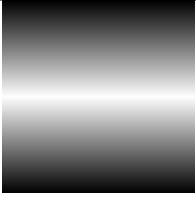
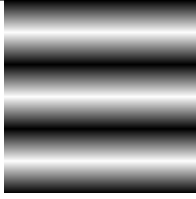
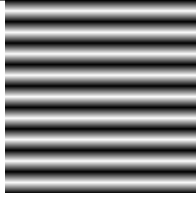
Continued on next page

Table B.1 – continued from previous page

Signal	Angle	Frequency		
		1	3	9
Sinusoidal	45			
	90			
Square-wave	0			
	45			
Square-wave	90			
Triangle	0			
	45			

Continued on next page

Table B.1 – continued from previous page

Signal	Angle	Frequency		
		1	3	9
Triangle	90			

# Appendix C

## Power Spectra-Based Features

### C.1 Features Derived by Liu and Jernigan

Liu and Jernigan [54] derived and investigated twenty eight features to discriminate and to classify samples of natural images distorted by additive noise. They presented the detail of how those 28 features were defined. Here, is the abbreviated names of those textures that are used in this report.

<b>emp</b>	: energy in major peak
<b>lmp</b>	: laplacian of major peak
<b>lsp</b>	: laplacian secondary peak
<b>smp</b>	: secondary major peak
<b>smf</b>	: squared major peak frequency
<b>rom</b>	: relative orientation of major and secondary peak
<b>isp</b>	: isotropy of power spectrum
<b>cps</b>	: circularity of power spectrum
<b>mph</b>	: major peak horizontal frequency
<b>mpv</b>	: major peak vertical frequency
<b>sph</b>	: secondary peak horizontal frequency
<b>spv</b>	: secondary peak vertical frequency
<b>sdb</b>	: squared distance between major and secondary peak
<b>pcm</b>	: principal component magnitude squared
<b>pcd</b>	: principal component direction
<b>rma</b>	: ratio of minor to major axis
<b>mi1</b>	: moment of inertia, quadrant I
<b>mi2</b>	: moment of inertia, quadrant II
<b>mra</b>	: moment ratio

---

<b>pe1</b>	: percentage energy, quadrant I
<b>pe2</b>	: percentage energy, quadrant II
<b>rnc</b>	: ratio of non-zero components
<b>lph</b>	: laplacian of major peak phase (not-used)
<b>lsh</b>	: laplacian of secondary peak phase (not-used)
<b>re1</b>	: relative entropy of power spectrum, $R_1$
<b>re2</b>	: relative entropy of power spectrum, $R_2$
<b>re3</b>	: relative entropy of power spectrum, $R_3$
<b>re4</b>	: relative entropy of power spectrum, $R_4$

## C.2 Proposed Features

Let  $P(u, v)$  be the power spectrum of the image and let

$$p(u, v) = \frac{P(u, v)}{\sum_{u \neq 0}^M \sum_{v \neq 0}^N P(u, v)} \quad (\text{C.1})$$

be the normalized power spectrum.

### C.2.1 Maximum value-based threshold of features

Let

$$p(u_1, v_1) = p(u, v)|_{p(u, v) > c, \quad c = \{0.5, 0.1, 0.01, 0.001\}} \quad (\text{C.2})$$

be the components of the normalized power spectrum above the threshold. The following power spectra-based features are defined as

*fro\_m* : Frobenius norm

$$\text{fro\_m} = \left[ \sum_{u_1=1} \sum_{v_1=1} \text{abs}(p[u_1, v_1]^2) \right]^{1/2} \quad (\text{C.3})$$

*mass* : mass of the frequency component greater than threshold

$$\text{mass} = \sum_{u_1=1} \sum_{v_1=1} p(u_1, v_1) \quad (\text{C.4})$$

*mom* : moment of the frequency component greater than threshold

$$\text{mom} = \left[ \sum_{u_1=1} \sum_{v_1=1} p(u_1, v_1) \cdot (u_1^2 + v_1^2) \right]^2 \quad (\text{C.5})$$



$rd\_m$  : maximum value of the frequency component greater than threshold

$$rd\_m = \max (u_1^2 + v_1^2)^{1/2} \quad (C.6)$$

$pts\_t$  : proportion of the number of the frequency component greater than threshold in X-axis

$$pts\_t = \frac{\sum_{u=1}(1)}{MN} \quad (C.7)$$

$pts\_h$  : density of the frequency component greater than threshold in X-axis within a convex hull boundary

$$pts\_h = \frac{\text{Conv}(p(u, v))}{\sum_{u=1}(1)} \quad (C.8)$$

$mass\_p$  : density in X-axis of frequency component greater than threshold

$$mass\_p = \frac{\sum_{u_1=1} p(u_1, v_1)}{\sum_{u_1=1}(1)} \quad (C.9)$$

$area\_h$  : proportion of the area of the convex hull boundary of the frequency component greater than threshold

$$area\_h = \frac{\text{Conv}(p(u_1, v_1))}{MN} \quad (C.10)$$

$corr$  : absolute value of the correlation between frequency component greater than threshold in X-axis and those in Y-axis

$$corr = |\text{Corr}(u_1, v_1)| \quad (C.11)$$

$var\_d$  : variance of the frequency component greater than threshold

$$var\_d = [\text{var}_{u_1}^2 + \text{var}_{v_1}^2]^{1/2} \quad (C.12)$$

where  $\text{var}_u$  is the PCA component in X-axis of frequency component greater than threshold and  $\text{var}_v$  the same component in Y-axis.

$ang\_p$  : angle of the vector  $\text{var}_u$  and  $\text{var}_v$  with respect to X-axis

$$ang\_p = \arctan \left( \frac{\text{var}_{v_1}}{\text{var}_{u_1}} \right) \quad (C.13)$$

$dens$  : the ratio between area within the convex hull boundary of frequency component greater than threshold and the mass within it

$$dens = \frac{\text{Conv}(p(u_1, v_1))}{\sum_{u_1=1} \sum_{v_1=1} p(u_1, v_1)} \quad (C.14)$$

## C.2.2 Circular boundary-based threshold of features

Let

$$p(u_1, v_1) = p(u, v)|_{(u^2+v^2) < c \cdot (u_m^2+v_m^2)}, \quad c=\{1, 2.25, 4\} \quad (\text{C.15})$$

where  $u_m, v_m = \operatorname{argmax}(P(u, v))$ , be the components of the normalized power spectrum inside a circular boundary with the radius is equals to the distance between the peak value of the spectrum and its centre. The following features are defined as

$rad\_m$  : radius of the circular boundary

$$rad\_m = \sqrt{u_m^2 + v_m^2} \quad (\text{C.16})$$

$area\_r$  : area of the circular boundary

$$area\_r = rad\_m^2 \quad (\text{C.17})$$

$pts\_r$  : number of the non-zero components of the power spectrum inside the circular boundary

$$pts\_r = \sum_{u_1=1} \sum_{v_1=1} (1) \quad (\text{C.18})$$

$mas\_r$  : mass of power spectrum within the circular boundary

$$mas\_r = 100 \cdot \sum_{u_1=1} \sum_{v_1=1} p(u_1, v_1) \quad (\text{C.19})$$

$mom\_r$  : total moment of power spectrum within the circular boundary

$$mom\_r = \sum_{u_1=1} \sum_{v_1=1} p(u_1, v_1) \cdot (u_1^2 + v_1^2) \quad (\text{C.20})$$

$dens\_r$  : inverse of the density of power spectrum within the circular boundary

$$dens\_r = \frac{area\_r}{mas\_r} \quad (\text{C.21})$$

$th\_m$  : angle of the radius vector of the peak value of the spectrum

$$th\_m = \arctan(v_m/u_m) \quad (\text{C.22})$$

### C.2.3 Quadrant area-based features

Let

$$Q_1 = \{u, v \ni 0 \leq u < M/2 \text{ and } 0 \leq v < N/2\} \quad (\text{C.23})$$

is the area of the first quadrant, and let

$$Q_2 = \{u, v \ni M/2 \leq u < M \text{ and } N/2 \leq v < N\} \quad (\text{C.24})$$

be the area of the second quadrant. The following features are defined as

$r\_cog1$  : radius of the centre of gravity of the spectrum in the first quadrant

$$r\_cog1 = \sqrt{cog\_x1^2 + cog\_y1^2} \quad (\text{C.25})$$

where  $cog\_x1 = \sum_{u,v \in Q_1} u \cdot p(u, v)$  and  $cog\_y1 = \sum_{u,v \in Q_1} v \cdot p(u, v)$ .

$th\_q1$  : angle of the vector of radius of the centre of gravity of the spectrum in the first quadrant

$$th\_q1 = \arctan\left(\frac{cog\_y1}{cog\_x1}\right) \quad (\text{C.26})$$

$sum\_rq1$  : mass of the spectrum in the first quadrant

$$sum\_rq1 = \sum_{u,v \in Q_1} p(u, v) |_{u^2+v^2 < r\_cog1} \quad (\text{C.27})$$

$count\_rq1$  : number of the non-zero components of the power spectrum in the first quadrant

$$count\_rq1 = \sum_{u,v \in Q_1} 1 |_{u^2+v^2 < r\_cog1 \text{ and } p(u,v) > 0} \quad (\text{C.28})$$

$r\_cog2$  : radius of the centre of gravity of the spectrum in the second quadrant

$$r\_cog2 = \sqrt{cog\_x2^2 + cog\_y2^2} \quad (\text{C.29})$$

where  $cog\_x2 = \sum_{u,v \in Q_2} u \cdot p(u, v)$  and  $cog\_y2 = \sum_{u,v \in Q_2} v \cdot p(u, v)$ .

$th\_q2$  : angle of the vector of radius of the centre of gravity of the spectrum in the second quadrant

$$th\_q2 = \arctan\left(\frac{cog\_y2}{cog\_x2}\right) \quad (\text{C.30})$$

$sum\_rq2$  : mass of the spectrum in the second quadrant

$$sum\_rq2 = \sum_{u,v \in Q_2} p(u, v) |_{u^2+v^2 < r\_cog2} \quad (\text{C.31})$$

*count\_rq2* : number of the non-zero components of the power spectrum in the second quadrant

$$count\_rq2 = \sum_{u,v \in Q_2} 1_{|u^2+v^2 < r\_cog2 \text{ and } p(u,v) > 0} \quad (C.32)$$

*rad\_cog* : sum of radius of the centre of gravity of the spectrum in the first and second quadrant

$$rad\_cog = \sqrt{r\_cog1^2 + r\_cog2^2} \quad (C.33)$$

*ang* : angle between *r\_cog1* and *r\_cog*

$$ang = \arctan\left(\frac{r\_cog1}{rad\_cog}\right) \quad (C.34)$$

## C.2.4 Wedge area-based features

*sum\_wm* : mass of the spectrum within the wedge area. The direction of the centre line of the wedge follows *th\_m*.

$$sum\_wm = \sum_{th\_m - 0.85 \leq \tan^{-1}(v/u) \leq th\_m + 0.85} p(u, v) \quad (C.35)$$

*count\_wm* : number of the non-zero components of the spectrum within the wedge area. The direction of the centre line of the wedge follows *th\_m*.

$$count\_wm = \sum_{th\_m - 0.85 \leq \tan^{-1}(v/u) \leq th\_m + 0.85} 1 \Big|_{p(u,v) > 0} \quad (C.36)$$

*sum\_wa1* : mass of the spectrum within the wedge area. The direction of the centre line of the wedge follows *th\_q1*.

$$sum\_wa1 = \sum_{th\_q1 - 0.85 \leq \tan^{-1}(v/u) \leq th\_q1 + 0.85} p(u, v) \quad (C.37)$$

*count\_wa1*

: number of the non-zero components of the spectrum within the wedge area. The direction of the centre line of the wedge follows *th\_q1*.

$$count\_wa1 = \sum_{th\_q1 - 0.85 \leq \tan^{-1}(v/u) \leq th\_q1 + 0.85} 1 \Big|_{p(u,v) > 0} \quad (C.38)$$

$sum\_wa2$  : mass of the spectrum within the wedge area. The direction of the centre line of the wedge follows  $th\_q2$ .

$$sum\_wa2 = \sum_{th\_q2-0.85 \leq \tan^{-1}(v/u) \leq th\_q2+0.85} p(u, v) \quad (C.39)$$

$count\_wa2$

: number of the non-zero components of the spectrum within the wedge area. The direction of the centre line of the wedge follows  $th\_q2$ .

$$count\_wa2 = \sum_{th\_q2-0.85 \leq \tan^{-1}(v/u) \leq th\_q2+0.85} \begin{cases} 1 \\ p(u, v) > 0 \end{cases} \quad (C.40)$$

### C.2.5 Standardized spectrum-based features

Let

$$p(u, v) = \frac{P(u, v)}{\max(P(u, v))} \quad (C.41)$$

be the standardized power spectrum. The following features are defined as

$sum\_$  : total mass of the standardized spectrum

$$sum\_ = \sum_{u, v} p(u, v) \quad (C.42)$$

$momen\_$  : sum of the moment of the standardized spectrum in the first and second quadrant

$$momen\_ = \sqrt{mx^2 + my^2} \quad (C.43)$$

where  $mx = \sum_{0 \leq u, v < M/2} (u^2 + v^2) \cdot P(u, v)$  and  $my = \sum_{M/2 \leq u, v < M} (u^2 + v^2) \cdot P(u, v)$ .

# Appendix D

## Results of Post-hoc Pairwise Comparisons Tests

Table D.1: Post-hoc pairwise comparisons of chi-squared test between FO visual textures

A	B	mean(A)	mean(B)	diff	SE	T	p-Tukey	efsize
10	20	1.300333	1.271000	0.029333	0.104	0.281	0.900000	0.051
10	30	1.300333	1.305333	-0.005000	0.104	-0.048	0.900000	-0.009
10	40	1.300333	1.183000	0.117333	0.104	1.124	0.900000	0.204
10	50	1.300333	1.012333	0.288000	0.104	2.759	0.654475	0.500
10	60	1.300333	0.820667	0.479667	0.104	4.594	0.001000	0.833
10	70	1.300333	0.789333	0.511000	0.104	4.894	0.001000	0.888
10	80	1.300333	0.614667	0.685667	0.104	6.567	0.001000	1.191
10	90	1.300333	0.574000	0.726333	0.104	6.957	0.001000	1.262
20	30	1.271000	1.305333	-0.034333	0.104	-0.329	0.900000	-0.060
20	40	1.271000	1.183000	0.088000	0.104	0.843	0.900000	0.153
20	50	1.271000	1.012333	0.258667	0.104	2.478	0.692862	0.449
20	60	1.271000	0.820667	0.450333	0.104	4.313	0.001000	0.783
20	70	1.271000	0.789333	0.481667	0.104	4.614	0.001000	0.837
20	80	1.271000	0.614667	0.656333	0.104	6.287	0.001000	1.140
20	90	1.271000	0.574000	0.697000	0.104	6.676	0.001000	1.211
30	40	1.305333	1.183000	0.122333	0.104	1.172	0.900000	0.213
30	50	1.305333	1.012333	0.293000	0.104	2.806	0.654475	0.509
30	60	1.305333	0.820667	0.484667	0.104	4.642	0.001000	0.842
30	70	1.305333	0.789333	0.516000	0.104	4.942	0.001000	0.897
30	80	1.305333	0.614667	0.690667	0.104	6.615	0.001000	1.200
30	90	1.305333	0.574000	0.731333	0.104	7.005	0.001000	1.271
40	50	1.183000	1.012333	0.170667	0.104	1.635	0.500000	0.297
40	60	1.183000	0.820667	0.362333	0.104	3.471	0.654475	0.630
40	70	1.183000	0.789333	0.393667	0.104	3.771	0.654475	0.684
40	80	1.183000	0.614667	0.568333	0.104	5.444	0.001000	0.988
40	90	1.183000	0.574000	0.609000	0.104	5.833	0.001000	1.058
50	60	1.012333	0.820667	0.191667	0.104	1.836	0.500000	0.333
50	70	1.012333	0.789333	0.223000	0.104	2.136	0.451574	0.387

Continued on next page

Table D.1 – continued from previous page

A	B	mean(A)	mean(B)	diff	SE	T	p-Tukey	efsize
50	80	1.012333	0.614667	0.397667	0.104	3.809	0.654475	0.691
50	90	1.012333	0.574000	0.438333	0.104	4.198	0.001000	0.762
60	70	0.820667	0.789333	0.031333	0.104	0.300	0.900000	0.054
60	80	0.820667	0.614667	0.206000	0.104	1.973	0.500000	0.358
60	90	0.820667	0.574000	0.246667	0.104	2.363	0.567662	0.429
70	80	0.789333	0.614667	0.174667	0.104	1.673	0.500000	0.304
70	90	0.789333	0.574000	0.215333	0.104	2.063	0.500265	0.374
80	90	0.614667	0.574000	0.040667	0.104	0.390	0.900000	0.071

Table D.2: Post-hoc pairwise comparisons of chi-squared test between SO visual textures

A	B	mean(A)	mean(B)	diff	SE	T	p-Tukey	efsize
10	20	0.837333	0.900333	-0.063000	0.052	-1.205	0.900000	-0.219
10	30	0.837333	0.972667	-0.135333	0.052	-2.589	0.654475	-0.470
10	40	0.837333	0.997667	-0.160333	0.052	-3.067	0.654475	-0.556
10	50	0.837333	1.029333	-0.192000	0.052	-3.672	0.654475	-0.666
10	60	0.837333	1.142000	-0.304667	0.052	-5.827	0.001000	-1.057
10	70	0.837333	1.237333	-0.400000	0.052	-7.651	0.001000	-1.388
10	80	0.837333	1.339000	-0.501667	0.052	-9.596	0.001000	-1.741
10	90	0.837333	1.352667	-0.515333	0.052	-9.857	0.001000	-1.788
20	30	0.900333	0.972667	-0.072333	0.052	-1.384	0.900000	-0.251
20	40	0.900333	0.997667	-0.097333	0.052	-1.862	0.500000	-0.338
20	50	0.900333	1.029333	-0.129000	0.052	-2.467	0.699285	-0.448
20	60	0.900333	1.142000	-0.241667	0.052	-4.622	0.001000	-0.839
20	70	0.900333	1.237333	-0.337000	0.052	-6.446	0.001000	-1.169
20	80	0.900333	1.339000	-0.438667	0.052	-8.391	0.001000	-1.522
20	90	0.900333	1.352667	-0.452333	0.052	-8.652	0.001000	-1.570
30	40	0.972667	0.997667	-0.025000	0.052	-0.478	0.900000	-0.087
30	50	0.972667	1.029333	-0.056667	0.052	-1.084	0.900000	-0.197
30	60	0.972667	1.142000	-0.169333	0.052	-3.239	0.654475	-0.588
30	70	0.972667	1.237333	-0.264667	0.052	-5.062	0.001000	-0.918
30	80	0.972667	1.339000	-0.366333	0.052	-7.007	0.001000	-1.271
30	90	0.972667	1.352667	-0.380000	0.052	-7.268	0.001000	-1.319
40	50	0.997667	1.029333	-0.031667	0.052	-0.606	0.900000	-0.110
40	60	0.997667	1.142000	-0.144333	0.052	-2.761	0.654475	-0.501
40	70	0.997667	1.237333	-0.239667	0.052	-4.584	0.001000	-0.832
40	80	0.997667	1.339000	-0.341333	0.052	-6.529	0.001000	-1.184
40	90	0.997667	1.352667	-0.355000	0.052	-6.790	0.001000	-1.232
50	60	1.029333	1.142000	-0.112667	0.052	-2.155	0.438889	-0.391
50	70	1.029333	1.237333	-0.208000	0.052	-3.978	0.654475	-0.722
50	80	1.029333	1.339000	-0.309667	0.052	-5.923	0.001000	-1.075
50	90	1.029333	1.352667	-0.323333	0.052	-6.184	0.001000	-1.122
60	70	1.142000	1.237333	-0.095333	0.052	-1.823	0.500000	-0.331
60	80	1.142000	1.339000	-0.197000	0.052	-3.768	0.654475	-0.684
60	90	1.142000	1.352667	-0.210667	0.052	-4.029	0.654475	-0.731

Continued on next page

Table D.2 – continued from previous page

A	B	mean(A)	mean(B)	diff	SE	T	p-Tukey	efsize
70	80	1.237333	1.339000	-0.101667	0.052	-1.945	0.500000	-0.353
70	90	1.237333	1.352667	-0.115333	0.052	-2.206	0.404687	-0.400
80	90	1.339000	1.352667	-0.013667	0.052	-0.261	0.900000	-0.047

Table D.3: Post-hoc pairwise comparisons of chi-squared test between TO visual textures

A	B	mean(A)	mean(B)	diff	SE	T	p-Tukey	efsize
10	20	1.024000	1.025000	-0.001000	0.037	-0.027	0.9	-0.005
10	30	1.024000	0.998000	0.026000	0.037	0.695	0.9	0.126
10	40	1.024000	1.023333	0.000667	0.037	0.018	0.9	0.003
10	50	1.024000	1.028333	-0.004333	0.037	-0.116	0.9	-0.021
10	60	1.024000	1.062667	-0.038667	0.037	-1.033	0.9	-0.187
10	70	1.024000	1.021333	0.002667	0.037	0.071	0.9	0.013
10	80	1.024000	0.996667	0.027333	0.037	0.731	0.9	0.133
10	90	1.024000	1.000000	0.024000	0.037	0.641	0.9	0.116
20	30	1.025000	0.998000	0.027000	0.037	0.722	0.9	0.131
20	40	1.025000	1.023333	0.001667	0.037	0.045	0.9	0.008
20	50	1.025000	1.028333	-0.003333	0.037	-0.089	0.9	-0.016
20	60	1.025000	1.062667	-0.037667	0.037	-1.007	0.9	-0.183
20	70	1.025000	1.021333	0.003667	0.037	0.098	0.9	0.018
20	80	1.025000	0.996667	0.028333	0.037	0.757	0.9	0.137
20	90	1.025000	1.000000	0.025000	0.037	0.668	0.9	0.121
30	40	0.998000	1.023333	-0.025333	0.037	-0.677	0.9	-0.123
30	50	0.998000	1.028333	-0.030333	0.037	-0.811	0.9	-0.147
30	60	0.998000	1.062667	-0.064667	0.037	-1.728	0.5	-0.314
30	70	0.998000	1.021333	-0.023333	0.037	-0.624	0.9	-0.113
30	80	0.998000	0.996667	0.001333	0.037	0.036	0.9	0.006
30	90	0.998000	1.000000	-0.002000	0.037	-0.053	0.9	-0.010
40	50	1.023333	1.028333	-0.005000	0.037	-0.134	0.9	-0.024
40	60	1.023333	1.062667	-0.039333	0.037	-1.051	0.9	-0.191
40	70	1.023333	1.021333	0.002000	0.037	0.053	0.9	0.010
40	80	1.023333	0.996667	0.026667	0.037	0.713	0.9	0.129
40	90	1.023333	1.000000	0.023333	0.037	0.624	0.9	0.113
50	60	1.028333	1.062667	-0.034333	0.037	-0.918	0.9	-0.166
50	70	1.028333	1.021333	0.007000	0.037	0.187	0.9	0.034
50	80	1.028333	0.996667	0.031667	0.037	0.846	0.9	0.154
50	90	1.028333	1.000000	0.028333	0.037	0.757	0.9	0.137
60	70	1.062667	1.021333	0.041333	0.037	1.105	0.9	0.200
60	80	1.062667	0.996667	0.066000	0.037	1.764	0.5	0.320
60	90	1.062667	1.000000	0.062667	0.037	1.675	0.5	0.304
70	80	1.021333	0.996667	0.024667	0.037	0.659	0.9	0.120
70	90	1.021333	1.000000	0.021333	0.037	0.570	0.9	0.103
80	90	0.996667	1.000000	-0.003333	0.037	-0.089	0.9	-0.016



Table D.4: Post-hoc pairwise comparisons of chi-squared test between FO tactile textures

A	B	mean(A)	mean(B)	diff	SE	T	p-Tukey	efsize
10	20	2.707667	1.898333	0.809333	0.083	9.743	0.001000	1.768
10	30	2.707667	1.757333	0.950333	0.083	11.441	0.001000	2.075
10	40	2.707667	1.261667	1.446000	0.083	17.408	0.001000	3.158
10	50	2.707667	1.023333	1.684333	0.083	20.277	0.001000	3.678
10	60	2.707667	0.884000	1.823667	0.083	21.954	0.001000	3.983
10	70	2.707667	0.559667	2.148000	0.083	25.859	0.001000	4.691
10	80	2.707667	0.535000	2.172667	0.083	26.156	0.001000	4.745
10	90	2.707667	0.438667	2.269000	0.083	27.316	0.001000	4.955
20	30	1.898333	1.757333	0.141000	0.083	1.697	0.500000	0.308
20	40	1.898333	1.261667	0.636667	0.083	7.665	0.001000	1.390
20	50	1.898333	1.023333	0.875000	0.083	10.534	0.001000	1.911
20	60	1.898333	0.884000	1.014333	0.083	12.211	0.001000	2.215
20	70	1.898333	0.559667	1.338667	0.083	16.116	0.001000	2.924
20	80	1.898333	0.535000	1.363333	0.083	16.413	0.001000	2.977
20	90	1.898333	0.438667	1.459667	0.083	17.572	0.001000	3.188
30	40	1.757333	1.261667	0.495667	0.083	5.967	0.001000	1.083
30	50	1.757333	1.023333	0.734000	0.083	8.836	0.001000	1.603
30	60	1.757333	0.884000	0.873333	0.083	10.514	0.001000	1.907
30	70	1.757333	0.559667	1.197667	0.083	14.418	0.001000	2.616
30	80	1.757333	0.535000	1.222333	0.083	14.715	0.001000	2.669
30	90	1.757333	0.438667	1.318667	0.083	15.875	0.001000	2.880
40	50	1.261667	1.023333	0.238333	0.083	2.869	0.654475	0.521
40	60	1.261667	0.884000	0.377667	0.083	4.547	0.001000	0.825
40	70	1.261667	0.559667	0.702000	0.083	8.451	0.001000	1.533
40	80	1.261667	0.535000	0.726667	0.083	8.748	0.001000	1.587
40	90	1.261667	0.438667	0.823000	0.083	9.908	0.001000	1.797
50	60	1.023333	0.884000	0.139333	0.083	1.677	0.500000	0.304
50	70	1.023333	0.559667	0.463667	0.083	5.582	0.001000	1.013
50	80	1.023333	0.535000	0.488333	0.083	5.879	0.001000	1.066
50	90	1.023333	0.438667	0.584667	0.083	7.039	0.001000	1.277
60	70	0.884000	0.559667	0.324333	0.083	3.905	0.654475	0.708
60	80	0.884000	0.535000	0.349000	0.083	4.201	0.001000	0.762
60	90	0.884000	0.438667	0.445333	0.083	5.361	0.001000	0.973
70	80	0.559667	0.535000	0.024667	0.083	0.297	0.900000	0.054
70	90	0.559667	0.438667	0.121000	0.083	1.457	0.500000	0.264
80	90	0.535000	0.438667	0.096333	0.083	1.160	0.900000	0.210

Table D.5: Post-hoc pairwise comparisons of chi-squared test between SO tactile textures

A	B	mean(A)	mean(B)	diff	SE	T	p-Tukey	efsize
10	20	0.907667	0.919667	-0.012000	0.047	-0.256	0.900000	-0.046
10	30	0.907667	0.920000	-0.012333	0.047	-0.263	0.900000	-0.048
10	40	0.907667	0.964333	-0.056667	0.047	-1.208	0.900000	-0.219
10	50	0.907667	0.992667	-0.085000	0.047	-1.812	0.500000	-0.329

Continued on next page

Table D.5 – continued from previous page

A	B	mean(A)	mean(B)	diff	SE	T	p-Tukey	efsize
10	60	0.907667	1.151000	-0.243333	0.047	-5.188	0.001000	-0.941
10	70	0.907667	0.999000	-0.091333	0.047	-1.947	0.500000	-0.353
10	80	0.907667	1.182667	-0.275000	0.047	-5.863	0.001000	-1.064
10	90	0.907667	1.170333	-0.262667	0.047	-5.600	0.001000	-1.016
20	30	0.919667	0.920000	-0.000333	0.047	-0.007	0.900000	-0.001
20	40	0.919667	0.964333	-0.044667	0.047	-0.952	0.900000	-0.173
20	50	0.919667	0.992667	-0.073000	0.047	-1.556	0.500000	-0.282
20	60	0.919667	1.151000	-0.231333	0.047	-4.932	0.001000	-0.895
20	70	0.919667	0.999000	-0.079333	0.047	-1.691	0.500000	-0.307
20	80	0.919667	1.182667	-0.263000	0.047	-5.607	0.001000	-1.017
20	90	0.919667	1.170333	-0.250667	0.047	-5.344	0.001000	-0.970
30	40	0.920000	0.964333	-0.044333	0.047	-0.945	0.900000	-0.171
30	50	0.920000	0.992667	-0.072667	0.047	-1.549	0.500000	-0.281
30	60	0.920000	1.151000	-0.231000	0.047	-4.925	0.001000	-0.893
30	70	0.920000	0.999000	-0.079000	0.047	-1.684	0.500000	-0.306
30	80	0.920000	1.182667	-0.262667	0.047	-5.600	0.001000	-1.016
30	90	0.920000	1.170333	-0.250333	0.047	-5.337	0.001000	-0.968
40	50	0.964333	0.992667	-0.028333	0.047	-0.604	0.900000	-0.110
40	60	0.964333	1.151000	-0.186667	0.047	-3.980	0.654475	-0.722
40	70	0.964333	0.999000	-0.034667	0.047	-0.739	0.900000	-0.134
40	80	0.964333	1.182667	-0.218333	0.047	-4.655	0.001000	-0.844
40	90	0.964333	1.170333	-0.206000	0.047	-4.392	0.001000	-0.797
50	60	0.992667	1.151000	-0.158333	0.047	-3.376	0.654475	-0.612
50	70	0.992667	0.999000	-0.006333	0.047	-0.135	0.900000	-0.024
50	80	0.992667	1.182667	-0.190000	0.047	-4.051	0.654475	-0.735
50	90	0.992667	1.170333	-0.177667	0.047	-3.788	0.654475	-0.687
60	70	1.151000	0.999000	0.152000	0.047	3.241	0.654475	0.588
60	80	1.151000	1.182667	-0.031667	0.047	-0.675	0.900000	-0.122
60	90	1.151000	1.170333	-0.019333	0.047	-0.412	0.900000	-0.075
70	80	0.999000	1.182667	-0.183667	0.047	-3.916	0.654475	-0.710
70	90	0.999000	1.170333	-0.171333	0.047	-3.653	0.654475	-0.663
80	90	1.182667	1.170333	0.012333	0.047	0.263	0.900000	0.048

Table D.6: Post-hoc pairwise comparisons of chi-squared test between TO tactile textures

A	B	mean(A)	mean(B)	diff	SE	T	p-Tukey	efsize
10	20	0.988333	0.976000	0.012333	0.055	0.223	0.900000	0.040
10	30	0.988333	1.164667	-0.176333	0.055	-3.184	0.654475	-0.578
10	40	0.988333	1.011000	-0.022667	0.055	-0.409	0.900000	-0.074
10	50	0.988333	1.189667	-0.201333	0.055	-3.636	0.654475	-0.660
10	60	0.988333	1.142667	-0.154333	0.055	-2.787	0.654475	-0.506
10	70	0.988333	0.781667	0.206667	0.055	3.732	0.654475	0.677
10	80	0.988333	0.881667	0.106667	0.055	1.926	0.500000	0.349
10	90	0.988333	0.803667	0.184667	0.055	3.335	0.654475	0.605
20	30	0.976000	1.164667	-0.188667	0.055	-3.407	0.654475	-0.618

Continued on next page

Table D.6 – continued from previous page

A	B	mean(A)	mean(B)	diff	SE	T	p-Tukey	efsize
20	40	0.976000	1.011000	-0.035000	0.055	-0.632	0.900000	-0.115
20	50	0.976000	1.189667	-0.213667	0.055	-3.858	0.654475	-0.700
20	60	0.976000	1.142667	-0.166667	0.055	-3.010	0.654475	-0.546
20	70	0.976000	0.781667	0.194333	0.055	3.509	0.654475	0.637
20	80	0.976000	0.881667	0.094333	0.055	1.703	0.500000	0.309
20	90	0.976000	0.803667	0.172333	0.055	3.112	0.654475	0.565
30	40	1.164667	1.011000	0.153667	0.055	2.775	0.654475	0.503
30	50	1.164667	1.189667	-0.025000	0.055	-0.451	0.900000	-0.082
30	60	1.164667	1.142667	0.022000	0.055	0.397	0.900000	0.072
30	70	1.164667	0.781667	0.383000	0.055	6.916	0.001000	1.255
30	80	1.164667	0.881667	0.283000	0.055	5.110	0.001000	0.927
30	90	1.164667	0.803667	0.361000	0.055	6.519	0.001000	1.183
40	50	1.011000	1.189667	-0.178667	0.055	-3.226	0.654475	-0.585
40	60	1.011000	1.142667	-0.131667	0.055	-2.378	0.572361	-0.431
40	70	1.011000	0.781667	0.229333	0.055	4.141	0.654475	0.751
40	80	1.011000	0.881667	0.129333	0.055	2.335	0.559723	0.424
40	90	1.011000	0.803667	0.207333	0.055	3.744	0.654475	0.679
50	60	1.189667	1.142667	0.047000	0.055	0.849	0.900000	0.154
50	70	1.189667	0.781667	0.408000	0.055	7.368	0.001000	1.337
50	80	1.189667	0.881667	0.308000	0.055	5.562	0.001000	1.009
50	90	1.189667	0.803667	0.386000	0.055	6.970	0.001000	1.264
60	70	1.142667	0.781667	0.361000	0.055	6.519	0.001000	1.183
60	80	1.142667	0.881667	0.261000	0.055	4.713	0.001000	0.855
60	90	1.142667	0.803667	0.339000	0.055	6.122	0.001000	1.111
70	80	0.781667	0.881667	-0.100000	0.055	-1.806	0.500000	-0.328
70	90	0.781667	0.803667	-0.022000	0.055	-0.397	0.900000	-0.072
80	90	0.881667	0.803667	0.078000	0.055	1.409	0.500000	0.256

## D.1 Post-hoc pairwise comparisons of Chi-squared test

Table D.7: Post-hoc pairwise comparisons of chi-squared test between MPs

MP	MP	P-val	P-val Corrected	Cramer's V	Significant?	Reject H0?
Saw_1.00	Saw_1.45	1.000	1.000	.000	(ns)	False
Saw_1.00	Saw_1.90	.332	.368	.022	(ns)	False
Saw_1.00	Squ_1.00	.466	.506	.016	(ns)	False
Saw_1.00	Squ_1.90	.490	.530	.016	(ns)	False
Saw_1.45	Saw_1.90	.308	.344	.023	(ns)	False
Saw_1.45	Squ_1.00	.436	.478	.018	(ns)	False
Saw_1.45	Squ_1.90	.521	.557	.014	(ns)	False
Saw_1.90	Squ_1.00	.847	.869	.004	(ns)	False

Continued on next page

Table D.7 – continued from previous page

MP	MP	P-val	P-val Corrected	Cramer's V	Significant?	Reject H0?
Saw_1.90	Squ_1.90	.087	.103	.039	(ns)	False
Saw_3.00	Saw_3.90	.408	.450	.019	(ns)	False
Saw_3.00	Sin_1.45	.120	.139	.035	(ns)	False
Saw_3.00	Squ_1.45	.072	.086	.041	(ns)	False
Saw_3.00	Squ_3.00	.314	.349	.023	(ns)	False
Saw_3.00	Squ_3.90	.443	.485	.017	(ns)	False
Saw_3.45	Saw_3.90	.174	.198	.031	(ns)	False
Saw_3.45	Sin_1.45	.530	.565	.014	(ns)	False
Saw_3.45	Squ_3.00	.238	.269	.027	(ns)	False
Saw_3.45	Squ_3.45	.748	.779	.007	(ns)	False
Saw_3.45	Squ_3.90	.156	.178	.032	(ns)	False
Saw_3.45	Too_1.45	.045	.054	.045	(*)	FALSE
Saw_3.90	Sin_1.45	.503	.539	.015	(ns)	False
Saw_3.90	Squ_3.00	.904	.925	.003	(ns)	False
Saw_3.90	Squ_3.45	.081	.096	.039	(ns)	False
Saw_3.90	Squ_3.90	1.000	1.000	.000	(ns)	False
Saw_9.00	Saw_9.90	.100	.117	.037	(ns)	False
Saw_9.00	Sin_1.90	.120	.139	.035	(ns)	False
Saw_9.00	Squ_9.00	.805	.832	.006	(ns)	False
Saw_9.00	Squ_9.45	.503	.539	.015	(ns)	False
Saw_9.00	Squ_9.90	.559	.591	.013	(ns)	False
Saw_9.45	Saw_9.90	.168	.191	.031	(ns)	False
Saw_9.45	Sin_1.00	.540	.574	.014	(ns)	False
Saw_9.45	Sin_1.90	.141	.162	.033	(ns)	False
Saw_9.45	Sin_9.45	.063	.075	.042	(ns)	False
Saw_9.45	Too_3.00	.364	.404	.020	(ns)	False
Saw_9.45	Too_3.45	.540	.574	.014	(ns)	False
Saw_9.45	Too_3.90	.477	.517	.016	(ns)	False
Saw_9.45	Too_9.45	.835	.861	.005	(ns)	False
Saw_9.45	Too_9.90	.047	.056	.045	(*)	FALSE
Saw_9.90	Sin_1.00	.503	.539	.015	(ns)	False
Saw_9.90	Sin_1.90	1.000	1.000	.000	(ns)	False
Saw_9.90	Squ_9.00	.188	.214	.030	(ns)	False
Saw_9.90	Squ_9.45	.372	.412	.020	(ns)	False
Saw_9.90	Squ_9.90	.328	.365	.022	(ns)	False
Saw_9.90	Too_3.00	.705	.737	.009	(ns)	False
Saw_9.90	Too_3.45	.503	.539	.015	(ns)	False
Saw_9.90	Too_3.90	.567	.599	.013	(ns)	False
Saw_9.90	Too_9.45	.284	.319	.024	(ns)	False
Sin_1.00	Sin_1.90	.446	.486	.017	(ns)	False
Sin_1.00	Squ_9.45	.099	.115	.037	(ns)	False
Sin_1.00	Squ_9.90	.082	.097	.039	(ns)	False
Sin_1.00	Too_3.00	.845	.868	.004	(ns)	False
Sin_1.00	Too_3.45	1.000	1.000	.000	(ns)	False
Sin_1.00	Too_3.90	1.000	1.000	.000	(ns)	False
Sin_1.00	Too_9.45	.762	.791	.007	(ns)	False
Sin_1.45	Squ_3.00	.624	.657	.011	(ns)	False

Continued on next page

Table D.7 – continued from previous page

MP	MP	P-val	P-val Corrected	Cramer's V	Significant?	Reject H0?
Sin_1.45	Squ_3.45	.311	.347	.023	(ns)	False
Sin_1.45	Squ_3.90	.465	.506	.017	(ns)	False
Sin_1.90	Squ_9.00	.221	.250	.028	(ns)	False
Sin_1.90	Squ_9.45	.424	.465	.018	(ns)	False
Sin_1.90	Squ_9.90	.376	.415	.020	(ns)	False
Sin_1.90	Too_3.00	.638	.669	.011	(ns)	False
Sin_1.90	Too_3.45	.446	.486	.017	(ns)	False
Sin_1.90	Too_3.90	.506	.541	.015	(ns)	False
Sin_1.90	Too_9.45	.245	.275	.026	(ns)	False
Sin_3.00	Sin_3.45	.304	.341	.023	(ns)	False
Sin_3.00	Sin_3.90	1.000	1.000	.000	(ns)	False
Sin_3.00	Sin_9.00	.822	.849	.005	(ns)	False
Sin_3.00	Sin_9.90	.061	.074	.042	(ns)	False
Sin_3.45	Sin_3.90	.421	.463	.018	(ns)	False
Sin_3.45	Sin_9.00	.554	.586	.013	(ns)	False
Sin_3.45	Sin_9.90	.495	.534	.015	(ns)	False
Sin_3.45	Too_9.00	.196	.222	.029	(ns)	False
Sin_3.45	Too_9.90	.047	.057	.045	(*)	FALSE
Sin_3.90	Sin_9.00	1.000	1.000	.000	(ns)	False
Sin_3.90	Sin_9.90	.098	.115	.037	(ns)	False
Sin_9.00	Sin_9.90	.148	.169	.033	(ns)	False
Sin_9.45	Sin_9.90	.197	.223	.029	(ns)	False
Sin_9.45	Too_9.00	.490	.530	.016	(ns)	False
Sin_9.45	Too_9.90	1.000	1.000	.000	(ns)	False
Sin_9.90	Too_9.00	.647	.679	.010	(ns)	False
Sin_9.90	Too_9.90	.247	.277	.026	(ns)	False
Squ_1.00	Squ_1.90	.142	.163	.033	(ns)	False
Squ_3.00	Squ_3.45	.118	.137	.035	(ns)	False
Squ_3.00	Squ_3.90	.857	.878	.004	(ns)	False
Squ_3.45	Squ_3.90	.071	.085	.041	(ns)	False
Squ_3.45	Too_1.00	.078	.092	.040	(ns)	False
Squ_3.45	Too_1.45	.105	.122	.037	(ns)	False
Squ_3.45	Too_1.90	.090	.106	.038	(ns)	False
Squ_9.00	Squ_9.45	.735	.766	.008	(ns)	False
Squ_9.00	Squ_9.90	.800	.829	.006	(ns)	False
Squ_9.00	Too_3.00	.074	.088	.040	(ns)	False
Squ_9.00	Too_3.90	.048	.058	.045	(*)	FALSE
Squ_9.45	Squ_9.90	1.000	1.000	.000	(ns)	False
Squ_9.45	Too_3.00	.173	.197	.031	(ns)	False
Squ_9.45	Too_3.45	.099	.115	.037	(ns)	False
Squ_9.45	Too_3.90	.120	.139	.035	(ns)	False
Squ_9.90	Too_3.00	.148	.169	.033	(ns)	False
Squ_9.90	Too_3.45	.082	.097	.039	(ns)	False
Squ_9.90	Too_3.90	.101	.118	.037	(ns)	False
Too_1.00	Too_1.45	.943	.962	.002	(ns)	False
Too_1.00	Too_1.90	1.000	1.000	.000	(ns)	False
Too_1.45	Too_1.90	1.000	1.000	.000	(ns)	False

Continued on next page

Table D.7 – continued from previous page

MP	MP	P-val	P-val Corrected	Cramer's V	Significant?	Reject H0?
Too_3_00	Too_3_45	.845	.868	.004	(ns)	False
Too_3_00	Too_3_90	.922	.942	.002	(ns)	False
Too_3_00	Too_9_45	.551	.584	.013	(ns)	False
Too_3_45	Too_3_90	1.000	1.000	.000	(ns)	False
Too_3_45	Too_9_45	.762	.791	.007	(ns)	False
Too_3_90	Too_9_45	.688	.720	.009	(ns)	False
Too_9_00	Too_9_90	.578	.608	.013	(ns)	False

Table D.8: The Value of Roughness parameters of the Six Tactile Stimuli

Image	Roughness Parameter						
	s_a	s_q	s_sk	s_ku	s_ds	s_al	s_tr
M1	29.815	36.950	0.456	2.860	0.066	2.236	0.006
M2	70.243	77.187	0.292	1.504	0.668	2.236	0.006
M3	31.864	39.805	0.792	3.178	0.058	9.487	0.026
P1	65.293	72.714	0.282	1.575	0.318	15.033	0.043
P2	56.500	64.356	-0.696	2.056	0.085	1.414	0.004
P3	45.416	55.172	0.745	2.596	0.117	1.414	0.004
D1	47.695	55.419	-0.243	1.983	0.029	1.414	0.004
M1_D1	30.375	37.724	0.075	2.810	0.005	1.414	0.004
M2_D1	34.982	42.800	0.439	2.743	0.011	1.414	0.004
M3_D1	31.274	38.357	0.049	2.586	0.000	1.414	0.004
D1_P1	28.217	34.997	0.157	2.821	0.008	47.170	0.134
D1_P2	34.487	42.282	-0.199	2.577	0.026	1.414	0.004
D1_P3	30.281	37.834	0.344	2.953	0.035	1.414	0.004

## References

- [1] Halimahtun M Khalid and Martin G Helander. Customer emotional needs in product design. *Concurrent Engineering*, 14(3):197–206, 2006. 1
- [2] Rosemary R Seva, Katherine Grace T Gosiaco, Ma Crea Eurice D Santos, and Denise Mae L Pangilinan. Product design enhancement using apparent usability and affective quality. *Applied ergonomics*, 42(3):511–517, 2011. 1
- [3] Sabrina Bruyneel, Siegfried Dewitte, Kathleen D Vohs, and Luk Warlop. Repeated choosing increases susceptibility to affective product features. *International Journal of Research in Marketing*, 23(2):215–225, 2006. 1
- [4] Cathy Barnes and Stephen Paul Lillford. Decision support for the design of affective products. *Journal of Engineering Design*, 20(5):477–492, 2009. 1
- [5] KY Fung, CK Kwong, Kin WM Siu, and KM Yu. A multi-objective genetic algorithm approach to rule mining for affective product design. *Expert Systems with Applications*, 39(8):7411–7419, 2012.
- [6] Jianxin Roger Jiao, Yiyang Zhang, and Martin Helander. A kansei mining system for affective design. *Expert Systems with Applications*, 30(4):658–673, 2006. 1
- [7] Sunkyoung Baek, Miyoung Cho, and Pankoo Kim. Matching colors with kansei vocabulary using similarity measure based on wordnet. In *Computational Science and Its Applications–ICCSA 2005*, pages 37–45. Springer, 2005. 1
- [8] Masataka Tokumaru, Noriaki Muranaka, and Shigeru Imanishi. Color design support system considering color harmony. In *Fuzzy Systems, 2002. FUZZ-IEEE’02. Proceedings of the 2002 IEEE International Conference on*, volume 1, pages 378–383. IEEE, 2002. 1
- [9] Yukari Nagai and Georgi V Georgiev. The role of impressions on users’ tactile interaction with product materials: An analysis of associative concept networks. *Materials & Design*, 32(1):291–302, 2011. 1
- [10] Lian-Yin Zhai, Li-Pheng Khoo, and Zhao-Wei Zhong. A rough set based decision support approach to improving consumer affective satisfaction in

- product design. *International Journal of Industrial Ergonomics*, 39(2):295–302, 2009. [1](#)
- [11] Inglen Lo and M Chuang. The effect of texture of lacquer coating on the kansei evaluation of plastic products. In *Proceedings of the 6th Asian Design Conference*, 2006. [1](#)
- [12] Hendrik NJ Schifferstein. The perceived importance of sensory modalities in product usage: A study of self-reports. *Acta psychologica*, 121(1):41–64, 2006.
- [13] Kai Wang. Research of the affective responses to product’s texture based on the kansei evaluation. In *Computational Intelligence and Design, 2009. ISCID’09. Second International Symposium on*, volume 2, pages 352–355. IEEE, 2009. [1](#)
- [14] Bianca Grohmann, Eric R Spangenberg, and David E Sprott. The influence of tactile input on the evaluation of retail product offerings. *Journal of Retailing*, 83(2):237–245, 2007. [2](#)
- [15] Simon Lacey, Jenelle Hall, and K Sathian. Are surface properties integrated into visuohaptic object representations? *European Journal of Neuroscience*, 31(10):1882–1888, 2010. [2](#)
- [16] MM Taylor, SJ Lederman, and RH Gibson. Tactual perception of texture. *Handbook of perception*, 3:251–272, 1973. [2](#)
- [17] Julien van Kuilenburg, Marc A Masen, and Emile van der Heide. A review of fingerpad contact mechanics and friction and how this affects tactile perception. *Proceedings of the Institution of Mechanical Engineers, Part J: Journal of Engineering Tribology*, 229(3):243–258, 2015. [2](#), [27](#), [34](#), [169](#)
- [18] Delphine Picard, Catherine Dacremont, Dominique Valentin, and Agnes Giboreau. Perceptual dimensions of tactile textures. *Acta psychologica*, 114(2):165–184, 2003. [2](#)
- [19] Shusuke Okamoto, Hidehisa Nagano, and Yoji Yamada. Psychophysical dimensions of tactile perception of textures. *Haptics, IEEE Transactions on*, 6(1):81–93, 2013. [2](#)



- 
- [20] M Hollins, R Faldowski, S Rao, and F Young. Perceptual dimensions of tactile surface texture: a multidimensional scaling analysis. *Perception & psychophysics*, 54(6):697–705, 1993. ISSN 0031-5117. doi: 10.3758/BF03211795. [2](#), [34](#)
- [21] MASAAKI YOSHIDA. Dimensions of tactual impressions (2). *Japanese Psychological Research*, 10(4):157–173, 1968.
- [22] T Yoshioka, SJ Bensmaia, JC Craig, and SS Hsiao. Texture perception through direct and indirect touch: An analysis of perceptual space for tactile textures in two modes of exploration. *Somatosensory & motor research*, 24(1-2):53–70, 2007. [2](#)
- [23] Louise Rosanna Manfredi. *The role of vibratory cues in affective responses to tactile textures*. University of Leeds, 2010. [2](#)
- [24] Wouter M Bergmann Tiest. Tactual perception of material properties. *Vision research*, 50(24):2775–2782, 2010. [2](#), [169](#)
- [25] John R Phillips and Kenneth O Johnson. Tactile spatial resolution. iii. a continuum mechanics model of skin predicting mechanoreceptor responses to bars, edges, and gratings. *Journal of Neurophysiology*, 46(6):1204–1225, 1981. [2](#)
- [26] Vinay Tannan, R Dennis, and M Tommerdahl. A novel device for delivering two-site vibrotactile stimuli to the skin. *Journal of neuroscience methods*, 147(2):75–81, 2005. [2](#)
- [27] Ian Darian-Smith. The sense of touch: performance and peripheral neural processes. *Comprehensive Physiology*, 1984. [2](#), [20](#)
- [28] Kenneth O Johnson, Takashi Yoshioka, and Francisco Vega-Bermudez. Tactile functions of mechanoreceptive afferents innervating the hand. *Journal of Clinical Neurophysiology*, 17(6):539–558, 2000. [19](#), [25](#)
- [29] Kenneth O Johnson. The roles and functions of cutaneous mechanoreceptors. *Current opinion in neurobiology*, 11(4):455–461, 2001.
- [30] Xavier Libouton, Olivier Barbier, Leon Plaghki, and Jean-Louis Thonnard. Tactile roughness discrimination threshold is unrelated to tactile spatial acuity. *Behavioural brain research*, 208(2):473–478, 2010. [3](#), [26](#), [27](#), [49](#), [156](#)

- 
- [31] Kenneth O Johnson and John R Phillips. Tactile spatial resolution. i. two-point discrimination, gap detection, grating resolution, and letter recognition. *Journal of neurophysiology*, 46(6):1177–1192, 1981. [2](#), [23](#), [24](#), [28](#), [49](#)
- [32] Morton A Heller. Texture perception in sighted and blind observers. *Perception & Psychophysics*, 45(1):49–54, 1989. [2](#), [27](#)
- [33] Ronald T. Verrillo, Stanley J Bolanowski, and Francis P McGlone. Subjective magnitude of tactile roughness. *Somatosensory & motor research*, 16(4):352–360, 1999. [2](#), [3](#), [17](#), [28](#), [34](#), [50](#)
- [34] Seung-Chan Kim, Ki-Uk Kyung, Jin-Hun Sohn, and Dong-Soo Kwon. An evaluation of human sensibility on perceived texture under variation of vibrotactile stimuli using a tactile display system. In *Haptic Interfaces for Virtual Environment and Teleoperator Systems, 2006 14th Symposium on*, pages 429–436. IEEE, 2006. [3](#)
- [35] CE Connor, SS Hsiao, JR Phillips, and KO Johnson. Tactile roughness: neural codes that account for psychophysical magnitude estimates. *The Journal of neuroscience*, 10(12):3823–3836, 1990. [3](#), [17](#), [19](#), [25](#), [26](#)
- [36] Charles E Connor and Kenneth O Johnson. Neural coding of tactile texture: comparison of spatial and temporal mechanisms for roughness perception. *The Journal of Neuroscience*, 12(9):3414–3426, 1992. [3](#), [26](#)
- [37] Adrian Sutu, El-Mehdi Meftah, and C Elaine Chapman. Physical determinants of the shape of the psychophysical curve relating tactile roughness to raised-dot spacing: implications for neuronal coding of roughness. *Journal of neurophysiology*, 109(5):1403–1415, 2013.
- [38] T Yoshioka, B Gibb, a K Dorsch, S S Hsiao, and K O Johnson. Neural coding mechanisms underlying perceived roughness of finely textured surfaces. *The Journal of neuroscience : the official journal of the Society for Neuroscience*, 21(17):6905–6916, 2001. ISSN 1529-2401. doi: 21/17/6905[pii]. [3](#), [50](#)
- [39] C J Cascio and K Sathian. Temporal cues contribute to tactile perception of roughness. *The Journal of neuroscience : the official journal of the Society for Neuroscience*, 21(14):5289–5296, 2001. ISSN 1529-2401. doi: 21/14/5289[pii].

- 
- [40] K Sathian, AW Goodwin, KT John, and I Darian-Smith. Perceived roughness of a grating: correlation with responses of mechanoreceptive afferents innervating the monkey's fingerpad. *The Journal of Neuroscience*, 9(4):1273–1279, 1989. 27, 35
- [41] T. Yoshioka, J. C. Craig, G. C. Beck, and S. S. Hsiao. Perceptual Constancy of Texture Roughness in the Tactile System. *Journal of Neuroscience*, 31(48):17603–17611, 2011. ISSN 0270-6474. doi: 10.1523/JNEUROSCI.3907-11.2011. URL <http://www.jneurosci.org/cgi/doi/10.1523/JNEUROSCI.3907-11.2011>. 3
- [42] Judith Eck, Amanda L Kaas, Joost LJ Mulders, and Rainer Goebel. Roughness perception of unfamiliar dot pattern textures. *Acta psychologica*, 143(1):20–34, 2013. 3
- [43] Sidney S Culbert and William T Stellwagen. Tactual discrimination of textures. *Perceptual and Motor Skills*, 16(2):545–552, 1963. 3, 30
- [44] Galal Elkharraz, Stefan Thumfart, Diyar Akay, Christian Eitzinger, and Brian Henson. Making tactile textures with predefined affective properties. *IEEE Transactions on Affective Computing*, 5(1):57–70, 2014. 3, 4, 5, 30, 35, 169
- [45] Chelsea Tymms, Esther P Gardner, and Denis Zorin. A quantitative perceptual model for tactile roughness. *ACM Transactions on Graphics (TOG)*, 37(5):168, 2018. 3, 5
- [46] D-M Tsai and C-Y Hsieh. Automated surface inspection for directional textures. *Image and Vision computing*, 18(1):49–62, 1999. 4
- [47] Manish H Bharati, J Jay Liu, and John F MacGregor. Image texture analysis: methods and comparisons. *Chemometrics and intelligent laboratory systems*, 72(1):57–71, 2004. 4, 35, 36, 37
- [48] Fahimeh Alaei, Alireza Alaei, Umapada Pal, and Michael Blumenstein. A comparative study of different texture features for document image retrieval. *Expert Systems with Applications*, 121:97–114, 2019. 4
- [49] Robert M Haralick. Statistical and structural approaches to texture. *Proceedings of the IEEE*, 67(5):786–804, 1979. 4, 35, 36

- [50] Jiahua Chen and Anil K Jain. A structural approach to identify defects in textured images. In *Proceedings of the 1988 IEEE International Conference on Systems, Man, and Cybernetics*, volume 1, pages 29–32. IEEE, 1988. [4](#)
- [51] Maroua Mehri, Pierre Héroux, Petra Gomez-Krämer, and Rémy Mullot. Texture feature benchmarking and evaluation for historical document image analysis. *International Journal on Document Analysis and Recognition (IJDAR)*, 20(1):1–35, 2017. [4](#)
- [52] Galal Elkharraz, Stefan Thumfart, Diyar Akay, Christian Eitzinger, and Brian Henson. Texture features corresponding to human touch feeling. In *Image Processing (ICIP), 2009 16th IEEE International Conference on*, pages 1341–1344. IEEE, 2009. [5](#), [35](#), [36](#), [47](#), [49](#), [169](#)
- [53] Mihran Tuceryan and Anil K Jain. Texture analysis. In *Handbook of pattern recognition and computer vision*, pages 235–276. World Scientific, 1993. [5](#), [36](#), [37](#), [169](#)
- [54] Song-Sheng Liu and ME Jernigan. Texture analysis and discrimination in additive noise. *Computer Vision, Graphics, and Image Processing*, 49(1): 52–67, 1990. [9](#), [45](#), [106](#), [187](#)
- [55] Georgios P Petropoulos, Constantinos N Pandazaras, and J Paulo Davim. Surface texture characterization and evaluation related to machining. In *Surface integrity in machining*, pages 37–66. Springer, 2010. [10](#), [13](#), [15](#)
- [56] PM Lonardo, H Trumpold, and Leonardo De Chiffre. Progress in 3d surface microtopography characterization. *CIRP Annals-Manufacturing Technology*, 45(2):589–598, 1996. [11](#)
- [57] I Sherrington and EH Smith. The significance of surface topography in engineering. *Precision engineering*, 8(2):79–87, 1986. [11](#)
- [58] Christina QL Chen, Will Scott, and Timothy M Barker. Effect of metal surface topography on mechanical bonding at simulated total hip stem–cement interfaces. *Journal of biomedical materials research*, 48(4):440–446, 1999. [11](#)
- [59] LT Drzal, N Sugiura, and D Hook. The role of chemical bonding and surface topography in adhesion between carbon fibers and epoxy matrices. *Composite Interfaces*, 4(5):337–354, 1996. [11](#)

- 
- [60] X Chen, CJ Barnes, THC Childs, B Henson, and F Shao. Materials' tactile testing and characterisation for consumer products' affective packaging design. *Materials & Design*, 30(10):4299–4310, 2009. [11](#)
- [61] Chris J Evans and James B Bryan. “structured”, “textured” or “engineered” surfaces. *CIRP Annals-Manufacturing Technology*, 48(2):541–556, 1999. [11](#)
- [62] WP Dong, PJ Sullivan, and KJ Stout. Comprehensive study of parameters for characterizing three-dimensional surface topography i: Some inherent properties of parameter variation. *Wear*, 159(2):161–171, 1992. [11](#), [16](#)
- [63] Ken J Stout. The development of methods for the characterisation of roughness in three dimensions. *Commission of the european communities. Luxembourg*, 130, 1993. [11](#), [16](#)
- [64] Richard K Leach. *Characterisation of areal surface texture*. Springer, 2013. [12](#)
- [65] Richard Leach. *Fundamental principles of engineering nanometrology*. Elsevier, 2014. [12](#), [13](#)
- [66] BSEN ISO. 4288: 1998, geometrical product specification–surface texture: profile method–rules and procedures for the assessment of surface texture. *British Standards Institution*, 1998. [13](#)
- [67] Evaristus Mainsah, Derek Chetwynd, et al. *Metrology and properties of engineering surfaces*. Springer Science & Business Media, 2013. [13](#), [15](#)
- [68] ISO Standard. 4287: 1997: Geometrical product specifications (gps)–surface texture: Profile method–terms, definitions and surface texture parameters. *International Organization for Standardization*, 1997. [13](#)
- [69] ES Gadelmawla, MM Koura, TMA Maksoud, IM Elewa, and HH Soliman. Roughness parameters. *Journal of Materials Processing Technology*, 123(1):133–145, 2002. [13](#), [14](#), [16](#), [159](#), [169](#)
- [70] ISO EN. 12805: 1997: Geometrical product specifications (gps)–surface texture: Profile method–terms, motif parameters. *International Organization for Standardization*, 1997. [15](#)
- [71] Shan Lou, Xiangqian Jiang, and Paul J Scott. Correlating motif analysis and morphological filters for surface texture analysis. *Measurement*, 46(2):993–1001, 2013. [15](#)

- [72] TR Thomas, B-G Rosen, and N Amini. Fractal characterisation of the anisotropy of rough surfaces. *Wear*, 232(1):41–50, 1999. [15](#)
- [73] Motoyoshi Hasegawa, Jiancheng Liu, Koichi Okuda, and Masayuki Nunobiki. Calculation of the fractal dimensions of machined surface profiles. *Wear*, 192(1):40–45, 1996. [15](#)
- [74] DJ Whitehouse. The parameter rash—is there a cure? *Wear*, 83(1):75–78, 1982. [15](#)
- [75] WP Dong, PJ Sullivan, and KJ Stout. Comprehensive study of parameters for characterising three-dimensional surface topography: Iii: Parameters for characterising amplitude and some functional properties. *Wear*, 178(1):29–43, 1994. [16](#)
- [76] TR Thomas and G Charlton. Variation of roughness parameters on some typical manufactured surfaces. *Precision Engineering*, 3(2):91–96, 1981. [16](#)
- [77] Ossama B Abouelatta. 3d surface roughness measurement using a light sectioning vision system. In *Proceedings of the World Congress on Engineering, London, UK*, volume 30, pages 698–703, 2010. [16](#)
- [78] Ghassan A Al-Kindi and Bijan Shirinzadeh. An evaluation of surface roughness parameters measurement using vision-based data. *International Journal of Machine Tools and Manufacture*, 47(3):697–708, 2007.
- [79] A Bengtsson and A Rönnerberg. Wide range three-dimensional roughness measuring system. *Precision engineering*, 6(3):141–147, 1984.
- [80] Quan Chen and Ngai Wong. New simulation methodology of 3d surface roughness loss for interconnects modeling. In *Design, Automation & Test in Europe Conference & Exhibition, 2009. DATE'09.*, pages 1184–1189. IEEE, 2009.
- [81] Anayet U Patwari, MD Arif, NA Chowdhury, and SI Chowdhury. 3-d contour generation and determination of surface roughness of shaped and horizontally milled plates using digital image processing. *Annals of the Faculty of Engineering Hunedoara*, 9(3):127, 2011. [16](#)
- [82] Liam Blunt and Xiang Jiang. *Advanced techniques for assessment surface topography: development of a basis for 3D surface texture standards” surf-stand”*. Elsevier, 2003. [16](#), [159](#), [160](#)

- 
- [83] François Blateyron. The areal feature parameters. In *Characterisation of Areal Surface Texture*, pages 45–65. Springer, 2013. [16](#)
- [84] Wouter M Bergmann Tiest and Astrid ML Kappers. Haptic and visual perception of roughness. *Acta psychologica*, 124(2):177–189, 2007. [17](#), [34](#), [159](#), [165](#), [169](#)
- [85] Susan J Lederman and Roberta L Klatzky. Haptic perception: A tutorial. *Attention, Perception, & Psychophysics*, 71(7):1439–1459, 2009. [17](#)
- [86] M Knibestöl and Åke B Vallbo. Single unit analysis of mechanoreceptor activity from the human glabrous skin. *Acta Physiologica Scandinavica*, 80(2):178–195, 1970. [18](#)
- [87] David E Sadava, David M Hillis, H Craig Heller, and May Berenbaum. *Life: the science of biology*, volume 2. Macmillan, 2009. [18](#)
- [88] Kenneth Johnson. Neural basis of haptic perception. *Stevens' handbook of experimental psychology*, 2002. [18](#), [19](#), [20](#)
- [89] Kenneth O Johnson, Steven S Hsiao, and Takashi Yoshioka. Book review: neural coding and the basic law of psychophysics. *The Neuroscientist*, 8(2):111–121, 2002. [19](#)
- [90] Vaughan G Macefield, Charlotte Häger-Ross, and Roland S Johansson. Control of grip force during restraint of an object held between finger and thumb: responses of cutaneous afferents from the digits. *Experimental Brain Research*, 108(1):155–171, 1996. [20](#)
- [91] Sliman J Bensmaïa and Mark Hollins. Complex tactile waveform discrimination. *The Journal of the Acoustical Society of America*, 108(3):1236–1245, 2000. [20](#)
- [92] JAB Gray and M Sato. Properties of the receptor potential in pacinian corpuscles. *The Journal of physiology*, 122(3):610, 1953. [20](#)
- [93] WR Loewenstein and R Skalak. Mechanical transmission in a pacinian corpuscle. an analysis and a theory. *The Journal of physiology*, 182(2):346–378, 1966. [20](#)
- [94] M Sato. Response of pacinian corpuscles to sinusoidal vibration. *The Journal of physiology*, 159(3):391–409, 1961. [20](#)

- [95] David Katz. *The world of touch*. Psychology Press, 2013. [20](#), [26](#)
- [96] Sliman Bensmaïa and Mark Hollins. Pacinian representations of fine surface texture. *Perception & psychophysics*, 67(5):842–854, 2005. [20](#)
- [97] Susan J Lederman, Jack M Loomis, and Deborah A Williams. The role of vibration in the tactual perception of roughness. *Perception & Psychophysics*, 32(2):109–116, 1982. [20](#), [169](#)
- [98] George A Gescheider, Bradley F Sklar, Clayton L Van Doren, and Ronald T Verrillo. Vibrotactile forward masking: psychophysical evidence for a triplex theory of cutaneous mechanoreception. *The Journal of the Acoustical Society of America*, 78(2):534–543, 1985. [21](#)
- [99] Ronald T Verrillo. Effect of contactor area on the vibrotactile threshold. *The Journal of the Acoustical Society of America*, 35(12):1962–1966, 1963. [21](#)
- [100] Stanley J Bolanowski Jr, George A Gescheider, Ronald T Verrillo, and Christin M Checkosky. Four channels mediate the mechanical aspects of touch. *The Journal of the Acoustical society of America*, 84(5):1680–1694, 1988. [21](#)
- [101] George A Gescheider, Stanley J Bolanowski, and Ronald T Verrillo. Some characteristics of tactile channels. *Behavioural brain research*, 148(1):35–40, 2004. [21](#), [22](#), [23](#)
- [102] Ronald T Verrillo and George A Gescheider. Enhancement and summation in the perception of two successive vibrotactile stimuli. *Perception & Psychophysics*, 18(2):128–136, 1975. [22](#)
- [103] RT Verrillo. Temporal summation in vibrotactile sensitivity. *The Journal of the Acoustical Society of America*, 37(5):843–846, 1965. [22](#)
- [104] Greg K Essick, Francis McGlone, Chris Dancer, David Fabricant, Yancy Rabin, Nicola Phillips, Therese Jones, and Steve Guest. Quantitative assessment of pleasant touch. *Neuroscience & Biobehavioral Reviews*, 34(2):192–203, 2010. [22](#)
- [105] Line S Löken, Jan Minde, Johan Wessberg, Irene Perini, Inger Nennesmo, and Håkan Olausson. Reduced c-afferent fibre density affects perceived pleasantness and empathy for touch. *Brain*, 134(4):1116–1126, 2011. [22](#)



- [106] Francis McGlone and David Reilly. The cutaneous sensory system. *Neuroscience & Biobehavioral Reviews*, 34(2):148–159, 2010.
- [107] Francis McGlone, Johan Wessberg, and Håkan Olausson. Discriminative and affective touch: sensing and feeling. *Neuron*, 82(4):737–755, 2014. [22](#)
- [108] F McGlone, H Olausson, JA Boyle, M Jones-Gotman, C Dancer, S Guest, and G Essick. Touching and feeling: differences in pleasant touch processing between glabrous and hairy skin in humans. *European Journal of Neuroscience*, 35(11):1782–1788, 2012. [22](#), [23](#)
- [109] Laura K Case, Claire M Laubacher, Håkan Olausson, Binquan Wang, Primavera A Spagnolo, and M Catherine Bushnell. Encoding of touch intensity but not pleasantness in human primary somatosensory cortex. *The Journal of Neuroscience*, 36(21):5850–5860, 2016. [23](#)
- [110] Qicai Wang, Weidong Yu, Kemin Chen, Zhongwei Zhang, and Rabie AM Asad. Brain cognitive comparison of fabric touch on human glabrous and hairy skin. *Textile Research Journal*, page 0040517515591785, 2015. [23](#)
- [111] Valeria Gazzola, Michael L Spezio, Joset A Etzel, Fulvia Castelli, Ralph Adolphs, and Christian Keysers. Primary somatosensory cortex discriminates affective significance in social touch. *Proceedings of the National Academy of Sciences*, 109(25):E1657–E1666, 2012. [23](#)
- [112] Ciara McCabe, Edmund T Rolls, Amy Bilderbeck, and Francis McGlone. Cognitive influences on the affective representation of touch and the sight of touch in the human brain. *Social Cognitive and Affective Neuroscience*, 3(2):97–108, 2008. [23](#)
- [113] Ryan M Peters, Erik Hackeman, and Daniel Goldreich. Diminutive digits discern delicate details: fingertip size and the sex difference in tactile spatial acuity. *The Journal of neuroscience*, 29(50):15756–15761, 2009. [23](#), [25](#)
- [114] James C Craig and Kenneth O Johnson. The two-point threshold not a measure of tactile spatial resolution. *Current Directions in Psychological Science*, 9(1):29–32, 2000. [23](#)
- [115] James C Craig. Grating orientation as a measure of tactile spatial acuity. *Somatosensory & motor research*, 16(3):197–206, 1999. [23](#)

- [116] JR Phillips and Kenneth O Johnson. Tactile spatial resolution. ii. neural representation of bars, edges, and gratings in monkey primary afferents. *Journal of neurophysiology*, 46(6):1192–1203, 1981. [24](#)
- [117] Kenneth O Johnson and Steven S Hsiao. Neural mechanisms of tactual form and texture perception. *Annual review of neuroscience*, 15(1):227–250, 1992. [24](#), [26](#), [49](#)
- [118] Esther P Gardner and Claude I Palmer. Simulation of motion on the skin. i. receptive fields and temporal frequency coding by cutaneous mechanoreceptors of optacon pulses delivered to the hand. *Journal of neurophysiology*, 62(6):1410–1436, 1989. [24](#)
- [119] Flavia Mancini, Armando Bauleo, Jonathan Cole, Fausta Lui, Carlo A Porro, Patrick Haggard, and Gian Domenico Iannetti. Whole-body mapping of spatial acuity for pain and touch. *Annals of neurology*, 75(6):917–924, 2014. [25](#)
- [120] Jack M Loomis. An investigation of tactile hyperacuity. *Sensory processes*, 3:289–302, 1979. [25](#), [49](#)
- [121] Jack M Loomis and Carter C Collins. Sensitivity to shifts of a point stimulus: An instance of tactile hyperacuity. *Perception & Psychophysics*, 24(6):487–492, 1978. [25](#)
- [122] HE Wheat, AW Goodwin, and AS Browning. Tactile resolution: peripheral neural mechanisms underlying the human capacity to determine positions of objects contacting the fingerpad. *The Journal of neuroscience*, 15(8):5582–5595, 1995. [25](#)
- [123] Robert O Duncan and Geoffrey M Boynton. Tactile hyperacuity thresholds correlate with finger maps in primary somatosensory cortex (s1). *Cerebral Cortex*, 17(12):2878–2891, 2007. [25](#)
- [124] Arthur C Grant, Mahesh C Thiagarajah, and K Sathian. Tactile perception in blind braille readers: A psychophysical study of acuity and hyperacuity using gratings and dot patterns. *Perception & Psychophysics*, 62(2):301–312, 2000. [25](#)
- [125] Hollins, Sliman J. Bensmaïa, Sean Washburn, and Mark. Vibrotactile adaptation impairs discrimination of fine, but not coarse, textures. *Somatosensory & motor research*, 18(4):253–262, 2001. [25](#)

- [126] Kenneth O Johnson and Graham D Lamb. Neural mechanisms of spatial tactile discrimination: neural patterns evoked by braille-like dot patterns in the monkey. *The Journal of physiology*, 310:117, 1981. [26](#)
- [127] M Hollins, SJ Bensmaia, and EA Roy. Vibrotaction and texture perception. *Behavioural brain research*, 135(1):51–56, 2002. [26](#)
- [128] Mark Hollins and S Ryan Risner. Evidence for the duplex theory of tactile texture perception. *Perception & psychophysics*, 62(4):695–705, 2000. [26](#)
- [129] FAA Kingdom and N Prins. *Psychophysics: a practical introduction*, 2010. [27](#), [50](#)
- [130] Susan J Lederman. Tactile roughness of grooved surfaces: The touching process and effects of macro-and microsurface structure. *Perception & Psychophysics*, 16(2):385–395, 1974. [27](#)
- [131] Alexandra Dépeault, El-Mehdi Meftah, and C Elaine Chapman. Tactile perception of roughness: raised-dot spacing, density and disposition. *Experimental brain research*, 197(3):235–244, 2009. [27](#)
- [132] Tetsu Miyaoka, Tadaaki Mano, and Masahiro Ohka. Mechanisms of fine-surface-texture discrimination in human tactile sensation. *The journal of the acoustical society of America*, 105(4):2485–2492, 1999. [27](#)
- [133] Susan J Lederman. The perception of surface roughness by active and passive touch. *Bulletin of the Psychonomic Society*, 18(5):253–255, 1981. [28](#)
- [134] Andrea Serino, Giulia Giovagnoli, Frederique de Vignemont, and Patrick Haggard. Spatial organisation in passive tactile perception: Is there a tactile field? *Acta psychologica*, 128(2):355–360, 2008. [28](#), [49](#)
- [135] James R Pomerantz and Michael Kubovy. Theoretical approaches to perceptual organization: Simplicity and likelihood principles. *Organization*, 36:3, 1986. [28](#), [29](#), [50](#)
- [136] Max Wertheimer. Laws of organization in perceptual forms. 1938. [28](#), [49](#)
- [137] Patrick Haggard and Giulia Giovagnoli. Spatial patterns in tactile perception: Is there a tactile field? *Acta psychologica*, 137(1):65–75, 2011. [28](#)

- 
- [138] Joseph S Lappin and Emerson Foulke. Expanding the tactual field of view. *Perception & Psychophysics*, 14(2):237–241, 1973. [28](#)
- [139] T Aisling Whitaker, Cristina Simões-Franklin, and Fiona N Newell. Vision and touch: Independent or integrated systems for the perception of texture? *Brain Research*, 1242:59–72, 2008. [29](#), [31](#)
- [140] Vanessa Harrar and Laurence R Harris. Multimodal ternus: Visual, tactile, and visuo—tactile grouping in apparent motion. *Perception*, 36(10):1455–1464, 2007. [29](#)
- [141] Alberto Gallace and Charles Spence. To what extent do gestalt grouping principles influence tactile perception? *Psychological bulletin*, 137(4):538, 2011. [29](#)
- [142] Krista E Overvliet, Ralf Th Krampe, and Johan Wagemans. Grouping by proximity in haptic contour detection. *PloS one*, 8(6):e65412, 2013. [29](#)
- [143] Dempsey Chang, Keith V Nesbitt, and Kevin Wilkins. The gestalt principles of similarity and proximity apply to both the haptic and visual grouping of elements. In *Proceedings of the eight Australasian conference on User interface-Volume 64*, pages 79–86. Australian Computer Society, Inc., 2007. [29](#)
- [144] Norimichi Kitagawa, Yuka Igarashi, and Makio Kashino. The tactile continuity illusion. *Journal of Experimental Psychology: Human Perception and Performance*, 35(6):1784, 2009.
- [145] Christian Frings and Charles Spence. Gestalt grouping effects on tactile information processing: when touching hands override spatial proximity. *Attention, Perception, & Psychophysics*, 75(3):468–480, 2013.
- [146] Krista E Overvliet, Ralf Th Krampe, and Johan Wagemans. Perceptual grouping in haptic search: the influence of proximity, similarity, and good continuation. *Journal of Experimental Psychology: Human Perception and Performance*, 38(4):817, 2012. [29](#)
- [147] Jack M Loomis. Tactile pattern perception. *Perception*, 10(1):5–27, 1981. [30](#), [49](#)
- [148] James C Bliss. A relatively high-resolution reading aid for the blind. *Man-Machine Systems, IEEE Transactions on*, 10(1):1–9, 1969. [30](#), [49](#)

- [149] Jack M Loomis. On the tangibility of letters and braille. *Perception & Psychophysics*, 29(1):37–46, 1981. [30](#), [49](#)
- [150] James C Craig. Tactile letter recognition: Pattern duration and modes of pattern generation. *Perception & Psychophysics*, 30(6):540–546, 1981. [30](#), [49](#)
- [151] Jack M Loomis. Tactile letter recognition under different modes of stimulus presentation. *Perception & Psychophysics*, 16(2):401–408, 1974. [30](#), [49](#)
- [152] Morton A Heller. Picture and pattern perception in the sighted and the blind: the advantage of the late blind. *Perception*, 18(3):379–389, 1989. [30](#), [31](#)
- [153] Galal Mohamed Elkharraz. *Selection of tactile textures with predetermined affective properties*. PhD thesis, University of Leeds, 2011. [30](#)
- [154] Olivier Collignon, Patrice Voss, Maryse Lassonde, and Franco Lepore. Cross-modal plasticity for the spatial processing of sounds in visually deprived subjects. *Experimental brain research*, 192(3):343, 2009. [31](#)
- [155] Lotfi Merabet, Gregor Thut, Brian Murray, Jessica Andrews, Steven Hsiao, and Alvaro Pascual-Leone. Feeling by sight or seeing by touch? *Neuron*, 42(1):173–179, 2004. [31](#)
- [156] Elisabeth Baumgartner, Christiane B Wiebel, and Karl R Gegenfurtner. A comparison of haptic material perception in blind and sighted individuals. *Vision research*, 115:238–245, 2015. [31](#)
- [157] Roberta L Klatzky, Susan J Lederman, and Catherine Reed. There’s more to touch than meets the eye: The salience of object attributes for haptics with and without vision. *Journal of experimental psychology: general*, 116(4):356, 1987. [31](#)
- [158] Alvaro Pascual-Leone, Amir Amedi, Felipe Fregni, and Lotfi B Merabet. The plastic human brain cortex. *Annu. Rev. Neurosci.*, 28:377–401, 2005. [31](#)
- [159] Lotfi B Merabet, Jascha D Swisher, Stephanie A McMains, Mark A Halko, Amir Amedi, Alvaro Pascual-Leone, and David C Somers. Combined activation and deactivation of visual cortex during tactile sensory processing. *Journal of neurophysiology*, 97(2):1633–1641, 2007. [31](#)

- [160] Harold Burton, Robert J Sinclair, and Donald G McLaren. Cortical activity to vibrotactile stimulation: an fmri study in blind and sighted individuals. *Human brain mapping*, 23(4):210–228, 2004. [31](#)
- [161] Andro Zangaladze, Charles M Epstein, Scott T Grafton, and Krish Sathian. Involvement of visual cortex in tactile discrimination of orientation. *Nature*, 401(6753):587, 1999. [31](#)
- [162] Daisuke N Saito, Tomohisa Okada, Yusuke Morita, Yoshiharu Yonekura, and Norihiro Sadato. Tactile–visual cross-modal shape matching: a functional mri study. *Cognitive Brain Research*, 17(1):14–25, 2003. [31](#)
- [163] K Sathian and A Zangaladze. Feeling with the mind’s eye: contribution of visual cortex to tactile perception. *Behavioural brain research*, 135(1-2):127–132, 2002. [31](#)
- [164] Hua-Chun Sun, Andrew E Welchman, Dorita HF Chang, and Massimiliano Di Luca. Look but don’t touch: Visual cues to surface structure drive somatosensory cortex. *Neuroimage*, 128:353–361, 2016. [31](#)
- [165] Krishnankutty Sathian. Visual cortical activity during tactile perception in the sighted and the visually deprived. *Developmental Psychobiology: The Journal of the International Society for Developmental Psychobiology*, 46(3):279–286, 2005. [31](#)
- [166] Xiaojuan Chen, Fei Shao, Cathy Barnes, Tom Childs, and Brian Henson. Exploring relationships between touch perception and surface physical properties. *International Journal of Design*, 3(2):67–76, 2009. [32](#)
- [167] Julien Scheibert, Sébastien Leurent, Alexis Prevost, and Georges Debrégeas. The role of fingerprints in the coding of tactile information probed with a biomimetic sensor. *Science*, 323(5920):1503–1506, 2009. [33](#)
- [168] Mark H Lee and Howard R Nicholls. Review article tactile sensing for mechatronics—a state of the art survey. *Mechatronics*, 9(1):1–31, 1999. [33](#)
- [169] Dennis Allerkamp, Guido Böttcher, Franz-Erich Wolter, Alan C Brady, Jianguo Qu, and Ian R Summers. A vibrotactile approach to tactile rendering. *The Visual Computer*, 23(2):97–108, 2007. [33](#)

- [170] Yasushi Ikei, Kazufumi Wakamatsu, and Shuichi Fukuda. Vibratory tactile display of image-based textures. *IEEE Computer Graphics and Applications*, 17(6):53–61, 1997. 33
- [171] Ryo Kikuuwe, Kenta Nakamura, and Motoji Yamamoto. Finger-mounted tactile sensor for evaluating surfaces. *Journal of Robotics and Mechatronics*, 24(3):430, 2012. 33
- [172] Masashi Konyo, Satoshi Tadokoro, Akinori Yoshida, and Naoki Saiwaki. A tactile synthesis method using multiple frequency vibrations for representing virtual touch. In *2005 IEEE/RSJ International Conference on Intelligent Robots and Systems*, pages 3965–3971. IEEE, 2005.
- [173] Akio Yamamoto, Shuichi Nagasawa, Hiroaki Yamamoto, and Toshiro Higuchi. Electrostatic tactile display with thin film slider and its application to tactile telepresentation systems. *IEEE Transactions on Visualization and Computer Graphics*, 12(2):168–177, 2006. 33
- [174] S. Chen, S. Ge, W. Tang, J. Zhang, and N. Chen. Tactile perception of fabrics with an artificial finger compared to human sensing. *Textile Research Journal*, 2015. ISSN 0040-5175. doi: 10.1177/0040517515586164. URL <http://trj.sagepub.com/cgi/doi/10.1177/0040517515586164>. 33
- [175] Xianming Ye, Byungjune Choi, Sungchul Kang, and Hyouk Ryeol Choi. Profile-based roughness discrimination with pen-type texture sensor. *International Journal of Control, Automation and Systems*, 8(4):793–800, 2010. 33
- [176] Florian De Boissieu, Christelle Godin, Bernard Guilhamat, Dominique David, Christine Serviere, and Daniel Baudois. Tactile texture recognition with a 3-axial force mems integrated artificial finger. In *Robotics: Science and Systems*, pages 49–56. Seattle, WA, 2009. 33
- [177] Mami Tanaka, Seiji Chonan, Zhongwei Jiang, and Hideki Nakajima. Measurement and valuation of touch sensation (tactile perception of forefinger compared with pvd sensor output). In *Ninth International Conference on Adaptive Structures and Technologies: October 14-16, 1998, Boston, Massachusetts, USA*, page 61. CRC, 1999. 33

- [178] Wei Tang, Nanxuan Chen, Jiankai Zhang, Si Chen, Shirong Ge, Hua Zhu, Shaogang Zhang, and Haifeng Yang. Characterization of tactile perception and optimal exploration movement. *Tribology Letters*, 58(2):1–14, 2015. [33](#)
- [179] Haihua Hu, Yezhen Han, Aiguo Song, Shanguang Chen, Chunhui Wang, and Zheng Wang. A finger-shaped tactile sensor for fabric surfaces evaluation by 2-dimensional active sliding touch. *Sensors*, 14(3):4899–4913, 2014. [33](#)
- [180] Diyar Akay, Xiaojuan Chen, Cathy Barnes, and Brian Henson. Anfis modeling for predicting affective responses to tactile textures. *Human Factors and Ergonomics in Manufacturing & Service Industries*, 22(3):269–281, 2012. [34](#), [159](#)
- [181] X Liu, Zhaoyang Yue, Z Cai, Derek G Chetwynd, and ST Smith. Quantifying touch–feel perception: tribological aspects. *Measurement Science and Technology*, 19(8):084007, 2008. [34](#)
- [182] CJ Barnes, THC Childs, B Henson, and CH Southee. Surface finish and touch—a case study in a new human factors tribology. *Wear*, 257(7):740–750, 2004. [34](#), [159](#)
- [183] Yasushi Ikei, Kazufumi Wakamatsu, and Shuichi Fukuda. Image data transformation for tactile texture display. In *Virtual Reality Annual International Symposium, 1998. Proceedings., IEEE 1998*, pages 51–58. IEEE, 1998. [35](#)
- [184] Paul F Whelan and Derek Molloy. *Machine vision algorithms in Java: techniques and implementation*. Springer Science & Business Media, 2012. [35](#), [36](#)
- [185] Piotr Szczypiński, Marcin Kociołek, Andrzej Materka, and Michał Strzelecki. Computer program for image texture analysis in phd students laboratory. In *International Conference on Signals and Electronic Systems, Łódź-Poland*, pages 255–262. Citeseer, 2001. [36](#)
- [186] Robert T Olszewski. Generalized feature extraction for structural pattern recognition in time-series data. Technical report, CARNEGIE-MELLON UNIV PITTSBURGH PA SCHOOL OF COMPUTER SCIENCE, 2001. [37](#)
- [187] Jianguo Zhang and Tieniu Tan. Brief review of invariant texture analysis methods. *Pattern recognition*, 35(3):735–747, 2002. [37](#)



- 
- [188] Fergus W Campbell and JG Robson. Application of fourier analysis to the visibility of gratings. *The Journal of physiology*, 197(3):551–566, 1968. [37](#)
- [189] MA Georgeson. Spatial fourier analysis and human vision. *Tutorial essays in psychology*, 2:39–88, 1979. [37](#)
- [190] Xiaou Tang and W Kenneth Stewart. Optical and sonar image classification: wavelet packet transform vs fourier transform. *Computer vision and image understanding*, 79(1):25–46, 2000. [37](#), [43](#)
- [191] P Scheunders, S Livens, G Van de Wouwer, P Vautrot, and D Van Dyck. Wavelet-based texture analysis. *International Journal on Computer Science and Information Management*, 1(2):22–34, 1998. [37](#)
- [192] Mingshi Wang and André Knoesen. Rotation-and scale-invariant texture features based on spectral moment invariants. *JOSA A*, 24(9):2550–2557, 2007. [37](#)
- [193] A Oppenheim, Jae Lim, Gary Kopec, and S Pohlig. Phase in speech and pictures. In *ICASSP’79. IEEE International Conference on Acoustics, Speech, and Signal Processing*, volume 4, pages 632–637. IEEE, 1979. [38](#), [149](#)
- [194] Leon N Piotrowski and Fergus W Campbell. A demonstration of the visual importance and flexibility of spatial-frequency amplitude and phase. *Perception*, 11(3):337–346, 1982. [38](#), [40](#), [99](#)
- [195] Alan V Oppenheim and Jae S Lim. The importance of phase in signals. *Proceedings of the IEEE*, 69(5):529–541, 1981. [38](#), [40](#), [99](#)
- [196] T Huang, J Burnett, and A Deczky. The importance of phase in image processing filters. *IEEE Transactions on Acoustics, Speech, and Signal Processing*, 23(6):529–542, 1975. [38](#), [99](#)
- [197] Joseph L Horner and Peter D Gianino. Phase-only matched filtering. *Applied optics*, 23(6):812–816, 1984. [38](#), [39](#)
- [198] W Pearlman and R Gray. Source coding of the discrete fourier transform. *IEEE Transactions on information theory*, 24(6):683–692, 1978. [38](#)
- [199] Andrew G Tescher. The role of phase in adaptive image coding. Technical report, UNIVERSITY OF SOUTHERN CALIFORNIA LOS ANGELES IMAGE PROCESSING INST, 1973. [38](#)

- [200] Navneet Upadhyay and Abhijit Karmakar. Speech enhancement using spectral subtraction-type algorithms: A comparison and simulation study. *Procedia Computer Science*, 54:574–584, 2015. [38](#)
- [201] M Ekstrom and JW Woods. Two-dimensional spectral factorization with applications in recursive digital filtering. *IEEE Transactions on Acoustics, Speech, and Signal Processing*, 24(2):115–128, 1976. [38](#)
- [202] Benjamin Friedlander. Recursive lattice forms for spectral estimation. *IEEE Transactions on Acoustics, Speech, and Signal Processing*, 30(6):920–930, 1982. [38](#)
- [203] Nivedita Chennupati, Sudarsana Reddy Kadiri, and Bayya Yegnanarayana. Significance of phase in single frequency filtering outputs of speech signals. *Speech Communication*, 97:66–72, 2018. [39](#)
- [204] D Wang and Jae Lim. The unimportance of phase in speech enhancement. *IEEE Transactions on Acoustics, Speech, and Signal Processing*, 30(4):679–681, 1982. [39](#), [42](#)
- [205] Pejman Mowlae, Rahim Saeidi, and Yannis Stylianou. Advances in phase-aware signal processing in speech communication. *Speech communication*, 81:1–29, 2016. [39](#), [41](#)
- [206] Kuldeep K Paliwal and Leigh Alsteris. Usefulness of phase spectrum in human speech perception. In *Eighth European Conference on Speech Communication and Technology*, 2003. [39](#)
- [207] Kuldeep Paliwal, Kamil Wójcicki, and Benjamin Shannon. The importance of phase in speech enhancement. *speech communication*, 53(4):465–494, 2011. [39](#)
- [208] Siarhei Y Barysenka, Vasili I Vorobiov, and Pejman Mowlae. Single-channel speech enhancement using inter-component phase relations. *Speech Communication*, 99:144–160, 2018. [39](#)
- [209] Xuelei Sherry Ni and Xiaoming Huo. Statistical interpretation of the importance of phase information in signal and image reconstruction. *Statistics & probability letters*, 77(4):447–454, 2007. [39](#), [99](#)
- [210] Waldemar Popiński. Statistical view on phase and magnitude information in signal processing. *Artificial Satellites*, 47(3):127–136, 2012. [39](#), [42](#)

- 
- [211] M Hayes, Jae Lim, and A Oppenheim. Phase-only signal reconstruction. In *ICASSP'80. IEEE International Conference on Acoustics, Speech, and Signal Processing*, volume 5, pages 437–440. IEEE, 1980. [40](#)
- [212] Monson Hayes, Jae Lim, and Alan Oppenheim. Signal reconstruction from phase or magnitude. *IEEE Transactions on Acoustics, Speech, and Signal Processing*, 28(6):672–680, 1980. [40](#), [42](#)
- [213] Changxue Ma. Novel criteria of uniqueness for signal reconstruction from phase. *IEEE Transactions on signal processing*, 39(4):989–992, 1991. [40](#), [41](#)
- [214] G Merchant and T Parks. Reconstruction of signals from phase: Efficient algorithms, segmentation, and generalizations. *IEEE transactions on acoustics, speech, and signal processing*, 31(5):1135–1147, 1983. [40](#)
- [215] V Tom, T Quatieri, M Hayes, and J McClellan. Convergence of iterative nonexpansive signal reconstruction algorithms. *IEEE Transactions on Acoustics, Speech, and Signal Processing*, 29(5):1052–1058, 1981. [40](#)
- [216] Sharon Urieli, Moshe Porat, and Nir Cohen. Image characteristics and representation by phase: from symmetric to geometric structure. In *Proceedings of 3rd IEEE International Conference on Image Processing*, volume 1, pages 705–708. IEEE, 1996. [40](#)
- [217] Athina P Petropulu and Chrysostomos L Nikias. Signal reconstruction from the phase of the bispectrum. *IEEE Transactions on Signal Processing*, 40(3):601–610, 1992. [40](#)
- [218] RP Millane and WH Hsiao. The basis of phase dominance. *Optics letters*, 34(17):2607–2609, 2009. [40](#), [44](#), [169](#)
- [219] Bernt C Skottun. Amplitude and phase in the müller-lyer illusion. *Perception*, 29(2):201–209, 2000. [40](#)
- [220] Jonathan D Victor and Mary M Conte. The role of high-order phase correlations in texture processing. *Vision Research*, 36(11):1615–1631, 1996. [41](#)
- [221] Bela Julész, Edgar N Gilbert, and Jonathan D Victor. Visual discrimination of textures with identical third-order statistics. *Biological Cybernetics*, 31(3):137–140, 1978. [41](#)

- 
- [222] Mitchell GA Thomson, David H Foster, and Robert J Summers. Human sensitivity to phase perturbations in natural images: a statistical framework. *Perception*, 29(9):1057–1069, 2000. [41](#)
- [223] Adolf W Lohmann, David Mendlovic, and Gal Shabtay. Significance of phase and amplitude in the fourier domain. *JOSA A*, 14(11):2901–2904, 1997. [41](#), [99](#)
- [224] John N Mc Donald. Phase retrieval and magnitude retrieval of entire functions. *Journal of Fourier Analysis and Applications*, 10(3):259–267, 2004. [41](#)
- [225] Igor Lyuboshenko and Alexander Akhmetshin. Stable signal and image reconstruction from noisy fourier transform phase. *IEEE transactions on signal processing*, 47(1):244–250, 1999.
- [226] Rima Alaifari, Ingrid Daubechies, Philipp Grohs, and Rujie Yin. Stable phase retrieval in infinite dimensions. *Foundations of Computational Mathematics*, pages 1–32, 2018.
- [227] Philipp Grohs, Sarah Koppensteiner, and Martin Rathmair. The mathematics of phase retrieval. *arXiv preprint arXiv:1901.07911*, 2019. [41](#)
- [228] Yonina C Eldar and Shahar Mendelson. Phase retrieval: Stability and recovery guarantees. *Applied and Computational Harmonic Analysis*, 36(3):473–494, 2014. [41](#)
- [229] Ju Sun, Qing Qu, and John Wright. A geometric analysis of phase retrieval. *Foundations of Computational Mathematics*, 18(5):1131–1198, 2018. [41](#)
- [230] Nicolas Sturmel, Laurent Daudet, et al. Signal reconstruction from stft magnitude: A state of the art. In *International conference on digital audio effects (DAFx)*, pages 375–386, 2011. [42](#)
- [231] Timo Gerkmann, Martin Krawczyk-Becker, and Jonathan Le Roux. Phase processing for single-channel speech enhancement: History and recent advances. *IEEE Signal Processing Magazine*, 32(2):55–66, 2015.
- [232] Mahdi Parchami, Wei-Ping Zhu, Benoit Champagne, and Eric Plourde. Recent developments in speech enhancement in the short-time fourier transform domain. *IEEE Circuits and Systems Magazine*, 16(3):45–77, 2016. [42](#)

- 
- [233] MJ Morgan, J Ross, and A Hayes. The relative importance of local phase and local amplitude in patchwise image reconstruction. *Biological Cybernetics*, 65(2):113–119, 1991. [42](#), [43](#), [45](#)
- [234] R Sarang, MR Jahed Motlagh, and P Eslami. Reconstruction of image using just magnitude information of fourier transform; is phase information really more important? In *2006 International Conference on Computational Intelligence for Modelling Control and Automation and International Conference on Intelligent Agents Web Technologies and International Commerce (CIMCA'06)*, pages 56–56. IEEE, 2006. [42](#)
- [235] James R Fienup. Reconstruction of a complex-valued object from the modulus of its fourier transform using a support constraint. *JOSA A*, 4(1):118–123, 1987. [42](#)
- [236] Norman E Hurt. *Phase retrieval and zero crossings: mathematical methods in image reconstruction*, volume 52. Springer Science & Business Media, 2001.
- [237] Kishore Jaganathan, Yonina C Eldar, and Babak Hassibi. Phase retrieval: An overview of recent developments. *arXiv preprint arXiv:1510.07713*, 2015. [42](#)
- [238] Radu Balan, Pete Casazza, and Dan Edidin. On signal reconstruction without phase. *Applied and Computational Harmonic Analysis*, 20(3):345–356, 2006. [42](#)
- [239] J He and SX Pan. Magnitude reconstruction of complex images from incomplete fourier phase data. In *[Proceedings] IECON'90: 16th Annual Conference of IEEE Industrial Electronics Society*, pages 357–362. IEEE, 1990. [42](#)
- [240] Bela Julesz. Visual pattern discrimination. *Information Theory, IRE Transactions on*, 8(2):84–92, 1962. [43](#), [50](#), [96](#), [170](#)
- [241] Nathalie Guyader, Alan Chauvin, Carole Peyrin, Jeanny Hérault, and Christian Marendaz. Image phase or amplitude? rapid scene categorization is an amplitude-based process. *Comptes Rendus Biologies*, 327(4):313–318, 2004. [43](#)

- [242] I Juvells, S Vallmitjana, A Carnicer, and J Campos. The role of amplitude and phase of the fourier transform in the digital image processing. *American Journal of Physics*, 59(8):744–748, 1991. [43](#)
- [243] Bela Julesz. Spatial nonlinearities in the instantaneous perception of textures with identical power spectra. *Phil. Trans. R. Soc. Lond. B*, 290(1038): 83–94, 1980. [43](#)
- [244] Y Tadmor and DJ Tolhurst. Both the phase and the amplitude spectrum may determine the appearance of natural images. *Vision research*, 33(1): 141–145, 1993. [43](#)
- [245] WH Hsiao, E Ip, and RP Millane. Effects of spectral amplitude and phase errors on interpretability of images. *Image and Vision Computing*, pages 175–180, 2003. [44](#)
- [246] WH Hsiao and RP Millane. Effects of fourier-plane amplitude and phase errors on image reconstruction. i. small amplitude errors. *JOSA A*, 24(10): 3180–3188, 2007. [44](#)
- [247] Eaton Lattman and David DeRosier. Why phase errors affect the electron function more than amplitude errors. *Acta Crystallographica Section A: Foundations of Crystallography*, 64(2):341–344, 2008. [44](#)
- [248] Joshua Gluckman. Visually distinct patterns with matching subband statistics. *IEEE transactions on pattern analysis and machine intelligence*, 27(2):252–264, 2005. [45](#)
- [249] Peyman Sheikholharam Mashhadi, Mahdi Aliyari Shoorehdeli, and Mohammad Teshnehlab. Patterns with different phases but same statistics. *JOSA A*, 30(9):1796–1805, 2013. [45](#)
- [250] Joan S Weszka, Charles R Dyer, and Azriel Rosenfeld. A comparative study of texture measures for terrain classification. *IEEE transactions on Systems, Man, and Cybernetics*, (4):269–285, 1976. [45](#), [46](#)
- [251] Du-Ming Tsai, Jeng-Jong Chen, and Jeng-Fung Chen. A vision system for surface roughness assessment using neural networks. *The International Journal of Advanced Manufacturing Technology*, 14(6):412–422, 1998. [45](#), [106](#)

- [252] BY Lee, SF Yu, and H Juan. The model of surface roughness inspection by vision system in turning. *Mechatronics*, 14(1):129–141, 2004. [46](#)
- [253] Rouzbeh Maani, Sanjay Kalra, and Yee-Hong Yang. Noise robust rotation invariant features for texture classification. *Pattern Recognition*, 46(8):2103–2116, 2013. [46](#)
- [254] Jun Zhang, Jimin Liang, Chunhui Zhang, and Heng Zhao. Scale invariant texture representation based on frequency decomposition and gradient orientation. *Pattern Recognition Letters*, 51:57–62, 2015. [46](#)
- [255] JO Eklundh. On the use of fourier phase features for texture discrimination. *Computer Graphics and Image Processing*, 9(2):199–201, 1979. [46](#)
- [256] Xinghui Dong, Ying Gao, Junyu Dong, and Mike J Chantler. The importance of phase to texture similarity. In *Proceedings of the IEEE International Conference on Computer Vision*, pages 2758–2766, 2017. [46](#), [130](#), [149](#)
- [257] Xinghui Dong, Thomas S Methven, and Mike J Chantler. How well do computational features perceptually rank textures? a comparative evaluation. In *Proceedings of International Conference on Multimedia Retrieval*, page 281. ACM, 2014. [46](#)
- [258] Ville Ojansivu and Janne Heikkilä. Blur insensitive texture classification using local phase quantization. In *International conference on image and signal processing*, pages 236–243. Springer, 2008. [46](#)
- [259] Sonia Kherchaoui and Amrane Houacine. Facial expression identification using gradient local phase. *Multimedia Tools and Applications*, 78(12):16843–16859, 2019. [46](#)
- [260] Ankan Kumar Bhunia, Alireza Alaei, and Partha Pratim Roy. Signature verification approach using fusion of hybrid texture features. *Neural Computing and Applications*, pages 1–12, 2019. [46](#)
- [261] Emanuela Marasco, Stefany Cando, Larry Tang, and Elham Tabassi. Cross-sensor evaluation of textural descriptors for gender prediction from fingerprints. In *2019 IEEE Winter Applications of Computer Vision Workshops (WACVW)*, pages 55–62. IEEE, 2019. [46](#)

- 
- [262] O Franzén. On summation: A psychophysical study of the tactual sense. *Quarterly progress and status report, Speech Transmission Laboratory, Royal Institute of Technology*, pages 14–25, 1966. [50](#)
- [263] Ronald T Verrillo, Anthony J Fraioli, and Robert L Smith. Sensation magnitude of vibrotactile stimuli. *Perception & Psychophysics*, 6(6):366–372, 1969.
- [264] George A Gescheider and Barbara A Hughson. Stimulus context and absolute magnitude estimation: A study of individual differences. *Perception & psychophysics*, 50(1):45–57, 1991. [50](#)
- [265] R Duncan Luce and Eugene Galanter. Psychophysical scaling. *Handbook of mathematical psychology*, 1:245–307, 1963. [50](#)
- [266] Raphael Vallat. Pingouin: statistics in python. *The Journal of Open Source Software*, 3(31):1026, nov 2018. [59](#)
- [267] Dietrich Samuel Schwarzkopf, Benjamin De Haas, and Geraint Rees. Better ways to improve standards in brain-behavior correlation analysis. *Frontiers in human neuroscience*, 6:200, 2012. [59](#)
- [268] Mavuto M Mukaka. A guide to appropriate use of correlation coefficient in medical research. *Malawi Medical Journal*, 24(3):69–71, 2012. [60](#), [72](#), [122](#)
- [269] Stephen Olejnik and James Algina. Measures of effect size for comparative studies: Applications, interpretations, and limitations. *Contemporary educational psychology*, 25(3):241–286, 2000. [61](#)
- [270] John TE Richardson. Eta squared and partial eta squared as measures of effect size in educational research. *Educational Research Review*, 6(2):135–147, 2011.
- [271] Jacob Cohen. *Statistical power analysis for the behavioral sciences*. Routledge, 2013. [61](#), [108](#), [165](#)
- [272] Hervé Abdi and Lynne J Williams. Tukey’s honestly significant difference (hsd) test. *Encyclopedia of Research Design. Thousand Oaks, CA: Sage*, pages 1–5, 2010. [61](#)
- [273] David Marr and A Vision. A computational investigation into the human representation and processing of visual information. *WH San Francisco: Freeman and Company*, 1(2), 1982. [98](#)



- 
- [274] Evgeny Gladilin and Roland Eils. On the role of spatial phase and phase correlation in vision, illusion, and cognition. *Frontiers in computational neuroscience*, 9, 2015. [98](#), [99](#)
- [275] Dorian Kermisch. Image reconstruction from phase information only. *JOSA*, 60(1):15–17, 1970. [99](#)
- [276] Fan Zhang, Wenfei Jiang, Florent Autrusseau, and Weisi Lin. Exploring v1 by modeling the perceptual quality of images. *Journal of vision*, 14(1):26–26, 2014. [99](#)
- [277] Nicolaas Prins et al. *Psychophysics: a practical introduction*. Academic Press, 2016. [104](#), [157](#)
- [278] Girish Chandrashekar and Ferat Sahin. A survey on feature selection methods. *Computers & Electrical Engineering*, 40(1):16–28, 2014. [107](#)
- [279] Isabelle Guyon and André Elisseeff. An introduction to variable and feature selection. *Journal of machine learning research*, 3(Mar):1157–1182, 2003. [107](#)
- [280] Ron Kohavi and George H John. Wrappers for feature subset selection. *Artificial intelligence*, 97(1-2):273–324, 1997. [107](#)
- [281] Jianyu Miao and Lingfeng Niu. A survey on feature selection. *Procedia Computer Science*, 91:919–926, 2016. [107](#)
- [282] Roger Bakeman. Recommended effect size statistics for repeated measures designs. *Behavior research methods*, 37(3):379–384, 2005. [122](#)
- [283] Thom Baguley. Standardized or simple effect size: What should be reported? *British journal of psychology*, 100(3):603–617, 2009. [122](#)
- [284] Concha Bielza, Víctor Robles, and Pedro Larrañaga. Regularized logistic regression without a penalty term: An application to cancer classification with microarray data. *Expert Systems with Applications*, 38(5):5110–5118, 2011. [127](#)
- [285] Yong Liang, Cheng Liu, Xin-Ze Luan, Kwong-Sak Leung, Tak-Ming Chan, Zong-Ben Xu, and Hai Zhang. Sparse logistic regression with a  $l_{1/2}$  penalty for gene selection in cancer classification. *BMC bioinformatics*, 14(1):198, 2013. [127](#)

- [286] Damjan Krstajic, Ljubomir J Buturovic, David E Leahy, and Simon Thomas. Cross-validation pitfalls when selecting and assessing regression and classification models. *Journal of cheminformatics*, 6(1):10, 2014. [127](#), [143](#)
- [287] Lars Buitinck, Gilles Louppe, Mathieu Blondel, Fabian Pedregosa, Andreas Mueller, Olivier Grisel, Vlad Niculae, Peter Prettenhofer, Alexandre Gramfort, Jaques Grobler, et al. Api design for machine learning software: experiences from the scikit-learn project. *arXiv preprint arXiv:1309.0238*, 2013. [127](#), [143](#)
- [288] Kenneth O McGraw and SP Wong. A common language effect size statistic. *Psychological bulletin*, 111(2):361, 1992. [142](#)
- [289] Dave S Kerby. The simple difference formula: An approach to teaching nonparametric correlation. *Comprehensive Psychology*, 3:11–IT, 2014. [142](#)
- [290] Rui Xu and Donald C Wunsch. Survey of clustering algorithms. 2005. [151](#)
- [291] Andreas Buja, Deborah F Swayne, Michael L Littman, Nathaniel Dean, Heike Hofmann, and Lisha Chen. Data visualization with multidimensional scaling. *Journal of Computational and Graphical Statistics*, 17(2):444–472, 2008. [151](#)
- [292] Christopher M Bishop. *Pattern recognition and machine learning*. springer, 2006. [151](#)
- [293] Jerome Friedman, Trevor Hastie, and Robert Tibshirani. *The elements of statistical learning*, volume 1. Springer series in statistics New York, 2001. [151](#)
- [294] Peter J Rousseeuw. Silhouettes: a graphical aid to the interpretation and validation of cluster analysis. *Journal of computational and applied mathematics*, 20:53–65, 1987. [153](#)
- [295] SM Aqil Burney and Humera Tariq. K-means cluster analysis for image segmentation. *International Journal of Computer Applications*, 96(4), 2014. [153](#)
- [296] Jess Hartcher-O’Brien, Jeremy Evers, and Erik Tempelman. Surface roughness of 3d printed materials: Comparing physical measurements and human perception. *Materials Today Communications*, 19:300–305, 2019. [169](#)